

# **Developing a tissue engineering strategy for cleft palate repair**



**Thesis submitted to the University of Sheffield  
for the degree of Doctor of Philosophy**

**Sasima Puwanun**

**Department of Materials Sciences and Engineering**

**October 2014**

## **ACKNOWLEDGEMENTS**

I would like to thank my supervisors Dr. Gwendolen Reilly and Prof. Sheila MacNeil for providing the opportunity for me to undertake this project, taking me under their care, teaching, continued support, patience and encouragement.

I would like to thank Naresuan University, Thailand for their financial support towards my studies in UK and the University of Sheffield for travel grants from the Learned Society Funding, without which I would not have been able to carry out this project.

I would like to show my appreciation towards many people at the University of Sheffield who have either given me training, advice, and help all they can, especially Robin-Delaine Smith, Mohsen Shaeri, Jennie Robertson, Rossukon Kaewhaw, Pallavi Deshpande, Frazer Bye, Claire Johnson, Sabiniano Roman, Saadi Bin Qasim, Vicki Yeung, Nicola Green, Anthony Bullock, Chris Hill, Helen Colley, Susan Clark, and Leslie A Couton.

I would like to say a big thank you to Assistant Prof. Anuphan Sittichokechaiwut, Naresuan University for suggesting the University of Sheffield for studying in PhD and supporting me by teaching me the cell culture technique in Thailand.

I would like to thank my family and friends for their support and for cheering me up over the course of these four years, without them I would not have been able to reach to this point.

Finally, I would like to thank Gwen once again, you have given me a great opportunity, supportive, be patience, and believing in me from the start. I am really grateful that to have you as my supervisor.

**ACRONYMS**

%	percentage
%BV	percentage bone volume
$\alpha$	alpha
$\beta$	beta
$\mu\text{g}$	microgram
$\mu\text{l}$	microliter
$\mu\text{M}$	micromolar
$\mu\text{m}^2$	square micrometre
2D	two dimensional
3D	three dimensional
AA	ascorbic acid-2-phosphate
Ab	antibody
ABTS	2,2'-Azino-bis(3-ethylbenzothiazoline-6-sulfonic acid)
Ag	antigen
ALP	alkaline phosphatase
ANOVA	analysis of variance
AP-1	activator protein 1
APC	allophycocyanin
ATF4	activating transcription factor 4
FCS	foetal calf serum
bFGF	fibroblast growth factor-basic recombinant human
$\beta$ -GP	$\beta$ -glycerolphosphate
BMP-2	bone morphogenic protein-2
BSA	bovine serum albumin
BV	Brilliant Violet
$\text{Ca}^{2+}$	Calcium
$\text{CaCl}_2$	calcium chloride
CD	cluster of differentiation
CFU-f	fibroblastic colony forming unit
CFS	carboxyfluorescein

## ACRONYMS

CLSM	confocal laser scanning microscopy
cm	centimetre
cm <sup>2</sup>	square centimetre
cm <sup>3</sup>	cubed centimetre
CO <sub>2</sub>	carbon dioxide
COL1	collagen type I
COX-2	cyclooxygenase 2
Ca/P	the mole fraction of calcium phosphate
CTan	CT analyse software
CTvol	CT volume software
DAPI	4',6 diamidino-2-phenylindole
DCM	dichloromethane
DCPD	dibasic calcium phosphate dehydrate (brushite)
Dex	Dexamethasone
dH <sub>2</sub> O	deionised water
DMEM	Dulbecco's Modified Eagle's Medium
DMSO	dimethyl sulphoxide
DNA	deoxyribonucleic acid
dsDNA	double stranded Deoxyribonucleic acid
ECM	extracellular matrix
EDTA	ethylenediaminetetraacetic acid
EDX	Energy-dispersive X-ray spectroscopy
ERK	extracellular signal-regulated kinase
F	fungizone
FACS	fluorescence activated cell sorting
FBS	foetal bovine serum
FDA	Food and Drug Administration
FITC	fluorescein isothiocyanate
FT-IR	Fourier transform infrared spectroscopy
g	gram
GSI	grey scale index

## ACRONYMS

IGF	insulin-like growth factors
IR	infrared
HA	hydroxyapatite
$\mu$ HA	micro-hydroxyapatite particle
nHA	nano-hydroxyapatite particle
HA-PCL	composite hydroxyapatite with electrospun poly( $\epsilon$ -caprolactone) Scaffold
hBMSCs	human mesenchymal stem cells derived from bone marrow
HDFs	human dermal fibroblasts
hESCs	human embryonic stem cells
hESMPs	human embryonic stem cell mesenchymal progenitor cells
HIF-1	hypoxia-inducible factor-1
HMDS	hexamethyldisilazane
HSP	heat shock protein
hUC-MSCs	human umbilical cord mesenchymal stem cells
HV	hydroxyvalerate
IBM	iliac bone marrow
kDa	kilodaltons
l	litre
M	molar
MAPK	mitogen-activated protein kinase
MEM	minimum essential medium
mg	milligram
MG63	human osteosarcoma cells
Micro-CT	micro computed tomography
min	minute
ml	millilitre
MLO-A5	murine lone bone osteocyte A5
mm	millimetre
mM	millimolar
MPa	megapascal

## ACRONYMS

MSCs	mesenchymal stem cells
MTS	(3-(4,5-dimethylthiazol-2-yl)-5-(3-carboxymethoxyphenyl)-2-(4-sulfophenyl)-2H-tetrazolium)
MTT	(3-(4,5-Dimethylthiazol-2-yl)-2,5-diphenyltetrazolium bromide)
N	biological repeat
n	technical repeat
Na <sub>2</sub> HPO <sub>4</sub>	disodium hydrogen phosphate
NaOH	Sodium hydroxide
nm	nanometre
nM	nanomolar
nmol	nanomole
NO	nitrogen oxide
O <sub>2</sub>	oxygen
OBM	orofacial bone marrow
OCN	osteocalcin
OFF	oscillatory fluid flow
ONN	osteonectin
OPG	osteoprotegerin
OPN	osteopontin
OSX	osterix
P/S	penicillin/streptomycin
Pa	Pascal
PAS-FTIR	photoacoustic fourier transform infrared spectroscopy
PBS	phosphate-buffer saline
PDGF	platelet-derived growth factor
PE	phycoerythrin
PerCP	peridinin chlorophyll protein complex
PGE <sub>2</sub>	prostaglandin E-2
pH	potential of hydrogen
PCL	poly (ε-caprolactone)
PH	polyhydroxybutyrate

## ACRONYMS

PHBV	Polyhydroxybutyrate-polyhydroxyvalerate
PI	propidium iodide
Pi	inorganic phosphate
PLA	poly-D-lactic acid
pNP	para-nitrophenol
pNPP	para-Nitrophenylphosphate
PPi	inorganic pyrophosphate
PU	polyurethane
PRP	Platelet-rich-plasma
RANKL	receptor activator of NF-kappa B ligand
RGD	arginine, glycine, and asparagine
RPM	round per minute
RUNX2	runt-related transcription factor 2
ROI	region of interest
SD	standard deviation
SE	standard error of the mean
SEM	scanning electron microscope
SM	supplemented medium consists of AA, $\beta$ -GP in the basic culture medium
SM+Dex10	supplemented medium added with 10nM of Dex
SM+Dex100	supplemented medium added with 100nM of Dex
TCP	tissue culture plastic
TGF- $\beta$	transforming growth factor-beta
TRITC	tetramethyl rhodamine isothiocyanate
v/v%	percentage by volume
VEGF	Vasculo endothelial growth factor
VitaminD	1,25-dihydroxyvitamin D
wt%	percentage by weight
XO	xylene orange
XPS	X-ray photoelectron spectroscopy
XRD	X-ray diffraction

### SUMMARY

The most common craniofacial birth defect is cleft defect with an incidence of 1.7:1000 live births. The current treatments involve many steps of surgical procedures and cause morbidity at the donor site when harvesting bone for filling the gap defect. It may be possible to treat cleft palate defects by tissue engineering strategies using osteoprogenitor cells on a biodegradable distensible electrospun scaffolds to form the hard palate. The aims of this project are to select the suitable cell sources, materials, chemical supplementation, and mechanical conditions to enhance matrix mineralization for repairing the bone part of a cleft palate.

Human jaw periosteal cells (HJPs), human mesenchymal stem cell derived from bone marrow (hBMSCs), and human embryonic stem cell mesenchymal progenitor (hESMPs) used in this project showed osteogenic potential by depositing calcium deposition on both monolayer and 3D constructs with the requirement of Dex in the culture media. Electrospun poly( $\epsilon$ -caprolactone) scaffolds (PCL) are a suitable temporary extracellular matrix for bone tissue engineering. Vascular endothelial growth factor (VEGF) is an important protein for new blood vessel formation. The VEGF secretion was reduced by Dex supplemented culture media in 3D culture, whereas, it was delayed in the monolayer culture. All cell types responded to oscillatory fluid flow (OFF) by using a standard see-saw rocker to stimulate osteogenic differentiation. The cells were more sensitive to OFF when they were supplemented with Dex for enhancing calcium deposition both in monolayer culture and 3D culture and the strongest effect was at the top surface of the scaffolds. The composite nano-hydroxyapatite PCL electrospun scaffold can enhance matrix mineralization compared to the standard PCL scaffold, but there were no additional effects of OFF on these scaffolds. A tri-layer PCL scaffold could support and separate two different cell types (human dermal fibroblasts and human osteoprogenitor cells: both hESMPs and hBMSCs) and also allow

## **SUMMARY**

osteogenic differentiation for 28 days. The novel tri-layer PCL electrospun membrane developed here is a promising scaffold for tissue engineering for cleft palate repair.

Tissue engineering strategy could benefit treatment cleft palate treatment compared to the current treatments (autologous bone graft from iliac crest) to promote bone formation at the defect area and allow normal development of facial structure in the future.

**CONTENTS**

ACKNOWLEDGMENTS.....	2
ACRONYMS.....	3
SUMMARY.....	7
<b>1. CHAPTER ONE: LITERATURE REVIEW.....</b>	<b>22</b>
1.1. Introduction.....	22
1.2. The structure of bone.....	23
1.2.1. Anatomy and function of bones.....	23
1.2.2. Macroscopic anatomy.....	23
1.2.3. Microscopic anatomy.....	25
1.2.4. Bone extracellular matrix component.....	26
1.3. Cell biology of bone.....	27
1.3.1. Osteoprogenitor cells.....	27
1.3.2. Osteoblasts.....	28
1.3.3. Osteocytes.....	28
1.3.4. Osteoclasts.....	29
1.4. Morphology of bone.....	29
1.4.1. Intramembranouse ossification.....	30
1.4.2. Endrochodral ossification.....	32
1.5. Bone healing and remodelling.....	34
1.6. Introduction of cleft palate.....	36
1.6.1. Development of palate.....	36
1.6.2. Incidence and causes of cleft palate.....	38
1.6.3. Current treatment of cleft palate repair.....	38
1.6.4. Controversy for timing of cleft palate repair.....	39
1.7. Tissue engineering for cleft palate/maxillofacial repair.....	41
1.8. Stem cells as an alternative source for bone tissue engineering.....	43
1.8.1. Human embryonic stem cells derived mesenchymal progenitor (hESMPs).....	43
1.8.2. Adult stem cells.....	44
1.8.2.1. Bone marrow mesenchymal stem cells.....	44
1.8.2.2. Human jaw periosteum cells (HJPs) as osteogenic progenitors.....	45
1.9. Scaffold for bone tissue engineering.....	46
1.10. Electrospinning.....	49
1.10.1. Introduction.....	49
1.10.2. Spinning mechanism and theory.....	49
1.10.3. Electrospinning and tissue engineering.....	50

## CONTENTS

1.10.4. Electrospinning rig set up.....	51
1.11. Polymer.....	53
1.11.1. Polyhydroxybutyrate-polyhydroxyvalerate.....	55
1.11.2. Poly( $\epsilon$ -caprolactone).....	56
1.11.3. Polylactic acid (PLA).....	57
1.11.4. Polyurethane.....	58
1.12. Bioactive composite electrospinning scaffold.....	58
1.13. Vascular endothelial growth factor (VEGF).....	60
1.14. Mechanical force.....	61
1.14.1. Introduction.....	61
1.14.2. Mechanical regulation of bone cells.....	61
1.15. Methods of mechanical stimulation.....	64
1.15.1. Introduction.....	64
1.15.2. Compression.....	64
1.15.3. Tension.....	66
1.15.4. Fluid flow-induced shear stress.....	67
1.16. Mechanical stimulation of osteoprogenitor cells on 3D culture.....	69
1.17. Mechanical stimulation of MSCs.....	70
1.18. Mechanotransduction.....	71
1.19. Aims and objectives of research project.....	74
<b>2. CHAPTER TWO: MATERIALS AND METHODS.....</b>	<b>76</b>
2.1. Materials.....	76
2.2. Methods.....	81
2.2.1. General cell culture conditions.....	81
2.2.2. Human dermal fibroblasts (HDFs).....	82
2.2.3. Human jaw periosteal cells (HJPs).....	83
2.2.4. Human mesenchymal stem cells from bone marrows (hBMSCs).....	84
2.2.5. Cell characterization (Flow cytometry).....	85
2.2.6. Cell culture in monolayer.....	88
2.2.7. Electrospinning rig set up.....	88
2.2.8. Physical characterization.....	89
2.2.9. Hydroxyapatite characterization.....	92
2.2.10. Scaffold preparation.....	94
2.2.11. Cell seeding for 3D culture.....	97
2.2.12. Assessment cell viability and cell number.....	98
2.2.13. Analysis of cell-deposited collagen using picro-sirius red staining.....	102
2.2.14. Assessment of osteogenesis.....	102

## CONTENTS

2.2.15. Fluorescent staining of cell nucleus and cytoskeleton.....	106
2.2.16. Mechanical loading of cells.....	108
2.2.17. Assessment of VEGF secretion using ELISA.....	109
2.2.18. Statistical analysis.....	110
<b>3. CHAPTER THREE: CELLS CHARACTERISATION AND EVALUATE THE SUITABLE OF CULTURE MEDIUM FOR OSTEOGENIC INDUCTION ON MONOLAYER CULTURED hESMPs AND HJPs.....</b>	<b>112</b>
3.1. Introduction.....	112
3.2. The effect of ascorbic acid-2-phosphate (AA) on collagen production of human dermal fibroblasts (HDFs).....	115
3.3. Osteoprogenitor cells characterization.....	117
3.4. Osteogenic differentiation of hESMPs in a monolayer culture.....	119
3.5. Comparisons of different culture media on the stimulation of human jaw periosteal cells (HJPs).....	123
3.6. The effect of varying concentrations of Dex on osteogenic differentiation of a monolayer cultured HJPs.....	126
3.7. Discussion.....	130
3.8. Summary of results.....	136
3.9. Future work.....	137
<b>4. CHAPTER FOUR: THE EFFECT OF A SIMPLE FLUID SHEAR STRESS STIMULUS OF OSTEOGENIC PROGENITOR MATRIX PRODUCTION.....</b>	<b>138</b>
4.1. Introduction.....	138
4.2. Methods.....	139
4.2.1. Cell culture.....	139
4.2.2. OFF application.....	140
4.3. The effect of oscillatory fluid flow (OFF) on osteogenic differentiation of hESMPs on monolayer culture.....	142
4.4. The effect of oscillatory fluid flow (OFF) on osteogenic differentiation of hBMSCs on monolayer culture.....	148
4.5. The effect of oscillatory fluid flow (OFF) on osteogenic differentiation of HJPs on monolayer culture.....	152

## CONTENTS

4.6. The effect of temperature on osteogenic differentiation of hESMPs compared between room temperature and physical cell culture temperature of 37°C and CO <sub>2</sub> on monolayer.....	158
4.7. The effect of temperature on osteogenic differentiation of HJPs compared between room temperature and physical cell culture temperature of 37°C and CO <sub>2</sub> on monolayer.....	163
4.8. Discussion.....	167
4.9. Conclusion.....	174
4.10. Summary.....	175
<b>5. CHAPTER FIVE: THE EFFECT OF OSCILLATORY FLUID FLOW AND NANOHYDROXYAPATITE ELECTROSPUN SCAFFOLD TO ENHANCE OSTEOGENIC DIFFERENTIATION OF OSTEOGENIC PROGENITOR CELLS.....</b>	<b>177</b>
5.1. Introduction.....	177
5.2. Fabrication and characterization of poly-D-lactide (PLA), polycaprolactone (PCL), and polyhydroxybutyrate-co-polyhydroxyvalerate (PHBV) electrospun scaffolds.....	179
5.3. Optimizing cell seeding methods on scaffolds.....	183
5.4. To evaluate cell viability on selected electrospun scaffolds (PLA, PCL, and PHBV) for hESMPs.....	186
5.5. To compare osteogenic differentiation of HJPs cultured on PCL and PLA scaffolds.....	188
5.6. Osteogenic differentiation of hESMPs on PCL scaffold.....	192
5.7. To evaluate the effect of oscillatory fluid flow (OFF) on hESMPs cultured on PCL electrospun scaffold.....	194
5.8. To evaluate the effect of oscillatory fluid flow (OFF) on human mesenchymal stem cells from bone marrow (hBMSCs) cultured on PCL electrospun scaffolds.....	198
5.9. To incorporate nano-hydroxyapatite (nHA) with PCL electrospun scaffolds for bone tissue engineering.....	202
5.10. To select an appropriate concentration of HA-PCL electrospun scaffold for enhancing osteogenic differentiation of hESMPs.....	209
5.11. To evaluate the effect of oscillatory fluid shear stress and HA-PCL electrospun scaffold for enhancing osteogenic differentiation of hESMPs.....	220
5.12. Discussion.....	233
5.13. Conclusion.....	245
5.14. Summary.....	245

5.15. Future work.....	246
<b>6. A TRI-LAYER POLYCAPROLACTONE MEMBRANE FOR CO-CULTURE OF FIBROBLASTS AND OSTEOGENIC PRECURSORS FOR CLEFT PALATE REPAIR.....</b>	<b>248</b>
6.1. Introduction.....	248
6.2. Methods.....	249
6.3. Results.....	252
6.4. Discussion.....	257
6.5. Conclusion.....	259
6.6. Summary.....	260
6.7. Future works.....	260
<b>7. CHAPTER SEVEN: CONCLUSION AND FUTURE DIRECTIONS.....</b>	<b>261</b>
7.1. Human mesenchymal progenitor/stem cells.....	261
7.2. 3D model for bone tissue engineering.....	262
7.3. External mechanical force.....	263
7.4. Tri-layer membrane scaffold.....	265
7.5. Clinical application of maxillofacial reconstruction.....	266
7.6. Final conclusions.....	268
8. APPENDIX 1.....	269
9. REFERENCES.....	271

**LIST OF FIGURES**

Figure 1.2.2 : The macroscopic anatomy of bone.....	24
Figure 1.2.3 : The microscopic anatomy of bone.....	26
Figure 1.3.1 : Phase contrast images of hESMPs.....	27
Figure 1.3.2 : Transverse section of a trabecular bone.....	29
Figure 1.4.1 : Histology images of intramembranous ossification.....	31
Figure 1.4.2 : Schematic showing endochondral ossification.....	33
Figure 1.6.1 : Schematic showing normal development stages of lip and palate.....	37
Figure 1.6.3 : Diagrams showing the complications of cleft palate post-operation.....	39
Figure 1.6.4 : Schematic showing the variety of cleft lip and/or palate.....	41
Figure 1.7 : Concept of tissue engineering.....	42
Figure 1.10.4 : Schematic of electrospinning apparatus.....	51
Figure 1.11.1 : Chemical formula of PHBV.....	56

## CONTENTS

Figure 1.11.2	: Chemical formula of PCL.....	56
Figure 1.11.3	: Chemical formula of PLA.....	57
Figure 1.14.2	: Schematic showing the anatomical area of osteocytes and osteoprogenitor cells.....	63
Figure 1.15.2	: Schematic of typical compression loading patterns.....	65
Figure 1.15.3	: Schematic of typical tension loading patterns.....	67
Figure 1.15.4	: Schematic of fluid flow-induced shear stress.....	69
Figure 1.18	: Schematic summarizing the mechanotransduction of MSCs.....	73
Figure 2.2.3	: Phase contrast images of HJPs.....	84
Figure 2.2.4	: Phase contrast images of hBMSCs.....	85
Figure 2.2.8	: The typical stress-strain curve of semi-crystalline polymer.....	92
Figure 2.2.10.1:	Electrospun PCL scaffolds were cut into ecliptic shapes.....	96
Figure 2.2.10.2:	Electrospun PCL scaffolds were inserted into the CellCrown™.....	96
Figure 2.10.11	: Schematic of cell seeding methods.....	97
Figure 2.2.12.1:	Schematic presentation of MTT.....	98
Figure 2.2.12.2:	Schematic presentation of MTS.....	99
Figure 2.2.12.3:	Schematic presentation of resazurin to resorufin.....	100
Figure 2.2.12.4:	Linear quantitation using the PicoGreen® reagent.....	101
Figure 2.2.16	: Standard see-saw rocker for stimulating fluid flow.....	109
Figure 3.2.1	: Effect of varying concentration of AA on cell viability and collagen production for HDFs on monolayer at days 7, 14, and 21...	116
Figure 3.3.1	: Immunophenotypic analysing of hESMPs.....	118
Figure 3.4.1	: Morphology of hESMPs under different concentration of Dex after day14.....	120
Figure 3.4.2	: Effect of varying concentration of Dex on DNA quantification, ALP activity, and VEGF secretion (during a 48 hour collection period) for hESMPs on monolayer at days 7, 14, and 21.....	121
Figure 3.4.3	: Effect of varying concentration of Dex on calcium deposition and collagen production for hESMPs on monolayer and their stained images after day 21.....	122
Figure 3.5.1	: Effect of different culture media condition for cell viability on HJPs at days 1, 4, and 7.....	124
Figure 3.5.2	: Comparison of the effect of basic culture media $\alpha$ -MEM and DMEM and cell viability between HJPs-1 and HJPs-2 at days 1, 4, and 7.....	125
Figure 3.6.1	: Morphology of HJPs under varying concentration of Dex after day 7.....	127

## CONTENTS

Figure 3.6.2	: Effect of varying concentration of Dex on DNA quantification and ALP activity for HJPs-1 (at days 7, 14, 21, and 28) and HJPs-2 (at days 7, 14, and 21) on monolayer.....	128
Figure 3.6.3	: Effect of varying concentration of Dex on calcium deposition and collagen production for HJPs on monolayer and their stained images after day 21.....	129
Figure 4.2.1	: The calculated oscillatory fluid flow (OFF) profiles experienced at the surface of circular 6-well plate for three different locations.....	141
Figure 4.3.1	: Morphology of hESMPs under different concentration of Dex after exposure to OFF on a standard rocking platform and static culture for 7 days.....	144
Figure 4.3.2	: Effect of OFF on DNA quantification and ALP activity for hESMPs on monolayer under different concentration of Dex at days 7, 14, and 21.....	145
Figure 4.3.3	: Effect of OFF on VEGF secretion (during a 48 hour collection period) for hESMPs on monolayer under different concentration of Dex at days 7, 14, and 21.....	146
Figure 4.3.4	: Effect of OFF on calcium deposition and collagen production for hESMPs on monolayer under different concentration of Dex and their stained images after day 21.....	147
Figure 4.4.1	: Morphology of hBMSCs under different concentration of Dex after exposure to OFF on a standard rocking platform and static culture for 7 days.....	149
Figure 4.4.2	: Effect of OFF on DNA quantification, ALP activity, and VEGF secretion (during a 48 hour collection period) for hBMSCs on monolayer under different concentration of Dex at days 7, 14, and 21.....	150
Figure 4.4.3	: Effect of OFF on calcium deposition and collagen production for hBMSCs on monolayer under different concentration of Dex and their stained images after day 21.....	151
Figure 4.5.1	: Effect of OFF on DNA quantification and ALP activity for HJPs-1 on monolayer under different concentration of Dex at days 7, 14, and 21.....	153
Figure 4.5.2	: The effect of OFF on calcium deposition and collagen production for HJPs-1 on monolayer under different concentration of Dex and their stained images after day 21.....	154

## CONTENTS

Figure 4.5.3	: Effect of OFF on DNA quantification and ALP activity for HJPs-2 on monolayer under different concentration of Dex at days 7, 14, and 21.....	156
Figure 4.5.4	: Effect of OFF on calcium deposition and collagen production for HJPs-2 on monolayer under different concentration of Dex and their stained images after day 21.....	157
Figure 4.6.1	: Morphology of hESMPs under different concentration of Dex after expose in room temperature, 0.04% CO <sub>2</sub> and culture incubator at 37°C, 5% CO <sub>2</sub> after 7 days.....	160
Figure 4.6.2	: Effect of temperature and CO <sub>2</sub> on DNA quantification, ALP activity, and VEGF secretion (during a 48 hour collection period) for hESMPs on monolayer under different concentration of Dex normalized to the static incubator group at days 7, 14, and 21.....	161
Figure 4.6.3	: Effect of temperature and CO <sub>2</sub> on calcium deposition and collagen production for hESMPs on monolayer under different concentration of Dex normalized to the static incubator group after day 21.....	162
Figure 4.7.1	: Effect of temperature and CO <sub>2</sub> on DNA quantification and ALP activity for HJPs-1 and HJPs-2 on monolayer under different concentration of Dex normalized to the static incubator group at days 7, 14, and 21.....	164
Figure 4.7.2	: Effect of temperature and CO <sub>2</sub> on calcium deposition for HJPs-1 and HJPs-2 on monolayer under different concentration of Dex normalized to the static incubator group after day 21.....	165
Figure 4.7.3	: Effect of temperature and CO <sub>2</sub> on collagen production for HJPs-1 and HJPs-2 on monolayer under different concentration of Dex normalized to the static incubator group after day 21.....	166
Figure 5.2.1	: Schematic of fibre diameter measuring form SEM images.....	180
Figure 5.2.2	: Morphology, distributions and means of fibre diameters, and porosity of electrospun PLA, PCL, and PHBV scaffolds.....	182
Figure 5.3.1	: Schematic of cell seeding methods.....	184
Figure 5.3.2	: Cell viability of hESMPs on different cell seeding methods at days 3, 5, and 7 and their Live/Dead staining images.....	185
Figure 5.4.2	: The ability of different electrospun scaffolds (PCL, PLA, and PHBV) on cell viability of hESMPs at days 1 and 7.....	187
Figure 5.5.2	: The ability of different electrospun scaffolds (PCL and PLA) on cell attachment of HJPs-1 and HJPs-2 after 1 day.....	189

Figure 5.5.3 : The ability of different electrospun scaffolds (PCL and PLA) on cell viability of HJPs-1 and HJPs-2 at days 7, 14, 21, and 28.....190

Figure 5.5.4 : The ability of different electrospun scaffolds (PCL and PLA) on calcium deposition of HJPs-1 and HJPs-2 after 28 days.....191

Figure 5.6.2 : The ability of electrospun PCL scaffold on cell viability at days 7, 14, 21, and 28, and calcium deposition, collagen production of hESMPs after 28 days.....193

Figure 5.7.2 : Effect of OFF on cell viability of hESMPs seeded PCL scaffolds at days 7, 14, 21, and 28.....195

Figure 5.7.3 : Effect of OFF on calcium deposition and collagen production of hESMPs seeded PCL scaffolds after 28 days.....196

Figure 5.7.4 : Effect of OFF on VEGF secretion of hESMPs seeded PCL scaffolds at days 7, 14, 21, and 28 (during a 48 hour collection period).....197

Figure 5.8.2 : Effect of OFF on cell viability of hBMSCs seeded PCL scaffolds at days 7, 14, 21, and 28.....199

Figure 5.8.3 : Effect of OFF on calcium deposition and collagen production of hBMSCs seeded PCL scaffolds after 28 days.....200

Figure 5.8.4 : Effect of OFF on VEGF secretion of hBMSCs seeded PCL scaffolds at days 7, 14, 21, and 28 (during a 48 hour collection period).....201

Figure 5.9.1 : Schematic of fabrication process for incorporated nano-hydroxyapatite PCL (HA-PCL) electrospun scaffolds.....203

Figure 5.9.2 : XPS survey spectrum of the HA-PCL from alternative soaking process.....206

Figure 5.9.3 : XRD pattern of the different HA-PCL fabrication technique.....207

Figure 5.9.4 : The ability of different HA-PCL fabrication scaffolds on cell viability of hESMPs at days 1, 4, and 7.....207

Figure 5.9.5 : The ability of different HA-PCL fabrication scaffolds on ALP activity of hESMPs after 7 days.....208

Figure 5.10.2 : Morphology and distribution of diameter of various percentages of HA-PCL fibres.....213

Figure 5.10.3 : Young's modulus, yield strength, and percentage porosity of various percentage of HA-PCL electrospun scaffold.....214

Figure 5.10.4 : Stress/strain curve of the various percentages of HA-PCL electrospun scaffolds.....215

Figure 5.10.5 : Photoacoustic amplitude spectra of the various percentages of HA-PCL electrospun scaffolds.....216

Figure 5.10.6 : XRD pattern of the various percentages of HA-PCL electrospun scaffolds.....217

## CONTENTS

Figure 5.10.7 : Effect of the various percentages of HA-PCL electrospun scaffolds on cell attachment of hESMPs after 1 day.....	217
Figure 5.10.8 : Effect of the various percentages of HA-PCL electrospun scaffolds on cell viability of hESMPs at days 1, 4, 7, 10, and 14.....	218
Figure 5.10.9 : Effect of the various percentages of HA-PCL electrospun scaffolds on ALP activity of hESMPs at days 7 and 14.....	219
Figure 5.11.1 : Schematic of sectioning of the electrospun scaffold for measuring mineralized deposition by using micro-CT.....	221
Figure 5.11.2 : A window form CTanalyze software for determining the threshold ranges of the standard PCL scaffold, mineralized deposition, and HA-PCL scaffold.....	222
Figure 5.11.3 : The grey scale distribution and threshold range table of the standard PCL scaffold, mineralized deposition, and HA-PCL scaffold....	225
Figure 5.11.4 : The ability of standard PCL and HA-PCL scaffolds on cell attachment after day 1 and effect of OFF on cell viability of hESMPs at days 7, 14, 21, and 28.....	226
Figure 5.11.5 : The ability of standard PCL and HA-PCL scaffolds and effect of OFF on VEGF secretion (a 48 hour collection period) of hESMPs at days 7, 14, 21, and 28.....	227
Figure 5.11.6 : Effect of OFF on mineralized deposition of hESMPs seeded on the standard PCL scaffolds after 28 days and their micro-CT images.....	228
Figure 5.11.7 : Effect of OFF on mineralized deposition of hESMPs seeded on the HA-PCL scaffolds after 28 days and their micro-CT images.....	229
Figure 5.11.8 : The ability of standard PCL and HA-PCL scaffolds and effect of OFF on total mineralized deposition of hESMPs after 28 days.....	230
Figure 5.11.9 : SEM images of the hESMPs seeded on the standard PCL scaffolds and exposed to OFF after 28 days.....	231
Figure 5.11.10: SEM images of the hESMPs seeded on the HA-PCL scaffolds and exposed to OFF after 28 days.....	232
Figure 6.3.1 : Effect of AA on cell viability and collagen production of HDFs seeded on the standard PCL scaffolds at days 14 and 21.....	252
Figure 6.3.2 : Morphology of tri-layer electrospun PCL scaffold and distribution of diameter fibre in different level.....	254
Figure 6.3.3 : Morphology of the co-culture hESMPs/HDFs and hBMSCs/HDFs on tri-layer PCL scaffold after 28 days in the osteoprogenitor cells side, after 7 days in the HDFs side, and side view of co-culture.....	255

Figure 6.3.4 : Confocal laser scanning microscopy fluorescence images of the side views of the co-culture hESMPs/HDFs and hBMSCs/HDFs on tri-layer PCL scaffold after 28 days.....256

**LIST OF TABLES**

Table 1.10.4 : Factors influence the morphology of an electrospun scaffold.....53

Table 1.11 : Advantages and disadvantages of natural and synthetic polymer used in bone tissue engineering.....54

Table 2.2.1: Complete list of culture conditions on both monolayer and 3D cultures.....82

Table 2.2.5 A : Complete list of components and experiment parameters for MSCs characterization in all cell types.....87

Table 2.2.5 B : Complete list of components and experiment parameters for Compbead™ characterization.....88

Table 2.2.11: Complete list of seeding cell densities on both monolayer and 3D cultures.....98

Table 3.3 : Information of the human mononuclear cells from different donors.....117

Table 3.3.1 : Surface antigen expression patterns of hESMPs, HJPs, and hBMSCs.....119

Table 5.9.2 : Complete list of XPS results: chemical components, spectral line, binding energy, and atomic percentage of the HA-PCL from alternate soaking process.....206

Table 5.10.1 : Complete list of components and experiment parameters for electrospinning of the standard PCL and HA-PCL scaffolds.....209

Table 5.10.2: Physical and mechanical properties of various percentage of HA-PCL electrospun scaffold.....215

## CONTENTS

Table 5.10.3: Observed infrared band position from the nHA particles and various percentage of HA-PCL electrospun scaffold.....	217
--	-----

### CHAPTER ONE: LITERATURE REVIEW

#### 1.1 Introduction

Cleft lip and/or cleft palate is a very common birth defect with an worldwide incidence of about 1.7 per 1000 live births (Mossey et al., 2009). Causes of the defect are suspected to include 1] environmental factors such as maternal disease, alcohol intake, excess anticonvulsant or exposed retinoic acid medication, 2] genetic factors. These affect early embryonic development during the fourth to tenth weeks of gestation (Stanier and Moore, 2004). Cleft defect is a non-life-threatening abnormality but may have significant effects on feeding, speaking, hearing, cause teeth and jaw problems, and social anxiety. Current treatments should be managed by a multidisciplinary team such as plastic surgeons, maxillofacial surgeons and dentists. These specialists would support and provide multiple surgical steps over the treatment course of many years (from the child is birth up to 20 years old). Where there is a bone defect the treatment is likely to include bone harvesting from a donor site. The post-operative complications from bone harvesting are 1] a high risk of donor site morbidity, 2] a temporary numbness of the leg from lateral femoral cutaneous paresthesia, 3] gait disturbances. Studies by Bergland et al., (1986) and Samee et al., (2008) stated that bone harvesting provided limited amount of bone available for grafting. Alternative cell sources for bone augmentation should be investigated further to improve cleft palate repair. Recently, tissue engineering strategies showed much promise for repairing a cleft defect on the alveolar ridge area, which supports the teeth. However, the cleft in the hard palate cleft was filled with soft tissue. Scar formation in the gap remaining in the hard palate is likely to affect facial development (Smahel et al., 2009).

This project will mainly focus on a tissue engineering approach for the bone part of the hard palate repair by investigating 1] selected cell sources, 2] a suitable condition for stimulating mineralized matrix formation by bone-like cells, and 3] scaffold materials. The current review of the literature will describe the basic principles of bone biology,

the development of cleft palate, current treatments of cleft palate, and bone tissue engineering as a clinical strategy.

### **1.2 The structure of bone**

#### **1.2.1 Anatomy and function of bones**

Bone is a rigid part of the body and serves many functions for movement, supporting the body structure, protecting internal organs, maintain mineral homeostasis. It stores growth factors, cytokines, and red bone marrow is which where red blood cells are produced. The adult human has a total of 206 bones. Bone is comprised of two structures: compact (or cortical) bone and cancellous (or trabecular) bone. The compact bone is a dense bone, its porosity is less than 5% (Clarke, 2008) and represents about 80 percent of adult bone. The cancellous bone has porous structure resembling sponge with strut thicknesses of around 50-400 $\mu$ m (Seeley et al., 2008) and represents about 20 percent of adult bone (Roger, 2011). It is located at some internal regions of bone and filled with bone marrow.

#### **1.2.2 Macroscopic anatomy**

Bones are organized into different shapes depending on their functions. The four categories of bone shapes are long bones, short bones, flat bones and irregular bones. Long bones include arm and leg bones. Short bones include the small bone in the ankles and wrists. Flat bones include the skull bones, mandible (jaw), hard palate, and the ribs (Figure. 1.2.2 A). Irregular bones include the vertebrae, sacrum and coccyx. The long bone length is longer than their width (Figure. 1.2.2 C). They include diaphysis (a hollow shaft), metaphysis (flared and cone shape), and epiphysis (at each end of the bone, and covered by articular cartilage). The primary diaphysis composition is cortical bone, whereas the metaphysis and epiphysis are trabecular bone. Flat bones have a broad surface to provide extensive protection and muscular attachment such as the

cranium of the skull, or mandible. They are composed of two layers of thin compact bone surrounding trabecular bone (Figure. 1.2.2 B).

Bone is tightly covered by periosteal membrane at the outer surface apart from where there is articular cartilage. The inner surface of cortical bone and trabecular bone are covered by endosteal membrane which contacts the bone marrow. Periosteal activity is important for bone apposition on the outer surface of bone while endosteal activity is for bone resorption and formation on the inner surface.

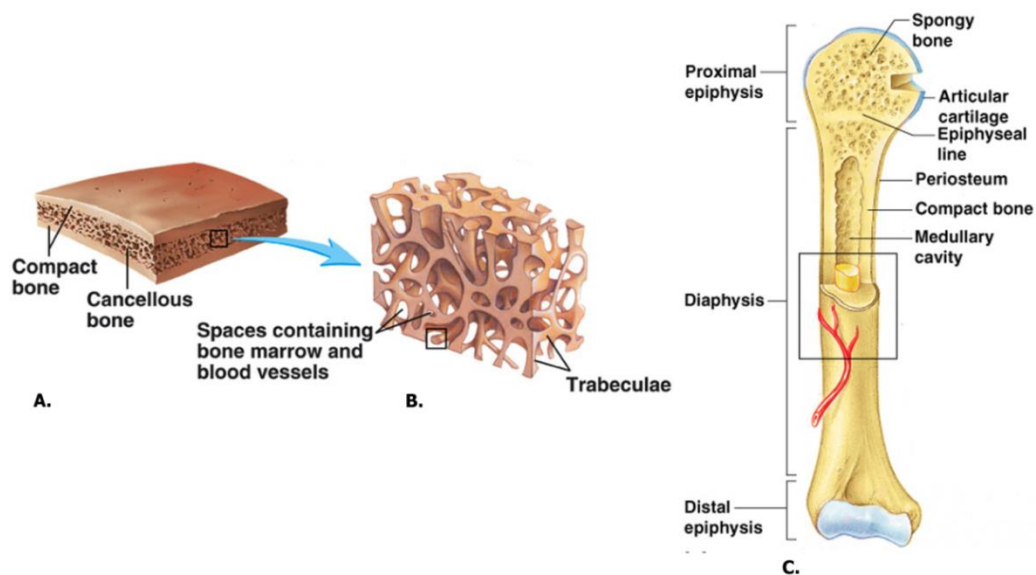


**Figure 1.2.2:** The diagram shows a flat bone which consist of 2 layers of compact bone and a cancellous bone (B) in between, like a sandwich. (C) The structure of long bone consists of diaphysis which has compact bone surrounding the hollow at the inner side and the epiphysis which locates at the end of the bone. Reprinted from Seeley et al., (2008) with kind permission of McGRAW-HILL.

### 1.2.3. Microscopic anatomy

At the microscopic level, bone is divided to two types, woven and lamellar bone, depending on the orientation of collagen type 1, which is the main component of bone matrix. Woven bone is an immature bone which has an irregular collagen fibre orientation. It has more mature bone cells per unit of volume, high turnover rate, and is more flexible but weaker than lamellar bone (Clarke, 2008). Lamellar bone is the dense organised bone which is created by remodelling of the woven bone. In humans, lamellar bone starts remodelling 1 month after birth. Most bone structures become lamellar bone by 4 years of age. Lamellar bone is composed of highly organized collagen fibres, aligned parallel within the same layer (lamellae) (Figure. 1.2.3 B). In humans the lamellae arrangement process leads to the formation of osteons surrounding a Haversian canal which contains blood vessels, nerves, and lymph vessels at the center to form a secondary osteon. Each Haversian canal interconnects with another canal by a Volkmann's canal. The mature bone cells occupy the small cavities, called lacunae which are located between lamellae. The lacunae have a connecting system to other lacunae for transferring nutrients which are called canaliculi. The osteon or Haversian system is a major structural unit which aligns parallel to the long axis of bone to provide strength. Cortical bone is created by many osteons, which combine with interstitial lamellae (the lamellae between osteons) and circumferential lamellae (the lamellae underlying periosteum and endosteum) (Doll, 2005). Osteons are the main component of both cortical and trabecular bone (Clarke, 2008). However, the trabecular bone's osteon does not have blood vessels at the center (Figure. 1.2.3A) (Seeley et al., 2008).

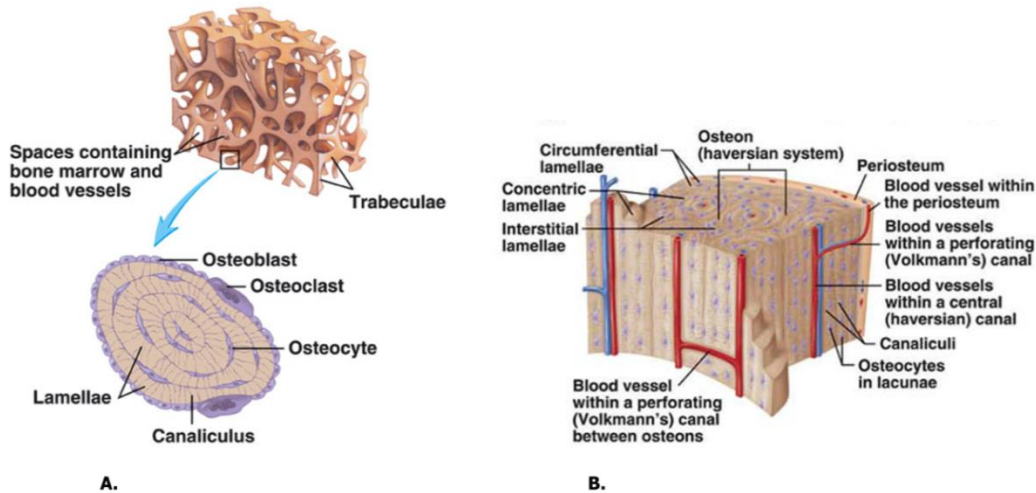


**Figure 1.2.3:** (A) The transverse section of trabecular bone shows the osteonal structure. (B) The osteon structure of compact bone. Reprinted from Seeley et al., (2008) with kind permission of McGRAW-HILL

#### 1.2.4. Bone ECM composition

Bone ECM is composed of inorganic component (about 60% of total bone ECM) organic matrix (up to 40% of total bone ECM) and trace amounts of water and lipids. The composition of the inorganic components is a mostly hydroxyapatite with small amounts of magnesium and carbonate to provide the mechanical compressive strength to bone. The organic matrix comprises protein and proteoglycans. Bone proteins can be divided into collagenous proteins (about 90%) which are mostly type I collagen and trace amounts of type III and V, which provide tensile strength to bone. The other bone protein components are non-collagenous proteins (about 10%) which are composed of proteoglycans, matrix proteins, cytokines, and growth factors. The proteoglycans regulate collagen fibre formation in the bone matrix. Three of the major proteoglycans are: osteocalcin (OCN), osteonectin (ONN), and osteopontin (OPN). The roles of bone matrix are to regulate bone cell activity, bone mineral deposition and resorption. There are cytokines and growth factors present in bone matrix such as TGF- $\beta$ , BMPs, and VEGF.

Their role is to contribute to bone cell proliferation, activation, and bone remodelling (Lamoureux et al., 2007, Clarke, 2008, Salbach et al., 2012).

### 1.3 Cell biology of bone

Bone contains of many cell types for maintaining stability. These are osteoprogenitor cells, osteoblasts (matrix-producing cells), osteocytes (matrix-maintaining cells), and osteoclasts (matrix-resorbing cells). Each cell has its own definite roles and functions.

#### 1.3.1 Osteoprogenitor cells

Osteoprogenitor cells or mesenchymal stem cells (MSCs) are fibroblast-like fusiform shaped, undifferentiated cells (Figure. 1.3.1). They give rise to the osteoblasts which produce new bone matrix. Bone marrow stroma contain a small population of MSCs that are capable of differentiation into either bone, cartilage, fat, or fibrous connective tissue depending on the circumstances. MSCs are promising cells for bone tissue engineering due to their ability to proliferate and differentiate into osteogenic cells.

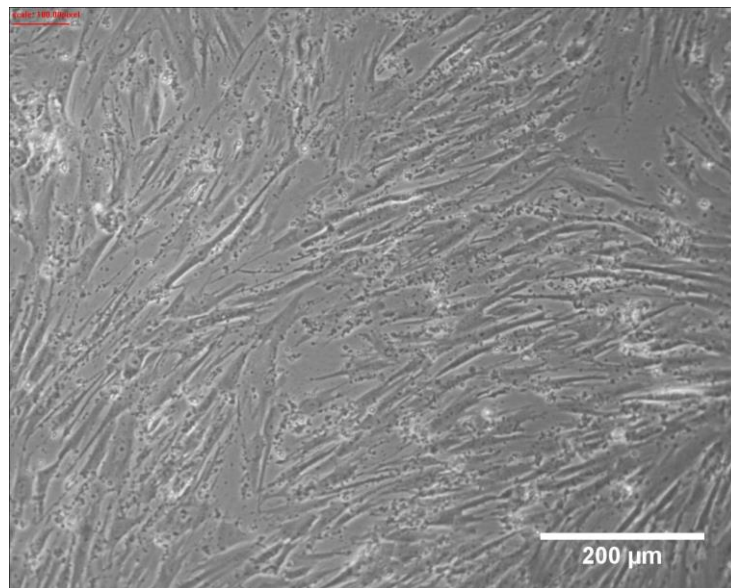


**Figure 1.3.1:** Phase contrast image of an osteoprogenitor cell (hESMPs). Scale bar 200μm. Image captured by author.

### 1.3.2 Osteoblasts

Osteoblasts are anchorage dependent cells which require an attachment to a surface to grow and survive. They are large cuboidal cells and usually located on the bone matrix surface, they rely on a cell-matrix and a cell-cell communication via specific receptors for signalling factors such as cytokines, hormones, and growth factors to maintain the cellular function. Moreover it has been found that the osteoblasts respond to mechanical stimuli (Sommerfeldt and Rubin, 2001). Osteoblasts synthesize and lay down collagen type I that is required for new bone formation. From *in vivo* studies it is known that osteoblasts can lay down 0.5-1.5 $\mu$ m of the non-mineralized organic part of bone matrix (called osteoid) per day (Sommerfeldt and Rubin, 2001). They also secrete non-collagenous proteins such as proteoglycans and glycosylated proteins. The glycosylated proteins, for example, alkaline phosphatase (early marker of osteoblasts: see chapter 2), regulate the mineralization process (Clarke, 2008), proteins bound to the cell surface and may help regulate matrix mineralization. Osteoblasts that become fully embedded in mineralized matrix transform their role to become osteocytes.

### 1.3.3 Osteocytes

Osteocytes are the terminally differentiated cells of the osteogenic lineage. Their shapes are smaller than osteoblasts and they have a number of cytoplasmic extensions. They lie within the lacunae in mineralized bone to support bone structure and metabolism. Osteocytes do not normally secrete alkaline phosphatase (an early marker of osteogenic differentiation) but express several other bone matrix proteins (Clarke, 2008). The functions of osteocytes are; facilitated intercellular adhesion and mineral exchange regulation in the bone fluid within lacunae. Osteocytes can communicate with adjacent cells via gap junctions of their cytoplasmic extensions in the canaliculi. Osteocytes can survive in the lacunae for decades. In contrast empty spaces in the lacunae can be

presented in an aging bone due to apoptosis of the cells or disturbance of cellular interactions (Verborgt et al., 2000).

### 1.3.4 Osteoclasts

Osteoclasts derive from hematopoietic stem cells (the cells that give that rise to blood cells) which are usually located within endosteal or periosteal surfaces. Osteoclasts are multinucleated cells from the fused monocyte progenitor cells, which contain around 6-12 nuclei, with a ruffled border on the cell periphery. Their function is bone resorption,

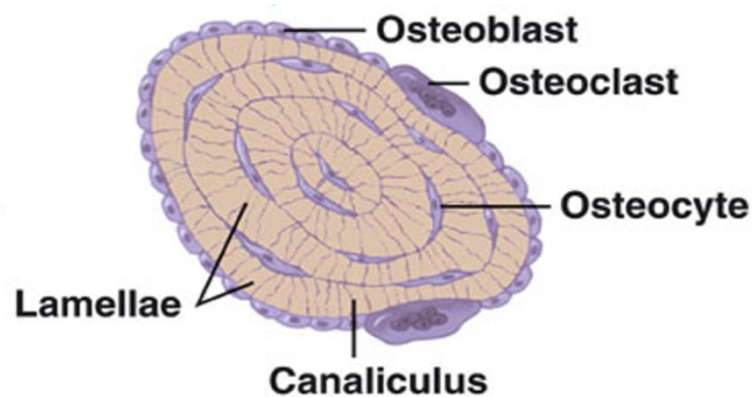


*Figure 1.3.2: Transverse section of a trabecula bone showing the three major bone cells which affect bone remodelling; osteoblasts, osteocytes and osteoclasts.*

*Reprinted from Seeley et al., (2008) with kind permission of McGRAW-HILL.*

which is the first step in the bone remodelling process. They secrete enzymes in lysosomes to increase the solubility of hydroxyapatite. Osteoclasts can resorb bone volume around  $200,000\mu\text{m}^3/7\text{days}$ , *in vitro* (Jeon et al., 2012).

### 1.4. Morphogenesis of bone

Bone is a rigid part of body and serves many functions, for instance, motion, supporting the body structure and protecting internal organs. Bone formation starts during the fetal period in gestation and has two modes, which are intramembranous and endochondral ossification.

### 1.4.1. Intramembranous ossification

This category of ossification takes place during embryonic development. Mostly it is responsible for formation of flat bones which are usually present in the craniofacial bones such as cranium, mandible and palate. Intramembranous ossification begins with MSCs which directly differentiate into mature osteoblasts. These osteoblasts can produce bone matrix that is mineralized within a few days. Osteoblasts that remain embedded in bone matrix then become osteocytes. As the result, many small trabecular of woven bone are created (Figure. 1.4.1 A). The network of trabeculae combines together to form trabecular bone (spongy bone). Some osteoblasts still locate at the surrounding surface of trabeculae to produce more or thicker trabeculae (Figure. 1.4.1 B). Finally the woven bone is replaced by the remodelling process with mature lamellar bone (blue staining in the Figure. 1.4.1 C) that is more organized and stronger than the woven bone. The cells within the trabecular bone space form red bone marrow and the cells surrounding the developing bone form periosteum. The osteoblasts from periosteum can continue to create bone matrix and develop into compact bone.

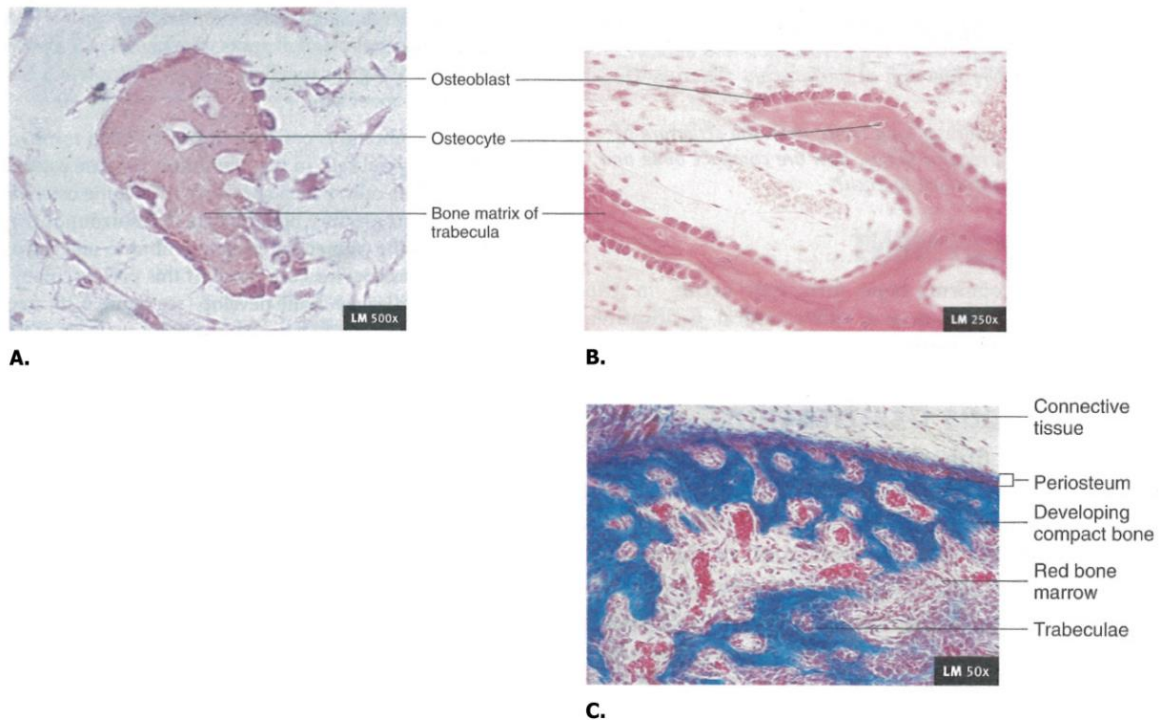


**Figure 1.4.1:** Intramembranous ossification: the 12<sup>th</sup> week of fetus, Paraffin section. (A) Osteoblasts at the outer surface create bone matrix and differentiate into osteocytes when they embed in the bone matrix. (B) Interconnection of many trabeculae forms cancellous bone. (C) The trabecular bone (blue colour) is in the centre and the spaces contain red bone marrow. Under the periosteum is developing compact bone. Reprint from Seeley et al., (2008) with kind permission of McGRAW-HILL.

### 1.4.2. Endochondral ossification

The second ossification mechanism of the mammalian skeletal system is endochondral ossification. Endochondral ossification is bone production that begins with the differentiation of MSCs (osteochondral progenitor cells) into cartilage cells (chondroblasts), which produce cartilage. Overtime the chondrocytes are less able to receive nutrients and they start to apoptose, then vasculature grows into the centre of the bone template. Perichondrium (the membrane at the outer part of cartilage) on the diaphysis becomes periosteum and osteochondral progenitor cells become osteoblasts. The outer side of the diaphysis area is covered by osteoblasts that produce bone which is called the bone collar (Figure. 1.4.2 A). The primary ossification center forms by bringing osteoblasts from the blood vessels which have penetrated into the medullary cavity. The osteoblasts begin to lay down bone matrix at the primary ossification center (Figure. 1.4.2 B). Secondary bone ossification centers form at the epiphysis regions. The cartilaginous framework on both sides of the ossification centers are replaced by woven bone, via a remodelling process into the lamellar bone (Figure. 1.4.2 C). The results of endochondral ossification are growth in two directions either height or width from the center of the long bone. Only articular cartilage remains at the joint ends (Figure. 1.4.2 D). This process is important in the formation of long bones, and natural fracture healing of bone (Yaszemski et al., 1996).

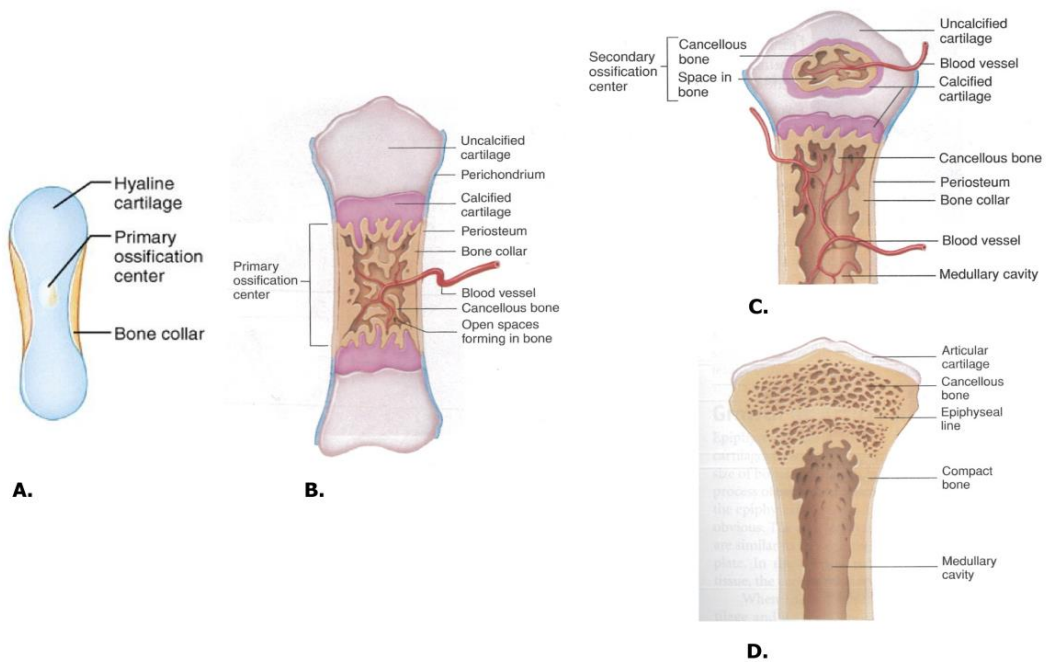


**Figure 1.4.2:** Endochondral ossification. (A) The cartilage was produced by chondroblasts. It has bone a collar at the diaphysis area. (B) The penetration of blood vessels becomes a primary ossification center and brings osteoblasts to this area. (C) Secondary ossification center occurs at the proximal of long bone. (D) The bone is fully developed, the cancellous and compact bones are mature, articular cartilage is the only cartilage present. Reprint from Seeley et al., (2008) with kind permission of McGRAW-HILL.

### 1.5. Bone healing and remodelling

Incorporation of a bone graft into a defected area is similar to the bone healing process. The healing process can be divided into three stages: 1] inflammatory stage, 2] reparative stage, and 3] remodelling stage. The inflammatory stage starts within the first hours and lasts a few days to produce hematoma which is composed of inflammatory cells and fibroblasts. Granulation tissue is produced which then initiates vascular ingrowth and MSCs migration.

In the reparative stage, the cells in the hematoma produce 'callus' which contain fibrous tissue, cartilage and immature bone to envelop the affected region. At the beginning of this stage, cartilage formation predominates followed by production of mineralized tissue.

In the remodelling stage, chondrocytes undergo terminal differentiation and become apoptotic. The ECM undergoes calcification, called cartilaginous calcification, at the junction between the mature chondrocytes and the new bone forming regions with new blood vessel invasion. The new bone formed is remodelled by the activity of osteoblasts and osteoclasts.

Bone remodelling maintains bone strength and mineral homeostasis throughout life. The homeostatic equilibrium between resorption and formation replaces the old bone, micro-damaged, or a fracture region with a new bone adapted to withstand the mechanical loads and strain applied to that bone. Remodelling of trabecular bone is more active than in cortical bone, because of the larger surface area per volume. The remodelling cycle is composed of three sequential phases: resorption, reversal, and formation. The length of the bone remodelling is thought to be several weeks to complete the process (Kini and Nandeesh, 2012).

The resorption process begins with migration and activation of mononuclear monocyte-macrophage osteoclast precursors to form multinucleated preosteoclast which bind to

bone matrix via the interaction between integrin receptor on cell membranes and RGD (arginine, glycine, and asparagine) on matrix proteins. They form deep folds in the membrane which are called the 'ruffled border' and surrounding this is a zone of attachment which is called the 'sealing zone'. Osteoclasts resorb bone by lysosomal enzymes and proteolysis of the bone matrix and finally the multinucleated osteoclasts undergo apoptosis. The reversal phase is a transition phase from bone resorption to bone formation. During bone formation, osteoblasts synthesize new collagen and mineral and regulate matrix mineralization. The osteoblasts surrounded by matrix become osteocytes embedded within lacunae. Osteoblasts secrete a range of growth factors including insulin-like growth factors (IGF), platelet-derived growth factor (PDGF), basic fibroblast growth factor (bFGF), transforming growth factor-beta (TGF- $\beta$ ), and bone morphogenetic proteins (BMP) to regulate themselves in an autocrine and paracrine manner. When bone formation is complete approximately 50-70% of osteoblasts undergo apoptosis (Clarke, 2008, Jilka et al., 1998).

The bone remodelling is controlled by the osteoprotegerin (OPG)/receptor activator of NF-kappa B ligand (RANKL)/RANK system. These mediators regulate the degree of osteoclast differentiation, activation, and apoptosis. RANKL present on the preosteoblastic cell surface binds to RANK present on the osteoclastic precursor cell membrane. It is a crucial interaction for differentiation, multinucleated cell formation, activation, and cell apoptosis. OPG is produced by the cells of the osteoblast lineage and bone marrow stromal cells and inhibits this interaction by blocking the effect of RANKL this is followed by the bone formation on the bone surface (Lamoureux et al., 2007, Clarke, 2008).

### **1.6. Introduction to cleft palate**

#### **1.6.1. Development of the palate**

Human face development normally begins in the fourth week post conception and is followed by the first appearance of palatal shelves at around the sixth week of gestation (Stanier and Moore, 2004). The complex processes of forming the mammalian secondary palate involves different cell states such as cell proliferation, migration, differentiation, and programmed cell death (Ferguson, 1988). In his study of facial development in mice, Stanier (2004) explains that there are three stages of palate formation; the first stage happens at mouse E12.5 (a twelve and half day old embryo) or about the seventh week of gestation in humans, the mammalian palatal shelves on the maxillary prominences grow vertically to horizontally above the dorsum of the tongue. Followed by, at mouse E13.5, or about the eighth week of gestation in humans the connection of palatine shelves at the midline of the palate. The final stage, at mouse E14.5 or approximately 9-10 weeks post conception in humans is the combining of the palatal shelves in the antero-posterior direction and uniting with the nasal septum (Figure. 1.6.1). The epithelial layer on the regions of the palate that fuse together are removed by programmed cell death, migration of epithelial cells to the oral and nasal epithelia, and trans-differentiation into mesenchyme (Martinez-Alvarez et al., 2000).

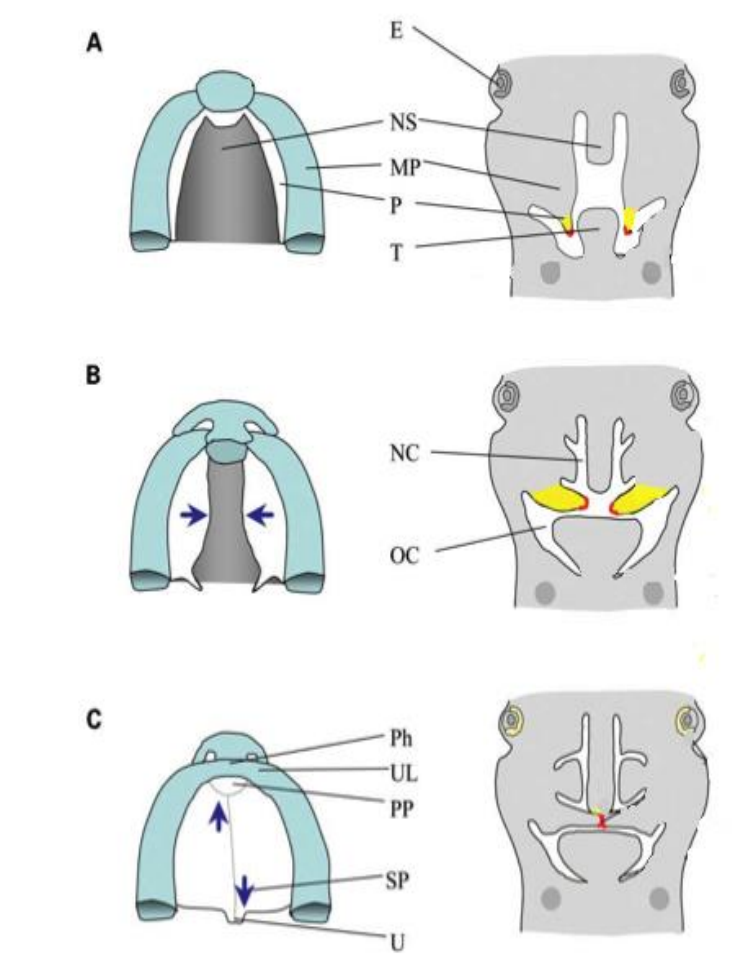


**Figure. 1.6.1:** The normal developmental stages of the lip and palate in paired horizontal and coronal planes of the head of mice. (Adapted from: Stanier, 2004) (A) At mouse E12.5 or about the seventh week of gestation in human, (B) At mouse E13.5 or about the eighth week of gestation in human, the blue arrows indicate the direction of palatal shelves fusion, (C) The mouse E14.5 or approximate 9-10 weeks post conception, the palatal shelves have combined in antero-posterior directions (blue arrows). Abbreviations: MP, maxillary prominences; P, palatal shelves; T, tongue; E, eye; NS, nasal septum; NC, nasal cavity; OC, oral cavity; Ph, philtrum; UL, upper lip; PP, primary palate; SP, soft palate; U, uvula. Reprint from *Human Molecular Genetics*, Stanier and Moore, (2004) with kind permission of Oxford journals.

### **1.6.2. Incidence and cause of cleft palate**

The most common craniofacial congenital anomaly is cleft defects that involve the lip and/or palate. The incidences of cleft lip with or without cleft palate are between 1/300 and 1/2500 live births and of cleft palate defect only are approximately 1/1500 live births. The incidence of these defects is affected by the geographic area, ethnicity and socio-economical status of the patients (Lidral and Murray, 2004). In their study in mice, Peters et al., (1998) found that cleft palate may be caused by abnormal characteristics of the palatal shelves which are broader and less elevated than in wild type mice. Cleft defects can be categorized into nonsyndromic and syndromic types. In nonsyndromic types, the patients do not have other physical and development disturbances, which is about 70 percent of cleft cases. However, the remaining 30 percent of patients are of the syndromic type and have physical or mental disabilities associated with the defects. The syndromic cleft defects can be subcategorized into 300 single-gene diseases (Mendelian disorders) which are inherited in families, (Murray, 2002). The single-gene diseases can be a recessive or dominant, either autosomal or sex-linked genes. Environmental factors, for instance, deficiency of nutrients or a toxic growth environment such as maternal alcohol or smoking during pregnancy are probably involved.

### **1.6.3. Current treatment of cleft palate repair**

The standard treatment for cleft lip and/or palate (National Health Service, 2010) states that the treatment begins with cleft lip and palate examination for diagnosis, hearing, and feeding including consultation with parents. Cleft lip is closed around the third months of age. Cleft palate is closed at the age of 6-12 months. Cleft palate is treated by using soft tissue to close the gap defect. The objectives of this treatment are to allow the acquisition of speech and encourage growth of maxillary bone (Rohrich et al., 1996). The patient might have complications after the operation, for instance, ossification of the growth suture of the maxilla and defects in the remaining alveolar cleft (Smahel et

al., 2009) which leads to maxilla distortion and a narrower, shallower palatal vault and short palate (Figure. 1.6.3). As a result, speech problems may occur. Patients are assessed for speech when the child starts to produce their first words around 13 months of age (Peterson-Falzone et al., 2001). Additional surgical procedures will be performed if defects involve the alveolar process (teeth bearing area). Secondary alveolar bone graft is usually performed at the age of 8 or 11 years to support tooth eruption. Currently, the bone defect is corrected by using autologous bone graft from iliac bone. This has a chance of causing donor site morbidity, numbness of legs, and gait disturbances. Additional surgery may be required to improve appearance and enhance the function of chewing. Ross, (1987b) reported that 73 percent of unilateral cleft lip and palate patients required orthodontic treatment to straighten their teeth. The other 27 percent of patients required surgery to correct the relationship between the maxilla and the mandible and increase the efficiency of the teeth during chewing and biting. The treatment of cleft palate is over a long period of time.

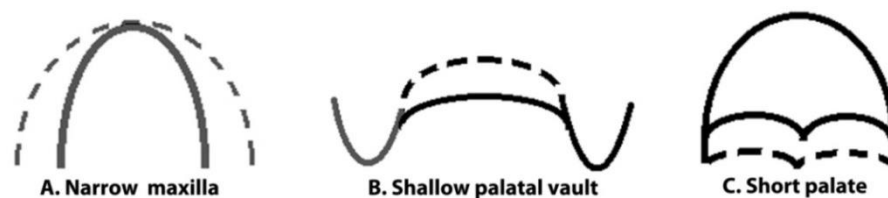


**Figure 1.6.3:** Diagrams of the complications of post-operation cleft palate which might occurred. The dash lines indicated normal maxilla and the black line indicates the complication. (A) is narrow maxilla, (B) is shallow palatal vault, and (C) is short palate.

#### 1.6.4. Controversy for timing of cleft palate repair

The protocols for cleft palate treatment are still controversial in that the ideal timing for the surgical procedure for closing the cleft defect is not fully established. This depends on many factors such as the type of cleft defect (cleft lip, cleft palate, and cleft lip and

palate: Figure 1.6.4), patient's condition, and the opinion of the medical team. Cleft palate children usually have delays in the onset at speech because there is no separate barrier between the nasal cavity and the mouth (Peterson-Falzone et al., 2001). The reviews of Berkowitz et al., (2005) and Saijo et al., (2010) claimed that a suitable age of the patient for undergoing cleft lip repair is around the third months of age, following by cleft palate repair is between 6 to 18 months. This timing benefits speech production, however, it may affect maxillary growth as previously mentioned. In the Ysunza et al., (2010) study, they described that an early cleft palate repair of hard palate at around 4-6 months of age can enhance speech development, and with orthodontic treatment allowed normal maxillary growth. However, some studies found mid face retrusion from scar tension in the antero-posterior direction (Ross, 1987b, Ortizmon.F et al., 1966). In bilateral cleft lip and palate patients, the development of the maxillary arch was narrower and shallower than in the non-cleft conditions, in addition, orthodontic treatment only provided small improvements in the maxillary structure (Smahel et al., 2009). Delay of cleft palate treatment may reduce maxillary growth disturbance. Because of this the two-stage procedure was introduced so as to balance the requirements for maxillary growth and speech development. The studies of Schweckendiek, (1978) and Pryds et al., (1974) reported that the defect of the soft palate could be repaired in the first year of age. Patients were found to improved speech development after this treatment and difficulties with speech diminished with age. The remaining defect on the hard palate was repaired at 12-14 years of age. This period of time is after complete maxillary growth has occurred to avoid maxillary growth disturbance. In contrast, Rohrich et al., (1996) followed up the patients who received early (10.8 months of age) and delayed (40.8 months of age) hard palate closure. The results showed that they did not significantly differ in the disturbance of maxillary growth. However, the delayed treatment group had significantly greater speech difficulties which can lead to hearing loss, and also incidence of palatal fistula (the abnormal connection between oral and nasal cavities) than the other groups. They

designed a procedure to complete a cleft palate repair before 2 years of age to allow the development of integrated speech and reduce risk of hearing loss (Rohrich and Gosman, 2004).

The suitable timings for cleft palate repair are still controversial and various surgical treatments are performed to treat cleft patients. Tissue engineering is a new strategy with potential to substitute for the missing organ (bone tissue and oral mucosa tissue) in cleft palate repair.

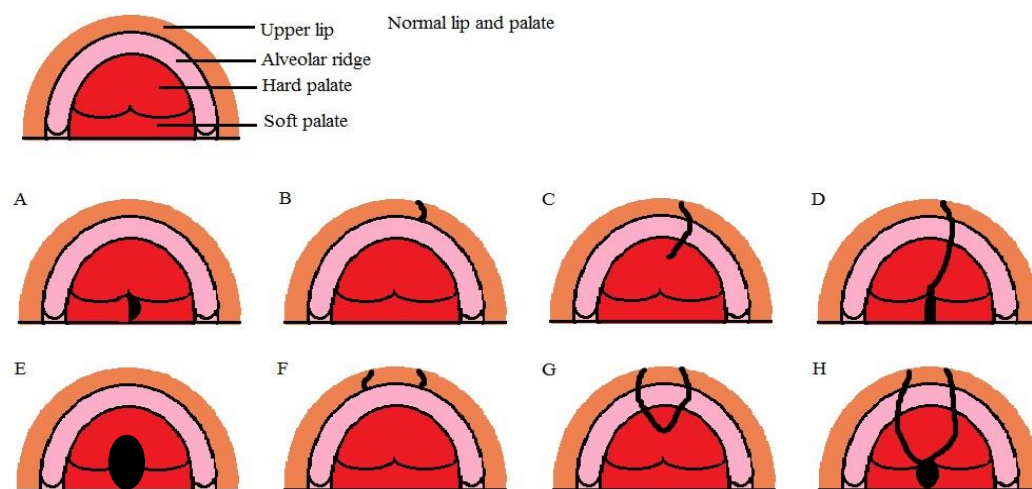


**Figure 1.6.4:** The variety of cleft lip and/or palate. The left side on top of picture is normal lip and palate. (A) Cleft in soft palate, (E) Cleft in hard palate; B,F: Unilateral and bi-lateral cleft lip; C, G: Unilateral and bi-lateral cleft lip involving hard palate; D,H: Unilateral and bi-lateral complete cleft lip and palate.

### 1.7. Tissue engineering for cleft palate/maxillofacial repair

A new treatment strategy for bone regeneration is tissue engineering. This technique would eliminate problems such as donor site morbidity, immune rejection, and pathogen cross-contamination. The conceptual model for bone tissue engineering is to take cells from the patient's tissues and then seed them back into a temporary scaffold before implantation back into the patient (Figure. 1.7).

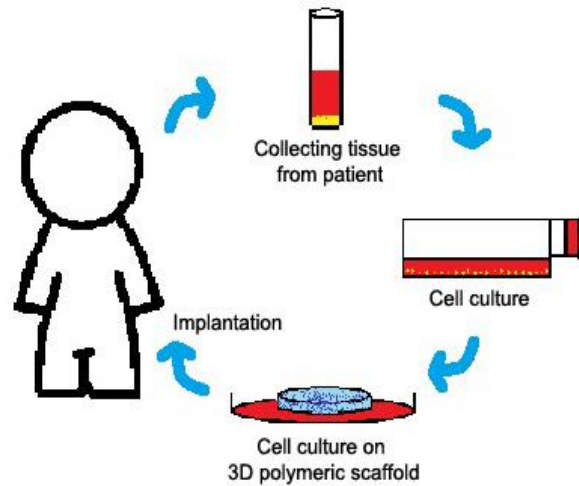


**Figure.1.7:** The concept of tissue engineering is to remove cells from the patient. The cells would be cultured and then seeded on a polymeric scaffold in a growth factor supplemented culture medium. Then, the cell seeded scaffold which forms a functional tissue would be implanted to the defect site.

A clinical study by Moy et al., (1993) found that the quantity of bone formed at the maxillary sinus after implantation of a mixture of cortical bone graft from chin and hydroxyl apatite (HA) granules was much more than after implantation of HA granules alone, about 44.4% and 20.3%, respectively. Therefore it seems that including cells in a bone tissue engineering procedure will increase the success rate of bone repair in the clinic. The cell sources for hard tissue engineering should incorporate with the surrounding area and be able to undergo osteogenic differentiation. For the polymeric scaffolds used in tissue engineering, many factors must be considered such as biocompatibility, porosity, mechanical integrity, and biodegradability. Tissue engineering techniques have been used for cleft defect reconstruction; Hibi et al., (2006), showed that the combination of a gel matrix, platelet-rich plasma (PRP), and autologous MSCs from bone marrow harvested from their patient's iliac crest, filled the alveolar cleft defect in a 9 year-old patient. The bone volume increased to 79.1% at 9 months post-operative. They also found that the maxillary lateral incisor and canine teeth which were located adjacent to the defect erupted 2 years post-operation. This case

study indicated that tissue engineering is promising for repairing cleft palate, however, cell sources and tissue engineering materials haven't been optimized. PRP which contains fibrinogen and chemical factors such as vascular endothelial growth factor (VEGF) was added to enhance matrix formation and tissue regeneration. The clinical results of tissue engineering repair are variable depending on each patient, considering factors such as gender, age, habit such as sucking behaviour, systemic conditions, and anatomy. The different regions of the maxillofacial bone will have different vascularization and functional loads. Therefore, the challenges in tissue engineering are to control these environments and, cell differentiation *in vitro* before implantation. This strategy will reduce subsequent healing time.

### **1.8. Stem cells as an alternative source for bone tissue engineering**

Stem cells are categorized into: 1] embryonic stem cells which are collected from embryos at the blastocyst stage and 2] adult stem cells which are collected from tissues throughout the body such as bone marrow, adipose tissue, dental pulp, and periosteal tissue. The characteristics of stem cells are firstly: self-renewal, as they undergo a number of cell divisions while still maintaining their non-differentiated cell state and, secondly, differentiation potential to other cell types including osteoblastic cells.

#### **1.8.1. Human embryonic stem cells derived mesenchymal progenitor (hESMPs)**

Cultured human embryonic stem cells have been used in cell therapy and tissue engineering (Karner et al., 2007). They have an unlimited ability to proliferate and the ability to differentiate in to the three germ lines which create all the cell types in the body. However, embryonic stem cells might induce a tumour risk. There are also many ethical issues to be considered when using them for research because a human embryo has to be destroyed. A study by Karlsson et al., (2009) developed hESMPs derived from an embryonic stem cell line which have been specifically pre-differentiated into the mesenchymal lineage in a commercial laboratory. They are a middle stage between embryonic stem cells and mesenchymal progenitor cells and have self-renewal and

differentiated potential into osteoblasts, chondroblasts, and adipocytes. These cells showed fibroblastic morphology and expressed markers similar to adult MSCs. hESMPs have advantages for use in research as they are homogeneous and easy to culture. It has been shown that they can grow in media without animal components, which makes them promising for cell toxicity, drug development, and tissue engineering in a clinical situation. In a study by de Peppo et al., (2010), hESMPs were used to screen metal scaffolds to investigate cell attachment, proliferation, and osteogenic differentiation. They showed gene expression profiles highly similar to the human MSCs. Their cell proliferations were significantly higher compare to the autologous cell MSCs. Therefore, hESMPs are a good cell model to select a suitable scaffold material for MSC differentiation.

### **1.8.2. Adult stem cells**

Adult stem cells are found in tissues throughout the body such as bone marrow, blood, adipose tissue, dental pulp (Sloan and Waddington, 2009) and periosteal tissue. The properties of adult stem cells are their ability to self-renew (with limited cell division due to a cellular senescence) and a multi-differentiation potential (Wagner et al., 2008). They are undifferentiated cells which can be differentiated into many cell types for tissue or organ regeneration.

#### **1.8.2.1. Bone marrow mesenchymal stem cells (hBMSCs)**

Bone marrow mesenchymal stem cells (hBMSCs) are used for regenerative medicine. They are capable of self-renewal and can be differentiated to adipocytes, chondroblasts, and osteoblasts under specific culture media (George et al., 2006). They can be harvested from human donors, then the cells are grown and expanded in the laboratory, finally, they can be used as autologous cells and introduced back to the same patient that donated them. This procedure would be a patient-specific treatment and avoid immune rejection. In case studies by Hibi et al., (2006) which performed in the 9 year old female

patient and Behnia et al., (2009) which performed in the 10 and 14 years old patients, autologous hBMSCs were seeded in biodegradable scaffolds to repair an alveolar cleft. The results showed new bone formation at the defect area post-operation. Sufficient bone was produced for the next step of treatment, which is orthodontic treatment. hBMSCs are typically collected from iliac crest (hip bone), therefore, there may be complications after isolation such as pain at the site of operation, imbalance, arterial and nerve injury and risk of infection. In addition, there are a limited amount of MSCs in bone marrow or about 0.01percent of the total of the mononucleated cells obtained. Moreover, hBMSCs have reduced progenitor and differentiation potential as the passage number increases (Jaquiery et al., 2005, Banfi et al., 2000, Caplan, 2005). Other cell sources may have advantages for use in bone regenerative medicine. The cell sources should have osteogenic potential, no risk of immunogenicity, and be easy to harvest. Recently, periosteal cells have been researched for using in bone regeneration, these cells have the ability to differentiate to chondroblasts and osteoblasts (Soltan et al., 2009, Frey et al., 2013, Samee et al., 2008).

### **1.8.2.2. Human jaw periosteum cells (HJPs) as osteogenic progenitors.**

Periosteum is a tri-layer membrane that covers the entire external surface of bone except at the joint surface (Olbrich et al., 2012). It aids in growth, remodelling, and healing of bone. The inner layer of the periosteal membrane consists of MSCs which can differentiate into chondroblasts and osteoblasts, these are similar to the MSCs which are collected from bone marrow aspiration (Soltan et al., 2009). The osteogenic potential of periosteal cells seems to be retained in aging donors, in contrast, this potential in bone marrow MSCs is reduced (Stolzing et al., 2008). There are controversies about a suitable harvesting area of MSCs for the reconstruction of facial bone defects. The original of the facial skeletal is the cranial neural crest, and the rest of the skeleton (limb and body) forms from mesoderm. Therefore, the periosteal tissue from the two different areas might be different in bone formation and bone healing (Opperman, 2000). In

previous animal studies Fujii et al., (2006) and Choi et al., (2002) showed different bone formation patterns from periosteum grafts between tibia and facial areas when they were grafted into suprahyoid muscle. The periosteum graft from facial bone induced intramembranous ossification (bone formation from fibrous tissue) alone. Whereas the periosteum graft from tibia induced endochondral ossification (bone formation from cartilage). The case studies in alveolar augmentation by D'Addona and Nowzari, (2001) showed that the intraoral bone graft produced bone formation without cartilage formation. A case report by Trautvetter et al., (2011) used mandibular periosteal cells seeded on polymer base scaffolds for maxillary sinus augmentation. Post-operative evaluation showed a mature bone appearance at 4 months. Dental implants were placed afterwards in the repaired area without any complications. This study reported that donor site morbidity and time of operation were significantly reduced compared with the autologous bone graft from iliac crest harvesting. However, these bone tissue engineering grafts were transplanted in the pre-osteogenic stage. The time for the healing process to take place may be longer than for autologous bone graft (mature osteogenic stage). These previous studies showed that HJPs might be a promising cell source for bone tissue engineering.

### **1.9. Scaffold for bone tissue engineering**

A scaffold can mimic the native extracellular matrix structure (ECM) with micro-and/or nano-fibres and provide an initial area for new tissue regeneration. The strategy of bone tissue engineering is to improve function and reconstruct damage or congenital defects by using engineered materials and biological methods. These methods consist of the osteogenic cells and suitable carriers, which are solid structures for supporting cell attachment, migration, proliferation and differentiation. In other cases the chemical agents are added to scaffolds then they are implanted into the defect areas, without cells. The chemical agents will attract the cells which surround the wound site of the patient. The cells will migrate and attach to the implanted scaffold. Another function of

scaffolds is to transfer cells from the laboratory to the patient for therapeutic replacement.

Various fabrication techniques for reconstruction scaffolds for bone tissue engineering have been developed in the last decade, including solvent casting, particulate-leaching (Mehrabanian and Nasr-Esfahani, 2011), phase-separation, freeze drying (Zhang and Ma, 1999), self-assembly, gas foaming, printed 3D structure (Leukers et al., 2005) and electrospinning (Lu et al., 2013). The requirements of the scaffold will vary depend on the type of the reconstructed tissue. The requirements of scaffolds for bone tissue engineering are biocompatibility, biodegradability, porosity, mechanical stability, ease of manufacture, sterilizability, and handleability. Features such as pore size and surface area need to be optimized for the application. In their review, Salgado et al., (2004) described the ideal properties of bone tissue engineering scaffolds

- **Biocompatibility:** scaffolds should incorporate into the surrounding tissue without immune rejection.
- **Porosity:** the pores should be highly interconnectivity to stimulate cell attachment, growth, nutrient diffusion, and metabolic waste removal.
- **Pore Size:** the pore diameter is an important factor for cell penetration, bone matrix production, and novel vasculature formation.
- **Surface properties:** the characteristics of the surface area of the scaffold influences cell attachment and proliferation.
- **Osteoinductivity:** the scaffold material should facilitate osteogenic differentiation.
- **Mechanical properties and biodegradability:** the scaffold should have sufficient strength to maintain a space for cell growth but totally degrade when tissue regeneration is complete.

The scaffold factors including diameter and pore size affect the biological response. The scaffolds with poor porosity found less cell infiltration than high porosity scaffolds. In

addition scaffolds containing micro-fibres (about 3-4 $\mu\text{m}$ ) showed that the cells could align on a single fibre and connect to adjacent fibres. The cells were able to penetrate below the surface of the scaffold. In contrast, scaffolds containing nano-fibres (about 200-300nm) showed most of the cells on the surface of the scaffold due to less penetration (Soliman et al., 2011). The pore size of the porous hydroxyapatite scaffold for bone ingrowth in 50 $\mu\text{m}$  sized pores was sufficient and 300 $\mu\text{m}$  sized pore was optimum (Chang et al., 2000a). For vascularization the scaffold should have at least 400 $\mu\text{m}$  sized pores (Woodruff et al., 2012). The result of smaller fibre diameter is a reduction in porosity and pore size but a higher fibre area and mechanical strength (Rim et al., 2013). The ECM is found in different architectures in the human body. For example in the skin and early states of bone formation ECM architectures are randomly woven fibres but in a tissue adapted to tension such as tendon to collagen is a highly organized aligned fibres. Therefore an ideal scaffold for tissue engineering should mimic native ECM at the affected site.

The advantages of solvent casting, particulate-leaching, phase-separation and freeze drying techniques are that they are simple procedures and minimal equipment is required. However, these techniques are dependent on the materials and solvents which needed to be optimized and sensitive to fabrication parameters. Self-assembly technique is suitable for producing a fine nanofibre scaffold due to organization of peptide sequences but the main disadvantages of this technique are that it is a complicated, elaborate process, and very expensive. The advantages of gas foaming are that organic solvent are not required and high temperatures, but the scaffold products are highly interconnected pore structure which will affect their strength. For printed 3D structures, the advantage is a control over structure and porosity, however, there are limited polymer materials that can be used and the equipment is very expensive (Subia et al., 2010). Most of the above techniques are not capable of producing polymeric fibre scaffolds ranging from microscale to nanoscale with special orientation, high surface

area, and adjustable pore geometry. Electrospinning technique is a promising technique for desired scaffold fabrication.

### **1.10. Electrospinning**

#### **1.10.1. Introduction**

Electrospinning is a versatile technique to prepare scaffolds for tissue engineering. It uses electric force to produce the polymer fibre in a certain diameter from a few micrometers to a few hundred nanometers. This technique can be used with many types of polymer. The advantages of electrospinning are the control over specific orientation, high surface area, and pore geometry of the fibres. It is a non-invasive technique that does not require high temperatures for fibre production, and is cost effective. However, this technique has a low production rate, making it difficult to scale-up (Rim et al., 2013, Blackwood et al., 2008, Delaine-Smith et al., 2014a).

#### **1.10.2. Spinning mechanism and theory**

The electrospinning technique was first described by Sir Geoffrey Ingram Taylor in 1964 (Burger et al., 2006). His work referred to the water droplets in the high electrical field. A high voltage was applied to a contained solution and the solution became charged with the electrostatic repulsion. The effect of repulsion counteracted the surface tension of the solution. The droplet was erupted and stretched which was called a Taylor cone. The fluid jet from the tip of the cone was emitted when the charge of the solution overcome the surface tension (Taylor, 1964). The solution jet dries during the path to the collector. The solution jet has 2 phases: the first phase, is called the stable phase which the jet emits from the needle tip at a straight line and an elongation of fibre along this phase. When the jet gradually evaporates, the solution concentration changes and thus the jet is a high velocity. The second phase, is called unstable phase, the jet present a random whipping movement to produce a thinner and non-woven fibre on the collector (Reneker et al., 2000).

### 1.10.3. Electrospinning and tissue engineering

Electrospun scaffolds have been developed to be used for tissue engineering in recent years as ECM to support cells. More than 100 types of polymer have been used in the electrospinning technique both synthetic and natural polymers (Burger et al., 2006). Since different native tissues have the specific requirement for a functional scaffold such as skin, nerve, heart, tendon, and bone, the electrospun scaffold technique can adjust and produce fibres which are suitable for the tissues. Many studies have used the electrospun scaffolds for supporting structure or cell delivery vehicles such as skin (Blackwood et al., 2008), nerve (Daud et al., 2012), heart (Zong et al., 2005), tendon (Yin et al., 2010), and bone (Ma et al., 2011). Furthermore, electrospun scaffolds can deliver bioactive agents such as drugs, proteins, and DNA if made with degradable polymers (Luu et al., 2003). The results in the rate of agent release depend on the methods of incorporation a bioactive agent into the scaffold (Liu et al., 2012). The properties of electrospun scaffold depended on the specific polymers and conditions. Therefore the choice of materials and conditions could be considered for the application.

#### 1.10.4. Electrospinning rig set up

The electrospinning apparatus consists of four main components: 1] a high voltage electricity source which applies the force to extend the charged to polymer solution, 2] a syringe pump which controls the dispensing rate of the polymer solution, 3] a syringe to carry the polymer solution and needle which charges the polymer solution in the high electric field, and 4] a ground platform for collecting the fibres such as an aluminum foil covered drum collector (Katta et al., 2004). Various types of collectors are designed to fit the purpose such as a flat plate or a rotating drum. The flat plate may produce an uneven scaffold distribution mat. Therefore, the rotating drum as a collector was used in this project (Figure. 1.10.4).

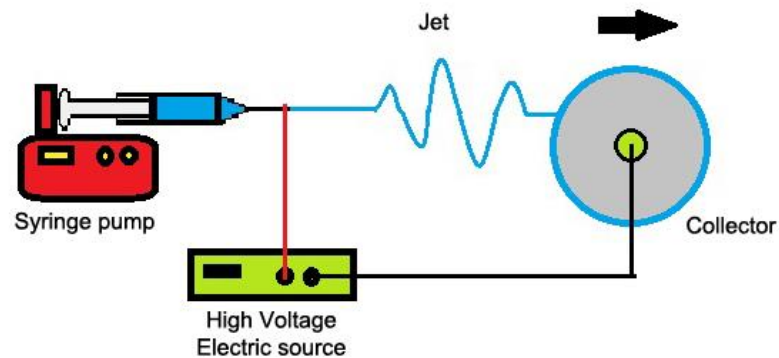


**Figure. 1.10.4:** Schematic of electrospinning apparatus. The green box is a high voltage electric supply and a ground is a collector, a rotating drum type. The red box is a syringe pump to hold a syringe and put force through a polymer solution to the collector. The blue line as a polymer solution jet is dispensed from the tip of syringe to the rotating drum.

A syringe pump forces the polymer solution which is contained inside a syringe. A high voltage electric source is applied between the needle and the ground collector. The electric charge carries the polymer solvent to form a cone and ejects a jet of the liquid at the tip of needle. The jet travels through the collector while the solvent evaporates and leaves behind the dry polymer fibre on the collector. The fibre morphology can be influenced by various process parameters such as applied voltage and needle collector distance (called working distance) (Table 1.10.4). However bead formation may occur on the resultant polymer fibres.

<b>Factors</b>	<b>The fibre structure</b>
<b>Polymer concentration</b> <ul style="list-style-type: none"> <li>• Too low</li> <li>• Too high</li> </ul>	The jet breaks up to form beading and droplets  The jet can't be initiated cause the droplets dry out at the tip of capillary
<b>Working distance</b> <ul style="list-style-type: none"> <li>• Too close</li> <li>• Too far</li> </ul>	Wet fibre and beading structure  Beading morphology
<b>Polymer flow rate</b> <ul style="list-style-type: none"> <li>• Low flow rate</li> <li>• High flow rate</li> </ul>	Decreased fibre diameter  Increased fibre diameter and beading morphology
<b>Applied voltage</b> <ul style="list-style-type: none"> <li>• Decreased voltage</li> <li>• Increased voltage</li> </ul>	Increased fibre diameter  Decreased fibre diameter and beading formation (Zuo et al., 2005).
<b>Humidity</b> <ul style="list-style-type: none"> <li>• High humidity (&gt;60%)</li> </ul>	Fibres do not dry properly and a formation of

	pore on the fibre surface which are called “breath figures”. The breath figures created from the air condenses on the fibre surface due to the jet cooled then they evaporated and formed pores (Casper et al., 2004).
<b>Temperature</b> • High temperature	Decreased fibre diameter

**Table 1.10.4:** Factors that influence the morphology of an electrospun scaffold

**1.11. Polymer**

Table 1.11, lists some commonly used scaffold materials, including 4 polymers used for tissue engineering relevant to this project: Polyhydroxybutyrate-polyhydroxyvalerate: PHPV, Poly ( $\epsilon$ -caprolactone): PCL, Polylactic acid: PLA, and Polyurethanes (PU). These scaffolds have all been approved by the Food and Drug Administration (FDA) for tissue replacement in medical devices, for instance in craniofacial reconstruction.

<b>Materials</b>	<b>Origin</b>	<b>Characteristics</b>
<b>Collagen</b>	Natural	Low immune activation Favorable cell adhesion Supporting to morphology modification, migration, and differentiation of cells Low mechanical properties (Kleinman et al., 1981)
<b>Chitosan</b>	Natural	Hemostatic Raise to osteoconductive and wound healing
<b>Poly(hydroxybutyrate)</b>	Natural	A natural resource Limited usefulness by its brittleness

		(Chen and Wang, 2002)
<b>Poly(<math>\epsilon</math>-caprolactone)</b>	Synthetic	Aliphatic polyester family U.S. Food and Drug Administration approved Hydrolysis degradation (Hutmacher et al., 2001) Produced biocompatible by-product (Langer and Tirrell, 2004) Slow degradation Lack of toxicity Low cost (Yoshimoto et al., 2003) Good mechanical properties
<b>Poly(lactic acid (PLA))</b>	Synthetic	Weak mechanical properties Controllable degradation by blending with Poly(glycolic acid):PGA Hydrolysis degradation By-products might generate inflammation, <i>in vivo</i> (Cheung et al., 2007)
<b>Polyurethane (PU)</b>	Synthetic	Biocompatibility. Degradable and nondegradable materials. Adjustable the wide range of biological and mechanical, and degradable properties. Toxicity of degradable products is a major problem (Gunatillake and Adhikari, 2003).

**Table 1.11:** Advantages and disadvantages of natural and synthetic polymers used in bone tissue engineering

### 1.11.1. Polyhydroxybutyrate-polyhydroxyvalerate

PHBV copolymer is a completely biodegradable plastic, the copolymer of hydroxybutyrate (HB) and hydroxyvalerate (HV) monomer produced and mixed by the fermentation of microorganisms (*Alcaligenes eutrophus*) (Kotnis et al., 1995) (Figure. 1.11.1). The usefulness of polyhydroxybutyrate (PH) is limited because of its brittleness, deficiency in thermal stability and difficulty of manufacture. These weaknesses are overcome by adding polyhydroxyvalerate (PV) into the polymer to increase the flexibility and firmness. PHBV has been used in various application areas such as disposable personal hygiene, packaging and medical devices. The beneficial properties of PHBV are its biodegradability by slow hydrolytic degradation (Holland et al., 1987).

PHBV has been evaluated for tissue response *in vivo*, Gogolewski et al., (1993) found that PHBV does not cause any adverse reaction such as pus or necrosis. However the animals, which were implanted with PHBV showed a continuous inflammatory response over three months. The high inflammatory response at the implanted area was related to the amount of HV ingredient. Although Shishatskaya et al., (2004) showed *in vivo* that there was no inflammatory affect at the implanted area where highly pure medical grade PHBV, which was not contaminated from protein or lipid of bacteria, was implanted. The PHBV polymer films were implanted, *in vivo*, and degraded until material was undetectable over an 18 month period (Sultana and Khan, 2012). Sombatmankhong et al., (2007) reported that PHBV scaffolds are biocompatible with fibroblastic cells by evaluating initial cell attachment and proliferation. In addition, enzyme activity (ALP: alkaline phosphatase) of human osteoblasts (Saos-2) seeded on PHBV indicated that the cells were osteogenic from 24-72hr after culture.

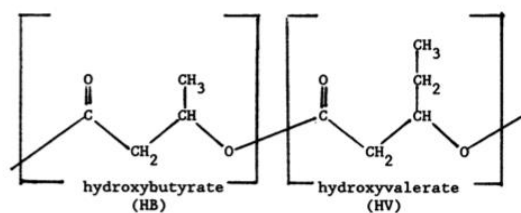


**Figure 1.11.1:** Chemical formula of Polyhydroxybutyrate-polyhydroxyvalerat

### 1.11.2. Poly( $\epsilon$ -caprolactone)

PCL is a biodegradable and biocompatible material, which is made from aliphatic polyester (Figure. 1.11.2). PCL is degraded by hydrolysis and its breakdown products are biocompatible. Monocryl<sup>®</sup> sutures are made from PCL. Several studies reveal that they have been used clinically and approved by the U.S. FDA for human use (Hutmacher et al., 2001, Reed et al., 2009). PCL has a slow degradation rate that is suitable for the bone part of a tissue engineering scaffold. The yield of PCL hydrolysis is the 6-hydroxycaproic acid which is a natural metabolite (Mishra et al., 2008). Because the material degrades slowly by hydrolysis PCL has been suggested as a bone replacement for a load-bearing area until bone cells grow into the mature phase and have sufficient ability to form functional tissue. Hutmacher et al., (2001) showed that a PCL scaffold could maintain its mechanical properties for 5-6 months and was completely metabolized over 2 years. Moreover, many people have used PCL as a material for *in vitro* studies and demonstrated that human fibroblastic and osteoblast-like cells attached, proliferated, produced extracellular matrix, and developed tissues (Delaine-Smith et al., 2014a, Tuan and Hutmacher, 2005, Williams et al., 2005). Furthermore, PCL is cheap and it is possible to produce in large quantities.

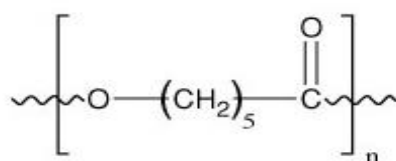


**Figure 1.11.2:** Chemical formula of caprolactone and polycaprolactone

### 1.11.3. Polylactic acid (PLA)

PLA is a Poly ( $\alpha$ -hydroxy esters) (Figure. 1.11.3). It is biocompatible, biodegradable and FDA approved for medical use (Bye et al., 2013, Tu et al., 2003, Ma and Zhang, 1999). PLA has the potential to provide an environment for attachment, growth, and differentiation of cells (Sikavitsas et al., 2005). The degradation of PLA is by hydrolysis to break the polyester bonds and this yields lactic acid as a by-product. Shishatskaya et al., (2004) reported that the degradation period of this scaffold is about 6 months. The drawbacks of PLA implanted materials are the residual products. These decrease the pH of the adjacent area and stimulate an inflammatory reaction. In addition, the by-products of PLA materials could increase the rate of degradation of the polyester. Thomson et al., (1995) observed that the degradation of the scaffold became more rapid when the acidic concentration of the adjacent area was increased *in vivo*. The acidic environment might induce an inflammatory reaction or tissue necrosis. Moreover, PLA has insufficient mechanical strength to support the reconstruction of hard tissue.

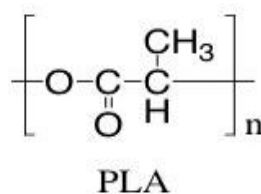


**Figure 1.11.3:** Chemical formula of the monomer of poly (lactic acid)

#### 1.11.4. Polyurethane (PU)

PU's have been used for biomedical purposes in cardiovascular implants for many years. But it was withdrawn from the market because of surface microcracking. In recent years improvements have been made in its toughness, elasticity, durability, biocompatibility, biodegradability, and it has been incorporated in several biomedical implant applications. PU consists of the three basic segments including;



Where P means the polyol which called the soft segment, D means the di-isocyanate which can react with either P or C, and C means the chain extender which is either a hydroxyl or amine group. The D and C combination creates the hard segment of PU.

PU has tunable biological, mechanical, and physicochemical properties by adjusting the combination of hard and soft segments resulting in PUs with different properties as desired for the final application (Takahara et al., 1992, Guan et al., 2005). Biodegradable PUs have been used in bone tissue engineering due to their elastic mechanical properties and low degradation rate. PU scaffolds can be produced by many methods including; electrospinning, salt leaching, and thermally induced phase separation (Guelcher, 2008). However, the degradation-products of PU particularly the diisocyanate component is a potential toxic chemical component (Gunatillake and Adhikari, 2003).

#### 1.12. Bioactive composite electrospun scaffold

Electrospun scaffolds can mimic the physical structure of native ECM. However, there are problems associated with synthetic polymer electrospun scaffold. These are; lack of cell recognition sites on the surface, hydrophobicity and no specific osteoinductive or osteoconductive properties of the majority of materials used in electrospinning.

Therefore, bioactive materials will be introduced in the polymer production for bone tissue engineering.

Composite materials by definition are composed from 2 or more components. Native bone is made from mostly collagen type I and HA that consists of calcium phosphate. Many studies in bone tissue engineering have developed electrospun scaffolds consisting of biodegradable materials and calcium phosphate particles or HA. Electrospun collagen type I has been used in tissue engineering, though they have the low mechanical properties and do not maintain their structure in a culture media environment for longer than 10 days (Jha et al., 2011). Therefore they are not material of choice for bone tissue engineering which needs time for cell development and mineralization, and also good mechanical properties. Nano-sized HA had been deposited on a knitted micro-porous silk scaffold by using a soaking process to produce a biocompatible, wettable, and osteoconductive scaffold that facilitates the attachment and ingrowth of cells into the implanted scaffold. The scaffold was also observed to be osteoinductive meaning that it could induce undifferentiated stem cells of osteoprogenitor cells to become osteoblast-like cells (He et al., 2013, Swetha et al., 2010). Utilising electrospinning, composite fibres can be created and produced in the form of composite blending (Nandakumar et al., 2010), submerging in a simulated body fluid, and the alternate soaking process (Meng et al., 2013). The traditional simulated body fluid (SBF) method typically requires an incubation time of more than 7 days for coating with continuous HA deposition via ion charging between the material surface which presents the negative charge (carboxyl and hydroxyl groups) and the positive charge (calcium ions) in the SBF. *In vitro* studies showed that HA alternate soaking process on PLA scaffold enhanced OCN expression and also increased mechanical strength (Jaiswal et al., 2012). On the other hand, Meng et al., (2013) found that calcium phosphate apatite surface coating didn't enhanced the cell adhesion, cell proliferation, or osteogenic differentiation.

### 1.13. Vacular endothelial growth factor (VEGF)

VEGF is a cellular glycoprotein which has an important role in the regulation of new blood vessel formation (vasculogenesis). Senger et al, (1983) discovered a vascular permeability factor from ascites tumor which rapidly produced a microvascular permeability, *in vivo*. They also found a similar result from the culture media of tumor cells, *in vitro*. Later VEGF research found that the VEGF family is composed of seven types; VEGF-A is the most vasculogenesis capable protein and can induce endothelial cell proliferation, vessel, and bone formation. The VEGF-A human gene has four different isoforms, VEGF-121, VEGF-165, VEGF-189, and VEGF-206. VEGF-189 and VEGF-206 are completely separated from ECM which is necessary for epiphyseal vascularization (secondary ossification) in endochondral bone formation. Whereas the VEGF-165 is mostly bound to ECM which takes an important role for primary ossification center (metaphyseal angiogenesis). VEGF-A binds to the VEGF receptors-1 (VEGFR-1), VEGFR-2, and the VEGF co-receptor neuropilin-1 (NRP1) on many cell surfaces such as hematopoietic stem cells, monocytes, neurons, and osteoblasts (Otrock et al., 2007, Thi et al., 2010). VEGFR-1 acts as the antagonist receptor to inhibit endothelial cell proliferation, while VEGFR-2 acts as the agonist for vasculogenesis. NRP1 can bind to VEGF-1 directly and also mediate the conversion of VEGF<sub>165</sub> to VEGFR-2. Clinical studies found that an overexpression of VEGF can cause diseases such as cancer and diabetic retinopathy in eyes. Several studies reported that late stage of human osteoblast-like cells produce VEGF. VEGF production is stimulated by hypoxic conditions, BMPs, transforming growth factor beta (TGF- $\beta$ ), prostaglandin, fibroblast growth factor 2 (FGF-2) and 1 $\alpha$ ,25-dihydroxyvitamin D<sub>3</sub>. In contrast, the production of VEGF is reduced by glucocorticoids (Maes and Carmeliet, 2008). Thi et al., (2010) reported that VEGFR-2 plays an important role in mediating fluid flow shear stress induced VEGF secretion by osteoblasts, *in vitro*. Fluid flow may release PGE<sub>2</sub> as mechano-signaling factor therefore this signal may stimulate VEGF production (see

1.17). Another hypothesis is that VEGF release by mechanical stimulation may induce vasculogenesis by two pathways. Firstly, the autocrine pathway may increase VEGFR-2 by actin adaptation of osteoblasts. The other is a paracrine pathway, the signal may communicate to other endothelial cells, osteoblasts, and osteocytes which are necessary for bone formation and fracture healing.

### **1.14. Mechanical force**

#### **1.14.1. Introduction**

Bone in healthy people is a dynamic tissue in which there is a balance between bone resorption and formation over time. The effect of mechanical forces on living bone has been studied for many years. Researchers found that the force below a bone micro damage threshold in a particular area affected the bone architecture by adaptation (Frost, 1994). For example, the bones of racket-holding arm in tennis players are much stronger than there of the other side. Mechanical force is applied to their arm whilst they play tennis. In contrast, an astronaut's bone mass decreases during long term space flight, since no gravity is present to enable sufficient loading on their bones. Various mechanical loading parameters such as compressive, tensile, or torsional strain and fluid shear stress may affect bone. Several studies have evaluated the effect of mechanical stimuli on osteoprogenitor cells used for bone tissue engineering (Li et al., 2004, Chen et al., 2010, Delaine-Smith et al., 2012).

#### **1.14.2. Mechanical regulation of bone cells.**

Typically in cortical bone, osteocytes are in lacuna and their cell processes are in canaliculi (Figure 1.14.2). The space between lacunae and canaliculi is filled with interstitial fluid. The fluid flows produced depend on the pressure gradients within the bone matrix. The oscillatory fluid shear stress on osteocytes was estimated to be approximately 0.8-3Pa (Weinbaum et al., 1994, Mi et al., 2005). Verbruggen et al., (2014) predicted the effect of shear stress on the cell membrane of osteocytes under a

physiological environment, *in vivo* by using computational methods. The shear stress was in the range of 0.1-2.2 Pa which had been shown in *in vitro* studies to enhance osteogenic differentiation (Delaine-Smith and Reilly, 2011, Bacabac et al., 2004). Osteoprogenitor cells located in the intramedullary cavity (bone marrow) may also be affected by fluid flow while there are volumetric changes in the cavity, muscle activity, and capillary filtration (Kwon et al., 2010). Osteoprogenitor cells reside not only in the bone marrow but also in many soft tissues including; vascular smooth muscle, capillary, and periosteum tissue. These tissues significantly deform under a physiological loading, therefore one would expect that fluid flow can affect the osteoprogenitor cells within these tissues (Chen et al., 2010).

How mechanical loading affects MSCs differentiation is still not clear, both *in vivo* and *in vitro*. Fluid flow can be applied to cells *in vitro* using a bioreactor (Datta et al., 2006, Sittichokechaiwut et al., 2010). Specific bioreactors design should be considered to enhance the current standard of tissue engineering. The important loading regime should be elucidated to ensure the best conditions of differentiation and extracellular matrix production, either *in vitro*: before implantation, or *in vivo*: after implantation.

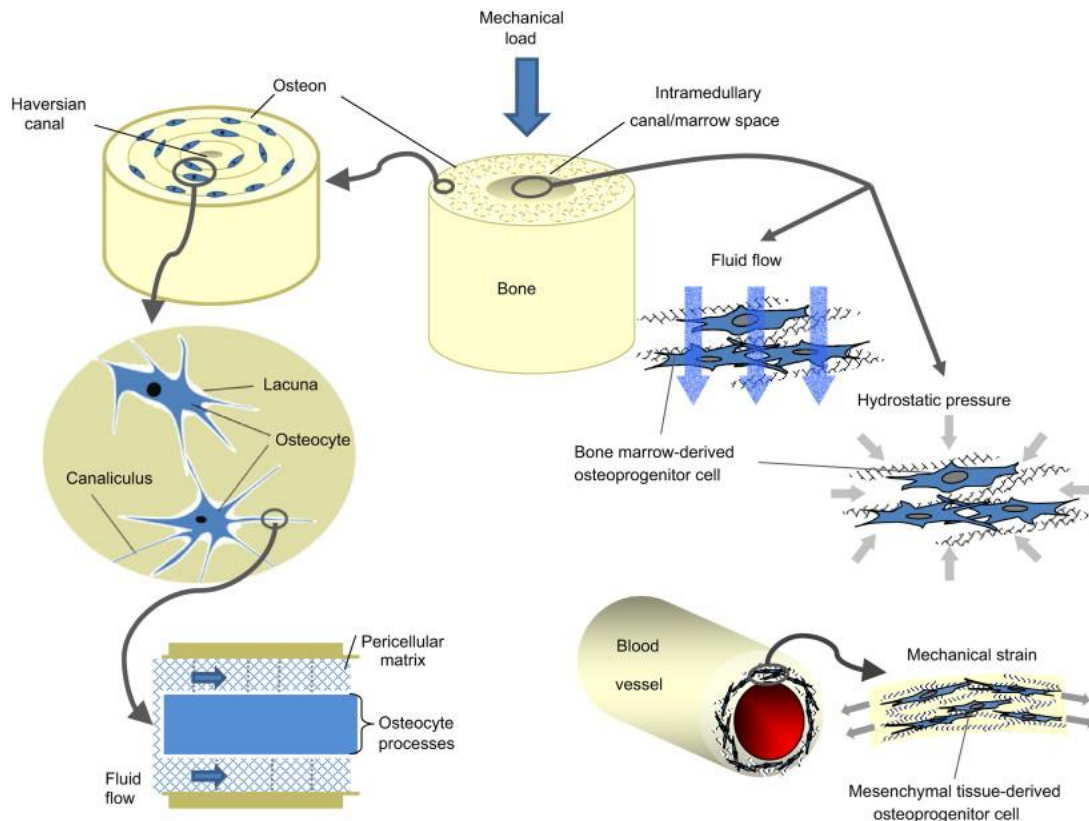


**Figure 1.14.2:** Schematic showing the anatomical area of osteocytes and osteoprogenitor cells in different areas. The figure on left side is a structure of cortical bone which has osteons arranged concentrically. An osteocyte locates in a lacuna and its processes connect with another osteocyte throughout the canaliculli. The space between the cells, lacuna, and canaliculli are filled with interstitial fluid. Fluid flow induced shear around the pericellular matrix could affect the biochemical response of the osteocyte. The figure on right side is a schematic of osteoprogenitor cells which locate in the intramedullary cavity and the mesenchymal tissues such as blood vessels (lower right corner). Fluid flow and hydrostatic pressure may affect the osteoprogenitor cells in intramedullary canal when bone deforms. The cells in mesenchymal tissues are subjected to the flow during the movement of tissues. Reprinted from (Chen et al., 2010) with kind permission of Elsevier.

### 1.15. Methods of mechanical stimulation

#### 1.15.1. Introduction

Bone is a dynamic organ able to adjust its architecture and resist physical forces. Mechanotransduction is a cell process which converts a mechanical stimulus into a cellular chemical response. The mechanotransduction mechanism of MSCs have been elucidated through both *in vivo* and *in vitro* studies by subjecting cells to various mechanical stimuli. The optimum conditions for mechanical stimulation such as amplitude, frequency, and duration are unknown. The MSC response to mechanical stimuli may also depend on the age of the donor, site of origin, stage of cell differentiation, and culture conditions. The cell culture environment, whether two-dimensional (2D) or three-dimensional (3D) affects the cells by affecting cell morphology, cellular matrix adhesion, cell migration, gene and protein expression, and mechanical response (Pedersen and Swartz, 2005). Three mechanical stimulation regimes which have been studied for osteogenic differentiation will be discussed here; compression, tension, and fluid flow induced shear stress.

#### 1.15.2. Compression

Cells will experience compressive strain when they are pressed by something. Two types of compressive loading which have been frequently studied are direct contact compression (Figure. 1.15.2 B) and hydrostatic pressure (Figure. 1.15.2 A). Hydrostatic pressure is an indirect contact pressure from the loading platform to the cells. The advantages of this pressure are simple to setup, homogenous pressure, no physical obstacle of the media to press the cells. The direct contact compression is a technique more close to the physiologic compression in the bone or cartilage. The side effects of the compressive pressure may produce a fluid shear stress from fluid moving in and out of the scaffold and nutrient transportation. Tanaka S. M. et al., (2005) suggested that the compression loading induce fluid flow was more influential than the direct strain created

by compressive loading. Compression loading can stimulate both osteogenic and chondrogenic differentiation in hMSCs (Chen and Jacobs, 2013). Studies by Saitoh et al., (2000), *in vivo*, showed that mechanical compression could stimulate cartilage formation in the mid-palatal suture by reprogramming MSC-like cells from osteogenic to chondrogenic. Orr et al., (2006) reported that the compressive strength could induce pressure gradients, resulting in stimulation of the interstitial fluid flow in the lacunar-canalicular space. In our group, Sittichokechaiwut et al., (2010), found that the short term of compressive cyclic loading and rest periods could enhance matrix production in hBMSCs in a 3D structure. These results also showed that compressive force on the scaffold could induce osteogenesis as well as dexamethasone (Dex).

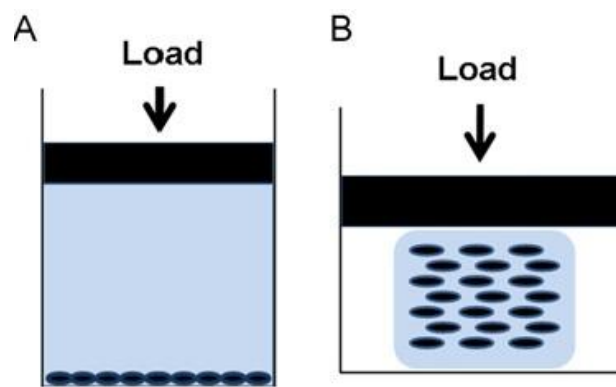


**Figure 1.15.2** : Schematic of typical compression loading patterns. (A) Hydrostatic pressure (or indirect contact pressure), (B) direct contact pressure. Adapted from Delaine-Smith and Reilly, (2011) with kind permission of Elsevier.

### 1.15.3. Tension

Tensional force arises by flexion of tendons or the muscle contraction pulling on bones. Cells will experience tension strain when they are stretched and their substrates also increase in length. The most two popular methods of tension which have been studied *in vitro* are uniaxial (or multi axial) grip tension (Figure. 1.13.3 B) and substrate bending (Figure. 1.15.3 A). Most studied involved cells seeded on flexible substrates. For example, the grips may be attached at the ends of a substrate and the cells seeded in the middle of the substrate. The cells are subjected to tensile strength when the substrates are pulled. In substrate bending, for example, the cultivated cells are subjected to tension strain when the substrates are bent by placing on two pivot points. The stretch can be; static or dynamic. For static stretch, the sample is held at a fixed strain for a period of time. For dynamic stretch, the sample is stretched cyclicly. Glucksmann A., (1942) and Takahashi et al., (2003) found that tensile stretch could transform a cartilaginous tissue into bone. Both tension stretch techniques may also create compressive stretch because of the Poisson effect which means contraction in the perpendicular direction to the direction of stretching. The cyclic tension may also applied fluid shear stress to the cells when the culture media moves over the cells. Cells seeded within a gel based scaffold (3D culture) which has mostly uniform deformation may receive the tensile loading homogenously. In contrast, a randomized fibrous scaffold on which cells attach in various directions on the fibres might receive heterogeneous strain.

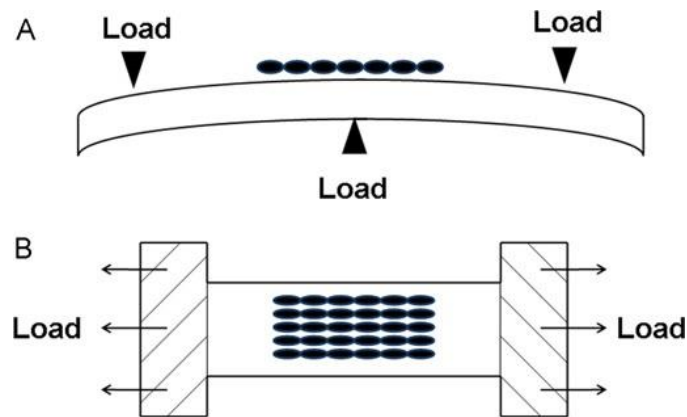


**Figure 1.15.3** : Schematic of typical tension loading configurations. (A) Substrate bending technique: The cells seeded on substrate are subjected to three point bending which results in tension strain on the convex surface. (B) Grip tension technique: The cells are seeded on substrate which is attached with the grip at the both end side. The substrate is pulled resulting in a uniaxial strain formation. Reprint from Delaine-Smith and Reilly, (2011) with kind permission of Elsevier.

#### 1.15.4. Fluid flow-induced shear stress

Fluid flow is the most widely used method of mechanical stimulation of osteocytes and osteoblasts. Several studies have shown that osteocytes and osteoblasts could respond to the fluid flow-induced shear stress similar to that is experienced in bone in the lacunar-canalicular system (Orr et al., 2006). Various apparatus configurations have been utilized to study the effect of shear stress on cells (monolayer '2D' culture). Typical apparatus that have been used include the cone and plate apparatus (Hermann et al., 1997), the parallel plate flow chamber (Li et al., 1996), the rotating disc apparatus (Reutelingsperger et al., 1994), the oscillatory orbital shaker system (Thomas et al., 2011), and oscillatory fluid flow (OFF) by using a standard see-saw rocking system (Zhou et al., 2010, Delaine-Smith et al., 2012). Firstly, the cone and plate apparatus comprises with a cone axis and a flat-plate for growing the cells. The fluid flow is homogenous relating to the velocity and the space between the cone and plate surface. The parallel plate flow chamber consists of two slits opening at the ends of a rectangular

chamber. A uniform laminar flow within a pressure gradient is created on the cell culture surface. See-saw rocking system comprises typical cell culture wells containing media placed on a standard see-saw rocker. The fluid flow relates to the speed, and flip angle of the rocker, in addition to the height, and viscosity of the culture media. The practical attractions of this apparatus include; simplicity of the apparatus, ease of culture media exchange, ease to monitor, both physically to visualize under a microscope, small volumetric culture media requirements, no special chamber requirement, and economical cost.

Various types of fluid flow have been studied including a unidirectional flow, divided into a steady perfusion and pulsatile flow, and oscillatory fluid flow. Pulsatile flow represents a typical continuous blood flow. Oscillatory flow represents the flow induced by the repetitive strain of tissue during locomotory (movement) activity. Steady perfusion has been reported to increase bone volume in 3D structures (Grayson et al., 2008). In addition, oscillatory fluid flow showed the ability to stimulate osteogenic differentiation and mineralization in both osteoprogenitor cells (hESMPs) with osteogenic induction medium and mature bone cells in monolayer (Delaine-Smith et al., 2012, Lim et al., 2013).

In 3D culture, it is difficult to quantify how much fluid flow are subjected to the cells. The cells arrangement on the scaffold may relate how much the fluid flow affects the cells (Figure. 1.15.4 A). Cells attached on a single layer on the scaffold surface may receive the similar experience as 2D culture on the parallel plate flow chamber (Figure. 1.15.4 B). However, the cells seeded on the hydrogel or bulk scaffold could transfer fluid flow to the cell surrounding structure similar to *in vivo* conditions (Delaine-Smith and Reilly, 2011).

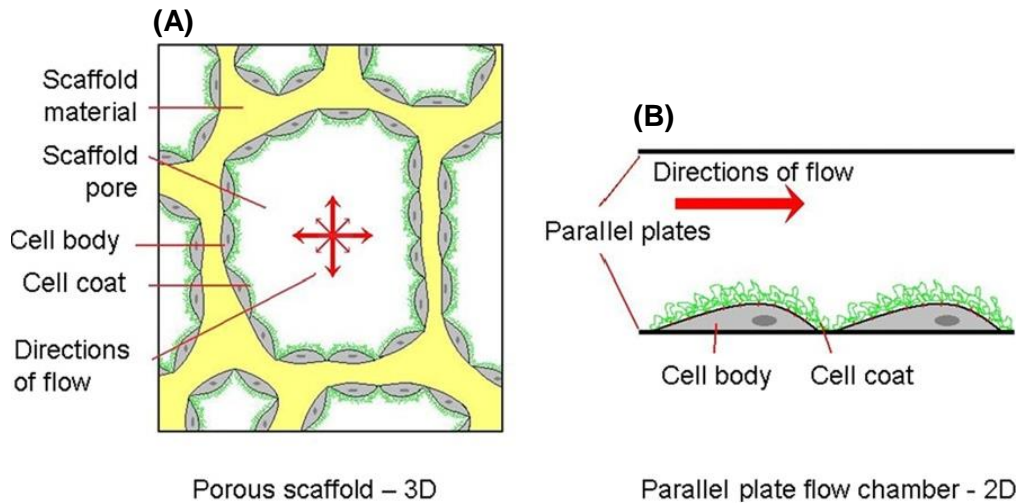


**Figure 1.15.4:** Schematic of fluid flow-induced shear stress the 3D culture (A) and monolayer '2D' culture (B). The directions of flow and flow magnitude in 3D culture are variable between regions. In contrast, the direction of flow in 2D culture is much more homogenous. Reprint from Delaine-Smith and Reilly, (2011) with kind permission of Elsevier.

### 1.16. Mechanical stimulation of osteoprogenitor cells in 3D culture.

Traditional cell culture on 3D scaffolds in static conditions, *in vitro*, leads to limitations such as providing non-homogenous nutrient and oxygen diffusion and eliminating waste products. *In vitro* studies, the distances between cells within the nonwoven polymer scaffold and the scaffold surface over which nutrients and oxygen can diffuse are around 100-200 $\mu\text{m}$  (Carrier et al., 2002, Volkmer et al., 2008). As a result there will be necrotic cells at the core and living cells at the outer shell of the construct over a long time in culture (McCoy and O'Brien, 2010). Recent studies showed a severe reduction in osteogenic differentiation and cell proliferation in 2% of oxygen condition compared with normal atmospheric oxygen, 21% of oxygen conditions (Malladi et al., 2006). To overcome these limitations of static culture, mechanical loading was introduced to enhance the quality of osteogenic differentiation and cell proliferation. Several

bioreactors were innovated for 3D constructs such as flow perfusion bioreactor (Datta et al., 2006), spinner flask (Mauney et al., 2004), cyclic compression (Sittichokechaiwut et al., 2010). These bioreactors showed an enhancement of osteogenic differentiation by osteoprogenitor cells. Therefore the mechanical stimuli influence the bone tissue engineering, *in vitro*. A porous scaffold with superior mechanical properties (able to withstand to load bearing) is ideal for bone tissue engineering when subjecting the construct to mechanical stimuli for enhancing osteogenic differentiation (McCoy and O'Brien, 2010).

### **1.17. Mechanical stimulation of MSCs**

MSCs differentiation can be stimulated *in vitro* under suitable conditions. The differentiation of MSCs into osteoblast has been extensively studied by adding chemical supplements or growth factors. This has previously been found that Dex may lead to osteonecrosis because of diminished stimulated VEGF secretion (Li et al., 2005). Therefore using Dex may not a desirable method for MSC implanted materials to be used clinic. Optional methods for the osteogenic differentiation of MSCs which withdraw the possible side effect of supplement additives are required. Therefore, external mechanical stimulation may be an optional method to overcome this problem. In physiological conditions, mechanical stimulation has an important role in the growth, development, and maintenance of cells and tissues with both differentiated and undifferentiated MSCs are mechanosensitive *in vitro*. Engler et al., (2006) found that MSCs can differentiation towards a specific lineage depend on the geometry and stiffness of their environment. However the mechanical properties of natural bone marrow environment have not been measured yet (Gurkan and Akkus, 2008). For tissue engineering, it is important to elucidate which regimes of mechanical stimulation will enhance bone matrix production and calcium deposition, *in vitro*. Moreover, MSCs could be pre-committed into a specific lineage by appropriate condition *in vitro*, which might overcome an inappropriate microenvironment *in vivo* (Engler et al., 2006).

### 1.18. Mechanotransduction

Mechanotransduction is a cellular mechanism which translates mechanical stimuli into the biochemical signals by using mechanosensitive receptors. This mechanism can be found in many types of cells such as osteocytes, osteoblasts and MSCs. Over the past decade studies have evaluated cellular mechanotransduction by several pathways. The effects of mechanical stimulation are translated via cellular components such as stretch-activated ion channels and G-protein coupled receptors in the cell plasma membranes. These cell components can respond when the cell membrane changes its shape. The result of this process is an influx of calcium and other ions into the cells (Figure. 1.18 a,h). The cell glycocalyx is a pericellular carbohydrate rich protein layer on the cell surface which is a potential sensor of external forces (Figure. 1.18 b). For example, on endothelial cells or in osteocyte's lacunar-canalicular system, the glycocalyx could respond to the fluid shear stress that moves over the cells to induce intracellular calcium influx and cyclooxygenase-2 (COX-2) gene expression. COX-2 is a critical enzyme for PGE<sub>2</sub> production during bone repair in both endochondral and intramembranous ossification (Einhorn, 2003) and osteopontin signalling (Reilly et al., 2003, Bonnet and Ferrari, 2010). Osteopontin is a glycosylated protein expressed in bone matrix. Its functions are to regulate cell proliferation and phagocyte activity in macrophages and to regulate mineralization in ECM (Sodek et al., 2000). Gap junction signalling also respond to external stimulations such as oscillatory fluid flow (Figure. 1.18 c). The effect of that stimulus is release of PGE<sub>2</sub> and up-regulation of osteopontin (Saunders et al., 2001, Schiller et al., 2001) which enhances the mineralization of bone cells *in vivo* (Yoshida et al., 2002).

Another part of mechanotransduction is the theory that integrin pulling causes cytoskeletal deformation. (Figure. 1.18 d,e). Integrins are transmembrane protein receptors which connect cytoskeleton filaments and ECM through focal adhesion (cellular junction between cell and ECM). The presence of tensile forces on cytoskeletal

is transferred to the nucleus membrane for activating ion-channels and changing DNA function (Ingber, 2006) (Figure. 1.18 g). Janmey and McCulloch, (2007) and Orr et al., (2006) reported that when cultured cell are exposed to fluid shear the magnitude of membrane deformation would induce a stress of only 0.1% of the shear stress applied in endothelial cell monolayer. They suggested that the physiological fluid flow was too small to stimulate stretch-activated ion channels. They necessary need the force enlargement to create strain. Some mechanical sensors may be more sensitive than the cell membrane or protrude into the ECM. One structure that projects from the cell membrane into ECM is primary cilium. Primary cilia have been found to respond to mechanical stimuli in many cells such as renal epithelial cells and osteocytes (Janmey and McCulloch, 2007). Hoey et al., (2012), reported that OFF could enhance mechanotransduction and mediate osteogenic differentiation in hBMSCs.

Osteoprogenitor cells responded to OFF by increasing intracellular calcium, producing nitric oxide (NO) and PGE<sub>2</sub>, activating mitogen-activated protein kinases (MAPKs) and ERK1/2, and regulating osteopontin gene expression (You et al., 2001). The activation of MAPKs and ERK1/2 will stimulate Runt-related transcription factor (Runx2) which is an important transcription factor for controlling osteogenic differentiation-related genes; such as ALP, OCN, bone sialoprotein, and collagen type I (Liu et al., 2010). OFF will increase intracellular calcium and is balanced by the released calcium from the (triphosphoinositol) IP<sub>3</sub> pathway from the storage organelles (Riddle et al., 2006). Osteopontin is a key factor at ECM involving bone cell attachment, regulation a late marker in osteogenic differentiation and mineralization (You et al., 2001, Bancroft et al., 2002).

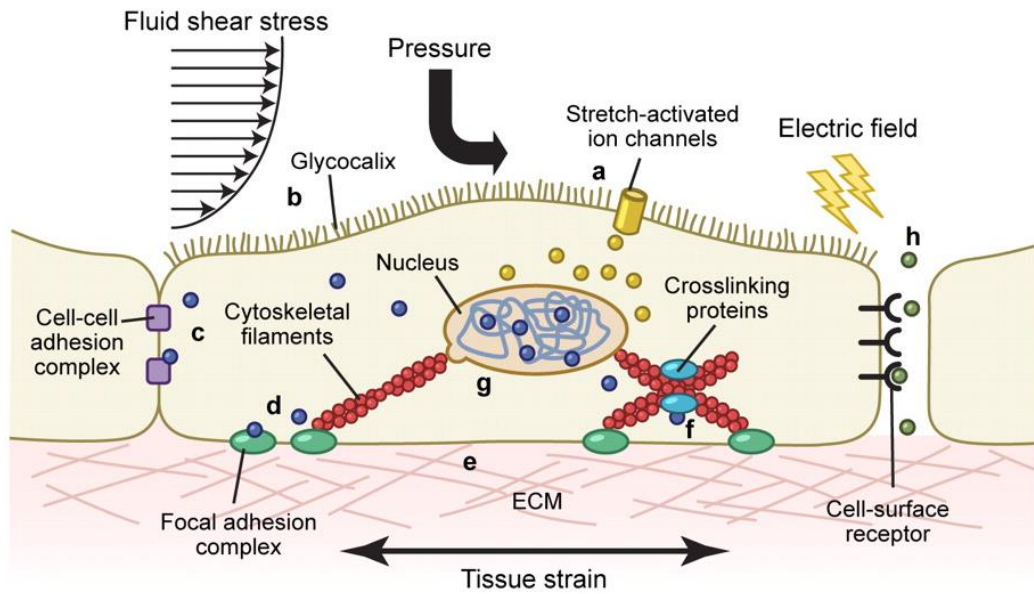


**Figure 1.18:** Schematic summarising the mechanotransduction of MSCs, osteoblasts, osteocytes and many other cells when fluid flow, pressure, or tissue strain is applied. Reprinted from Bonnet and Ferrari, (2010) with kind permission from Nature Publishing group.

### 1.19. Aims and objectives of research project

#### Hypothesis

The main hypothesis of the project is that tri-layer scaffolds seeded with human primary osteoprogenitor cells can be differentiated into osteoblastic cells on one side and fibroblastic cells on the other side. This strategy could be used in the future to fill the space in the roof of the mouth in patients with cleft palate.

#### Objectives

The objectives of my PhD project were to understand how to engineer bone tissue by selected cell sources, materials, and conditions for developing cleft palate repair. The combination of tri-layer scaffolds was in collaboration with another student who is selecting the soft tissue part. In our design the tri-layer scaffold can separate the two different cell types where one is human dermal fibroblastic cells (HDFs) and the other side could be human primary mesenchymal stem cells (hESMPs and hBMSCs). This method can allow normal facial development and decrease the surgical steps required to reconstruct the cleft palate. Therefore, from these objectives, the aims of this study were:

1. Evaluate suitable conditions to stimulate osteogenic differentiation of human mesenchymal progenitor cells including; hESMPs, hBMSCs, and HJPs.
  - 1.1 Suitable osteogenic media conditions will be selected to be used for stimulating osteogenic differentiation of HJPs.
  - 1.2 Various concentrations of Dex supplements for inducing osteogenic differentiation on hESMPs and HJPs will be tested.
  - 1.3 The effect of Dex on vascular endothelial growth factor (VEGF) secretion of the cell types will be determined.

- 2.** Finding the appropriate materials for the scaffold.
  - 2.1.** Appropriate scaffold materials will be selected by evaluating cell attachment, viability, and matrix mineralization.
  - 2.2.** The potential of a composite hydroxyapatite PCL electrospun scaffold (HA-PCL) to support cells will be investigated.
  - 2.3.** Both PCL and HA-PCL physical and mechanical properties will be characterized.
  - 2.4.** A suitable percentage of HA incorporated into PCL scaffold will be selected for osteogenic differentiation.
- 3.** Evaluate OFF stimulate osteogenic-progenitor cells.
  - 3.1.** The ability of OFF to stimulate osteoprogenitor cells (hESMPs, hBMSCs, and HJPs) in both the monolayer and 3D culture will be examined.
  - 3.2.** The effect of OFF on VEGF secretion of hESMPs and hBMSCs under monolayer and 3D culture will be evaluated.
- 4.** Study how a tri-layer scaffold separates two cell types on either side.
  - 4.1.** The osteogenic differentiation and also separation of osteoprogenitor cells (hESMPs and hBMSCs) on one side and HDFs cells on the other side at suitable times (28 days for culturing osteoprogenitor cells and 7 days for culturing HDFs) will be visualised.
  - 4.2.** The mineralization of the osteoprogenitor cells and the separation of co-culture will be evaluated using confocal fluorescence microscopy.

### CHAPTER TWO: MATERIALS AND METHODS

#### 2.1. Materials

1. Primary human dermal fibroblasts were isolated from skin donated by patients undergoing abdominoplasty or breast reduction under informed consent. (Ethical approval for the tissue acquisition was granted by the local ethical approval committee of the NHS Trust, Sheffield, UK). The tissue and isolated primary cells were stored in the Kroto Research Institute's tissue bank, University of Sheffield (License number 12179).
2. Primary human jaw periosteum cells were isolated from periosteum membrane which was donated by 2 patients undergoing maxillofacial operations who's periosteum was removed because of jaw fracture with informed consent. The periosteum was considered to be waste tissue in these operations. (Ethical approval for the tissue acquisition was granted by the local ethical approval committee of the NHS Trust, Sheffield, UK).
3. Human bone marrow mononuclear cells (Lonza<sup>®</sup>, Castleford, UK).
4. Human embryonic stem cell-derived mesenchymal progenitor hES-MP 002.5 (hESMP) cells (Cellartis, Gothenburg, Sweden).
5. Poly( $\epsilon$ -caprolactone) (PCL), 80kDa (Sigma, Dorset, UK) to produce electrospun scaffolds.
6. Polylactic-D-acid (PLA), 152kDa (Sigma, Dorset, UK) to produce electrospun scaffolds.
7. Polyhydroxybutyrate-co-polyhydroxyvalerate 8% (PHBV) in ratio PHB92:PHV8 (Goodfellow, Huntingdon, UK) to produce electrospun scaffolds.
8. Dichloromethane (Sigma, Dorset, UK) for dissolving polymers for electrosinning.
9. Nano-hydroxyapatite (HA) powder, particle size less than 200nm, 97% pure (Sigma, Dorset, UK).

## CHAPTER TWO

10. Human dermal fibroblasts basal culture media: Dulbecco's Modified Eagle's Medium (DMEM) (Biosera, East Sussex, UK) supplemented with 10% Fetal calf serum (FCS), 2mM L-glutamine (L-G) and 1% of 100mg/mL penicillin and streptomycin (P/S) (All products obtained from Sigma, Dorset, UK).
11. HJPs and hBMSCs basal culture media: Minimum Essential Medium Alpha Eagle ( $\alpha$ -MEM) (Lonza<sup>®</sup>, Castleford, UK) supplemented with 10% FCS, 1% L-G, and P/S.
12. hESMPs basal culture media: Minimum Essential Medium Alpha Eagle ( $\alpha$ -MEM) (Lonza<sup>®</sup>, Castleford, UK) supplemented with 10% FCS, 1% L-G and P/S, and 4ng/ml fibroblast growth factor-basic recombinant human (bFGF) (Invitrogen, Paisley, UK)
13. Fibroblastic media (FM): basal DMEM supplemented with 50 $\mu$ g/mL ascorbic acid-2-phosphate (AA) (Sigma, Dorset, UK).
14. Media with the supplements required for matrix mineralisation but NOT the osteogenic factor dexamethasone (Dex) was termed 'supplemented media' (SM): basal  $\alpha$ -MEM supplemented with 50 $\mu$ g/mL AA and 5mM  $\beta$ -glycerolphosphate ( $\beta$ -GP) (Sigma, Dorset, UK).
15. Dex containing osteogenic media (SM+Dex10, SM+Dex100): basal  $\alpha$ -MEM supplemented with 50 $\mu$ g/mL AA, 5mM  $\beta$ -GP, and either 10nM or 100nM Dexamethasone (Dex) (Sigma, Dorset, UK), respectively.
16. Trypsin-EDTA (Sigma, Dorset, UK).
17. Porcine gelatine (Sigma, Dorset, UK).
18. Phosphate buffered saline (DulbeccoA) (OXOID Limited, Hamshire, England ).
19. Collagenase from *Clostridium histolyticum* (Sigma, Dorset, UK).
20. Dimethyl Sulfoxide (DMSO) (Sigma, Dorset, UK).
21. DNaseI (Stemcell<sup>®</sup>, France).
22. Trypan blue dye (Sigma, Dorset, UK) for detecting dead cells.
23. MTT (3-(4,5-Dimethylthiazol-2-yl)-2,5-diphenyltetrazolium bromide) cell viability assay (Sigma, Dorset, UK).

## CHAPTER TWO

24. MTS (3-(4,5-dimethylthiazol-2-yl)-5-(3-carboxymethoxyphenyl)-2-(4-sulfophenyl)-2H-tetrazolium) (CellTiter 96<sup>®</sup> Aqueous Non-radioactive Cell Proliferation Assay) (Promega, Southampton, UK).
25. DAPI (4'-6-Diamidino-2-phenylindole) (Sigma, Dorset, UK) at 1mg/mL
26. Phalloidin-TRITC (Phalloidin-Tetramethylrhodamine B isothiocyanate) (Sigma, Dorset, UK) at 0.5mg/mL
27. Live/Dead staining: Live-cell SYTO<sup>®</sup> 9 (Life technologies, Paisley, UK) and dead cell Propidium Iodide (Molecular Probe<sup>®</sup>, Oregon, US)
28. Picro-Sirius red stain: at 1mg/mL direct red dye and saturated Picric acid (Sigma, Dorset, UK) for collagen staining.
29. Alizarin red staining (Sigma, Dorset, UK): at 1mg/mL diH<sub>2</sub>O, pH 4.2, for calcium staining.
30. Xylenol Orange tetrasodium salt (Sigma, Dorset, UK): at 20 $\mu$ M in culture media for labelling mineralized nodules.
31. Quant-iT<sup>™</sup> PicoGreen<sup>®</sup> dsDNA Reagent assay Kits (Invitrogen<sup>™</sup>, Paisley, UK) for total cellular DNA quantification.
32. Alkaline Phosphatase Yellow (pNPP) Liquid Substrate System for ELISA (Sigma, Dorset, UK) for quantitative determination of cellular alkaline phosphatase (ALP) activity.
33. Human VEGF standard ELISA Development Kit (PeproTech<sup>®</sup>, London, UK) for measuring of VEGF secretion in cell culture supernatants.
34. 2,2'-Azino-bis(3-ethylbenzothiazoline-6-sulfonic acid) (ABTS) liquid substrate (Sigma, Dorset, UK) for colour developing in VEGF quantification assay.
35. Formaldehyde (37%, grade 1 for SEM) (Sigma, Dorset, UK).
36. Hexamethyldisilazane (HMDS) (Sigma, Dorset, UK) for SEM.
37. Human mesenchymal stem cells multi-color flow cytometry kit contained four different antibodies conjugated fluorochromes [CD146 conjugated with carboxyfluorescein (CFS), CD90 conjugated with allophycocyanin (APC), CD105

## CHAPTER TWO

conjugated with peridinin chlorophyll protein complex (PerCP), and CD45 conjugated with phycoerythrin (PE)] and their isotype controls for each antibody (R&Dsystem, UK).

38. Brilliant Violet 421™ anti-human CD105: CD105 conjugated with Brilliant Violet (BV) and its isotype control (BioLegend, US)

39. Microcentrifuge tube (Eppendorf, Hamburg, Germany)

40. PBS without calcium (Ca<sup>2+</sup>) and magnesium (Mg<sup>2+</sup>) (Sigma, dorset UK)

41. Non-enzymatic cell diassociation solution (Sigma, dorset UK)

42. Compensation particles (BD™ CompBeads, Oxford, UK)

43. BD LSRII flow cytometer (BD Biosciences, UK) (the Mellanby Centre, Medical school, University of Sheffield).

44. Electrospinning apparatus consists of a syringe pump (Genie™ Plus, Kent Science, USA), a high voltage electric source (Genvolt, UK), a rotating motor (Heidolph Instrument, Germany).

45. BOSE ElectroForce 3200 (ELF3200) for mechanical testing (ElectroForce System Group, BOSE, Minnesota, USA)

46. Standard see-saw rocker (STR6) (Stuart equipment, Staffordshire, UK) for producing oscillatory fluid flow.

47. Spectrophotometer (ELx800, BioTek, UK)

48. FLx800 microplate fluorescence reader (BioTek, UK)

49. ImageXpress™ is an epifluorescent microscope (Axon Instrument, Inc., UK)

50. Zeiss Axiokop 2 FS MOT laser-scanning confocal microscope (upright) provided with LSM 510 Meta detector (Carl Zeiss MicroImaging GMBH, Germany)

51. Chameleon Ti:sapphire tunable (700-1060nm) multiphoton laser (Coherent, CA, USA)

52. Argon/2 laser with wavelength 488nm (LSM 510 laser module, Carl Zeiss, Germany)

53. HeNe laser with wavelength 543 nm (LSM 510 laser module, Carl Zeiss, Germany)

## CHAPTER TWO

54. EC-plan-Neofluar objective with magnification 20X (Carl Zeiss, Germany)
55. Ziess LSM Image Browser software package (Carl Zeiss, Germany)
56. Scanning electro microscope (SEM, Philips XL-20 SEM, Netherlands)
57. Micro-computed tomography (micro-CT) (Skyscan 1172, Kontich, Belgium) (the Mellanby Centre, Medical school, University of Sheffield) for quantifying bone volume.
58. X-ray diffractometer (XRD) D500 Diffractometer (Siemens, Germany)
59. X-ray photoelectron spectroscopy (XPS) (Axis Ultra DLD spectrometer) (Kratos Analytical, UK)
60. Casa XPS software (Casa Software Limited, Devon, UK) for processing XPS spectra.
61. Photoacoustic Fourier transform infrared spectroscopy (PAS-FTIR) (Nicolet Nexus 8700 FT-IR, Thermo Fisher Scientific Inc, USA)
62. Omnic 7.4 software (Thermo Scientific, UK) for processing PAS-FTIR spectra.
63. Medical grade steel ring (2cm diameter, 1.2cm inner hole diameter) (produced by NHS medical workshop) for seeding cells and immobilizing cell in the cell culture medium during experiment.
64. Medical grade stainless steel dental wire (0.8mm diameter) (OthoCare<sup>®</sup>, Bradford, UK) for immobilizing and flattening scaffold in the culture medium during experiment.
65. CellCrown<sup>™</sup> (made from polyethylene terephthalate: PET) (Scaffdex<sup>®</sup>, Tampere, Finland) for seeding cells and immobilizing cells in the cell culture medium during experiments.
66. Laboratory digital balance (Mettler toledo, UK)
67. Image processing software: image analysis and processing in Java-base (ImageJ) (developed by National Institutes of Health, USA)
68. Image processing software: LSM Image Browser (downloaded from Carl Zeiss microscopy)

69. Image processing software: CT-Analyser (CTAn) (kindly obtained from Dr Les Coulton, the Mellanby Centre, Medical school, University of Sheffield) for measuring the percentage of bone volume.

70. Image processing software: CT-Volume (CTVol) (kindly obtained from Dr Les Coulton, the Mellanby Centre, Medical school, University of Sheffield) for constructing visual model.

71. Data analysis software: GraphPad Prism6, SPSS (Statistic 21, IBM)

72. Graphic program: Adobe Photoshop (Developed by Adobe System) for arranging graphs and images.

### **2.2. Methods**

#### **2.2.1. General cell culture conditions**

Cells were grown in T-75 flasks and cultured by using the appropriate basal culture media at 37°C in 5% CO<sub>2</sub> and a humidified atmosphere. The cells were observed daily for cell morphology, colour of the medium, and cell density. The medium was changed every 2-3 days. Passages were performed when cells reached 80% confluency. To begin with, the medium was removed and washed twice with PBS; 2.5ml of trypsin-EDTA solution was used to enzymatically release the cells from the old tissue culture plate. The enzyme was stopped by using a fresh basal culture media. Cell suspension was centrifuged at 1,000 revolutions per minute for 5 minutes. The supernatant was removed and a known volume of the basal culture media was added. The cell pellet was resuspended in 1ml medium, 40µl of cell working solution was mixed with another 40µl of trypan blue dye. A number of cells were counted by using a hemacytometer. Finally, a minimum 10<sup>5</sup> cells were transferred to a new flask or seeded onto samples. Cryopreservation of cells for future experiments used DMSO as a cryoprotectant at 10% final concentration in FCS. The cells were transferred to a cyrovial and stored at -80°C for one day and then moved to -196 °C the next day for long term storage.

Culture condition	Compositions
SM	basal $\alpha$ -MEM supplemented with 50 $\mu$ g/mL AA and 5mM $\beta$ -GP.
SM+Dex10	basal $\alpha$ -MEM supplemented with 50 $\mu$ g/mL AA, 5mM $\beta$ -GP, and 10nM Dex
SM+Dex100	basal $\alpha$ -MEM supplemented with 50 $\mu$ g/mL AA, 5mM $\beta$ -GP, and 100nM Dex

**Table 2.2.1:** Complete list of culture conditions on both monolayer and 3D cultures.

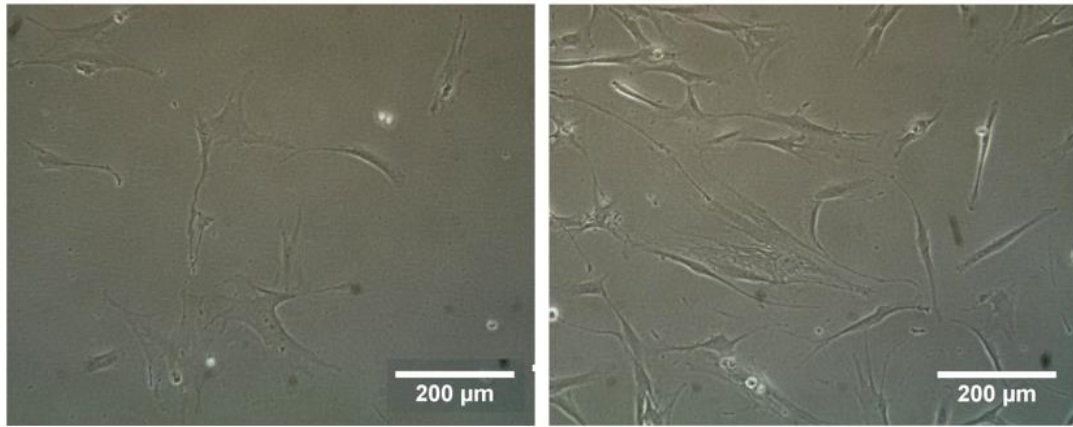
### 2.2.2. Human dermal fibroblasts (HDFs)

The cells were kindly provided by Julio Bissoli (Kroto Research Institute, the University of Sheffield). Briefly, the cells were extracted from dermis layer of skin where dermal fibroblastic cells are found. Firstly, the harvested skin were removed from the epithelium layer and then mechanically separated from the dermis tissue. They were then added to 10-15ml of collagenase A solution overnight at 37 °C for dissociating the tissue. The working solution was washed with PBS to remove the collagenase, following with centrifugation at 2000 rpm for 10 minutes to obtain a cell pellet. The cell pellet was resuspended and placed into T-25 flasks. The first culture following the cell isolation was called the primary culture (or passage 0, P0). The unattached cells were removed from the flasks and the remaining cells that were attached onto the flasks were subcultured by dividing 1:10 dilutions for passaging. These cells were called a secondary culture (or passage 1, P1). The cells that were used for experiments from passage 2 to 8 to ensure their initial functions were maintained.

### 2.2.3. Human jaw periosteal cells (HJPs)

Human jaw periosteum consists of three-layers; the inner layer is called cambium layer which contains osteoprogenitor cells; the following layer contains mostly fibroblastic

cells and the outer most layer contains mainly collagen fibres. The periosteum tissues were harvested from the upper (maxilla) or lower (mandible) jaw of two patients undergoing maxillofacial treatment in the University of Sheffield, Dental School; with informed consent. The periosteum tissues were stored in the  $\alpha$ -MEM basic culture media, at 4°C for less than 24 hours before they underwent cell isolation. The periosteum tissues were control bacterial contamination with 1% of 100 mg/ml P/S in PBS, then mechanically separated into smaller tissue pieces. They were added to 0.25% collagenase type II and incubated at 37 °C for 3 hours (Samee et al., 2008). The working solution was resuspended with  $\alpha$ -MEM basic culture media; centrifuged at 2000 rpm for 5 minutes to obtain cell pellet, the supernatant was then emptied to remove the collagenase. The cell pellet was resuspended and placed into T-25 flasks and 2ml of fresh basic culture media was added to the flasks every 2-3 day for 7 days. After 7 days the old culture media and non-adherent cells were removed. The adherent cells are expected to be MSCs, under basic culture media (Dominici et al., 2006, Chao et al., 2012). It has been suggested that HJPs can be used between passages 3 to 10 (De Bari et al., 2006), however, cells were only used between passages 3-8 for all experiments. From studies comparing DMEM and  $\alpha$ -MEM as suitable basal culture media for HJPs; the HJPs cultured in  $\alpha$ -MEM showed better cell proliferation than those cultured in DMEM. Therefore  $\alpha$ -MEM was used for all HJP experiments. The HJPs morphology obtained from 2 donors exhibited 2 different cell shapes; HJPs-1 cell morphology was more cuboidal shape, while HJPs-2 was spindle cell shaped (Figure. 2.2.3).

**A. HJPs-1****B. HJPs-2**

**Figure 2.2.3:** Phase contrast images of the HJPs cells from two donors on day 7 of culture. (A) The cell morphology of HJPs-1 shows a distinct cuboidal cell shape. (B) The cell morphology of HJPs-2 shows a spindle cell shape similar to fibroblast-like cells. Images captured by author. Scale bar = 200 $\mu$ m.

#### 2.2.4. Human mesenchymal stem cells from bone marrow (hBMSCs)

The bone marrow mononuclear cell samples were purchased from a registered company (Lonza<sup>®</sup>) for each of the 3 donors. The samples consisted of hematopoietic cells and MSCs. MSCs are isolated based on their ability to adhere to plastic tissue culture dishes (Chao et al., 2012, Dominici et al., 2006). To receive maximum yield of the MSCs from the frozen cell samples; the cell samples were placed in a distilled water bath at 37°C until the last ice crystal melted. The cell solutions were transferred to pre-warmed basal culture media containing 0.1mg/ml DNaseI. The viable cells were counted by using a hemacytometer and trypan blue dye. The dead cells were presented as dark blue in contrast to the live cells and were therefore excluded. The cells were plated at a density of  $1.25 \times 10^5$  cells per  $\text{cm}^2$  in T-25 flasks. 2ml of fresh basic culture media was added to the samples every 2-3 day for 7 days. Non-adherent cells were removed and replaced by fresh culture media. The adherent cells which were fibroblast-like cells showed a number of fibroblastic colony forming units (CFU-f) (Figure. 2.2.4). The cells from this stage were called passage 0 and were cultured until reaching 70-80% confluence. The

adherent cells were detached from the flasks with Trypsin-EDTA and were re-plated at a density of  $4 \times 10^3$  cells per  $\text{cm}^2$  in T-75 flasks. The cells were serially sub-cultured up to passage four for experiments (Lee et al., 2013).

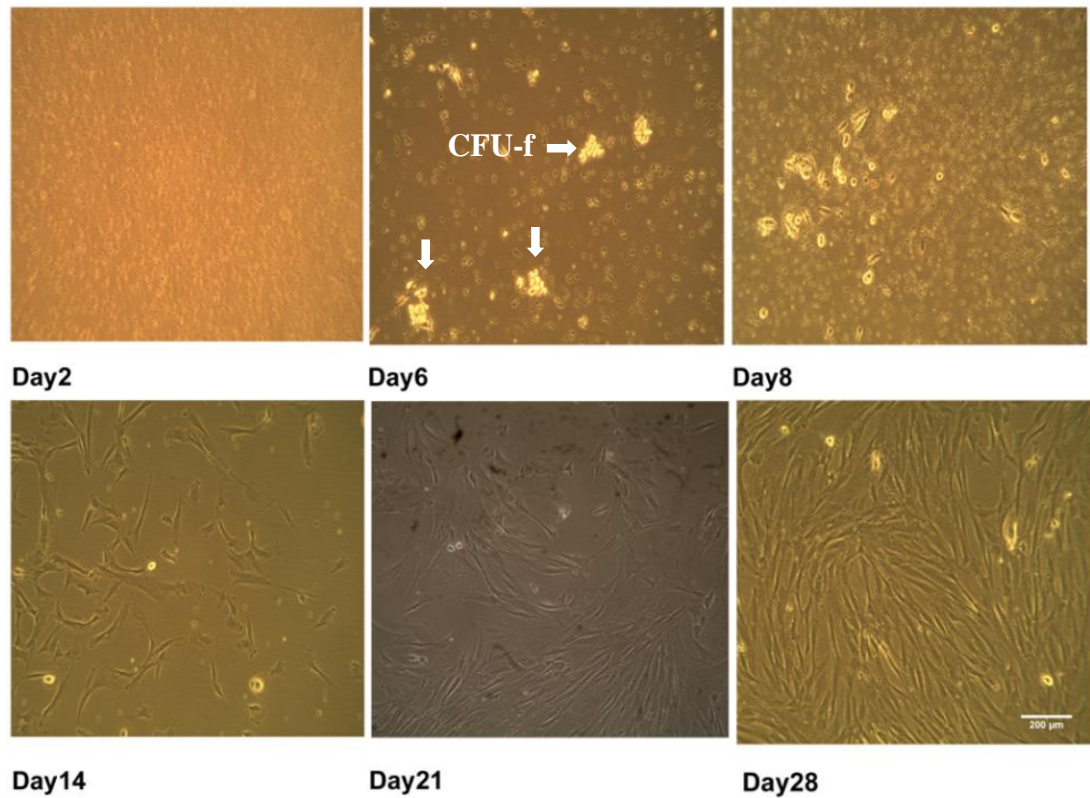


**Figure 2.2.4 :** Phase contrast images present the adherent cells of human MSCs which are fibroblast-like cells and form fibroblastic colony forming units (CFU-f) over 28 days. Scale bar is 200μm.

### 2.2.5. Cell characterization

The Mesenchymal and Tissue Stem Cell Committee of the International Society for Cellular Therapy suggested the criteria to clarify cells as MSCs that 1] MSCs must adhere to plastic tissue culture surface under a standard culture condition, 2] MSCs showed express the surface antigens (Ag); CD 73 (known as an ecto 5' nucleotidase), CD 105 (known as an endoglin), CD 90 (known as a Thy-1), and CD 146 (known as a melanoma cell adhesion molecule: MCAM) (Tormin et al., 2011), and lack expression

of the surface antigens; CD 45 and CD 34 which normally indicate hematopoietic stem cells (Ogata et al., 2005), and CD 14 (known as monocyte and macrophage markers) (Zieglerheitbrock and Ulevitch, 1993) by using flow cytometry, “CD” is an abbreviation for cluster of differentiation (Boxall and Jones, 2012), 3] MSCs are be able to differentiate to chondroblasts, adipocytes and osteoblasts (Dominici et al., 2006).

Flow cytometry is a method for identification and characterization of MSCs. It is used to characterise cell properties, count cells, sort cells, and identify biomarkers. It allows each cell to be characterised and sorted from a heterogenous cell mixture depending on the specific proteins on the cell that are labelled with fluorescent antibodies. The usefulness of this method is that it is fast, objective and quantitaive record of fluorescent signal from individual cells and can physically separate the cells of interest.

The cells cultured in the T-75 flasks were removed from the culture media and washed with PBS without calcium ( $\text{Ca}^{2+}$ ) and magnesium ( $\text{Mg}^{2+}$ ). 6 ml of non-enzymatic cell diassociation solution was added and incubated at 37°C and monitored to detach cells from the flask. This was followed by neutralising with basal culture media and centrifuging at 1000 rpm for 5 minutes. The supernatant was removed and 1 ml of FACS solution (0.1% BSA, 0.1% sodium azide in PBS solution) was added to resuspend and count the cells. The desired cells were divided into the microcentrifuge tube, centrifuged, and the supernatant removed. The following tabulated list of all components for analysing all types of MSCs which have been used in all experiments (hESMPs, HJPs, and hBMSCs) (table 2.2.5 A). Then they were incubated at room temperature for 45 minutes under dark environment.

Conditions	Staining buffer (µl)	Primary antibody (µl)	Isotype control antibody (µl)	Excitation and emission (nm)
Unstained	50	0	0	
All Isotypes	30	0	5 µl X 4 Isotypes	
CD90/APC	45	5	0	660/20
CD105/BV	45	5	0	450/50
CD146/ CFS	45	5	0	530/30
CD-45/PE	45	5	0	575/26
All antibodies	30	5 µl X 4 antibodies	0	

*Table 2.2.5 A: Complete list of components and experiment parameters for MSCs characterization of hESMPs, HJPs, and hBMSCs by using FACS.*

For each experiment, anti-rat Ig,  $\kappa$ -chain and negative control CompBeads™ particles were stained with the corresponding fluorochrome-stained antibodies. Compensation particles were used to optimize the setting of fluorescence compensation for analysing with multicolour flow cytometry. The advantages of the compensation particles are that they provide more accurate results and reduce overlap from the combination of fluorescence-stained antibodies.

The staining process followed the company instructions briefly; 100µl of staining buffer was added into a microcentrifugation tube. One full drop (approximate 60µl) of the CompBead™ anti-rat Ig (positive particles) and the other full drop of the negative control particles were added into each tube and vortexed. 10µl of primary antibody was added to the tube, and incubated for 30 minutes at room temperature in a dark environment. 1ml of FAC buffer was added to each tube and vortexed. All samples including the cells and the CompBead™ were centrifuged at 6000 rpm for 2 minutes

and the supernatant removed. 300 µl of FACs buffer solution was added to each tube and kept at 4°C, under dark environment.

Conditions	Staining buffer (µl)	Primary antibody (µl)	Excitation and emission (nm)
Unstained	100	0	
CD90/APC	90	10	660/20
CD105/BV	90	10	450/50
CD146/ CFS	90	10	530/30
CD-45/PE	90	10	575/26

*Table 2.2.5 B: Complete list of components and experiment parameters for CompBead™ characterization of control compensation particle set by using FACS.*

The stained CompBead™ and negative control particles were analyzed on a BD LSRII flow cytometer with 4 lasers as 355, 405, 488, and 633 nm. Using excitation and emission setting as listed in table 2.2.5 B compensation was adjusted automatically using the BD FACS Diva acquisition software. Then, the samples were analysed using the same settings. Data of flow cytometry data were analysed as geometric means of fluorescence intensity.

### **2.2.6. Cell culture in monolayer**

In the monolayer experiments (termed ‘2D’) cells were detached from T-75 flasks, and counted to calculate cell number. The determination of cell number and volume of media depended on the length of experiment, cell shape, and size of cell culture well plate. The required cell and culture media volumes were mixed into one container and were resuspended to ensure even distribution. They were then divided into individual cell

culture wells. Sterile 0.1% Gelatin in PBS was precoated on the well plate half an hour before cell seeding to enhance cell attachment of the hESMPs.

### **2.2.7. Electrospinning rig set up**

Polymer electrospun scaffolds were created from a specific polymer concentration in a suitable solvent as detailed in chapter 5. A polymer solution was made by dissolving in either dichloromethane (DCM) or a mixture of DCM and methanol. The solutions were left on a magnetic stirrer plate overnight to ensure homogeneity. The electrospinning apparatus was set up as seen in (Figure. 1.10.4). Scaffolds were synthesized at 17 kV, with a flow rate of 40 $\mu$ l/min, a working distance of 17 cm, and a drum rotation speed of 300 rpm. The solutions were released by 4 needles (0.6 mm internal diameter) to the rotating drum, ground collector. The collector was covered with aluminum foil to support a fibrous sheet. After emptying the polymer solution in the syringes, the fibrous sheets were moved to a vacuum at room temperature for 24 hours to allow any excess solvent to evaporate. The fibrous sheet was then stored in a self-sealed plastic bag at 4°C and used within 6 months.

### **2.2.8. Physical characterisation**

#### **• Electrospun scaffold without cells**

The morphology of electrospun scaffolds was observed and their morphologies were analysed by measuring fibre diameter by SEM from two different sample batches. The SEM is an electron microscope which can visual the surface topography and composition of the samples. SEM has a wide range capacity of magnification from 10 to 500,000 times while a light microscope has a limitation of magnification of only 250 times. The scanning process begins with an electron gun emitting the electron beams to interact on the sample surface. The secondary electron beams are released and detected by the special detectors.

The scaffold sample was cut into a 10 mm diameter circle shape and mounted onto a specimen stub using an electrically conductive double sided adhesive tape. The scaffolds were sputter coated with an gold ultrathin layer because the sample surface must be electrically conductive to avoid electrical charge. The sample was visualised with accelerating voltages of 20kV and spot size of 3.0.

### • **Electrospun scaffolds with cells**

The sample for visualising by SEM was required to be completely dry due to the SEM chamber being under high vacuum. A living cell sample was removed from culture media and washed with PBS 3 times (5 minutes each) and fixed with 10% formalin in PBS for 20 minutes at room temperature to preserve the cell structure. A dehydration step was undertaken to replace water in the cells with ethanol. The sample was submerged in the following series: 35%, 60%, 80%, 90% of ethanol in distilled water, and 100% ethanol for 15 minutes at each concentration. Following this, the solution was replaced with HMDS as a drying agent by submerging the sample in 1:1 ethanol and HMDS solution for 1 hour and subsequently rinsing with 100% HMDS for 5 minutes twice. The sample was then removed and left to dry in a desiccator for at least 1 hour, the sample was stored in a dry and clean place until coated with the gold layer and visualised.

Scaffold porosity was calculated by determining the density of the scaffold and the density of the bulk material. To determine the scaffold density, the scaffolds were cut into 1cm<sup>2</sup> squares, the thickness measured with a micrometer, and the weight determined using a laboratory analytical balance, which can measure mass in the sub-milligram range, to determine the scaffold volume. The scaffold porosity was calculated using the following formula:

$$\varepsilon = (1 - \rho/\rho_0)*100$$

(where  $\rho$  refers to the density of scaffold and  $\rho_0$  refers to the density of the bulk material)

### • Mechanical characterisation

The mechanical characteristics of electrospun scaffolds was determined by using a BOSE ELF 3200 with WinTest 4.1 software package. The scaffold was cut into cylindrical shapes, 5 mm in width and 12 mm in length. The scaffold was gripped at both ends of the sample with 6 mm guage length and strained until the maximum deformation was 6mm (100% strain). The force was recorded using a 22 N load cell. Both the force and displacement results were plotted to generate a stress against strain graph. The graph was used to determine the Young's modulus of elasticity and the yield strength of each scaffold.

Young's modulus is a ratio of stress divided by strain in the elastic region of the stress against strain curve. The elastic region where the material can return to its initial shape after the strain has been removed, this value represents the stiffness of the material. Yield strength is the first stress point at the which material begins plastic deformation. The yield strength is the maximum point on the curve after the region of elastic deformation. Ultimate (tensile) strength is the maximum point of stress which begins as the material show a necking shape before the material is broken.

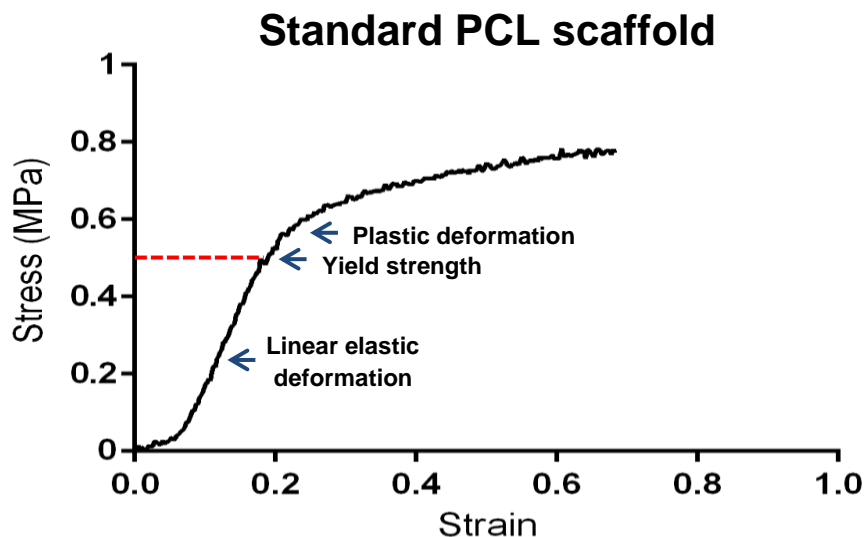


**Figure 2.2.8:** The stress-strain curve of the standard electrospun PCL scaffold. Young's elastic modulus of elasticity can be determined from the gradient of the maximum slope in the elastic region. Linear elastic deformation is the recoverable deformation region and its slope is the Young's Modulus. Yield strength is the stress point when the sample initially deviated after the elastic region. Plastic deformation is the permanent deformation that occurs after yield.

### 2.2.9. Hydroxyapatite characterisation

#### • X-ray Diffraction (XRD)

XRD is a crystal analytical technique that does not destroy the sample. The data obtained includes a chemical composition, morphology, and crystal structure by using the principle of Bragg diffraction. W. L. Bragg and W. H. Bragg in 1913 explained that the crystal structures arrange in the parallel planes which have a specific distance. The incident x-ray beams at a specific angle could produce the intense peak of reflected beams. The Bragg's law formula is:

$$n\lambda = 2d\sin\theta$$

(Where  $n$  refers to integer,  $\lambda$  refers to the incidence wavelength,  $d$  refers to the distance between the parallel planes in the crystal structure,  $\theta$  refers to the angle between the incidence radiation and the crystal parallel plane).

XRD could determine a sample in either a thin film or a powder. An intense peak reveals where the particular atoms are arranged in the structure and the data is compared

with known standard data. Moreover, this technique may quantify the amount of atoms and the crystalline size of the sample. However, the limitations of XRD are single crystal determination and the length of particle size for analysing must be between 0.1 $\mu\text{m}$ -40 $\mu\text{m}$ .

The sample was flattened on the holder and measured by a x-ray diffractometer using copper K-alpha (Cu K $\alpha$ ) radiation ( $\lambda=1.54(\text{A})$ ) at 40kV and 30mA to obtain the data. The range of  $2\theta$  between 25° to 35° was measured with at a scan speed of 0.1 degrees per minute (Ishikawa et al., 1993). The data was compared with a known standard graph to identify the sample component.

### • **Fourier transform infrared spectroscopy (FTIR)**

FTIR is a chemical component analytical technique that is widely used in biomaterials. This technique can identify the presence of functional groups in a sample molecule. Mostly the biomaterials are opaque which obstructs analysis of the material with a direct transmission analysis in the mid-infrared regions (Rehman and Bonfield, 1997). Reduction in material density can change the original material components. An alteration in the infrared (IR) wavelength from mid-IR region to near-IR region which avoids the opaque side effect of materials may limit the obtained data, therefore photo-acoustic sampling (PAS)-FTIR may be used as a solution to these problems. The principle of this technique is that a specific frequency of IR beams are absorbed when they equal the vibrational frequency of a molecular bond in the sample. Subsequently they are converted into heat and diffused to the sample surface and the surrounding environment. A gas thermal expansion generates the PAS signal which could be identified by the detector (Rehman and Bonfield, 1997). Advantages of this technique are that there is no sample preparation, and there is more depth of detection than any other FTIR technique.

The sample was scanned in the sample chamber of the PAS cell which was purged with dry helium gas. The obtained spectra was recorded in the IR range between 400-4000

$\text{cm}^{-1}$  at  $8 \text{ cm}^{-1}$  resolution with 128 scans. The carbon black specimen was scanned for calibration before scanning the sample and the received data were processed using Omnic 7.4 software package.

### • X-ray photoelectron spectroscopy (XPS)

XPS is a chemical analysis technique of the surface of material to reveal a chemical elemental composition and an empirical formula. A sample is irradiated with x-ray beams resulting in electrons being released to the ultra-high vacuum chamber. An electron detector measures the electron binding energy (y-axis) which represents the specific element and the number of released electrons which represents the amount of elements on the sample (x-axis). The limitation of this technique is that it is not suitable to analyse samples which contain water as water might evaporate and change the material structure during the reading.

The obtained XPS data were used an Axis Ultra DLD spectrometer. The material surface was scanned at 160eV pass energy, 1eV step size from 1200 to -5eV to reveal the XPS spectra. The data was determined using Casa XPS software. The sample scans were performed in duplicate.

### 2.2.10. Scaffold preparation

A day before experiments began, scaffolds were cut into either a circular shape by using a circular cork borer (15mm diameter) or an elliptic shape (15mm in width and 35mm in length) (Figure. 2.2.10.1 A) by using a scalpel blade. The scaffold mat was wrapped with aluminium foil. A template was drawn with pen on the cover of the aluminium foil and then cut with a scalpel blade. The appropriate sized scaffolds were soaked with PBS to increase the hydrophilicity of the scaffold. The scaffolds were sterilised with 0.1% peracetic acid in PBS under steady rocking conditions for 3 hours. Peracetic acid is an anti-microbiological agent and has therefore been used to sterilise scaffolds; however a side effect of peracetic acid can be damage the nano-HA particles on the scaffold (Kim et al., 2006a). Therefore in experiments where HA scaffolds were used all scaffolds

## CHAPTER TWO

(HA containing and control polymer scaffolds) were sterilised with 80% ethanol in distilled water for 2 hours. After sterilisation, the scaffolds were washed three times with PBS, left for 5 minutes in each wash to ensure the removal of either the peracetic acid or ethanol remaining. Two different scaffold immobilizers were used during cell culturing; a customised bended medical grade stainless steel wire (Figure. 2.2.10.1 C) and a CellCrown™ application (Figure. 2.2.10.2 A). The steriled CellCrown™ and scaffold were assembled and submerged overnight in the basal culture media which contained FCS to enhance cell attachment, under sterile and room temperature condition (Figure. 2.2.10.2. B-D). For the wire-held group, the scaffolds were placed in a 12-well plate and stainless steel rings were placed on top; 1mL of basal culture media was added to each well and left overnight to allow for serum protein attachment under sterile and 37°C incubator condition. Before cell seeding, the cell culture media was removed.

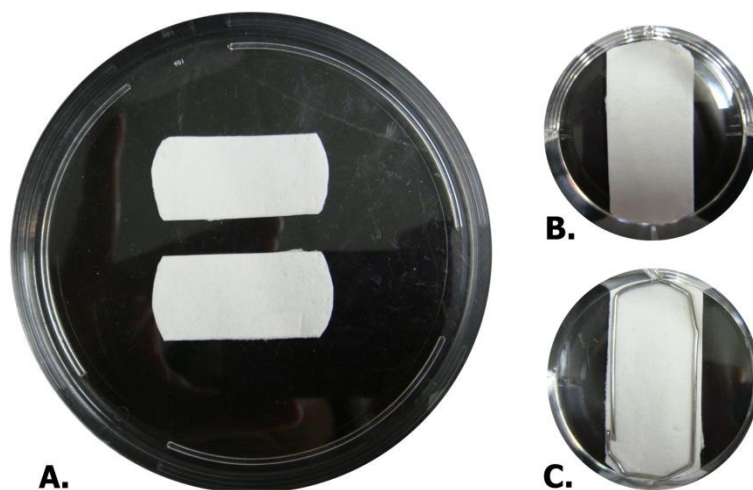


**Figure. 2.2.10.1 :** (A) Electrospun PCL scaffolds were cut into ecliptic shapes. (B) The scaffolds were laid flat in the 6-well plate . (C) The bent wire is placed on top of the scaffold. Images captured by author.

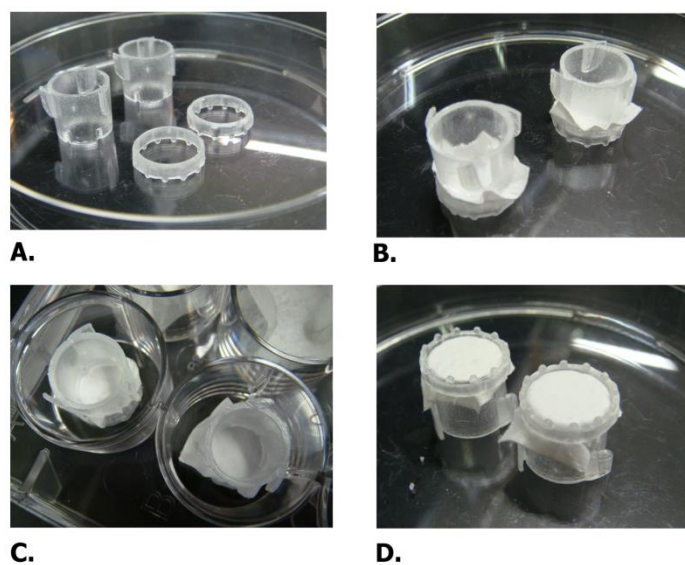


**Figure 2.2.10.2 :** (A) CellCrown™. (B) The scaffolds were inserted into the CellCrown™ and (D) inverted side. (C) The scaffold inserted CellCrown™ were cultured in the 12-well plate. Images captured by author.

### 2.2.11. Cell seeding for 3D culture

A cell seeding study was carried out to determine the most effective of cell seeding techniques; (Figure. 2.2.11 A) small volume technique + 1hr, (Figure. 2.2.11 B) small volume technique + 2hr; (Figure. 2.2.11 C) low volume of media technique, and (Figure. 2.2.11 D) large volume of media technique.

There were no significant differences between the methods used however the large volume technique presented less variation than the others; therefore the large volume technique was chosen for all future experiments. After the culture media was removed, 1mL of media was added to each well. The media leaked through the scaffolds until the inner and outer parts of the immobilized materials were at equilibrium. The small volume suspension (no more than 100 $\mu$ l) was seeded on top of the inner ring and left for 24 hours in a cell culture incubator for cell attachment. The following day the wire-holder group of scaffolds were removed to fresh well plates (Figure. 2.2.10.1 B) and fresh wire was placed on top to ensure immobilisation and that the scaffolds were submerged in the culture media (Figure. 2.2.10.1 C). The scaffolds inserted in the CellCrown™ were also moved to a fresh well plate (Figure. 2.2.10.2 D). All cell seeded scaffolds were cultured with fresh culture media along with the required supplements on day1.

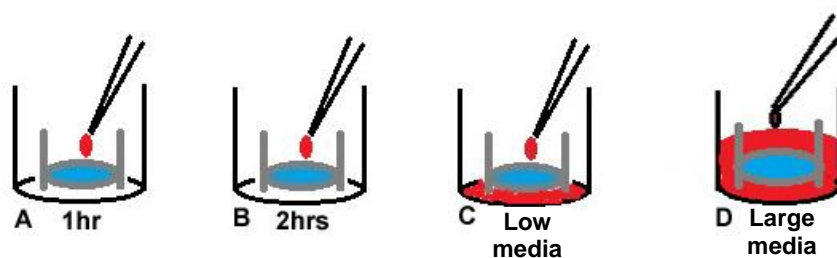


**Figure 2.2.11:** Schematic of cell seeding methods. A: small volume technique+1 hour, B: small volume technique+2 hours, C: low volume of media technique, and D: large volume of media technique. In the technique A, B, and C, after the samples were incubated, the appropriate media were added until 1mL into the well plate. The cells were allowed for attachment for overnight in the cell culture incubator.

Conditions	Number of cell per sample	Cell density
Monolayer culture	10,000	11 cells/mm <sup>2</sup>
<b>3D culture</b>		
Experiment 5.4	50,000	1473 cells/mm <sup>2</sup>
General experiment	100,000	2,946 cells/mm <sup>2</sup>
Experiment 6.3	200,000	2,946 cells/mm <sup>2</sup>

**Table 2.2.11:** Complete list of seeding cell densities on both monolayer and 3D cultures.

### 2.2.12. Assessment cell viability and cell number

#### • MTT assay

MTT (3-(4,5-Dimethylthiazol-2-yl)-2,5-diphenyltetrazolium bromide) assay is a colorimetric assay for examining relative cell number and viability by using metabolic activity. The yellow dye of MTT (tetrazole) is reduced by mitochondrial reductase enzyme in living cells to purple formazan (Figure. 2.2.12.1). Acidified isopropanol is added to dissolve the product of purple formazan into a dark blue or purple formazan salt solution. The colour of the solution is removed and measured with a spectrophotometer at wavelength 570nm.

Cell-seeded scaffolds were washed with PBS, and then 0.5mg/mL of MTT in PBS was added into the sample in the volume 0.5 and 1.0mL for 2D and 3D samples, respectively. The scaffolds were then incubated in a cell culture incubator for 40 minutes. The purple formazan product was dissolved using 0.125% acidified isopropanol (25µL of HCL with 20mL of isopropanol), subsequently 100 µL of the dissolved solution was pipetted into 96-well plate and the OD read spectrophotometer.

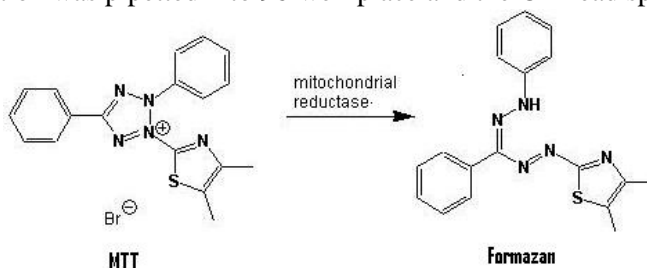


**Figure 2.2.12.1:** Schematic presentation of MTT is reduced in living cells by mitochondrial reductase enzyme, resulting is purple insoluble formazan salt.

Picture from (Peter and Peter, 2009).



• **Resazurin reduction test (Alamar blue<sup>®</sup>)**

The resazurin reduction test has been used for examining cytotoxicity and cell proliferation in different types of cells such as fibroblasts, cancer cell lines, mouse cells, and human cells. The test has increased in popularity due to it being a simple method, minimally toxic to cells, non-carcinogenic and cost-effective. The method can also measure continuous cell growth and the samples can be used for further experiments. The blue, non-fluorescent colour of the resazurin solution is reduced to resorufin which is pink and highly fluorescent in the media (Figure. 2.2.12.3). The pathway of reduction is not completely known. It may occur due to the intracellular activity of mitochondria enzyme or in the medium as a chemical reaction. The test can be measured by an absorbance or a fluorescence micro-plate reader, however, the fluorescence measurement has greater sensitivity than the absorbance reading (O'Brien et al., 2000).

The resazurin working solution is a 0.1mM or 25.1µg/mL of the resazurin salt solution in basal culture media (1mM of resazurin salt powder in distilled water as stock solution, MW=251.16). The media was removed from the cell seeded scaffolds, and 2 mL of resazurin working solution was added. The samples were wrapped in aluminum foil and incubated for 4 hours at 37°C. 200µL of pink resorufin product was transferred to a 96-well plate, and measured with a spectrofluorometer at an excitation wavelength of 540/35, and emission wavelength of 630/32nm.

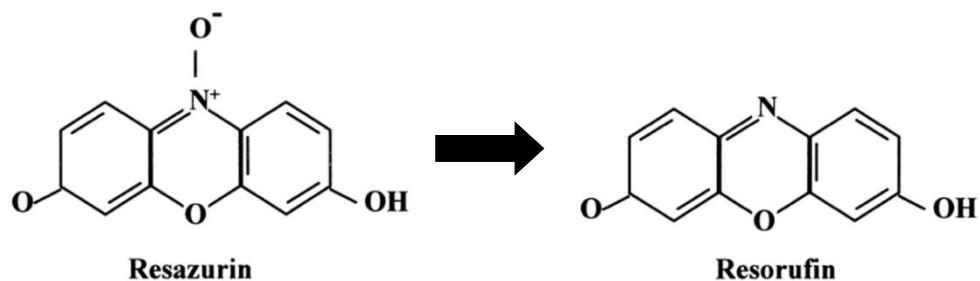


*Figure 2.2.12.3: A schematic presentation of non-fluorescent resazurin reduction to fluorescent resorufin. Adapted from (O'Brien et al., 2000) with kindly permission Wiley.*

### •DNA quantification

Fluorescent dye (PicoGreen<sup>®</sup>) was used to evaluate double stranded DNA (dsDNA). The dye specifically binds to dsDNA, enhancing the fluorescent properties of dsDNA. The cells were added to the cell digestion buffer to extract cellular DNA; stored at -80°C for 10 minutes; incubated at 37°C for 1 hour and vortexed for 15 seconds. PicoGreen<sup>®</sup> working solution was made by mixing a 20-times dilution of TE buffer and 200-times dilution of PicoGreen<sup>®</sup> reagent as commercially available in distilled water. 100µl of the 1:1 ratio mixture of samples and PicoGreen<sup>®</sup> working solution was transferred into opaque 96-well plates, mixed well, and incubated for 10 minutes at room temperature. The expression of fluorescent dye in the samples was evaluated by a spectrofluorometer at excitation 480nm, and emission 520nm (Oliveira et al., 2006). The intensity of fluorescence emission was plotted against the known DNA concentration (calf thymus DNA) to create a standard curve (n=6). As a result, the formula from the standard curve was created to convert a number of fluorescence emission intensities to a volume of DNA (ng/ml):

$$\text{DNA (ng/ml)} = (\text{Fluorescence emission} - 17.827) / 3.7593$$

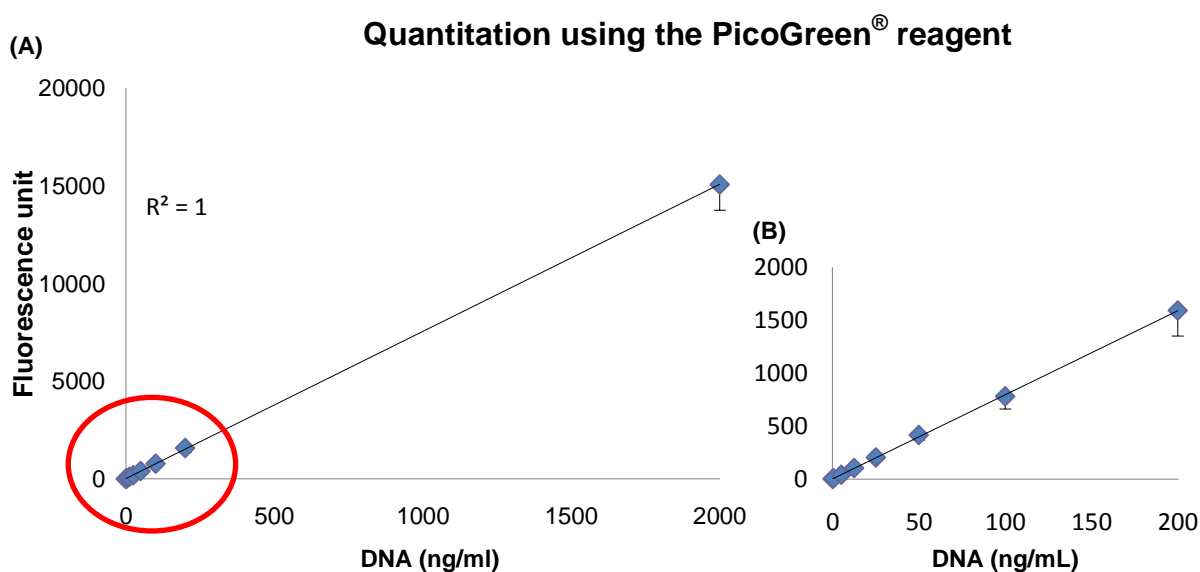


**Figure. 2.2.12.4:** Linear quantitation of calf thymus DNA by using PicoGreen reagent, from 0 to 2000 ng/ml with linear regression analysis (A), The data points in the red circle region from 0 to 200ng/ml are shown in figure B.

### **2.2.13. Analysis of cell-deposited collagen using picro-sirius red staining**

Picro-sirius red staining has been used for many years to stain collagen in histochemistry and quantify collagen in the culture plate. Picro-sirius red is an anionic dye; it can bind to a cation (the guanidine group of arginine) on the collagen molecule. This assay is a simple procedure and has been stated to specifically label collagen types I and III (Tullberg-Reinert and Jundt, 1999).

The media was removed from the cell-seeded scaffolds and they were washed 3 times with PBS. Samples were then fixed with 10% formalin for 20 minutes at room temperature, and washed 3 times with PBS. Picro-sirius red solution was made by dissolving 1mg/ml of Sirius red powder in saturated picric acid, 1mL was added to each well, and placed under mild shaking for 18 hours. The dye was removed, washed with distilled water until no more dye solution was eluted, and air-dried. The stained collagen was observed by light microscopy. The samples were destained with 0.2M sodium hydroxide (NaOH) and Methanol in a ratio 1:1 under mild shaking for 15 minutes. 200  $\mu$ L of the dissolved solution was pipetted into the 96-well plate and assessed in an absorbance plate reader at 490nm.

### **2.2.14. Assessment of osteogenesis**

#### **• Alkaline phosphatase activity**

ALP is an enzyme which can be used to predict the early stages of osteogenic differentiation. ALP can hydrolyze inorganic pyrophosphate (PPi) and generate inorganic phosphate (Pi) to promote mineralization. PPi can inhibit mineralization (Douglas et al., 2012, Orimo, 2010). Cells were evaluated for ALP activity by washing 3 times with PBS. 500 $\mu$ L of cell digestion buffer was added; 10% of cell assay buffer (1.5M Tris-HCL, 1mM ZnCL<sub>2</sub>, 1mM MgCL<sub>2</sub> in double-distilled water, ddH<sub>2</sub>O) in ddH<sub>2</sub>O, and subsequently 1% of Triton X-100 and samples were left at 37°C for 30 minutes. The cells which were cultured onto tissue culture plates were scraped to

remove cell lysate (the mixture of cell debris and cell digestion buffer solution) into a micro-centrifuge tube and left overnight at 4°C. Whereas the cells seeded onto scaffolds were dipped into cell digestion buffer in a micro-centrifuge tube; vortexed briefly, and left overnight at 4°C. The samples were then placed in a -80°C freezer for 10 minutes, then in a 37°C for 15 minutes and switched back and forth 2 more times; vortexed for 15 seconds, and centrifuged at 1,000 rpm for 5 minutes. 10µL of cell lysate was mixed with 190µl of Alkaline Phosphatase Yellow Liquid Substrate for ELISA in a 96-well plate and incubated at 37°C for 10 minutes. The samples were measured by absorbance plate reader at 405nm every minute for 30 minutes. The enzyme activity was calculated as nmol para-nitrophenol/min (nmol pNP/min). The plate reader was calibrated so that 1 absorbance value equals 22.5nmol product. The ALP activity was normalized by dividing by the DNA quantification from the same sample.

### • Alizarin red Staining

A measurement of calcium deposition *in vitro* is Alizarin red staining. Alizarin red binds to calcium-containing mineral which can be observed as an orange-red colour by eye and under a light microscope. The amount of stain can be measured by extracting the red dye with 5% perchloric acid from monolayer culture plates and scaffolds.

After the samples were measured by the resazurin reduction assay, they were washed 3 times with PBS, fixed with 10% formalin for 20 minutes at room temperature and washed again 3 times with PBS. 1ml of 1mg/ml alizarin red in dH<sub>2</sub>O, adjusted to pH 4.1 by adding ammonium hydroxide and left at room temperature for 20 minutes under a standard rocking platform. The unstained dye was removed with distilled water until no more red colour was eluted, and left to dry. The monolayer samples were observed by light microscopy. The stained samples were dissolved by adding 500µl of 5v/v% Perchloric acid into each well for 30 minutes under shaker at room temperature. 150 µl

of the dissolved solution was transferred to a 96-well plate and the OD measured at 405nm (Hild et al., 2011).

### • Xylenol orange (XO) fluorescence staining

XO ( $C_{31}H_{28}N_2O_{13}SNa_4$ ) is a non-toxic fluorochrome label when bound to calcium ions (Wang et al., 2006, van Gaalen et al., 2010). This staining has been using for labelling sequentially formed bone *in vivo* by intraperitoneal injection at different time points (van Gaalen et al., 2010) and *in vitro* to detect the mineralized matrix of vital osteoblastic cells on hydroxyapatite component biomaterials (Kuhn et al., 2010). Advantages of this stain are the continuous monitoring of osteogenic response without requiring the sacrifice of the samples; the ease of the method and a high-throughput.

20mM stock solution of XO powder was made up with distilled water and stored at 4°C. The stock XO solution was added to the culture medium in a 1:1000 dilution, with a final concentration of 20µM. The final concentration was added to the samples for a minimum of 12 hours before imaging (Kuhn et al., 2010). The XO solution was removed and washed with PBS twice and replaced with fresh medium without β-GP to reduce the fluorescent background from unbound XO. Visualised images of XO staining were taken with a confocal microscope at an excitation wavelength of 543nm. XO also absorbs into HA particles therefore no-cell control scaffolds were also stained to assess the effect of HA incorporation into polymer scaffolds on XO staining.

### • Micro-computed tomography (*micro-CT*) imaging

To evaluate mineralised matrix in tissue engineering construct 2D histological and x-ray radiographic techniques were used in combination. The x-rays beams pass through the target area and are absorbed at a detector and presented in a 2D representation. Recently, 3D techniques have been developed and applied *in vivo* and *in vitro* for detecting osteoporosis and bone aging. This application has been used recently in bone tissue engineering (Tuan and Hutmacher, 2005, He et al., 2010). For the micro-CT

technique, the samples were taken in many different angles of radiographs, followed by a computed reconstruction which produced 3D models of the samples.

The samples were fixed with 10% formalin in PBS for 20 minutes and washed twice with PBS. 12 samples were stacked by separating using foam sheets and were placed on a 20 mm diameter brass tray. The samples were adjusted to a width and height parallel to the scanning plane. The micro-CT parameters were set at 17.5 $\mu$ m/voxel resolution, the two images at each point were merged to present more accurate image, the filter was 1 mm of aluminium and a rotation step of 0.8°, 360° was applied. Approximately 750 slices were obtained. Two software packages (CTan and CTvol) provided by Skyscan were used to quantify the percentage of 'bone volume' (in this case 'bone volume' refers to any mineralized composite e.g. a composite HA-PCL electrospun scaffold and cell mineralized deposited collagen and HA) and to reconstruct the 3D structure of the samples, respectively. The region of interest (ROI) was cubic with dimensions of 18 mm in length and 35mm in width which covered the entire sample stack chosen for scanning. For measuring bone volume percentage (%BV), a cylindrical ROI with a diameter of 1.2 mm (inner diameter of metal ring) and height of 390 $\mu$ m (approximate scaffold thickness) was chosen. The ROI was sectioned into top, mid, and bottom portions with 130  $\mu$ m in each (Figure 5.11.1, chapter 5). Micro-CT measurement of the samples were received by evaluating on the threshold of the grey scale index (GSI). The threshold values were evaluated by analysing the GSI distribution. After scanning data set were divided into two different arbitrary thresholds (see result in the experiment 5.11, chapter 5). The first threshold was set in the range 30-70 GSI to analyse the standard PCL scaffold; the second threshold was set in the range more than 70 GSI to analyse the calcium deposition or hydroxyapatite (Figure 5.11.3, chapter 5). The value of a particular portion was presented as a percentage of the bone volume (%BV). The %BV of without cells on both unfilled PCL and HA-PCL samples as control was subtracted.

### 2.2.15. Fluorescent staining of cell nucleus and cytoskeleton

#### • DAPI and TRITC

DAPI (4',6-diamidino-2-phenylindole) is a fluorescent dye which binds to A-T rich regions on dsDNA. DAPI can pass through both live and fixed cells; however, the efficiency of staining for live cells is less than that for fixed cells (Zink et al., 2003). DAPI absorbs at a maximum wavelength of 358nm (ultraviolet) and emits at a maximum wavelength of 461nm which is detected by a blue filter in fluorescence microscopy (ImageXpress™) or confocal microscope at an excitation wavelength of 800nm.

Phalloidin binds to F-actin in fixed cells; either muscle or non-muscle cells. Phalloidin is an extracted peptide from the mushroom *Amanita phalloides*. The dye is mostly used in imaging applications conjugated with a fluorescent tag.

TRITC (Tetramethyl Rhodamine Iso-Thiocyanate) is a commonly used reagent for fluorescent conjugation with phalloidin. TRITC is excited at a wavelength of 540-547nm and emitted at a wavelength 570-573nm.

Cells seeded onto scaffolds were fixed in 10% formalin for 20 minutes at room temperature, then washed 3 times with PBS. 1% Triton X-100® in PBS was added to the samples and left for 10 minutes for cell membrane permeabilization, samples were then washed with PBS. The working solution of DAPI and Phalloidin-TRITC was a 1:1000 dilution of DAPI and a 1:250 dilution of Phalloidin-TRITC stock (commercially available) in PBS. The DAPI and Phalloidin-TRITC at the final concentration of 1µg/ml of DAPI and 2 µg/ml of Phalloidin-TRITC were added to the samples, samples were covered in aluminum foil and left for 15 minutes. Samples were washed twice with PBS, and visualized by fluorescent microscopy.

### • **CellTracker™**

Two colours of CellTracker™ were used, CellTracker™Red and CellTracker™Green. CellTracker™ (Molecular Probe®) is a fluorescent marker in which the dye binds to the inside of the cell cytoplasm. The stained cells are still viable and pass the fluorescence to daughter cells through approximately four cell divisions (Yang et al., 2001). In a study by (Puelacher et al., 1996) bovine periosteal cells were stained with CellTracker™ Green. The dye was freely passed to the cell cytoplasm. The glutathione S-transferase-mediated reaction will conjugate partially the chloromethyl into thiol components in the cells. Then, the fluorescent dye thiol-ether product is permanently trapped inside the cell cytoplasm. The stained cell preparation was optimized for human jaw periosteum to be seeded on to the scaffolds. The optimal concentration of the fluorescent dye and revolutions of the centrifuge (rounds per minute) were assessed using fluorescence microscopy. The suitable CellTracker™ staining cell conditions demonstrated that 10µM of CellTracker™ combined with 1000 rpm centrifugation gave the highest fluorescence resolution images and cell number compared with the other groups. Moreover, preliminary experiments showed that adding CellTracker™ to the cells in monolayer in the T-75 flasks prior to trypsinization, was more effective than adding it to a cell suspension. Therefore this method was adopted for the remainder of the experiments. Trypsin-EDTA was then added to the flasks which were centrifuged at 1000 rpm to obtain the cell pellet. The cells was mixed with trypan blue solution in a 1:1 ratio; counted using a haemocytometer and seeded on to the scaffolds.

### • **Live/Dead staining**

Live/Dead staining can distinguish between live and dead cells via the expression of two fluorescent colours. The fluorescence dies can penetrate into cells depending on the cell membrane permeability. The Live/Dead stain is a mixture of SYTO®9 which is the green-fluorescent nucleic acid stain and propidium iodide (PI) which is the red-fluorescence nucleic acid stain. The stains differ in their spectral expression and their

ability to penetrate healthy cells. SYTO<sup>®</sup>9 can generally bind to both live (intact membrane) and dead cells (damaged membrane). In contrast, PI can only penetrate cells with damaged membranes and this reduces the green-fluorescent staining. Therefore, the cells with intact cell membranes express green-fluorescence and the damaged membrane cells express red-fluorescence.

Cells seeded onto scaffolds were washed with PBS. The working solution of Live/Dead staining is a 1:1000 dilution of SYTO<sup>®</sup>9 and a 1:100 dilution of PI (commercially available) in PBS. 1mL of the final concentration at a 5 $\mu$ M of SYTO<sup>®</sup>9 and 10 $\mu$ g/mL of PI were added to the samples; covered with aluminum foil and left on a shaker at room temperature for 30 minutes. The samples were then washed with PBS and PBS was added to each sample to just cover the sample and they were visualized with fluorescence microscopy.

### **2.2.16. Mechanical loading of cells**

#### **• Application of oscillatory fluid flow (OFF) to cells**

Oscillatory motion is motion that moves back and forth repeatedly in a constant cycle. OFF conditions were applied using a standard laboratory rocking platform ‘a see-saw rocker’. Cells were subjected to OFF when they were placed on a see-saw rocker (Figure. 2.2.16). The rocking platform which was used in the experiments had a fixed maximum tilt angle of 6° and an adjustable speed. During all OFF experiments, cells were cultured in 6 well-culture plates which contained 2 ml of culture media in each well. Pre-coated well plates with 0.1% sterilised gelatin were required to enhance cell attachment for only the hESMPs experiment. The samples were subjected to OFF at room temperature, atmosphere CO<sub>2</sub> (0.04% CO<sub>2</sub>) for 1 hour a day, 5 days a week for all experiments (Delaine-Smith and Reilly, 2011). Control condition were as described in chapter 4.



*Figure. 2.2.16 : Image of a standard see-saw rocker to conduct OFF. The static group was placed beside the standard see-saw rocker. The rocking groups were placed on the standard see-saw rocker. Image was captured by author.*

### **2.2.17. Assessment of vascular endothelial growth factor (VEGF) secretion using enzyme-linked immunosorbent assay (ELISA)**

ELISA is a quantified laboratory technique used to determine the concentration of specific antigens (Ag) or antibodies (Ab) in cell lysates and other solutions. A polystyrene plate was used to support and capture the Ag test. The developing colour of samples from a colourless to an intense solution which was measured by a absorbance plate reader at the optimum wavelength. The obtained results compared to a standard curve to convert the absorbance to the concentration of the samples in each well. The disadvantage of the direct ELISA is that the Ag can bind to the polystyrene plates poorly, resulting in a potentially inaccurate measurement. To overcome this limitation, sandwich ELISA have been used by a matching pair between Ag and specific Ab. This technique can enhance sensitivity and a specificity of the quantified assay into picogram, therefore sandwich ELISA is a suitable technique to quantify cytokine and hormones in supernatant.

An ELISA kit was used for quantification of VEGF production in the cells. The supernatant was collected to measure the VEGF production produced by cells after 48 hours after the media was changed. The assay protocol was followed according to the manufactures instructions. Briefly, the 96-well immunomicro plates were each coated with 100µl of 0.5µg/ml antigen-specific Ab (capture Ab), then the plate was sealed and incubated overnight. All methods were performed at room temperature. The plates were then washed four times with wash buffer solution (0.05% Tween-20 in PBS). The wells were blocked with 300 µl of 1% bovine serum albumin (BSA) in PBS, and incubated for 1 hour. After being washed, 100 µl of standard or supernatant were added to the wells in duplicate, incubated for 2 hours and washed. They were then incubated with 100 µl of 0.25 µg/ml biotinylate antigen-specific Ab (detection Ab) for 2 hours. The plates were washed and then incubated with 100 µl of avidin-horseradish peroxidase conjugate at 1:2000 in diluent (0.1% BSA in the wash buffer) per well for 30 minutes. After washing, the colour solution in the well was developed for 20 minutes by adding 100 µl of 2,2'-Azino-bis(3-ethylbenzothiazoline-6-sulfonic acid) ABTS liquid substrate. Absorbance was measured by using an absorbance microplate reader at a 405nm wavelength. The absorbance was normalised by dividing by the fluorescent unit of resazurin reduction test from the same sample.

### **2.2.18. Statistical analysis**

Statistical analysis was performed using SPSS (IBM SPSS statistics 21). Calcium deposition and collagen production were analysed by One-way ANOVA. Cell viability, DNA quantification, ALP activity, and VEGF secretion were analyzed by Two-way ANOVA (for two factors), followed by Tukey's multiple comparison test. Data was expressed as mean values  $\pm$  SE (standard error of mean). Numbers of replicates are as stated in each figure legend. 'N' represents a biological repeat (separate experiment) and 'n' represents a technical repeat (different samples within one experiment). The differences were considered to be statistically significant when the *p-value* was less than

## CHAPTER TWO

or equal to 0.05 ( $p \leq 0.05$ ). Prism6 (GraphPad) was used to analyse the frequency of distribution of fibre diameter of the materials.

**CHAPTER THREE: CELL CHARACTERIZATION AND EVALUATION OF THE MOST SUITABLE CULTURE MEDIUM FOR OSTEOGENIC INDUCTION ON MONOLAYER CULTURED hESMPs AND HJPs**

A key requirement of bone tissue engineering for cleft palate repair is a cell source which has osteogenic differentiation potential. Cells that have been used in many clinical studies for intra-oral bone repairs such as alveolar cleft bone graft and maxillary sinus augmentation for dental implantation, as mentioned in the previous chapter are: hBMSCs (Behnia et al., 2009, Hibi et al., 2006) and HJPs (D'Addona and Nowzari, 2001, Trautvetter et al., 2011). Therefore, the selected cell sources that will be used in this chapter are hESMPs as a model cell for MSCs and HJPs. However, there is little information about the best culture conditions for osteogenesis differentiation using Dex for hESMPs and HJPs.

**3.1 Introduction**

hESMP 002.5 is a human embryonic stem cell-derived mesenchymal progenitor cell line. The cells were derived from human embryonic stem cells (hESCs). The hESMPs do not express pluripotent hESCs markers but are reported to express surface markers similar to human MSCs; CD105, CD166, CD10, and CD13. According to the literature hESMPs have been used in several studies as a model cell for bone tissue engineering. hESMPs were chosen for these studies due to 1] their homogeneity, to avoid the donor variation that occurs in a primary human cells (Marolt et al., 2010), 2] their ability to maintain their cell viability up to passage 20 (Karlsson et al., 2009) whereas usually primary human cells may lose their stem cell potential after passage 8 (Khoo et al., 2008, Min et al., 2011) and 3] they are straightforward cells to culture with high proliferation capability. Both hESMPs and human MSCs are similar in that they require

Dex for osteogenic differentiation. The osteogenic induction medium for MSCs is supplemented with ascorbic acid (AA), beta-glycerophosphate ( $\beta$ -GP), and Dex. AA is very important in the production of a stable collagen (hydroxyproline) which is a major component of ECM of bone.  $\beta$ -GP is important to provide an inorganic phosphate for the mineralization of osteoblastic cells whereas Dex is a glucocorticoid steroid drug which can stimulate osteogenic differentiation of MSCs (Advani et al., 1997, Coelho and Fernandes, 2000). This study also evaluates the effect of osteogenic differentiation of progenitor cells on VEGF secretion. VEGF is an important vasculogenesis growth factor which is produced by many cells including osteoblasts. Vasculogenesis is important as for a tissue engineered bone to survive *in vivo* as it needs to induce blood vessel formation to supply nutrients and oxygen into the cells within the implanted structure. Primary human dermal fibroblasts were used to evaluate the suitable concentration of AA for producing collagen.

In bone reconstruction surgery, an autologous bone graft is the gold standard due to its biochemical properties and ability to integrate to the surrounding tissue. Periosteum is a tri-membrane that covers the outer surface of all bones except at the joints of long bones while endosteum lines the inner surface of all bone (Olbrich et al., 2012) (see chapter 1). Cells that are extracted from periosteum are called periosteal cells which are a sub-population of MSC. In this study, periosteal cells were extracted from HJP. Studies showed that HJP derived cells could be a promising source for cell based therapies for bone tissue engineering due to less risk of donor site morbidity, reduced time of operation and also easy harvesting technique compared to the extraction of autologous bone graft from iliac crest (Trautvetter et al., 2011). HJP is easy to harvest during wisdom tooth removal (a routine dental procedure). Whereas the mononuclear bone marrow cells are harvested from the inner (trabecular) part of the bone. Fujii et al., (2006) and Choi et al., (2002) reported that facial periosteum graft induced intramembranous ossification was similar to maxillofacial skeletal osteogenesis. The

tibia periosteum graft induced endochondral ossification in a similar way to limb skeletal osteogenesis. The approach of using HJPs in the construction or formation of bone may be an optional method for bone reconstruction. Flow cytometry showed that human periosteal cell expressed specific cell surface markers; Stro-1 for progenitor cells and ALP for osteoblastic cells (Ball et al., 2011). They also reported that the surface marker expression of MSCs on periosteal cells was maintained up until passage 10 while ALP showed a high expression up until to passage 5 before starting to decline. Cicconetti et al., (2007) found that maxillary and mandibular periosteal cells did not express the negative markers of CD34: an endothelial cell marker, CD45: a leukocyte marker while they did express the mesenchymal phenotypic markers of CD 105, CD49a, CD63, CD90, and CD140b.

DMEM was used in the Stolzing group or  $\alpha$ -MEM was used in the Yang and Cicconetti groups in the culturing of HJP cells (Stolzing et al., 2008). There are controversies in the selection of medium for HJP cell culture due to the differences in cellular bioactivities and expressions. Ascorbic acid-2-phosphate (AA) and fibroblast growth factor-basic recombinant human (bFGF) have been used to increase MSCs proliferation and maintain their multipotency (Ramasamy et al., 2012).

The aims of present study were to characterise the cells have been using in my study and evaluate suitable culture conditions for cell proliferation and osteogenic differentiation for both HJPs and hESMPs that have not been previously optimised. In order to do this;

1. Analysed three cell sources for bone formation; hESMPs, HJPs, and hBMSCs.
2. A comparison was made between DMEM and  $\alpha$ -MEM
3. The effects of AA, bFGF, and a combination of AA and bFGF supplementation on primary HJPs was investigated.

4. The effect of varying the concentration of Dex (without Dex, 10nM, and 100nM) on cell proliferation and osteogenic differentiation of both hESMPs and HJPs was tested.
5. The effect of Dex on VEGF secretion of hESMPs was analysed.

### **3.2 The effect of AA on collagen production of HDFs**

The aim of this study is to evaluate the concentration of AA for collagen production by HDFs.

#### **3.2.1 Results**

The cell viability of HDF cells was assessed using a MTT cell viability test after day 7, 14, and 21. The cell viability increased in all conditions (5, 25, 50, and 100µg/mL) from 7 to 21 days (Figure 3.2.1 A). The cell viability was highest in the 100µg/mL group which was significantly different, whereas the 5µg/mL group was the lowest at every time point ( $p < 0.05$ ). Collagen production per viable cell of the 50µg/mL group was slightly higher than the other groups at every time-point (Figure 3.2.1 B). The 5µg/mL group was significantly lower at all the experiment time-points ( $p < 0.05$ ).

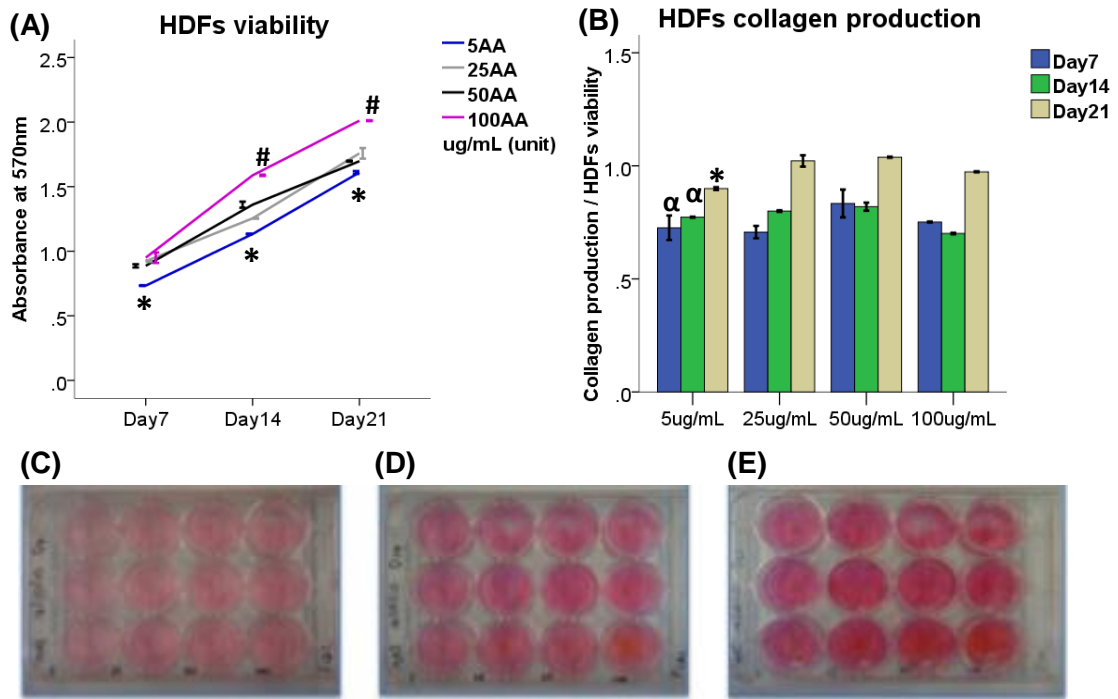


**Figure 3.2.1:** The effect of varying concentration of AA: 5, 25, 50, and 100µg/mL on HDFs on monolayer culture after 7, 14 and 21 days. The cell viability (A) and collagen production of HDF cells were measured using MTT cell viability test and picro-sirius red staining, respectively. (B) Collagen production was normalised to MTT absorbance. Photoimages of picro-sirius red staining of HDF cells cultured on a monolayer in different concentration of AA after 7 (C), 14 (D), and 21 days (E). Data is presented as mean  $\pm$  SE, (N=1, n=3), \* =  $p < 0.05$  comparison between 5 µg/mL of AA and the other groups, # =  $p < 0.05$  comparison between 100 µg/mL of AA and the other groups,  $\alpha$  =  $p < 0.05$  comparison between 5 and 50 µg/mL of AA, Two-way ANOVA, Tukey's multiple comparison test.

**3.3. Osteoprogenitor cells characterisation**

**3.3.1. Materials**

hESMPs (passage number 4 to 8), 2 different donors of HJPs (passage number 6 to 8), and 3 different donors of hBMSCs (passage number 2 and 3) were evaluated for surface antigen expression. Further information about hBMSCs is in table 3.3). The method for surface antigen fluorescence staining has been described in chapter 2.

<b>Donor(Lot No.)</b>	<b>Date of cryopreservation</b>	<b>Age</b>	<b>Gender</b>	<b>Passage No.</b>
hMSCs-1 :080900C	4 <sup>th</sup> June2008	30	Male	2
hMSCs-2 :080917A	6 <sup>th</sup> June 2008	23	Male	2
hMSCs-3 :080926B	9 <sup>th</sup> June 2008	40	Female	2

*Table 3.3: Information of the human mononuclear cells obtained from three different donors.*

**Immunophenotypic analysing results**

hESMPs (Figure 3.3.1), a combination from 2 donors of HJPs (HJPs-pool), and a combination from 3 donors of hBMSCs (hBMSCs-pool) were used to detect the expressions of cell surface antigens by using flow cytometry. The results showed that both hESMPs and hBMSCs-pool expressed the MSCs markers CD146, CD105, and CD90 in the majority of cells (more than 95%), while they did not express the hematopoietic maker (CD45) or less than 15% (Table 3.3.1). This implies that the cell population’s MSCs following the minimal criteria for MSCs specified by the international Society for Cellular Therapy (ISCT) (Dominici et al., 2006). Surprisingly, the HJPs-pool expressed CD105 and CD90 in the majority of cells (more than 95%) but did not express the CD146. CD45 was also little expressed as expected or less than 10%.

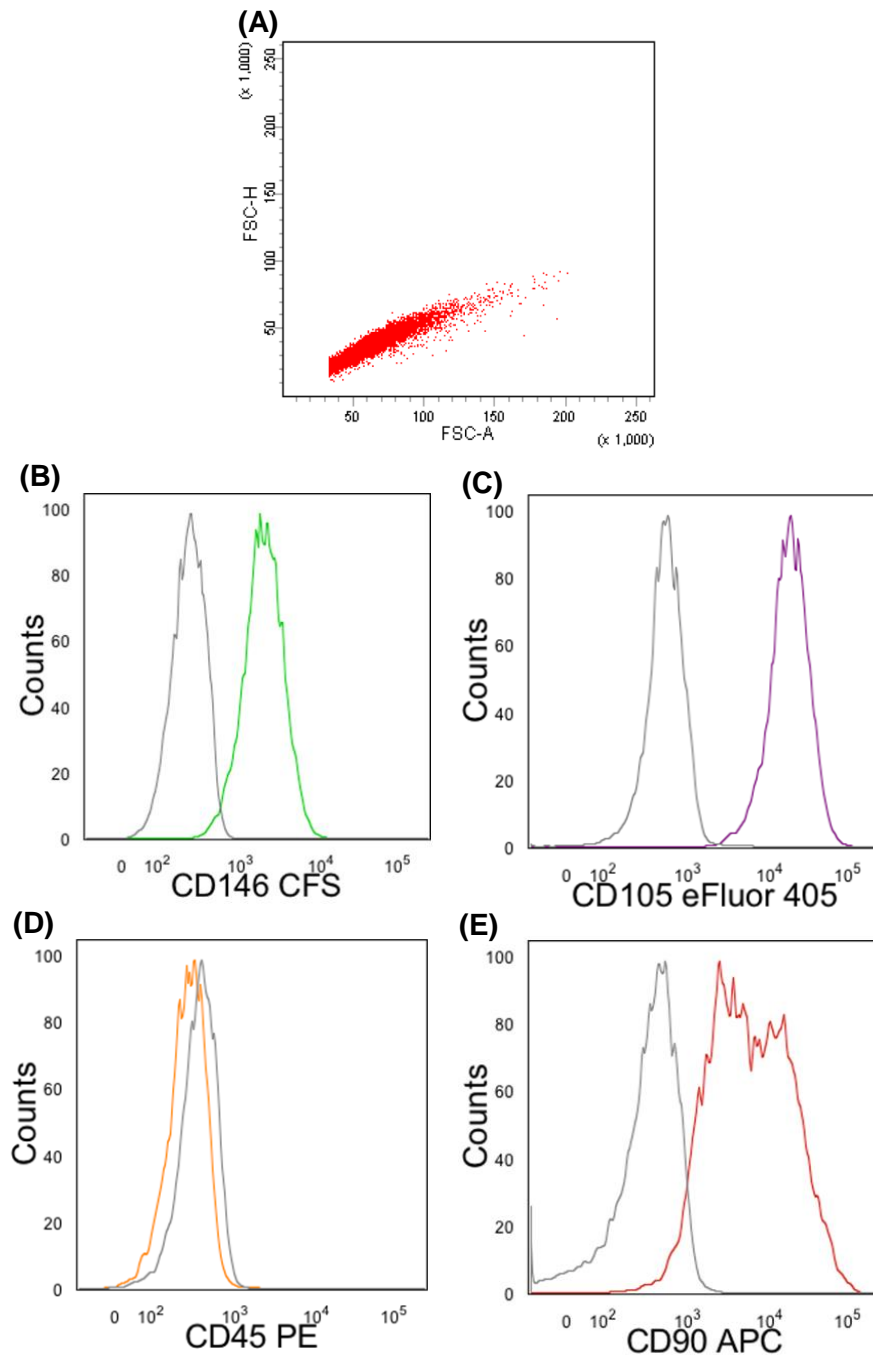


**Figure 3.3.1:** hESMPs were stained with CD146, CD105, CD90, and CD45 and analyzed by flow cytometry. (A) Sorting gate from a representative hESMPs sample for CD 146, CD105, CD45 and CD90 expressions. (B-E) Colour histograms represented FACS profile of hESMPs single cell and grey histograms represent the corresponding isotype controls.

Cell types	CD146	CD105	CD90	CD45
hESMPs (cell line)	+ <b>96.7</b>	+ <b>99.9</b>	+ <b>86.1</b>	- <b>0.8</b>
HJPs-pool	- <b>8.6</b>	+ <b>96.4</b>	+ <b>98.9</b>	- <b>7.4</b>
hBMSCs-pool	+ <b>95.7</b>	+ <b>100.0</b>	+ <b>99.6</b>	- <b>11.0</b>

*Table 3.3.1: Surface antigen expression patterns of hESMPs, HJPs-pool (combination of HJPs from 2 donors), and hBMSCs-pool (combination of hBMSCs from 3 donors) were measured. Their expressions were decided into 3 categories: 1] positive (+) when more than 70%, 2] weakly positive (+-) when 20-70%, and 3] negative (-) when less than 20% of the population showed the specific marker (Marolt et al., 2010).*

### 3.4. Osteogenic differentiation of hESMPs in a monolayer culture

#### 3.4.2. Results

After 7 days, hESMP cell morphology showed changes under SM+Dex100 medium from a fibroblastic cell shape to a cuboidal shape which is similar to a typical osteoblastic cell shape (Cheng et al., 1994, Kaveh et al., 2011) (Figure 3.4.1). DNA increased in all conditions (SM, SM+Dex10, and SM+Dex100) from day 7 to 14. The SM group had higher cell numbers than the other groups on day 14. However by day 21 there were no significant differences between the groups (Figure 3.4.2 A). The SM group had the lowest ALP activity normalized to DNA, whereas the SM+Dex100 group was the highest ALP activity at all time-points (Figure 3.4.2 B). The VEGF secretion (during a 48 hours collection period) was normalized to DNA ( $\mu\text{g/ml}$ ) of hESMPs after day 7, 14 and 21. The secretion of VEGF at all conditions increased over the 3 weeks. The VEGF secretion by the SM group was significantly higher than the SM+Dex100 groups by 171% on day 14 ( $p < 0.05$ ). From 14 to 21 days, the amount of VEGF secreted by cells in both the SM+Dex10 and SM+Dex100 groups was higher compared to the SM group, however there were no differences between the groups by day 21 (Figure

3.4.2 C). Total calcium deposition of hESMPs when cultured with varying concentrations of Dex was measured after 21 days. Total calcium deposition was highest in the SM+Dex100 group followed by SM+Dex10 and SM groups. However, there were no significant differences between the SM+Dex10 and SM+Dex100 groups (Figure 3.4.3 A). Total collagen production by hESMPs when cultured with varying concentrations of Dex was measured after 21 days. All culture groups were not significantly different. However, the cells cultured with SM+Dex100 showed the lowest total collagen followed by SM+Dex10 and SM groups (Figure 3.4.3 B). The photographs of whole well alizarin red staining show that the SM+Dex100 group contained the darkest staining after 21 days in cell culture (Figure 3.4.3 C: upper row) indicating that this group had a higher calcium deposition than the SM+Dex10 and SM groups. In contrast, the picro-sirius red staining showed an inverse relationship between picro-sirius red staining in the cells with an increased concentration of Dex (Figure 3.4.3. C: lower row), indicating that the SM group had the highest collagen production.

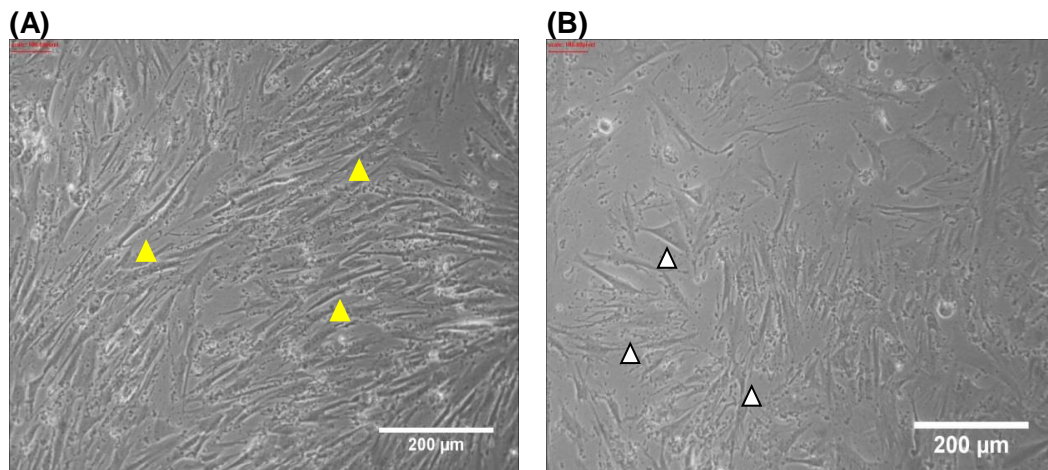


**Figure 3.4.1:** Microphotographs of the morphology of hESMPs under different culture media. (A) Cells in supplemented media (SM: AA and  $\beta$ -GP) were more fibroblastic in shape (yellow arrow heads) while (B) cells in SM+Dex100nM (AA,  $\beta$ -GP, and 100nM of Dex) media were more cuboidal in shape similar to osteoblastic cells (white arrow heads) after day 14. Scale bar : 200 $\mu$ m

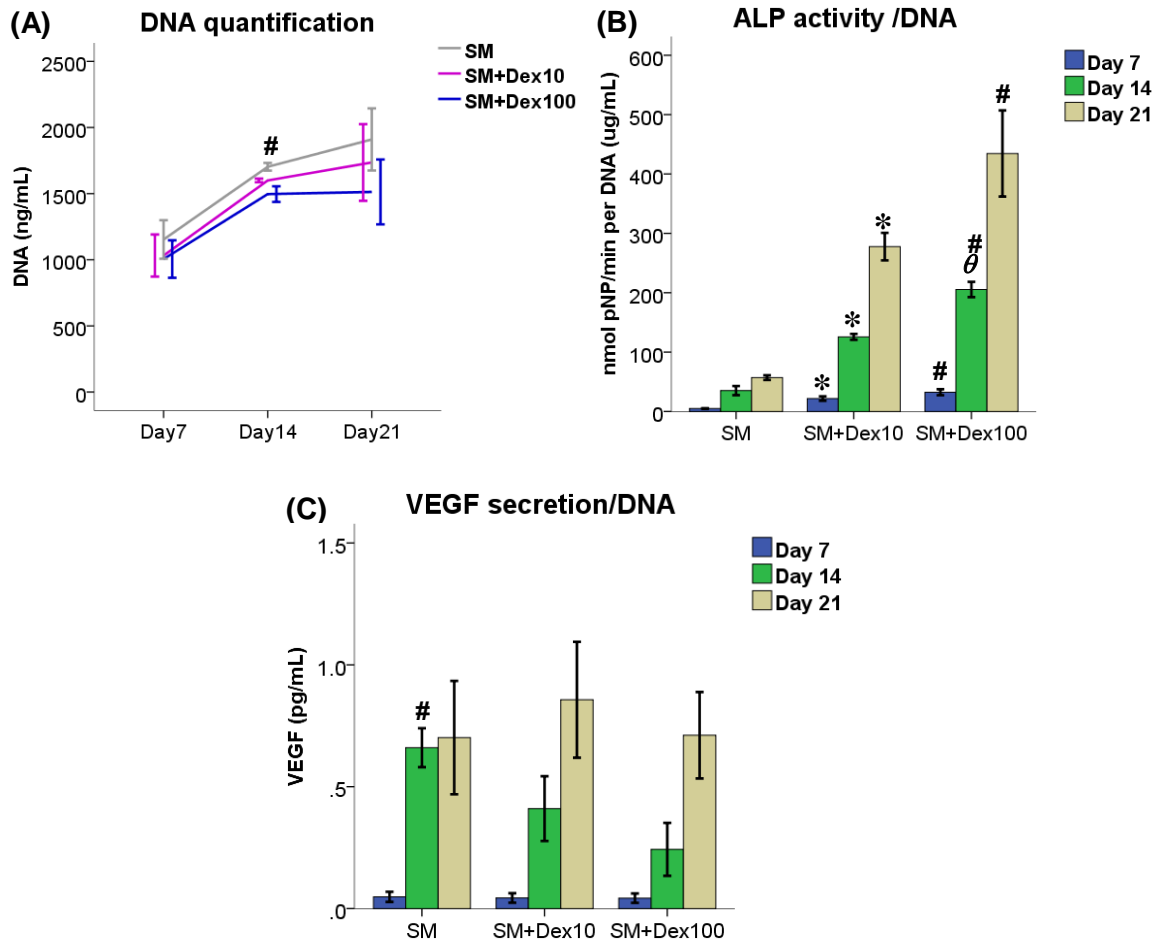


**Figure 3.4.2:** The effect of varying concentrations of Dex: supplemented media (SM), supplemented media with 10nM of Dex (SM+Dex10), and supplemented media with 100nM of Dex (SM+Dex100) on hESMPs in monolayer culture after 7, 14 and 21 days. DNA quantification measured by Quant-Ti™ PicoGreen® (A), ALP activity normalised to DNA ( $\mu\text{g/ml}$ ) (B), and VEGF secretion ( during a 48 hour collection period) normalised to DNA ( $\mu\text{g/ml}$ ) (C). Data are presented as mean  $\pm$  SE, ( $N=2$ ,  $n=3$ ), and  $*$  =  $p<0.05$  comparison between SM and SM+Dex10,  $\#$  =  $p<0.05$  comparison between SM and SM+Dex100,  $\theta$  =  $p<0.05$  comparison between SM+Dex10 and SM+Dex100, using Two-way ANOVA, Tukey's multiple comparison test.

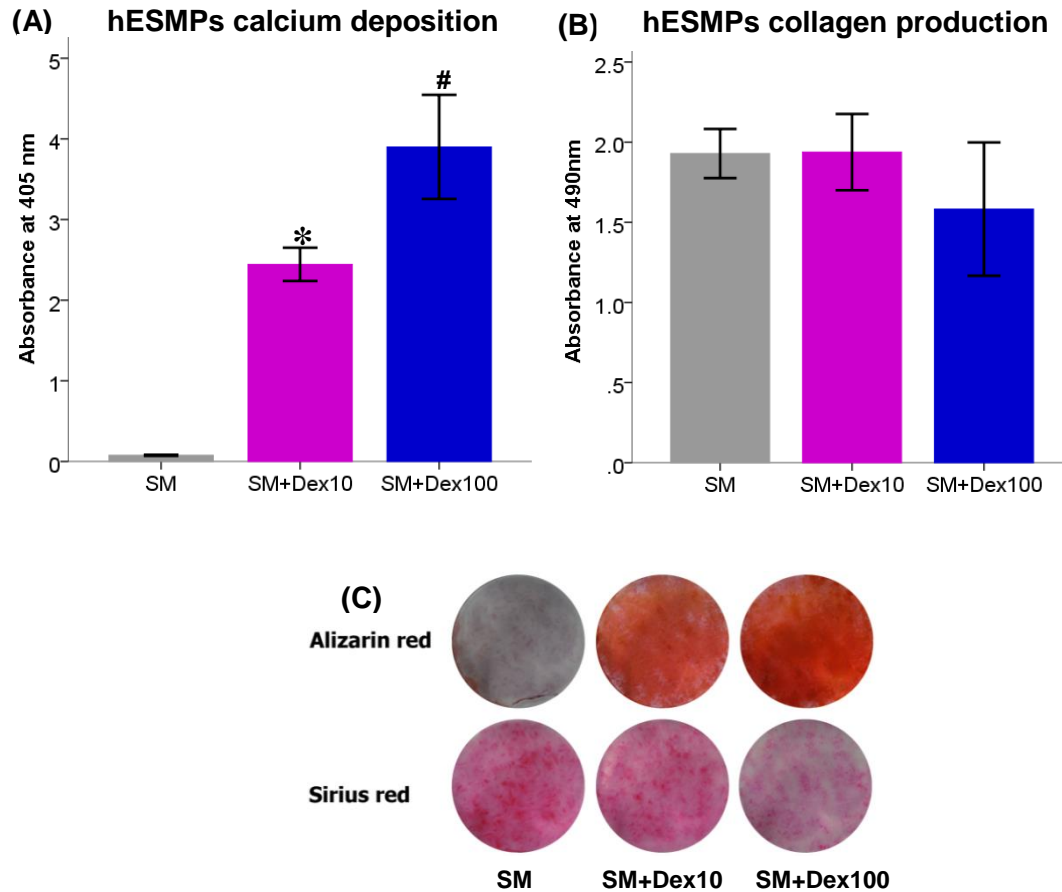


**Figure 3.4.3:** The effect of varying concentrations of Dex: supplemented media (SM), supplemented media with 10nM of Dex (SM+Dex10), and supplemented media with 100nM of Dex (SM+Dex100) on hESMPs in monolayer culture after 21 days, hESMPs calcium deposition (A) using alizarin red staining and hESMPs collagen production (B) using picro-sirius red staining. (C) The photoimages show a representative set of alizarin red staining (upper row) and sirius red staining (lower row) of hESMPs. (A,B) Data is presented as mean  $\pm$  SE, (N=2, n=3), \*= $p$ <0.05 comparison between the SM and SM+Dex10 groups, # = $p$ <0.05 comparison between the SM and SM+Dex100 groups, using two-way ANOVA, Tukey's multiple comparison test.

### 3.5. Comparisons of different culture media on the stimulation of human jaw periosteal cells (HJPs)

#### 3.5.1 Results

The HJPs-1 cell viability in the  $\alpha$ -MEM media increased over time for 7 days. The plain  $\alpha$ -MEM media group had the highest cell viability (Figure 3.5.1 A: left). Whereas HJPs-1 cell viability cultured in the DMEM media was slightly reduced from day 1 to 4 (Figure 3.5.1 A: right). This was followed by an increasing of cell viability from day 4 to 7 with no difference between the different groups. However, the overall comparison of the cells cultured whether in  $\alpha$ -MEM or DMEM after 7 days showed that the  $\alpha$ -MEM group was higher than the group culture in DMEM media.

HJPs-2 cell viability in the  $\alpha$ -MEM media slightly increased on day 1 to 4, followed by a sharp increase on day 4 to 7. There were no differences between the conditions (Figure 3.5.1 B: left). The cells cultured in the DMEM media had similar cell viability pattern as in the  $\alpha$ -MEM media (Figure 3.5.1 B: right). However, the comparison of cells cultured between  $\alpha$ -MEM and DMEM found that the cell viability in the  $\alpha$ -MEM groups was higher than the DMEM groups. The overall cell viabilities of HJPs-1 were significantly lower than the HJPs-2, around 4 fold, whether they were cultured in  $\alpha$ -MEM or DMEM media over 7 days (Figure 3.5.2). Cell viability for HJPs-2 cultured in  $\alpha$ -MEM was significantly higher than for the DMEM ( $p < 0.05$ ). Indicating the cells cultured in the  $\alpha$ -MEM group had higher cell proliferation than the DMEM group. In addition, the HJPs-2 had a higher cell proliferation rate than the HJPs-1.

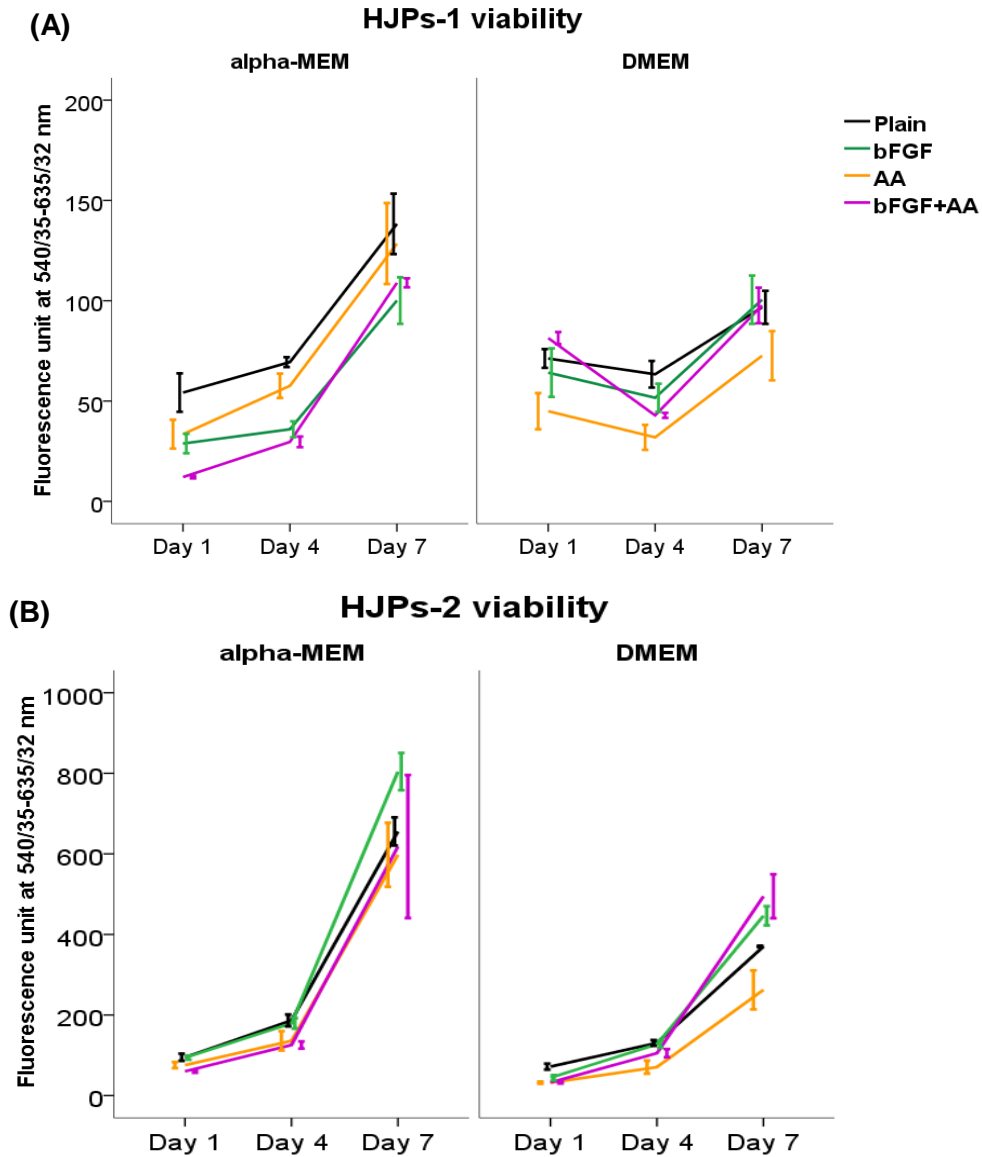


**Figure 3.5.1** The effect of culture medium,  $\alpha$  MEM (left) and DMEM (right) which were divided into 4 different groups: 1] basic culture medium (plain), 2] basic culture medium containing ascorbic acid-2-phosphate (AA), 3] basic culture medium containing a human beta-fibroblast growth factor (bFGF), and 4] the combination of AA and bFGF were assayed by the resazurin reduction test for HJPs-1 (A) and HJPs-2 (B) on a monolayer cell culture after 1, 4, and 7 days. (A) HJPs-1 was cultured in  $\alpha$ -MEM and DMEM. (B) HJPs-2 was cultured in  $\alpha$ -MEM and DMEM. Noticeably, the scale bar of y axis on Figure A is from 0 to 200 but Figure B is from 0-1000 fluorescence unit. mean $\pm$ SE, (N=1, n=3), \* =  $p < 0.05$ , Two-way ANOVA, Tukey's multiple comparison test.

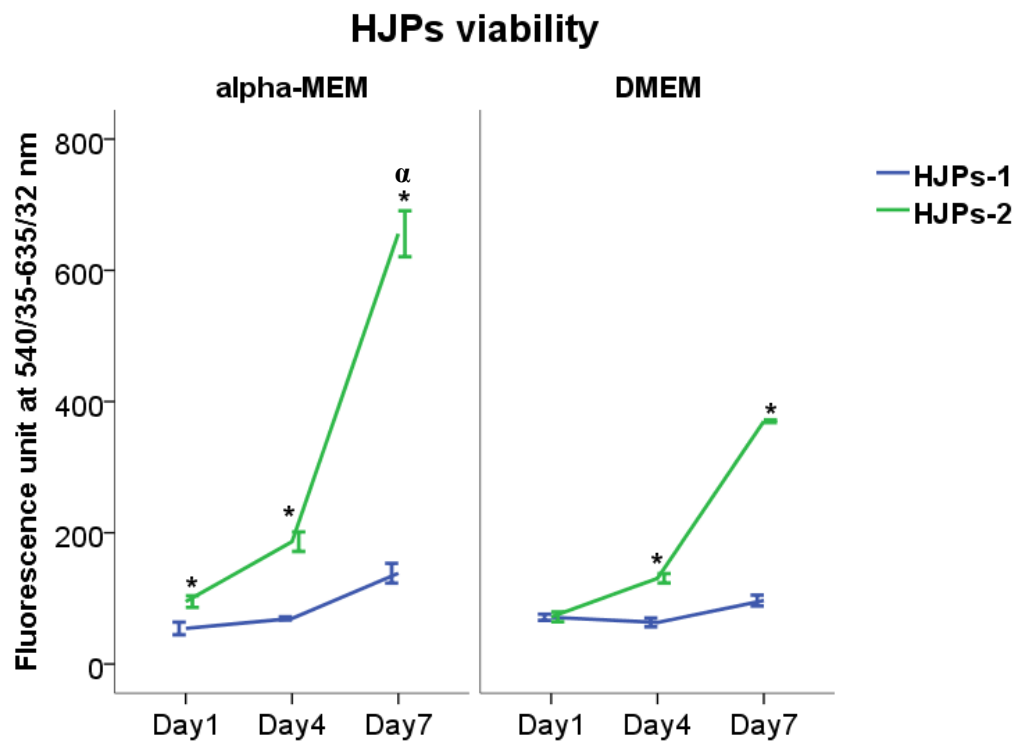


*Figure 3.5.2: Comparison of the effect of basic culture medium  $\alpha$ -MEM (left) and DMEM (right) assayed by the resazurin reduction test of HJPs-1 and HJPs-2 on a monolayer cell culture after 1, 4, and 7 days. mean $\pm$ SE, (N=1, n=3), \* =  $p < 0.05$  comparison between the HJPs-1 and HJPs-2 cell viability,  $\alpha$  =  $p < 0.05$  comparison between the HJPs-2 cultured in the  $\alpha$ -MEM and DMEM, Two-way ANOVA, Tukey's multiple comparison test.*

### 3.6. The effect of varying concentrations of Dex on Osteogenic differentiation HJPs cultured as monolayer.

#### 3.6.1. Results

On day 7 the cells under the SM groups were fusiform in shape similar to fibroblastic cells (Figure 3.6.1 A for HJPs-1 and D for HJPs-2, red arrow heads). While the cells in the SM+Dex10 and SM+Dex100 groups were of more cuboidal cell shape similar to osteoblastic cells (Figure 3.6.1 B for HJPs-1 and E for HJPs-2 under the SM+Dex10 medium, white arrow heads and C for HJPs-1 and F for HJPs-2 under the SM+Dex100 medium, yellow arrow heads) (Cheng et al., 1994, Kaveh et al., 2011). The cell viability of HJPs-1 increased overtime for 28 days in all conditions and the SM+Dex10 group was higher than the other groups after 21 to 28 days (Figure 3.6.2 A). ALP activity normalized to DNA ( $\mu\text{g/ml}$ ) was lowest in the SM group of HJPs-1, in contrast, the SM+Dex100 group had the highest ALP activity compared to the other groups (Figure 3.6.2 C). There were no differences between the SM+Dex10 and SM+Dex100 groups ( $p < 0.05$ ). The cell number of HJPs-2 increased overtime for 21 days in all conditions except the SM group slightly decreased between day 14 to 21 (Figure 3.6.2 B). The SM+Dex10 group showed a significantly higher DNA content than the SM group after 21 days ( $p < 0.05$ ). Indicating that both HJPs-1 and HJPs-2 in the SM+Dex10 had a higher cell proliferation than the other groups. ALP activity normalized to DNA of the SM group of HJPs-2 was the lowest at all time-points. In contrast, the ALP activity of the SM+Dex10 group was the higher than the other groups after day 21, significantly ( $p < 0.05$ ). Total calcium deposition was highest in the SM+Dex10 group both for HJPs-1 and HJPs-2 (Figure 3.6.3 A and B). The cells cultured in the SM+Dex10 group showed the darkest staining after 28 days for HJPs-1 (Figure 3.6.3 C) and after 21 days for HJP-2 (Figure 3.6.3 D). Both HJPs-1 (E) and HJPs-2 (F) in the SM groups had significantly higher collagen production than the other groups after 21 days for HJPs-2 and 28 days for HJPs-1, while, the lowest total collagen production was in the SM+Dex100 groups ( $p < 0.05$ ).

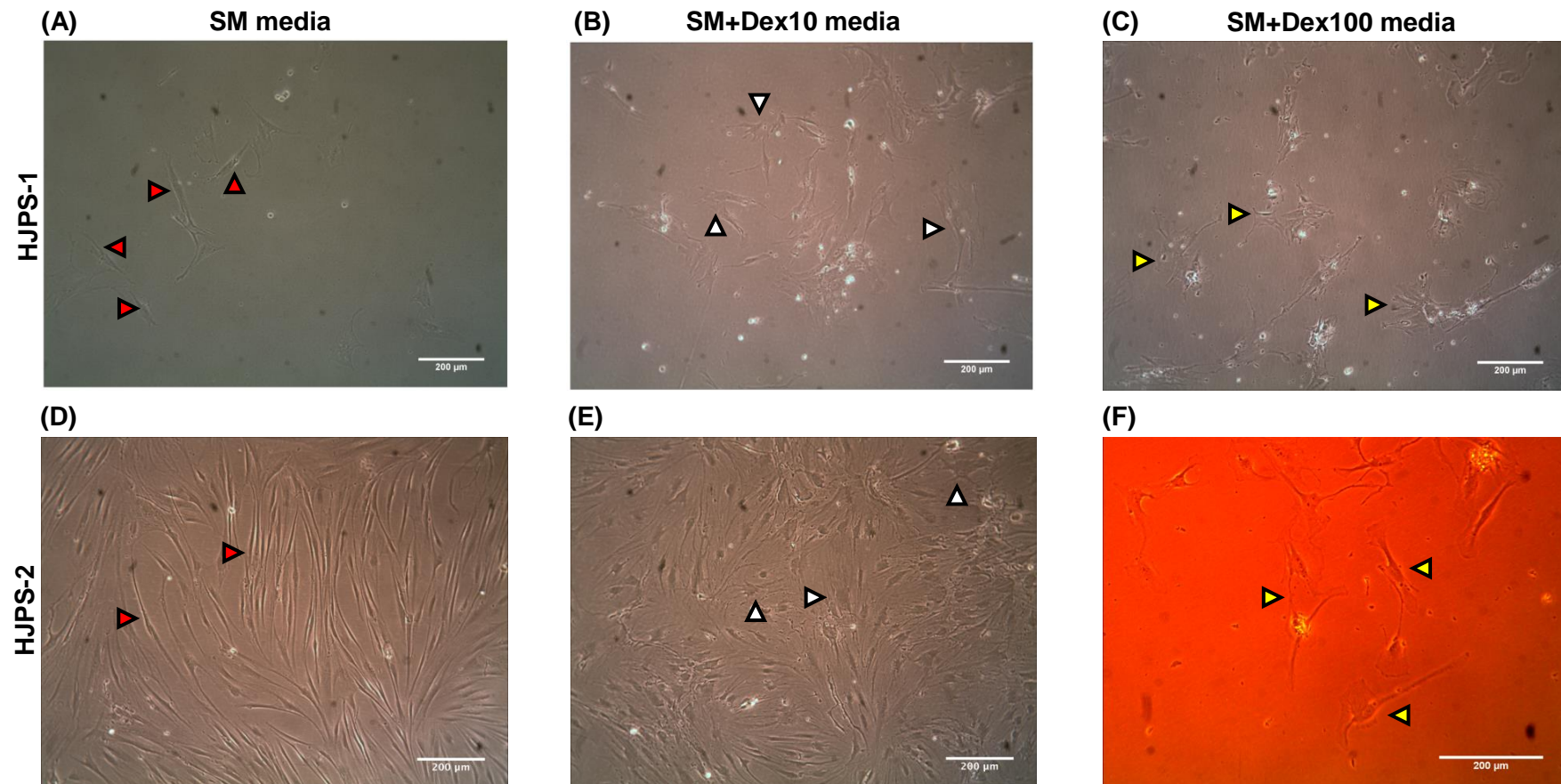


**Figure 3.6.1:** Microphotographs of the morphology of Human jaw periosteal cells (HJPs) cultured in varying concentrations of Dex after 7 days. (A) The HJPs-1 and (D) HJPs-2 in supplemented media (SM) which contained AA and  $\beta$ -GP were more fibroblast fusiform in shape (red arrow heads). (B) The HJPs-1 and (E) HJPs-2 in SM+Dex10 media which contained 10nM of Dex were more cuboidal in shape similar to osteoblast-like cells (white arrow heads). (C) The HJPs-1 and (F) HJPs-2 in SM+Dex100 media which contained 100nM of Dex were more expanded in shape (yellow arrow heads). Scale bar : 200 $\mu$ m.

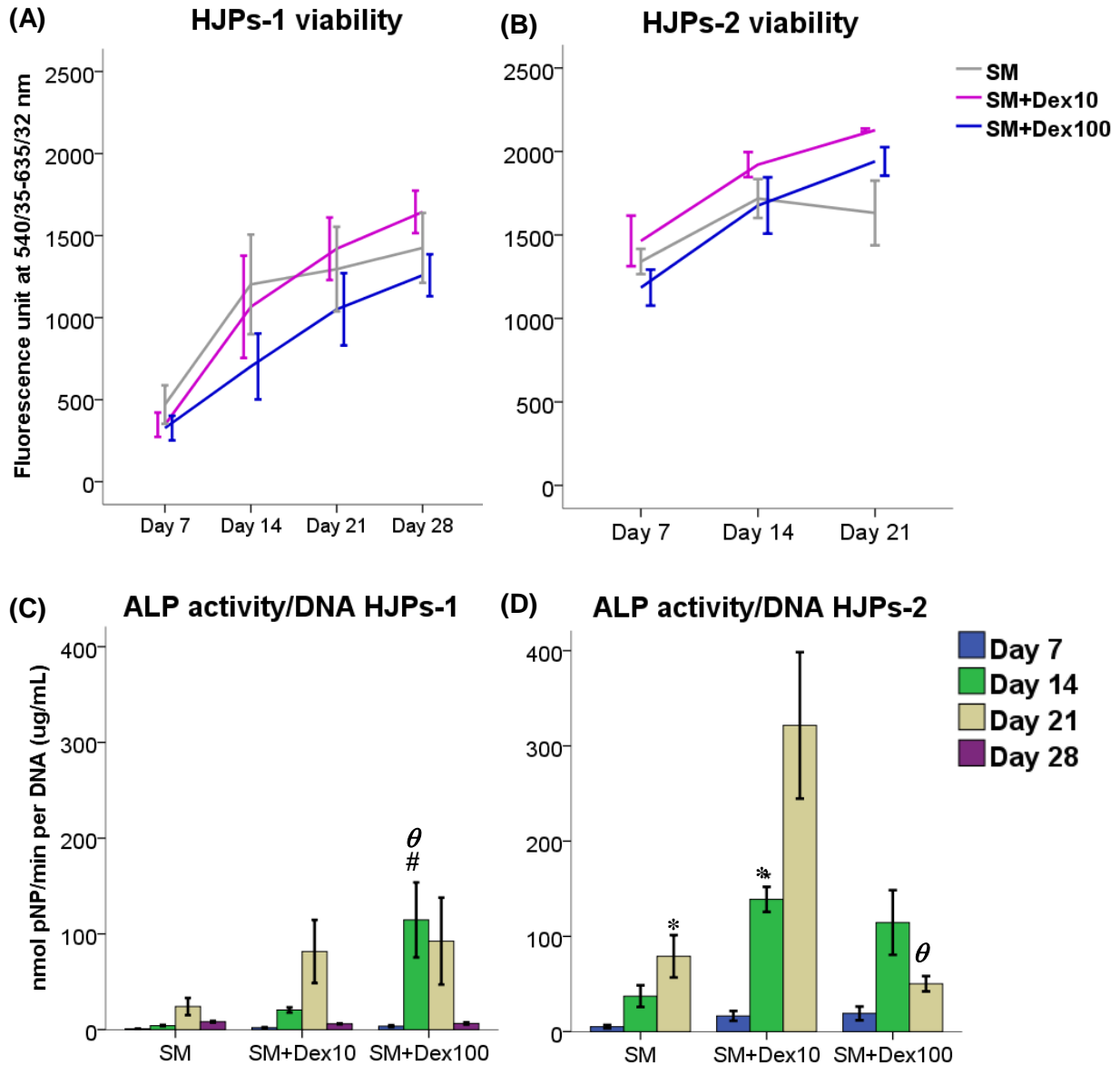


**Figure 3.6.2:** The effects of varying concentrations of Dex (SM, SM+Dex10, and SM+Dex100) on HJPs-1 from 7 to 28 days and HJPs-2 from 7 to 21 days on a monolayer culture in  $\alpha$ -MEM. The cell viability measured by resazurin reduction test of HJP-1 (A) and HJP-2 (B), ALP activity normalized to DNA ( $\mu\text{g/ml}$ ) of HJP-1 (C) and HJPs-2 (D). mean $\pm$ SE, (N=2, n=3), \* =  $p < 0.05$  comparison between the SM and SM+Dex10, # =  $p < 0.05$  comparison between the SM and SM+Dex100 groups, and  $\theta$  =  $p < 0.05$  comparison between the SM+Dex10 and SM+Dex100 groups, Two-way ANOVA, followed by Tukey's multiple comparison test.

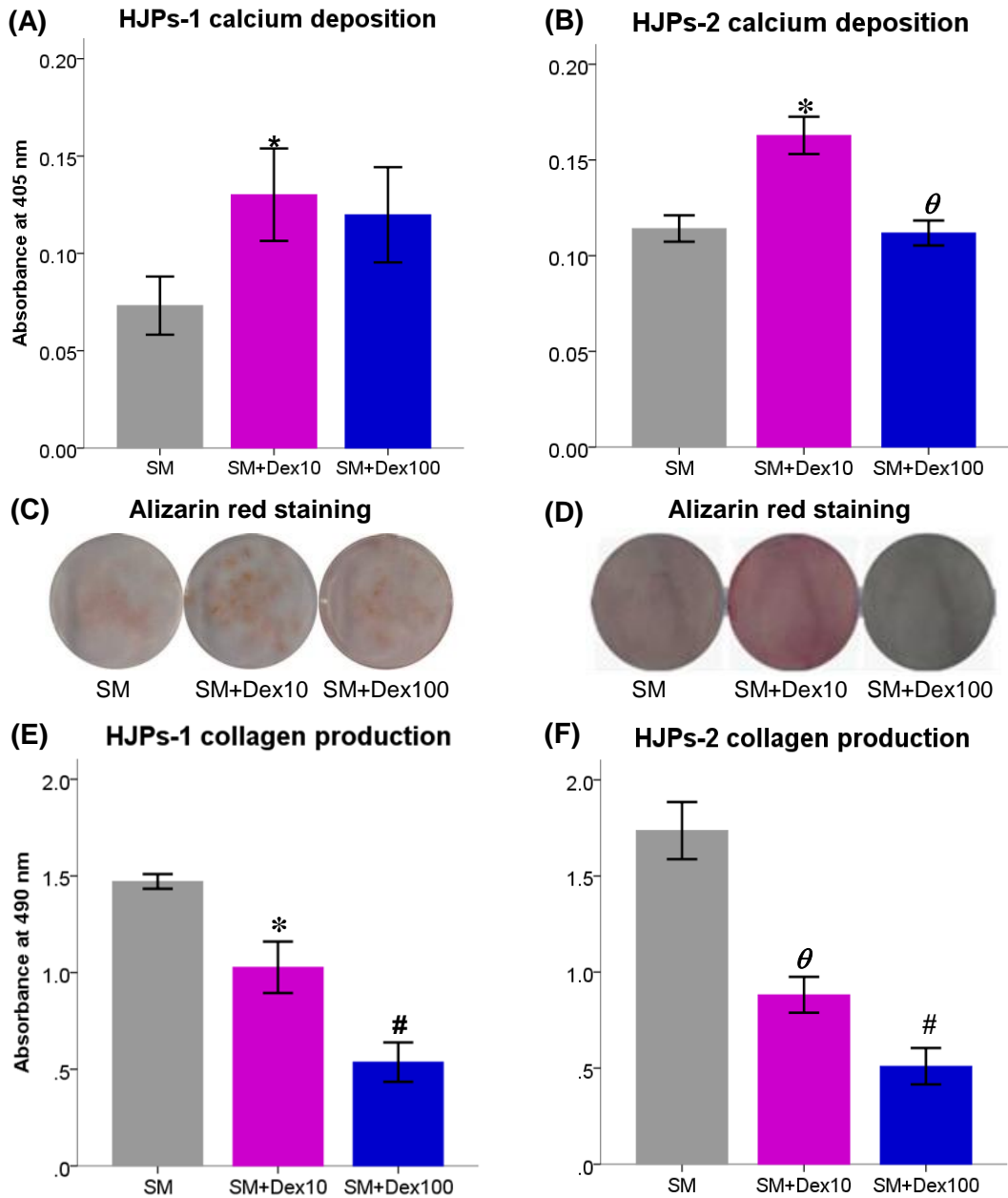


**Figure 3.6.3:** The effects of varying concentrations of Dex (SM, SM+Dex10, and SM+Dex100) on monolayer culture of HJPs. Total calcium deposition using alizarin red staining of HJPs-1 was assayed after 28 days (A) while the HJPs-2 was assayed after 21 days (B). Collagen production using picro-sirius red staining assay of HJPs-1 was assayed after 28 days (E) and the HJPs-2 were assayed after 21 days (F). Photoimages of alizarin red staining of HJPs cultured on a monolayer in different concentration of Dex after 28 days for HJPs-1 (C) and after 21 days for HJPs-2 (D). mean $\pm$ SE, (for Figure A, B, C and D (N=2, n=3) and figure E and F (N=1, n=3)), \* =  $p < 0.05$  comparison between the SM and SM+Dex10, # =  $p < 0.05$  comparison between the SM and SM+Dex100 groups, and  $\theta = p < 0.05$  comparison between the SM+Dex10 and SM+Dex100 groups, one-way ANOVA, followed by Tukey's multiple comparison test

**3.7 Discussion**

Bone tissue engineering may become an option for clinical cleft palate reconstruction. One important part of this strategy is the osteogenic cell source and the biochemical agents used for bone formation and vasculogenesis. The main aims of this chapter were to evaluate suitable cell sources and culture condition for proliferation and osteogenic differentiation of both hESMPs and HJP cells, and the effect these conditions have on VEGF secretion of hESMPs in monolayer culture. In order to do this the first experiments evaluated a suitable concentration of AA as a component in the osteogenic induction medium for MSC cells. The experiment showed that the effect of increasing the concentration of AA on HDFs was higher cell viability over time indicating higher cell proliferation. In our experiment we found that the best concentration of AA is 50µg/mL which gave a higher collagen per viable cell than the other concentrations. Phillips et al., (1994) and Choi et al.,(2008) reported that AA can stimulate cell proliferation and up-regulate collagen synthesis in HDFs and also in MSCs. ECM which is a collagen component mediates the chemical and mechanical signals to enhance cell proliferation and differentiation (Hitomi et al., 1992), and also provide the cell attachment (Wei et al., 2012). Therefore, the optimized concentration of AA for future experiments was chosen as 50µg/ml. A limitation of this study lack of control group (the no AA supplementation) however the studies of Pinnell (1985) and Geesin et al, (1988) showed that AA could stimulates collagen production on HDFs compared to the control group.

All cell types that have been used in this thesis were analysed for their surface antigen expression. Both hESMPs and hBMSCs were confirmed to be MSCs by expression of cell surface antigens (CD146, CD105, and CD90) and no expression of CD45 indicating that the cell population contained MSCs. CD45 would indicate the presence of hematopoietic cells which may contaminate the osteoprogenitor cells. However, in the HJPs-pooled cells surface antigen failed to bind with the CD146 antibody. CD146

is known as a melanoma cell adhesion molecule and it has been found that it has positive expression in human bone marrow cells that contribute to the vascular niche whereas a negative expression in the cells that contribute to the osteoblastic niche (Watt et al., 2013). Human MSCs reside in either osteoblastic or vascular niches which are the specific sites near the endosteal membrane or sinusoidal vessels in adult tissue, respectively (Yin and Li, 2006). Therefore HJPs may derive from osteoblastic niche because the periosteum is a similar membrane to the endosteal membrane while both hESMPs and hBMSCs derive from vascular niche. However, the HJPs detected in this study were also of late passage number (passage number 8), and it's possible that the CD146 cell surface antigen may reduce in expression over passage number (Osipova et al., 2011).

A limitation of this study is that in many cases only 2 experiments were performed in triplicate, however, some interesting differences were identified were found to be significant as follows. It is known that a combination of Dex, AA and  $\beta$ -GP can be used to enable calcified matrix deposition by MSCs. Both the hESMPs and HJPs used in these experiments are relatively understudied cells compared to bone marrow derived MSC hence there is limited literature on the optimum conditions to enable differentiation and bone matrix formation by these cells. Therefore hESMPs were evaluated to investigate whether they respond to osteogenic medium in the same way as mature MSCs. Our study found that the DNA in the SM+Dex100 group increased between the first to second weeks but slightly decreased after the second week onwards indicating that cells proliferated but then cell proliferation slowed after they differentiated into osteoblastic cells, there may also have been some cell death. Media supplemented with Dex promoted ALP activity (an early marker for osteogenic differentiation) over time points and total calcium deposition (a late marker for osteogenic differentiation) after 21days in a dose dependant manner, however, it reduced collagen production. This experiment showed the lowest cell proliferation and collagen production in the high concentration of Dex group

(SM+Dex100) whereas the lower concentration of Dex (SM+Dex10) and without Dex (SM) show no differences both cell proliferation and collagen production. Dex is a synthetic corticosteroid which is usually used to support osteogenic differentiation in MSCs. The supplementation of Dex in culture media would change the cells phenotype to be osteoblastic cells (Cheng et al., 1994) and irreversible enhance ALP activity (Hitomi et al., 1992). However, Dex also reduced cell proliferation and collagen production in the high concentration (100nM) which has been found in several studies on bone marrow stromal cells (Walsh et al., 2001, Advani et al., 1997, Chen, 2006). In this study the calcium deposition play a role as a late marker of osteogenic differentiation but they did not prove the matrix mineralising phenotype. An additional assay such as osteogenic gene expression: RUNX2, OCN, or OPN that could have been performed alongside the presented data to make the conclusions more robust.

VEGF is an important cytokine to recruit endothelial cells for vasculogenesis and is an essential cytokine in bone formation and bone healing after fracture. In this study it was shown that VEGF secretion (during a 48 hour collection period) increased over time for 21 days. The SM+Dex10 group secreted the highest amount of VEGF per viable cell compared to the other groups after 21 days. Wang et al., (2012) found that the 10nM of Dex significantly increased VEGF secretion of human umbilical cord MSCs (hUC-MSCs) compared to treating with 100nM of Dex ( $p < 0.01$ ). The VEGF gene composes of a promoter region called AP-1 which is a potential binding site to initiate transcription factors and lead to regulate gene expression (Tischer et al., 1991). A complex formation between Dex and Dex-glucocorticoid receptor can inhibit the VEGF induction by binding on the AP-1 promoter regions. Resulting in, prevention of AP-1 dependent transcription processes and inhibition of VEGF production (Heiss et al., 1996, Jonat et al., 1990). This implies that Dex affected the VEGF secretion from the cells in a concentration dependent manner. Interestingly, the VEGF secretion per viable cell increased over time and by day 21 there was no difference between the

groups (SM, SM+Dex10, and SM+Dex100). The increase over time may be related to cell density; one could speculate that there is less oxygen available per cell at higher densities. It is known that expression of VEGF is highly sensitive to the oxygen. Pham et al., (2002) showed that hypoxia induced angiogenesis by up-regulation of VEGF in rat alveolar epithelial cells in monolayer culture. Several studies both *in vivo* and *in vitro* reported that cells cultured under a hypoxia condition (2% O<sub>2</sub>) for at least 30 minutes could up-regulate hypoxia inducible factor-1 (HIF-1), which can enhance VEGF secretion compared to the normal O<sub>2</sub> condition (Semenza, 1999, Machein et al., 1999, Wang et al., 2007). At this stage it is not clear why the inhibitory effect of Dex on VEGF diminishes over time in culture, but it may be related to the osteogenic pathways which are stimulated by Dex and are known to up-regulate VEGF overcoming the Dex inhibition that occurs in more immature MSCs. Furumatsu et al., (2003) *in vitro* study found that the VEGF secretion on hBMSCs under continuous 10nM of Dex supplementation for 3 weeks showed an increasing of VEGF secretion while they also majority expressed OCN gene, indicating that the osteoblastic cells may secrete the VEGF for their own survival.

HJPs have been chosen for this study, but there was limited information in the literature on the suitable culture conditions for osteogenic differentiation. Therefore, the first step for HJPs culture was to compare the various types of culture media to stimulate proliferation of HJPs. A limitation of this study is that only one experiment was performed in triplicate, however, some interesting differences were identified and found to be significant. The cell number of HJPs from 2 donors increased in the  $\alpha$ -MEM media while the additional supplements did not affect cell proliferation. A study by Coelho et al., (2000) and Chen et al., (2009) reported that  $\alpha$ -MEM media is suitable to use for isolation and culturing bone marrow cells. The  $\alpha$ -MEM media itself includes Vitamin B12, AA and non-essential amino in addition to the components of DMEM media. This medium may facilitate HJPs cell proliferation and enable HJPs to differentiate

into the osteoblastic lineage in a similar way as bone marrow cells. Several studies used  $\alpha$ -MEM to culture these types of cells. However, Nakamura et al., (2008) found that human MSCs cultured on both DMEM media and specific MSC basal medium were no different in their cell behaviour including growth rate and an osteogenic differentiation. The difference in cell proliferation between the two HJPs sources may be due to variation between patients, and site of extraction. HJPs are a heterogeneous population of cells. Therefore fluorescence activated cell sorting or fibronectin coated culture plate could distinguish the MSCs from the heterogeneous cell population for the future work (Ogura et al., 2004, De Bari et al., 2008). For the remaining experiments the  $\alpha$ -MEM media was used to culture HJPs.

The next aim was to optimize osteogenic media condition for HJPs. This study showed that HJPs from two donors had the ability to undergo osteogenic differentiation similar to hESMP osteogenic progenitors. Both donors of HJPs have different characteristics with regards to cell morphology and cell proliferation, but similar conditions were required; 10nM of Dex (SM+Dex10) for osteogenic differentiation, and a reduction of collagen production at the high concentration of Dex (SM+Dex100). Li et al., (2005) and Walsh et al., (2001) reported that the higher concentrations of Dex and prolonged treatment can induce osteoporosis by three mechanisms: 1] reduction in cell number of osteogenic precursor cells and activity of osteoblastic cells, 2] increase in cell number and activity of osteoclast cells, and 3] reduced VEGF secretion. Consistent with a clinical study by Dempster et al., (1983), Walsh and Avashia, (1992), and Labar et al., (2010) found that patients treated with prednisolone which is a derivative of glucocorticoid group, similar to Dex, reduced the active period of osteoblastic cells for bone formation and increased resorption surface areas, compared to control groups. HJPs have been used in many studies as an osteoprogenitor cell source (Samee et al., 2008). Cicconetti et al., (2007) found that HJPs from maxilla and mandible under a basic culture media expressed surface

markers similar to MSC markers. HJPs could express the high levels of positive markers of CD 105, CD 49, CD 63, CD90, and CD 140. The differences are most likely due to patient variability and site of tissue harvesting (Marolt et al., 2010). Akintoye et al., (2006) found that the expression of periosteal cell specific markers was different depending on the harvesting site and patient variability caused by factors such as individual habit, age, and health. Our studies found that the ALP activity of hESMPs was higher than the HJPs possibly indicating that the hESMPs had more osteogenic potential than the HJPs. The reason may be that the HJPs were derived from adult donors in which only a sub-population of cells could undergo osteogenic differentiation (Caplan, 2005). Whereas, the hESMPs derived from embryonic stem cells had a homogenous population of cells which were able to undergo osteogenic differentiation (Karlsson et al., 2009). The expression profile of MSCs can be different depending on the harvesting site, it has been found that the orofacial bone marrow (OBM) shows more osteogenic differentiation and quantity of bone regeneration than iliac bone marrow (IBM) (Akintoye et al., 2006, Osyczka et al., 2009). The OBM may contain less hematopoietic marrow cells compare to the IBM. Comparison of four differences cell sources from rabbits; JPO: periosteum from mandible, JBM: bone marrow from mandible, LPO: periosteum from tibia, and LBM: bone marrow from tibia indicated the stem cell potential of these cells *in vitro*, this study found that JPO showed the highest osteogenic differentiation (Park et al., 2012). The JPO have been recommended to be a first choice for repairing a maxillofacial region. Previous work within our group has showed that hBMSCs incubated with 10nM of Dex undergo osteogenic differentiation *in vitro* study (Sittichokechaiwut et al., 2010). Therefore, hBMSCs were not included in this chapter for evaluating the suitable osteogenic induced culture condition.

Chen et al., (2011) compared the osteogenic potential of between human MSCs from periosteal and bone marrow derived cells at the same harvesting site (metaphyseal

region) from the same donors found that the MSCs from periosteal derived cells showed the higher osteogenic gene expression (BMP-2, OPN, and OCN) and mineralization than the hBMSCs. Age of donor also influence the MSCs potential as younger IBM have a more osteogenic response than the older IBM when they were cultured under recombinant human BMP-2 (Osyczka et al., 2009). HJPs could be used as an autologous cell source in the treatment of cleft palate defects due to their potential to undergo osteogenic differentiation in a laboratory for clinical use. Therefore, it would be ideal to test the osteogenic potential of HJPs from higher number of patients in order to compare the outcome and from child donors. Unfortunately we had insufficient human jaw periosteum supply.

### 3.7. Summary of results

One important part of bone tissue engineering is the cell source which should have osteogenic potential. The aims of this chapter were to evaluate suitable culture conditions for both hESMPs and HJPs for osteogenic differentiation. From these studies we found that;

- A suitable concentration of AA is 50 $\mu$ g/mL which produces the highest collagen per HDF cell of the concentrations tested. This concentration will be used for the future experiments.
- Dex induced a change in morphology of hESMPs from a fibroblastic fusiform shape to an osteoblastic cell shape.
- Dex stimulated osteogenic differentiation by increasing ALP activity and calcium deposition, whereas it also reduced cell number, collagen production, and VEGF secretion in a dose-dependent manner.
- The SM+Dex100 medium condition will be used for osteogenic differentiation of hESMPs in future experiments due to the significantly higher ALP and calcium deposition induced in this medium.

- Both donors of HJPs have the ability to undergo osteogenic differentiation showing similar outcomes to the hESMP osteogenic progenitors.
- The  $\alpha$ -MEM media and SM+Dex10 media conditions will be used for culturing and inducing osteogenic differentiation of HJPs in the future experiments due to having the same or even a more stimulatory effect on ALP and calcium deposition compared to SM+Dex100.

HJPs collected from 2 different donors showed variability in growth rate and differentiation ability, therefore it would be ideal to test the osteogenic potential of HJPs from more patients to compare the outcomes. Unfortunately the insufficient HJP tissue supplied to do this, however, these cell characterizations and selected suitable culture conditions will be used in future experiments described in subsequent chapters.

### **3.8. Future work**

Characterisation of all cells from individual donors to evaluate surface antigen expression of known MSCs markers.

**CHAPTER FOUR: THE EFFECT OF A SIMPLE FLUID SHEAR STRESS STIMULUS OF OSTEOGENIC PROGENITOR MATRIX PRODUCTION.**

**4.1 Introduction**

MSCs have been used in bone tissue engineering for several years. The work reported in chapter 3 showed that hESMPs and HJPs differentiate into osteoblastic cells by biochemical stimulation by adding Dex supplementation. Behnia et al., (2009) and Hibi et al., (2006) reported that a patient's own MSCs from bone marrow could be used as the cell sources in bone tissue engineering for alveolar reconstruction. Therefore, all three cell types will be used in these studies to evaluate osteogenic differentiation. Cells can be stimulated by many pathways to differentiate into osteoblastic lineage cells, for example biochemical, mechanical and environmental stimulation. Many studies have shown that fluid flow created mechanical stress can enhance MSC's osteogenic differentiation (Yourek et al., 2010, Bancroft et al., 2002, Sikavitsas et al., 2003, Delaine-Smith et al., 2012). These studies have used different types of flow stimulus for example laminar flow versus pulsatile flow versus oscillatory flow both in monolayer and through 3D porous scaffolds. OFF is thought to be similar to the flow found in the canalicular system in mature bone structure (see chapter1) and flow in the bone marrow (Gurkan and Akkus, 2008). Previous work from our group, Delaine-Smith et al, (2012) studied the effects of OFF *in vitro* on hESMPs cultured in a typical 6-well plate using a standard see-saw rocker to produce the OFF (described in chapter 2). They found that the OFF successfully increased collagen production and mineralized matrix in osteoprogenitor cells in monolayer culture. Our group found that a suitable OFF loading regime, using a standard see-saw rocker to increase osteogenic differentiation is a speed of 45 rounds per minutes, flip angle of 6°, for 1 hour per day, 5 days per week. Therefore this regime will be used in the experiments (Delaine-Smith et al., 2012).

Therefore this simple mechanical stimulation system was chosen for all of the following experiments in this chapter. This method may increase osteogenic differentiation and mineralization of osteoprogenitor cells for use for the construct for cleft palate patients. The advantages of this system are cost effectiveness, straight forward pre-treatment method, and high throughput for bone tissue engineering.

Therefore the aim of these experiments is to evaluate the effects of OFF, using a standard see-saw rocker, on cell proliferation, osteogenic differentiation, extracellular matrix production and VEGF secretion by hESMPs, hBMSCs, and HJPs in monolayer.

## 4.2 Methods

### 4.2.1 Cell culture

Three cell types were used for each study; hESMPs, HJPs, and hBMSCs. The HJPs and hBMSCs isolation methods were described in chapter 2. hESMPs (passage number 4 to 8), 2 different donors HJPs (passage number 6 to 8), and 3 different donors of hBMSCs (as described and characterized in chapter 3) (passage number 2 and 3) were used for OFF studies. Media which was used in all studies was basal  $\alpha$ -MEM supplemented with AA and  $\beta$ -GP medium which will be designated 'SM' group, SM supplemented with 10nM of Dex will be designated 'SM+Dex10', and the SM supplemented with 100nM of Dex will be designated 'SM+Dex100'.

### 4.2.2. OFF application

For experiments, hESMPs were cultured in gelatine-coated standard circular 6-well plates at a density of  $10^4$  cells per well, the other cells were cultured on the non-coated well plates. All cell types were cultured in their basic culture medium on the day of seeding cell (day 0). The following day, the culture media were changed to either SM, SM+Dex10 or SM+Dex100. From day 4 of culture, the samples were divided into 2 different groups: 1] the 'Rocking group' is the cells subjected to continuous OFF with 45 cycles/minutes for an hour/day, and 5 days/week, 2] the static group is cells that were moved to the laboratory bench when the rocking group was undergoing OFF then they were moved back to the cell incubator. Delaine-Smith et al, (2012) calculated the OFF stress on the 6-well plate in 3 different points parallel to the diameter ( $x/L=0.25, 0.5, \text{ and } 0.75$ , where 'x' is a distance from the reference point to the edge of the well and 'L' is a diameter of the well)

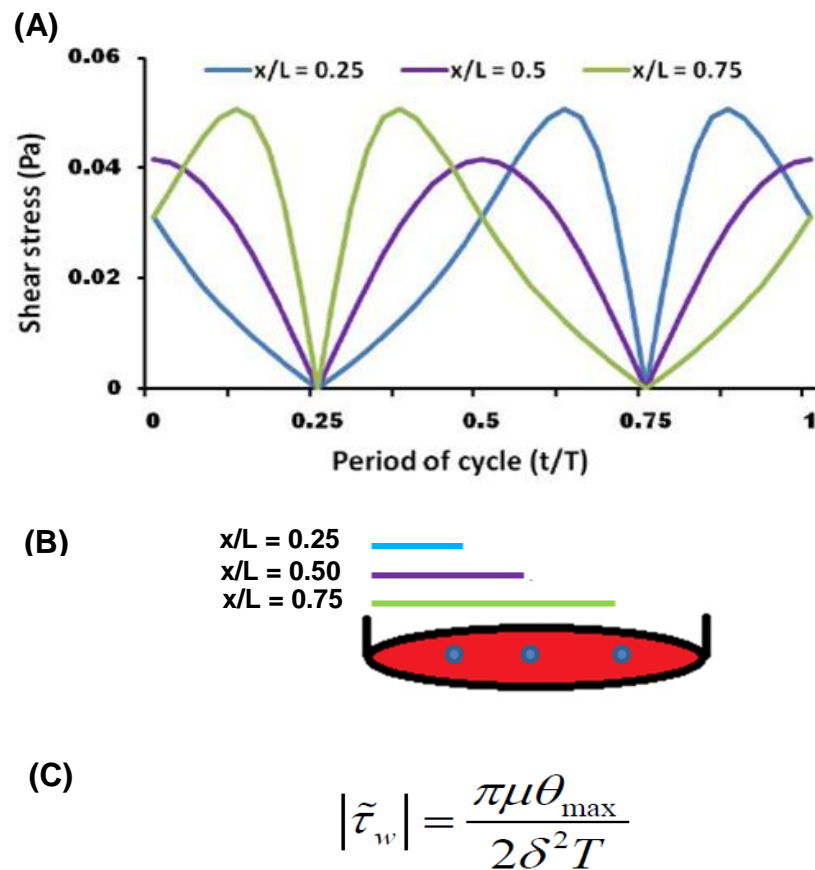


**Figure 4.2.1:** (A) The calculated OFF stress in 3 different points parallel the with diameter at the circular culture surface of the 6-well plate for one cycle;  $x/L = 0.25, 0.5,$  and  $0.75$ . (B) Where  $x$  is a distance from the reference point to the edge of the well and  $L$  is the diameter of the well in the axis of rotation. (C) The value of fluid flow stress on the circular culture dish received from the formula. Where  $\mu$  is the fluid viscosity ( $10^{-3}$  Pa s),  $\theta_{\max}$  is the maximum flip angle. (6.8 degree in the 2 ml of media condition),  $\delta$  is the ratio between the depth of fluid and the length of well,  $T$  is the period of time per one cycle. Reprinted from (Delaine-Smith et al., 2012) for figure A and (Zhou et al., 2010) for figure C with kind permission of European Cells and Materials and Elsevier, respectively.

### 4.3. The effect of OFF on osteogenic differentiation of hESMPs on monolayer culture.

#### 4.3.1. Results

On day 7, the cell morphology of the rocking (upper row) and static (lower row) groups cultured under SM medium (A,D) showed a more fibroblastic fusiform shape (red arrow heads), while the cells cultured under both SM+Dex10 (B,E) and SM+Dex100 (C,F) media were more cuboidal in shape which is similar to a typical osteoblastic cell (white and yellow arrow heads, respectively) (Figure 4.3.1). The DNA increased at all conditions (SM and SM with varying concentrations of Dex) from day 7 to 21. However the SM+Dex100 group had a slight decrease in DNA after 14 to 21 days in both the rocking and static groups indicating that there were lower cell numbers than the other groups (Figure 4.3.2 A). The SM group showed the lowest ALP activities normalized to DNA from day 7 to 21. By day 21, the highest ALP activity in the rocking group was in the SM+Dex10 condition but this was not significantly different from the SM+Dex100 group. The highest ALP activity of the static group was the SM+Dex100 condition (Figure 4.3.2 B). The secretion of VEGF (during a 48 hour collection period) increased in all conditions at all time-points. By day 14, the SM groups showed higher VEGF secretion than others while the SM+Dex100 groups showed the lowest, indicating that Dex inhibits VEGF. After day 21 the highest VEGF secretion was in the SM+Dex10 groups; for both the rocking and static groups (Figure 4.3.3) although there was no statistically significant difference between any treatments groups in VEGF secretion by this time-point ( $p \leq 0.05$ ). Total calcium deposition by the SM+Dex100 rocking group was significantly higher than for any other group by day 21 ( $p \leq 0.05$ ). The SM group produced the lowest calcium deposition in both the rocking and static groups (Figure 4.3.4 A). The effect of Dex on collagen production confirmed the results of chapter 3 and rocking had no further statistically significant effect (Figure 4.3.4 B). The SM+Dex100 group under rocking conditions (upper row) had the darkest alizarin red

## CHAPTER FOUR

staining after 21 days compared to the other groups indicating that there was more calcium deposition than the other groups. For the SM+Dex10 group under rocking conditions there was a small area of staining whereas there was none present on the static group (Figure 4.3.4 C) and this matched the small but not statistically significant difference in quantitated alizarin red between the two groups. The picro-sirius red staining of SM groups was the darkest staining whereas the SM+Dex100 groups were the lightest staining compared to the other both the rocking and static conditions (Figure 4.3.4 D).

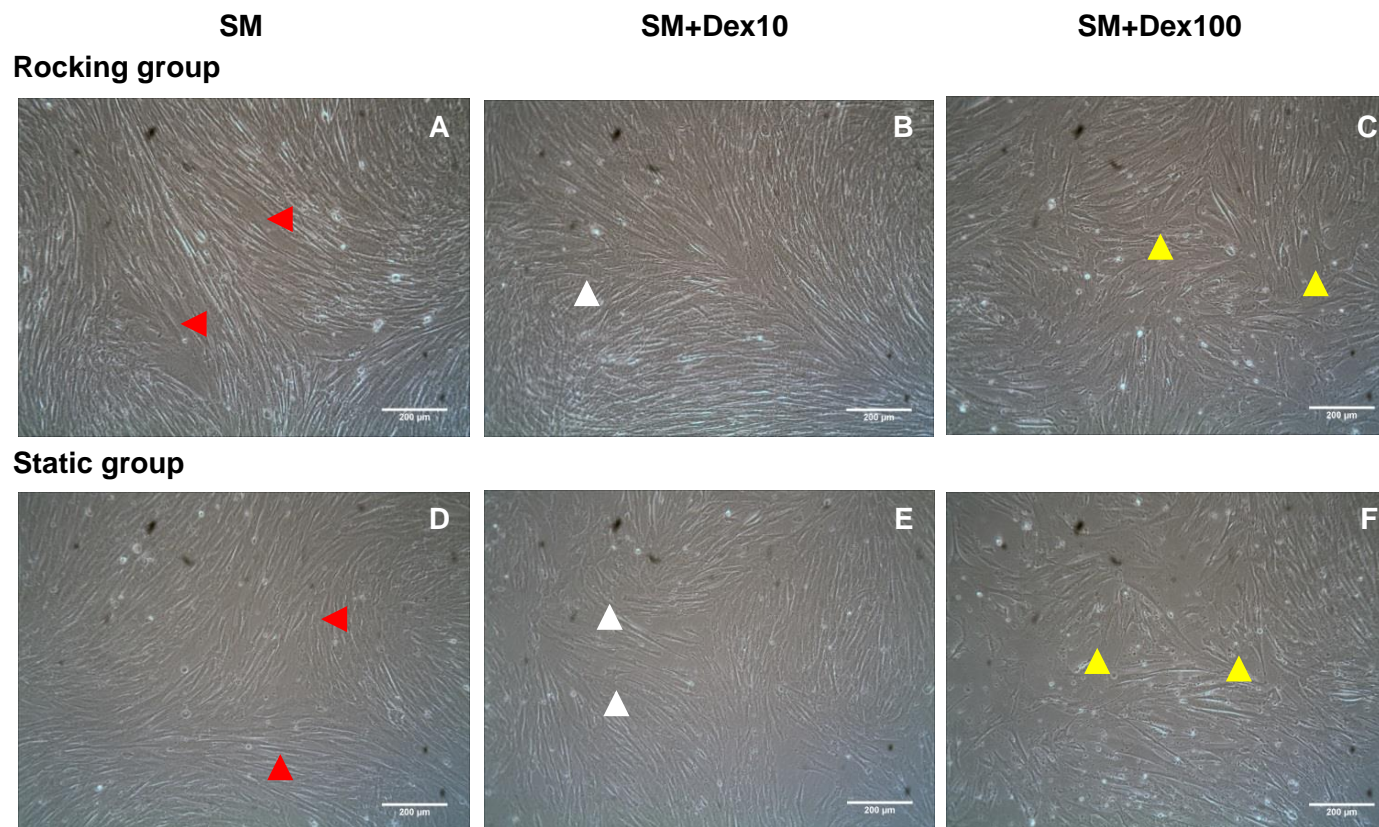


**Figure 4.3.1:** Microphotographs of the morphology of hESMPs for the rocking group (upper row) which was subjected to OFF for 1 hour/day, 5 days/week, and static group (lower row) at room temperature. The cells were cultured in the varying concentrations of Dex: supplemented media (SM) which contained AA and  $\beta$ -GP, supplemented media with 10nMDex (SM+Dex10), and supplemented media with 100nMDex (SM+Dex100) for 7 days. (A and D) The SM group were more fibroblastic in shape (red arrow heads) while the SM+Dex10 (B and E) and SM+Dex100 (C and F) groups were more cuboidal in cell shape similar to osteoblastic cells (white and yellow arrow heads, respectively). There were no differences between the rocking and static groups. Scale bar: 200 $\mu$ m

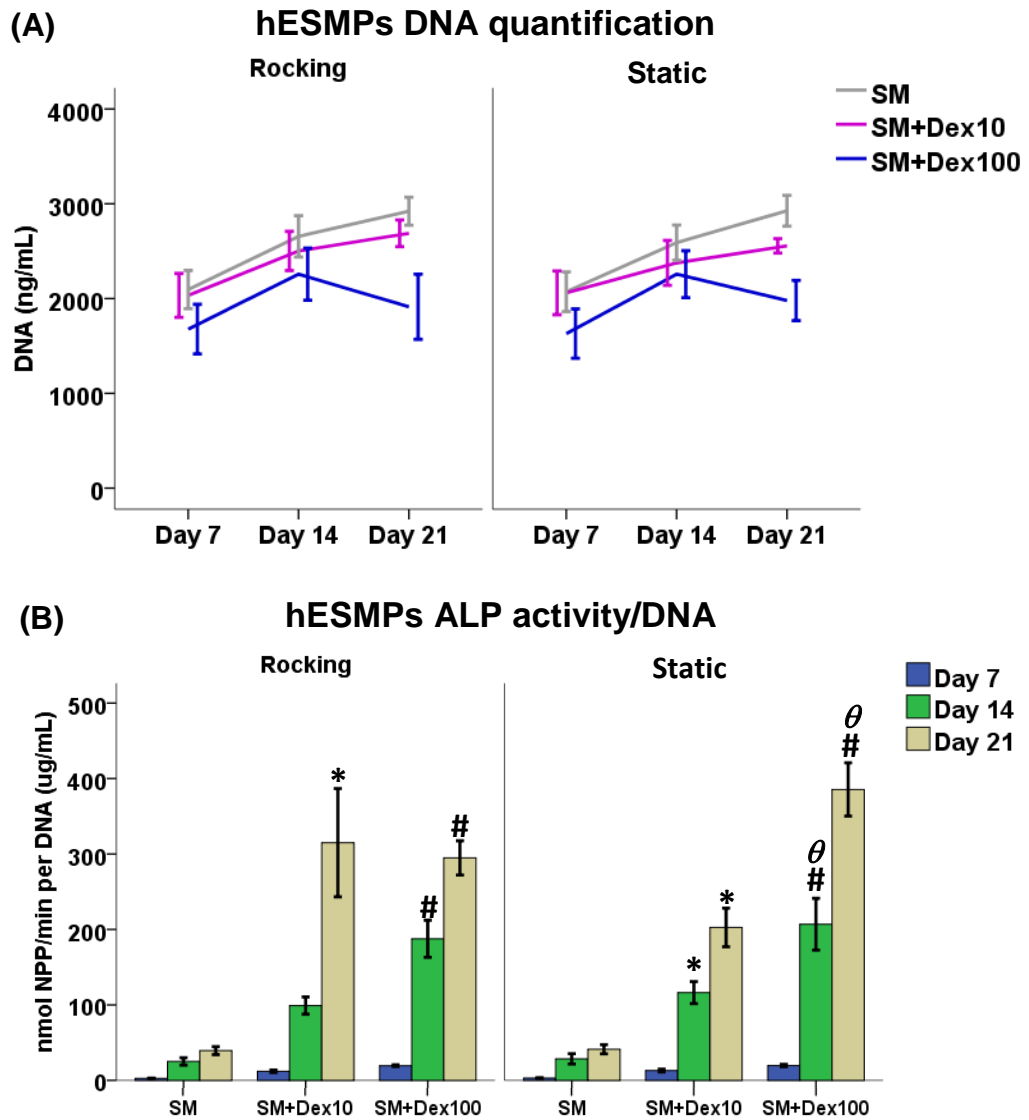


**Figure 4.3.2:** The effect of OFF on hESMPs between the rocking and static groups under varying concentrations of Dex: supplemented media (SM), supplemented media with 10nM of Dex (SM+Dex10), and supplemented media with 100nM of Dex (SM+Dex100) on monolayer culture after 21 days. DNA quantification (A), ALP activity normalised to DNA ( $\mu\text{g/ml}$ ) (B). mean  $\pm$  SE, (N=4, n=3),  $*$ = $p < 0.05$  comparison between SM and SM+Dex10, # =  $p < 0.05$  comparison between SM and SM+Dex100,  $\theta$  =  $p < 0.05$  comparison between SM+Dex10 and SM+Dex100, using Two-way ANOVA, Tukey's multiple comparison test.

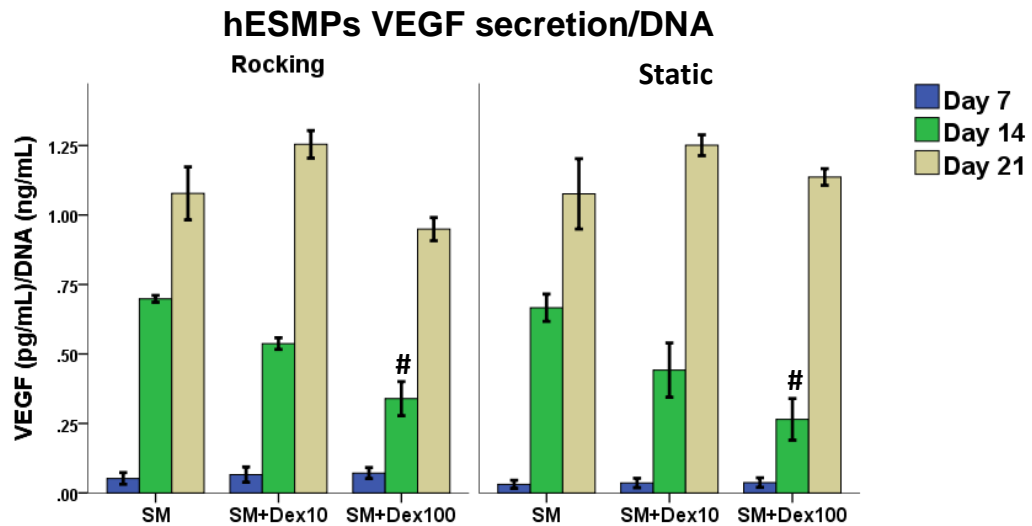


**Figure 4.3.3:** The effect of OFF on hESMPs between the rocking and static groups under varying concentrations of Dex: supplemented media (SM), supplemented media with 10nM of Dex (SM+Dex10), and supplemented media with 100nM of Dex (SM+Dex100) on monolayer culture after 21 days. Data is a VEGF secretion (during a 48 hour collection period) normalised to DNA (ng/ml) presented as mean  $\pm$  SE, (N=2, n=3), # =  $p < 0.05$  comparison between SM and SM+Dex100, using Two-way ANOVA, Tukey's multiple comparison test.

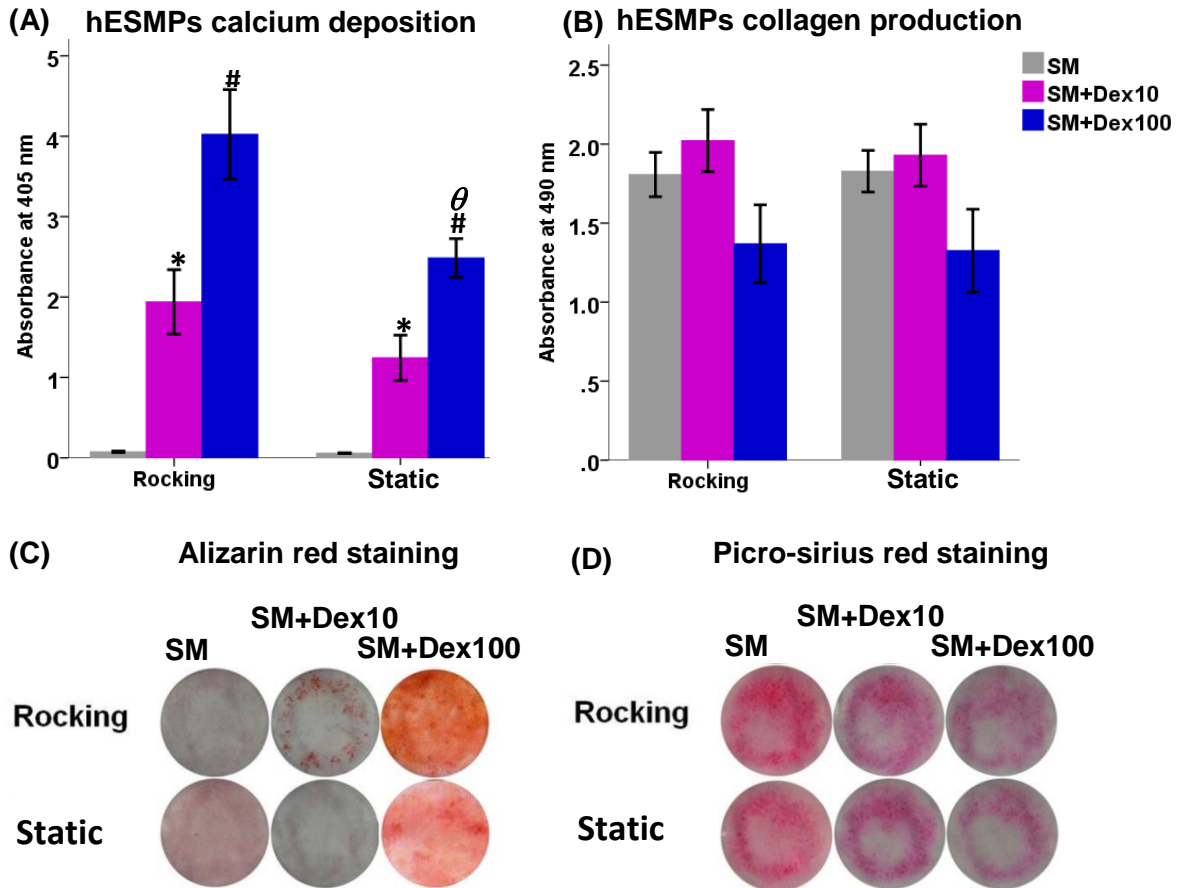


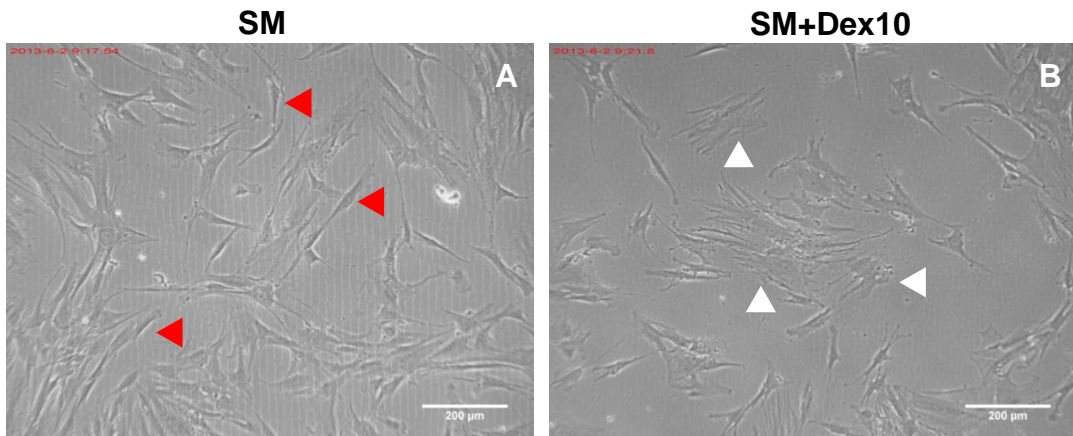
**Figure 4.3.4:** The effect of OFF on hESMPs between the rocking and static groups under varying concentrations of Dex: supplemented media (SM), supplemented media with 10nM of Dex (SM+Dex10), and supplemented media with 100nM of Dex (SM+Dex100) on monolayer culture after 21 days. Total calcium deposition (A) using alizarin red staining and total collagen production (B) using picro-sirius red staining. The photoimages show representative sets of alizarin red staining (C) and picro-sirius red staining (D) on monolayer cultured of hESMP. (A,B) Data is presented as mean  $\pm$  SE, (N=4, n=3),  $*$ = $p < 0.05$  comparison between the SM and SM+Dex10 groups, #= $p < 0.05$  comparison between the SM and SMDex100 groups,  $\theta$ = $p < 0.05$  comparison between rocking and static groups, using two-way ANOVA, Tukey's multiple comparison test.

**4.4. The effect of OFF on osteogenic differentiation of hBMSCs on monolayer culture.****4.4.1. Results**

The cell morphology of the rocking (upper row) and static (lower row) groups cultured under the SM medium (Figure 4.4.1 A,C) were more fibroblast fusiform in shape (red arrow heads). While the cell morphology cultured under SM+Dex10 medium were more cuboidal in shape which is similar to a typical osteoblastic cell shape (white arrow heads, Figure 4.4.1 B,D) similar to hESMPs (Figure 4.3.1 C,F). The DNA increased at all conditions (SM and SM+Dex10) from day 7 to 14 while the SM+Dex10 groups had higher DNA than the other by day 14. The SM+Dex10 group under rocking condition had slightly lower DNA by day 21 indicating that they were fewer cells than the other groups (Figure 4.4.2 A). The SM group showed the lowest ALP activity normalized to DNA from day 7 to 21. By day 21, the highest ALP activity in the rocking group was the SM+Dex10 condition but there were no differences between the rocking and static groups (Figure 4.4.2 B). The secretion of VEGF (during a 48 hour collection period) increased overtime at all conditions over 21 days. By day 14, the SM groups showed higher VEGF secretion than other group in both the rocking and static conditions, indicating that Dex inhibits VEGF secretion. On day 21, there were no significant differences between any treatment groups by this time-point (Figure 4.4.2 C). Total calcium deposition by the SM+Dex10 rocking group was higher than for any other groups by day 21. The SM group produced the lowest calcium deposition in both the rocking and static groups (Figure 4.4.3 A) whereas the SM groups gave no staining by day 21. The SM and SM+Dex10 groups had no significant differences in collagen production. The rocking groups produced the highest collagen compared to the static groups after 21 days. However, the SM+Dex10 groups had lower collagen production than in the SM medium (Figure 4.4.3 B). The SM+Dex10 group subjected to OFF showed the darkest staining, compared to the SM+Dex10 static group after 21 days. The

SM+Dex10 group under rocking conditions was the darkest and most uniform alizarin red staining after 21 days, compared to the other groups, indicating that there was more calcium deposition (Figure 4.4.3 C). The picro-sirius red staining of the rocking group gave a darker staining than the SM+Dex10 group. There were no differences between the SM and SM+Dex culture media (Figure 4.4.3 D).

**Rocking**



**Static**

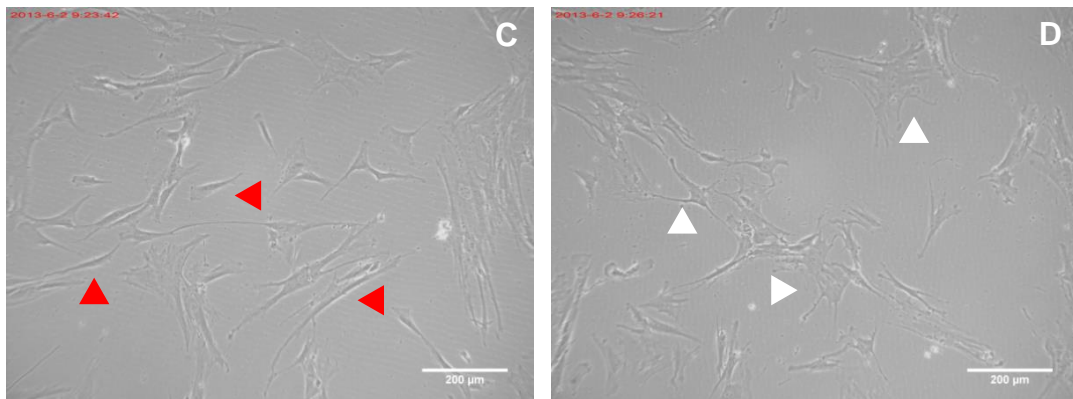


**Figure 4.4.1:** Microphotographs of the morphology of hBMSCs under the rocking and static groups for 1 hour/day, 5 days a week. The cells were cultured in the supplemented media (SM), which contained AA and  $\beta$ -GP and supplemented media with 10nMDex (SM+Dex10) of hBMSCs on monolayer culture after 7 days. (A and C) The SM group were more fibroblastic in shape (red arrow heads) while the SM+Dex10 (B and D) groups were more cuboidal in cell shape, similar to osteoblastic cells (white arrow heads). Scale bar: 200 $\mu$ m

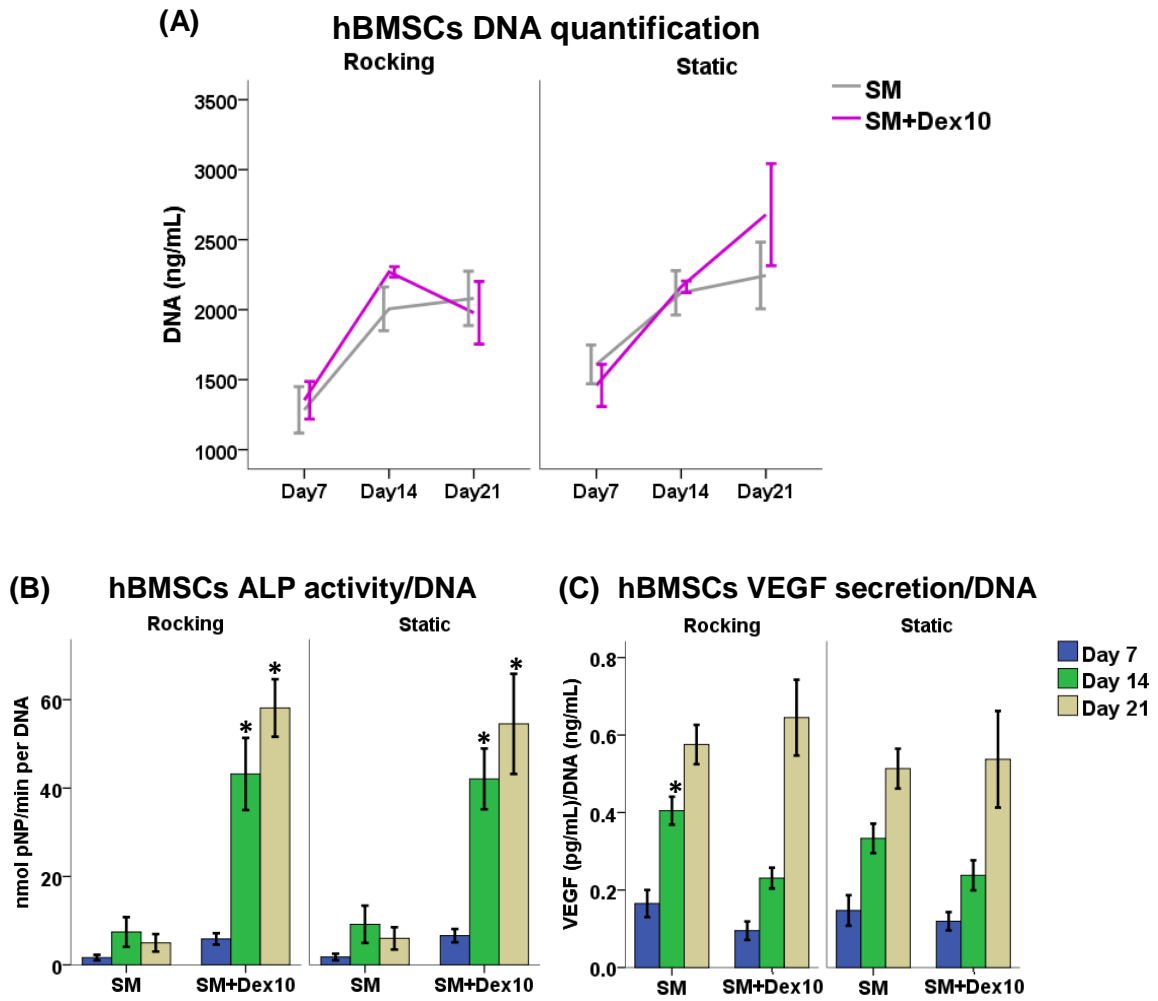


*Figure 4.4.2: The effect of OFF on hBMSCs under supplemented media (SM) and supplemented media with 10nM of Dex (SM+Dex10) of hBMSCs on monolayer culture after 7, 14, and 21 days. DNA quantification (A), ALP activity normalised to DNA (B), and VEGF secretion (during a 48 hour collection period) normalised to DNA (ng/ml) (C). Data is presented as mean  $\pm$  SE, (N=3, n=3), \*= $p$ <0.05 comparison between SM and SM+Dex10, using Two-way ANOVA, Tukey's multiple comparison test.*

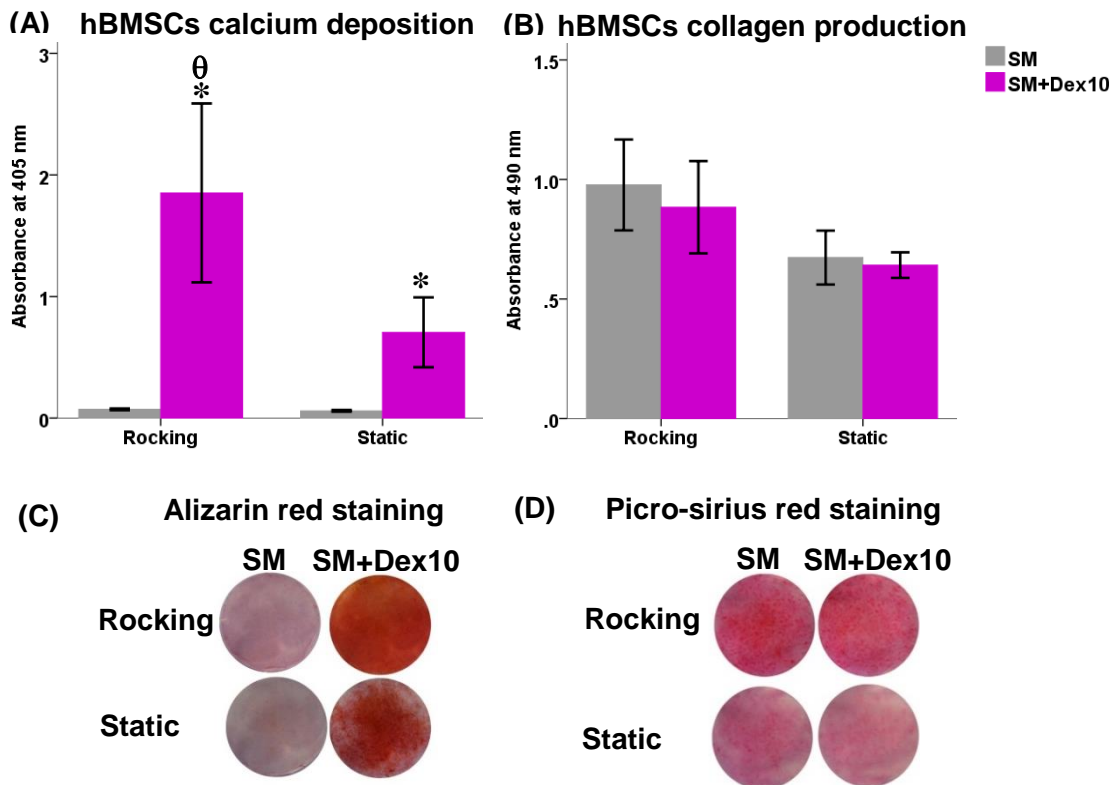


**Figure 4.4.3:** The effect of OFF on hBMSCs under the supplemented media (SM) and supplemented media with 10nM of Dex (SM+Dex10) on monolayer culture after 21 days. Total calcium deposition (A) using alizarin red staining and total collagen production (B) using picro-sirius red staining. (C) The photoimages show representative set of alizarin red staining and (D) picro-sirius red staining on monolayer cultured of hBMSCs. (A,B) Data is presented as mean  $\pm$  SE, (N=3, n=3),  $\ast = p < 0.05$  comparison between the SM and SM+Dex10 groups,  $\theta = p < 0.05$  comparison between the rocking and static groups, using Two-way ANOVA, Tukey's multiple comparison test.

### **4.5. The effect of OFF on osteogenic differentiation of HJPs on monolayer culture.**

#### **4.5.1. Results**

This experiment evaluated the effect of OFF on 2 different donors of HJPs: HJPs-1 and HJPs-2 which showed different responses, therefore, we present them in separate results.

#### **Results of HJPs-1**

The DNA of HJPs-1 increased at all conditions (SM and SM+Dex10 groups) from 7 to 28 days (Figure 4.5.1 A). The SM groups were slightly higher than the SM+Dex10 groups both for rocking and static groups, implying that the SM groups had higher cell proliferation than the SM+Dex10 groups. The SM groups showed a lower ALP activity normalized to DNA than the SM+Dex10 groups in both rocking and static groups at all time-points (Figure 4.5.1 B). By day 14, the highest ALP activity in the rocking group was the SM+Dex10 condition, compared to any other groups, then this gradually decreased after 14 to 28 days. By day 21, the highest ALP activity was the SM+Dex10 in the static group which was followed by a slight decrease afterwards. Total calcium deposition by the SM+Dex10 rocking group was higher than for any other groups by day 21 (Figure 4.5.2 A). The SM group produced the lowest calcium deposition in both the rocking and static groups. The SM+Dex10 groups produced the lowest amount of collagen indicating that Dex inhibits collagen production compared to the other group in both the rocking and static groups on day 21 (Figure 4.5.2 B). The SM+Dex10 group under rocking conditions (upper row) gave the darkest alizarin red staining after 28 days compared to the other groups indicating that there was the more calcium deposition than the other groups (Figure 4.5.2 C). The SM static group (lower row) contained patchy staining and was faint at the center and periphery indicating that there was lower calcium deposition. The picro-sirius red staining images of the SM+Dex10 groups

indicated lighter staining compared to the SM groups in both of the rocking and static groups (Figure 4.5.2 D).

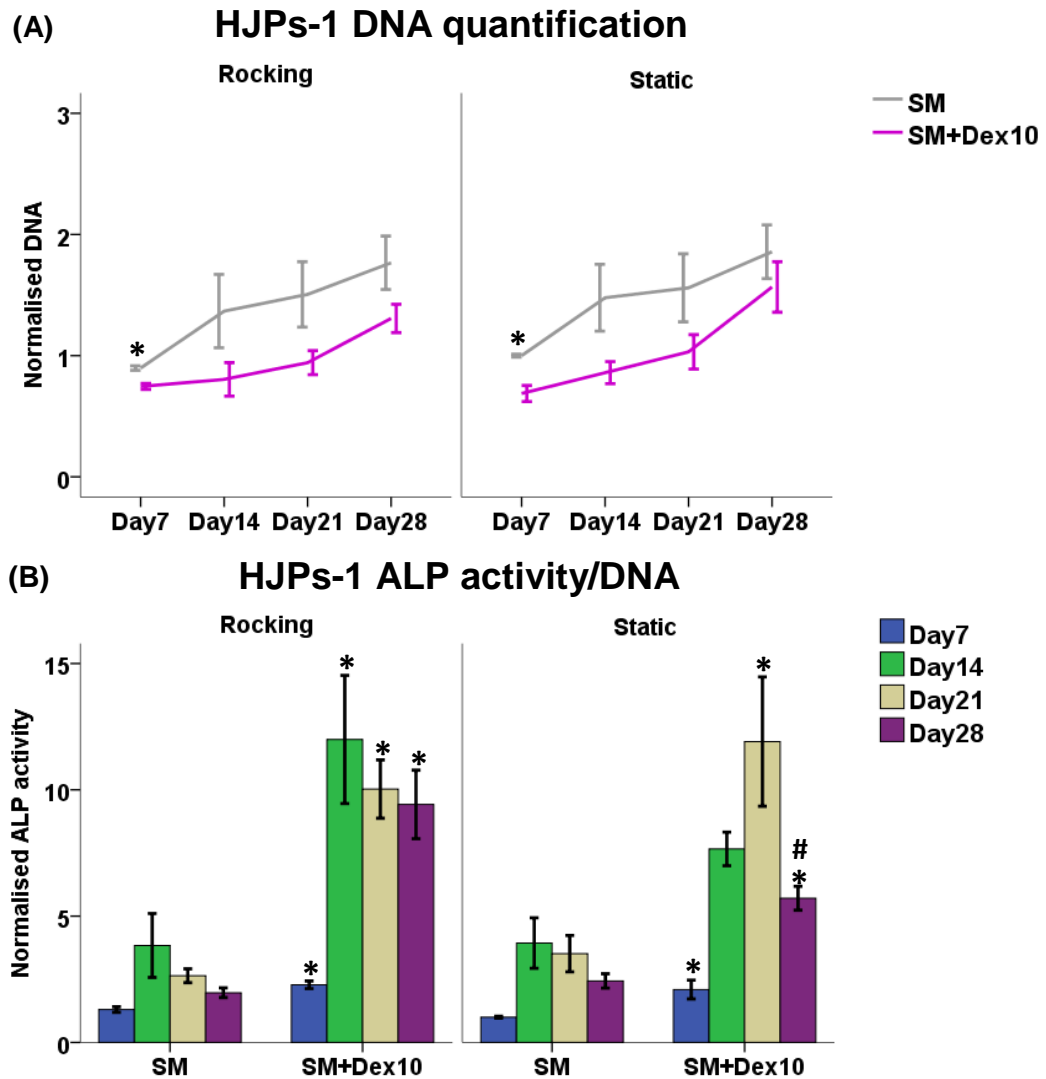


**Figure 4.5.1:** The effect of OFF on HJPs-1 under supplemented media (SM) and supplemented media with 10nM of Dex (SM+Dex10) on monolayer culture after 7 to 28 days. DNA quantification (A) and ALP activity normalised to DNA (B). mean  $\pm$  SE, (N=2, n=3), \*=p<0.05 comparison between SM and SM+Dex10, #=p<0.05 comparison between rocking and static groups, Two-way ANOVA, Tukey's multiple comparison test.

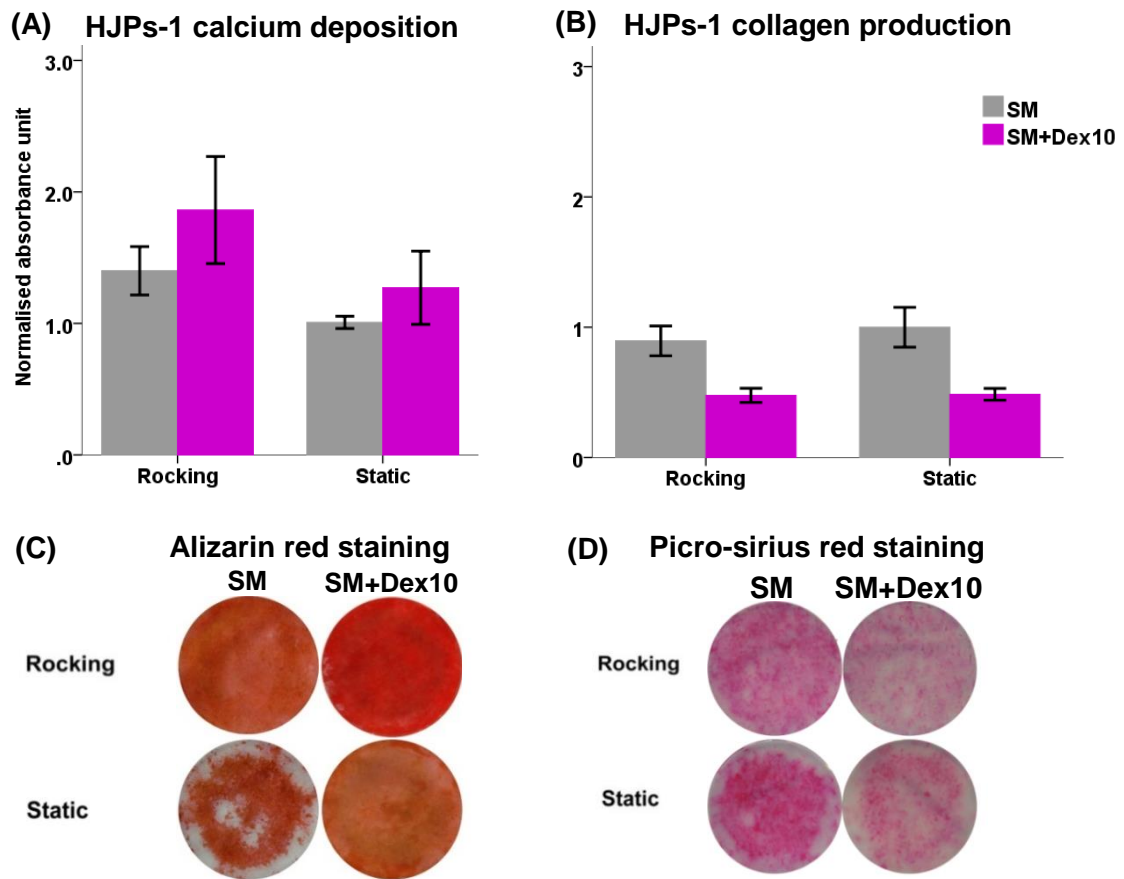


**Figure 4.5.2:** The effect of OFF on HJPs-1 under the supplemented media (SM) and supplemented media with 10nM of Dex (SM+Dex10) on monolayer culture after 28 days. Total calcium deposition (A) using alizarin red staining and total collagen production (B) using picro-sirius red staining. (C) The photoimages show representative set of alizarin red staining and (D) picro-sirius red staining on monolayer cultured of HJPs. (A,B) Data is presented as mean  $\pm$  SE, ( $N=2$ ,  $n=3$ ),  $*=p<0.05$  comparison between the SM and SM+Dex10 groups), Two-way ANOVA, Tukey's multiple comparison test.

### Results of HJPs-2

The DNA of HJPs-2 increased at all conditions (the SM and SM+Dex10 groups) from 7 to 21 days (Figure 4.5.3 A). The SM+Dex10 groups were higher than the SM groups in both the rocking and static groups indicating that there were higher cell numbers than the other group. The SM groups showed the lower ALP activity normalized to DNA than the SM+Dex10 groups in both the rocking and static conditions at all time-points (Figure 4.5.3 B). Both rocking and static groups were not significantly different. Total calcium deposition by the SM+Dex10 rocking groups was the highest than for any other groups by day 21 (Figure 4.5.4 A). The SM+Dex10 groups produced a higher amount of collagen than the SM groups in both the rocking and static groups after 21 days (Figure 4.5.4 B). The SM+Dex10 group under rocking condition (upper row) had the darkest alizarin red staining after 21 days compared to the other groups indicating that there was more calcium deposition than for the other groups (Figure 4.5.4 C). The picro-sirius red staining images of the SM+Dex10 groups (right column) were darker stained compared to the SM groups (left column) in both the rocking and static conditions (Figure 4.5.4 D).

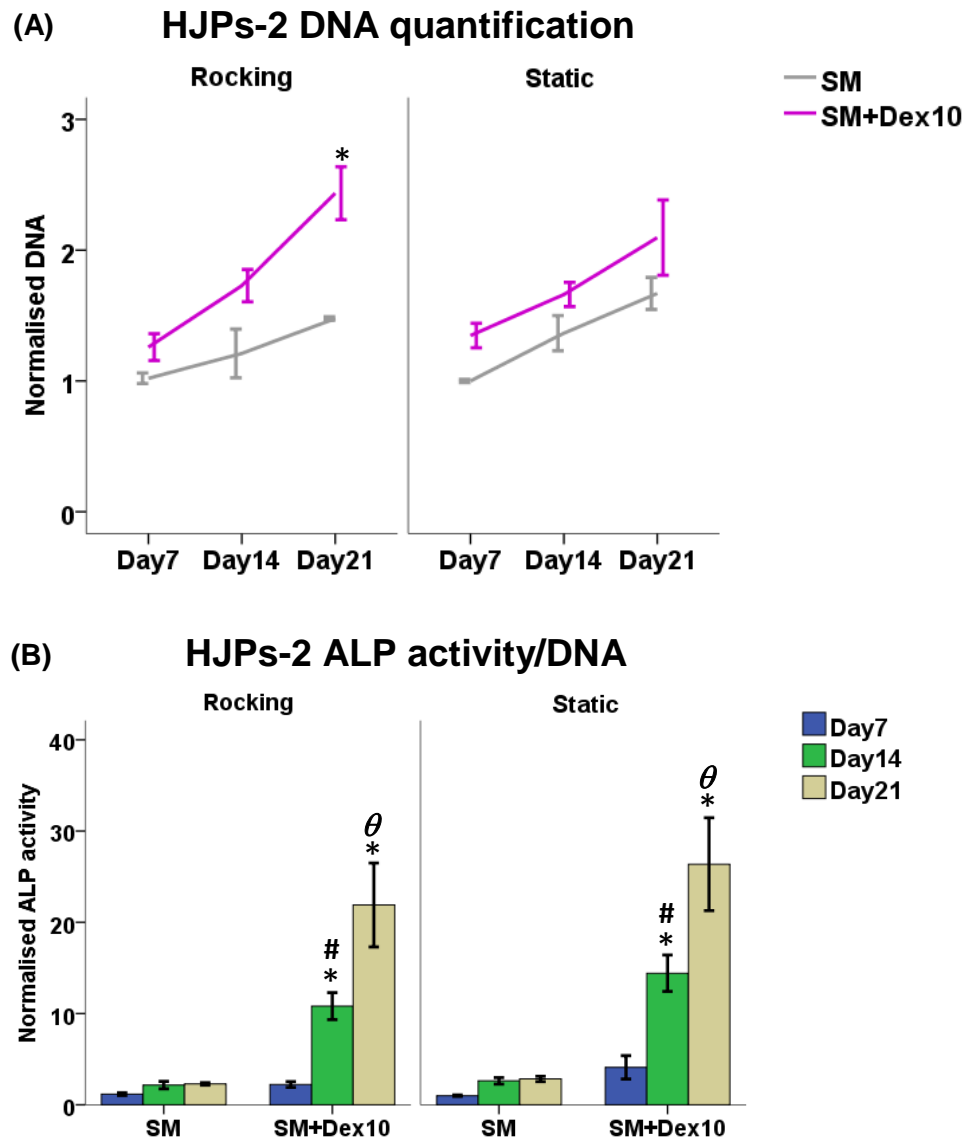


*Figure 4.5.3: The effect of OFF on HJPs-2 under supplemented media (SM) and supplemented media with 10nM of Dex (SM+Dex10) on monolayer culture after 7 to 21 days. DNA quantification (A) and ALP activity normalised to DNA (B). mean  $\pm$  SE, (N=2, n=3),  $\ast$ = $p < 0.05$  comparison between SM and SMDex10, Two-way ANOVA, Tukey's multiple comparison test.*

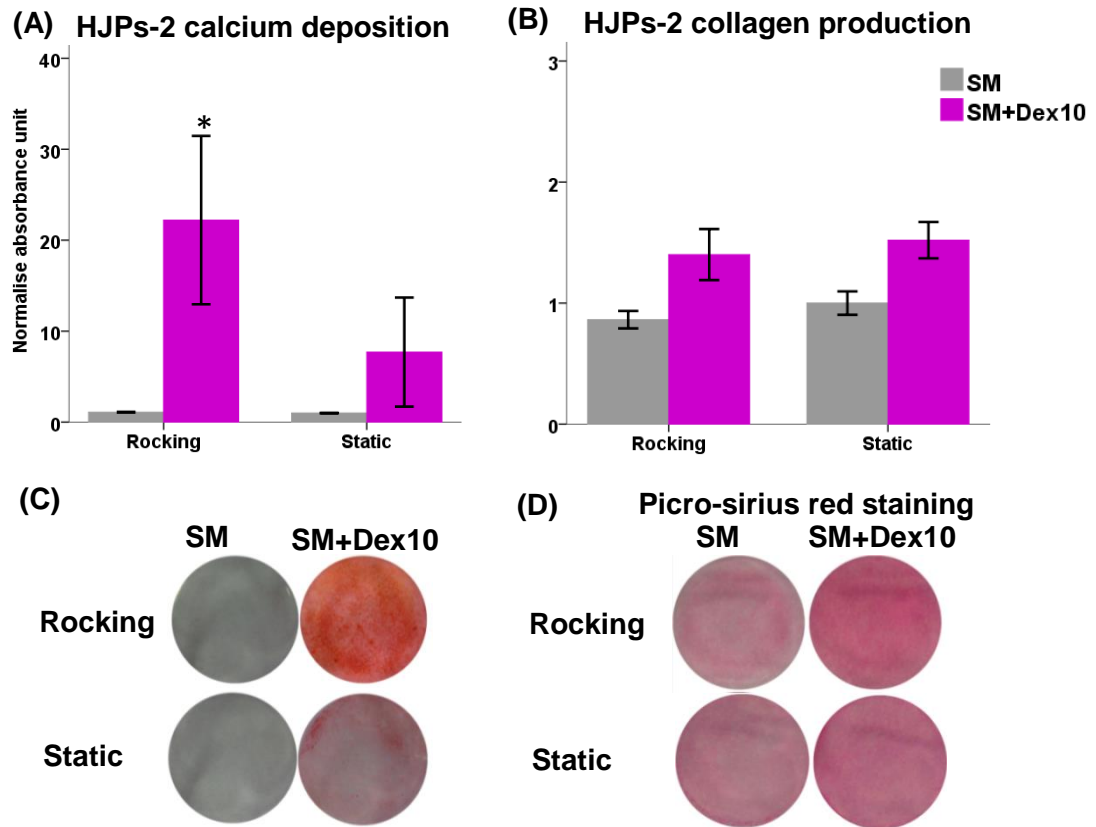


**Figure 4.5.4:** The effect of OFF on HJPs-2 under the supplemented media (SM) and supplemented media with 10nM of Dex (SM+Dex10) on monolayer culture after 21 days. (A) Total calcium deposition by using alizarin red staining and (B) total collagen production by using picro-sirius red staining. (C) The photoimages show representative sets of alizarin red staining and (D) picro-sirius red staining on monolayer culture of HJPs. (A,B) Data is presented as mean  $\pm$  SE, (N=2, n=3), \*=p<0.05 comparison between the SM and SM+Dex10 groups, Two-way ANOVA, Tukey's multiple comparison test.

### **4.6. The effect of temperature on osteogenic differentiation of hESMPs compared between room temperature and physical cell culture temperature of 37°C and Carbon dioxide (CO<sub>2</sub>) on monolayer.**

#### **4.6.1. Introduction**

Because the standard see-saw rocker available in our laboratory could only operate at room temperature all our static controls were also placed at room temperature for the same length of time. Therefore, we set another group of samples to compare between continuous static incubator culture and static at room temperature to certain whether this switch to a short period of time at room temperature and standard atmospheric gas concentrations (0.04% CO<sub>2</sub>) in itself had any relevant effects on the cells. These temperature effect tests were performed on hESMPs and HJPs. For the purposes of the rest of this chapter, ‘static’ means the cultured cells were moved to room temperature for the same time of rocking and ‘static incubator’ means a continuous culture in the cell incubator at 37°C, 5% CO<sub>2</sub>.

#### **4.6.2. Results**

On day 7, the cell morphology of the static incubator (upper row) and static (lower row) groups cultured under the SM medium (A,D) was more fibroblast fusiform in shape (red arrow heads), while the cells cultured under the SM+Dex10 (B,E: white arrow heads) and SM+Dex100 media (C,F: yellow arrow heads) were more cuboidal shaped, similar to a typical osteoblastic cell (Figure 4.6.1). There were no differences between the static incubator and static groups. DNA quantification (Figure. 4.6.2 A), ALP activity normalized to DNA (Figure. 4.6.2 B), VEGF secretion (during a 48 hour collection period) normalized to DNA (Figure. 4.6.2 C), total calcium deposition (Figure. 4.6.3 A), and total collagen production (Figure. 4.6.3 B) of the static compared to the static incubator groups (dashed line) showed that they were no differences in any culture media: SM, SM+Dex10 or SM+Dex100 over 21 days of culture.

## CHAPTER FOUR

While the total calcium deposition was significantly different between the static and static incubator groups under the SM+Dex10 medium this difference was less than 20% at day 21 ( $p < 0.05$ ). The alizarin red stained cells of SM+Dex100 groups after 21 days showed the darkest staining for both the static and static incubator groups, confirming that the SM+Dex100 groups deposited the highest amount of calcium compared to the others (Figure. 4.6.3 C). The picro-sirius red staining images of the SM+Dex100 group indicate there was less collagen production (lighter staining) compared to SM and SM+Dex10 in both the static and static incubator groups, this confirmed that the high concentration of Dex inhibited collagen production by cells (Figure 4.6.3 D)

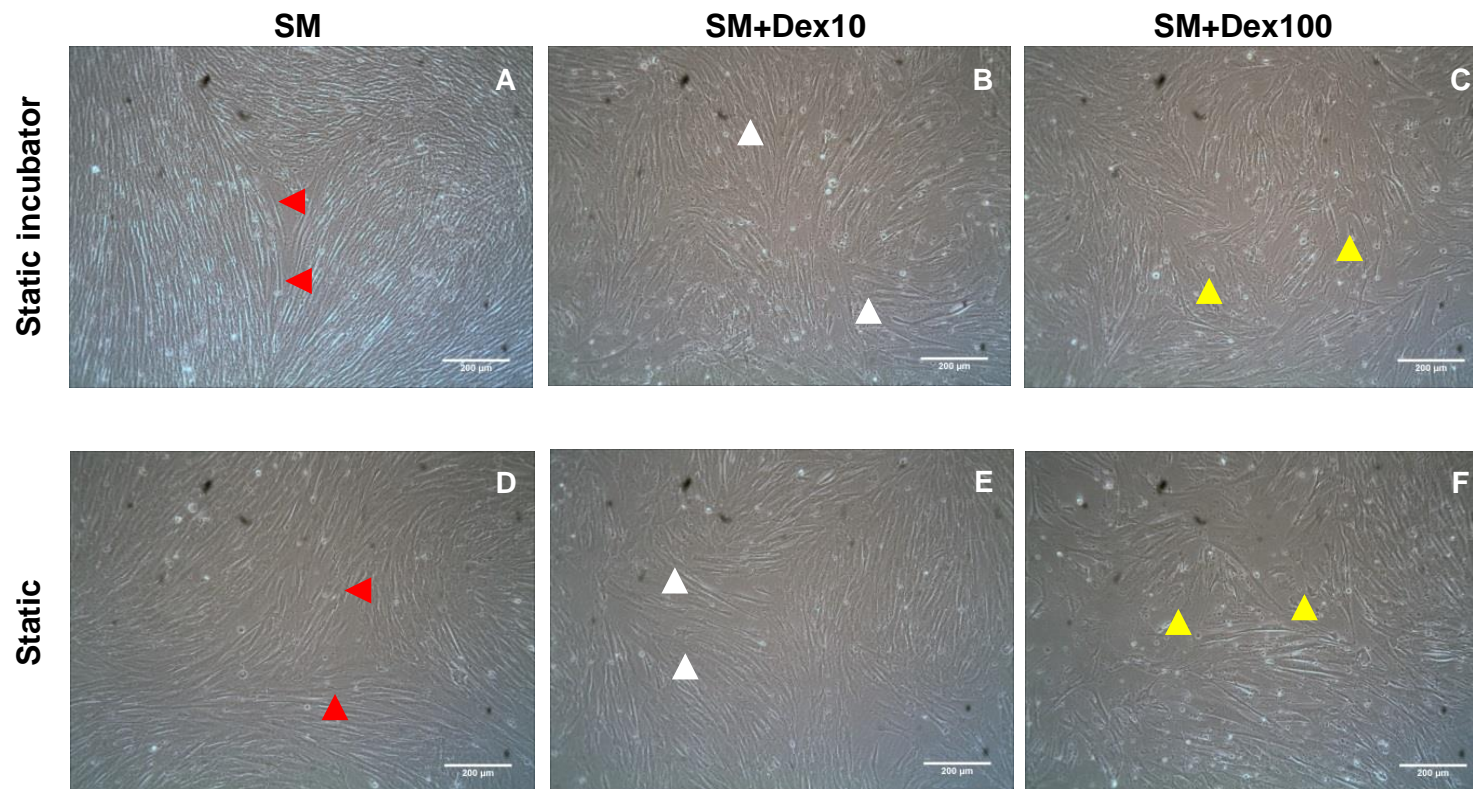


**Figure 4.6.1:** Microphotographs of the morphology of hESMPs under different temperatures for the static incubator group and the static group at room temperature for 1 hour/day after 7 days. The cells were cultured in the varying concentrations of Dex: supplemented media (SM) which contained AA and  $\beta$ -GP, supplemented media with 10nM of Dex (SM+Dex10), and supplemented media with 100nM of Dex (SM+Dex100) of hESMPs. The SM group (A,D) were more fibroblastic in shape (red arrow heads) while the SM+Dex10 (B, E) and SM+Dex100 (C, F) groups were more cuboidal in shape similar to osteoblastic cells (white and yellow arrow heads, respectively). Scale bar : 200 $\mu$ m

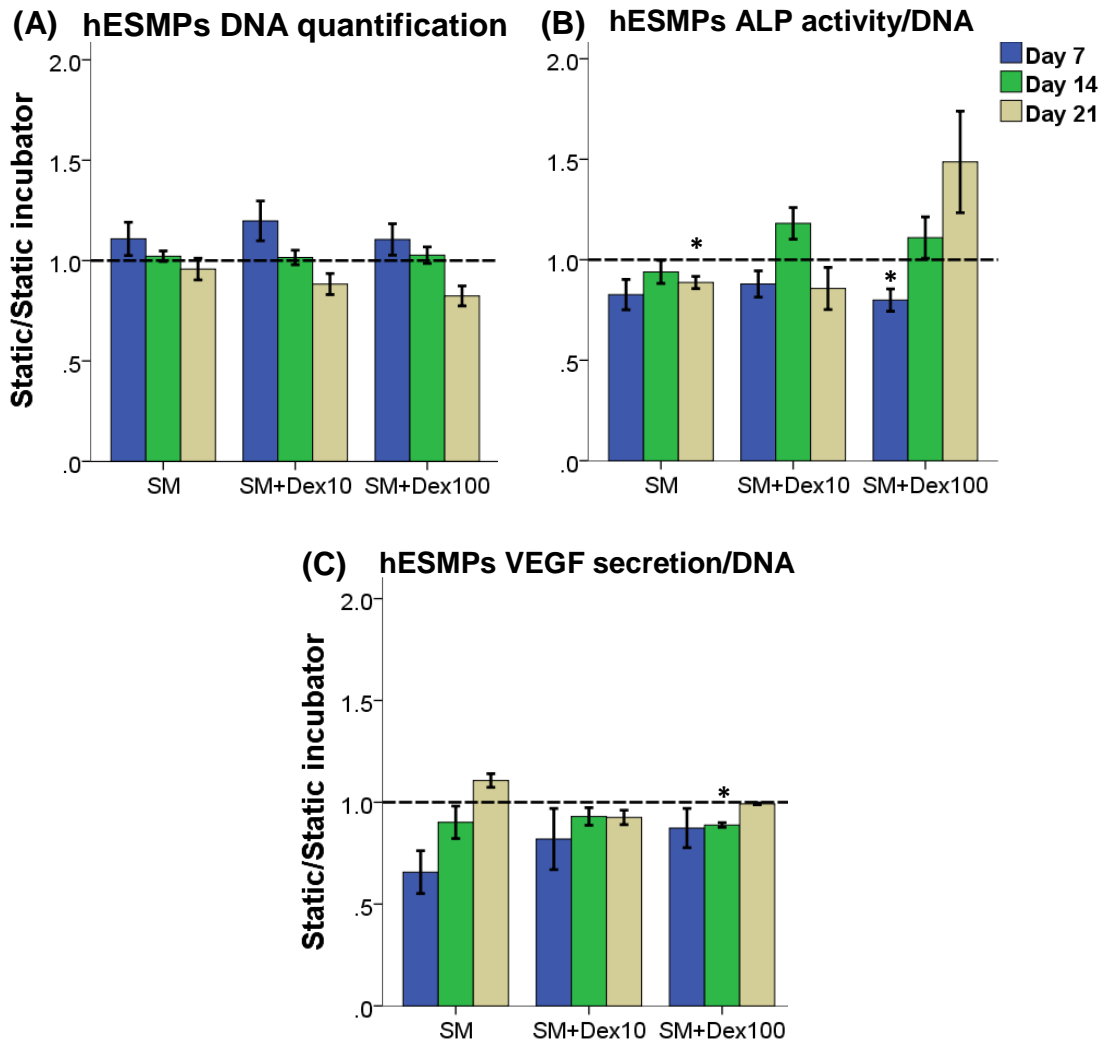


**Figure 4.6.2:** The effect of different temperature for hESMPs cells cultured between the static and static incubator groups. The cells were cultured in the SM, SM+Dex10, and SM+Dex100 media on monolayer and collected at 7, 14 and 21 days. DNA quantification (A), ALP activity normalised to DNA (B), and VEGF secretion (during a 48 hour collection period) normalised to DNA (ng/ml) (C) of the static groups were normalised to static incubator groups presented as mean  $\pm$  SE, (N=3, n=3:for DNA and ALP activity, N=2, n=3:for VEGF),  $*=p<0.05$  comparison between the static and the static incubator groups (dashed line), using One sample T test.

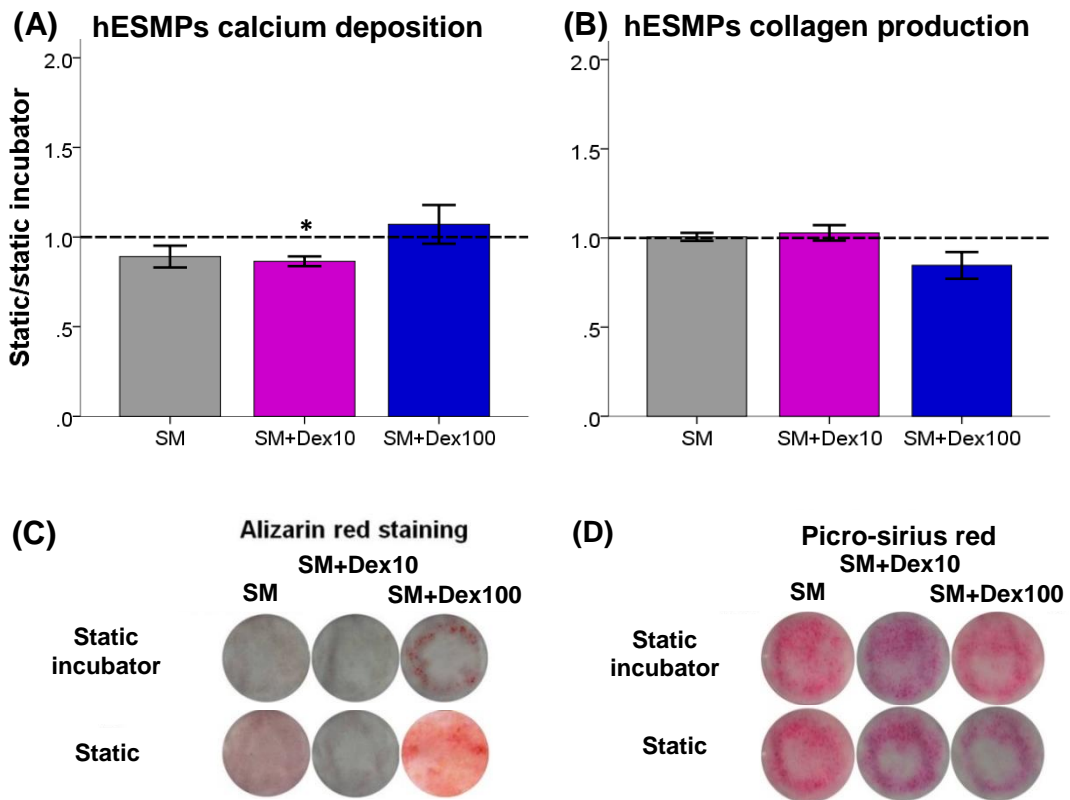


**Figure 4.6.3:** The effect of different temperature for hESMPs cells cultured between the static and static incubator groups. The cells were cultured in the SM, SM+Dex10, and SM+Dex100 media on monolayer culture after 21 days showed total calcium deposition (A) using alizarin red staining and total collagen production (B) using picro-sirius red staining. The photoimages show representative set of alizarin red staining (C) and picro-sirius red staining (D) on monolayer cultures of hESMPs. (A,B) Data is presented as mean  $\pm$  SE, (N=4, n=3),  $*=p<0.05$  comparison between the static and the static incubator groups (dashed line), using One sample T test.

#### **4.7. The effect of temperature on osteogenic differentiation of HJPs compared between room temperature and physical cell culture temperature of 37°C and CO<sub>2</sub> on monolayer.**

##### **4.7.1. Results**

In HJPs-1, DNA quantification (Figure. 4.7.1 A) and total collagen production (Figure. 4.7.3 A) of static compared to the static incubator groups (dashed line) showed that they were no significant differences or differences were less than 20%, ( $p < 0.05$ ). There were no differences between the static and the static incubator groups for the cell proliferation or collagen production. The picro-sirius red staining of the cells show no differences between the static and static incubator groups (Figure 4.7.3 C). ALP activity normalized to DNA of the SM+Dex10 groups were significantly different ( $p < 0.05$ ), or about 35% differences (Figure 4.7.1 C). Calcium deposition by the static normalized to the static incubator groups under the SM medium showed a highly significant difference (Figure 4.7.2 A). HJPs-1 under the SM medium deposited much more calcium in the static condition (moved to room temperature for short periods) compared to the static incubator. The alizarin red staining was also visibly darker for the static group staining compared to the static incubator group (Figure 4.7.2 C).

In contrast, HJPs-2, DNA quantification (Figure. 4.7.1 B), ALP activity normalized to DNA (Figure. 4.7.1 D), total calcium deposition (Figure. 4.7.2 B), and total collagen production (Figure. 4.7.3 B) of the static compared to the static incubator groups (dashed line) showed that there were no differences ( $p < 0.05$ ) or less than 20% differences in all culture media: SM, and SM+Dex10 over 21 days of culture. The alizarin red staining of the cells under the SM+Dex10 static group did appear darker compared to the static incubator group and the quantification indicated higher calcium content however there was large variability within this group and no statistically significant effect (Figure 4.7.2 D). The picro-sirius red staining of the cells showed no

difference between the static and static incubator groups in all media: the SM and SM+Dex10 (Figure 4.7.3 D).

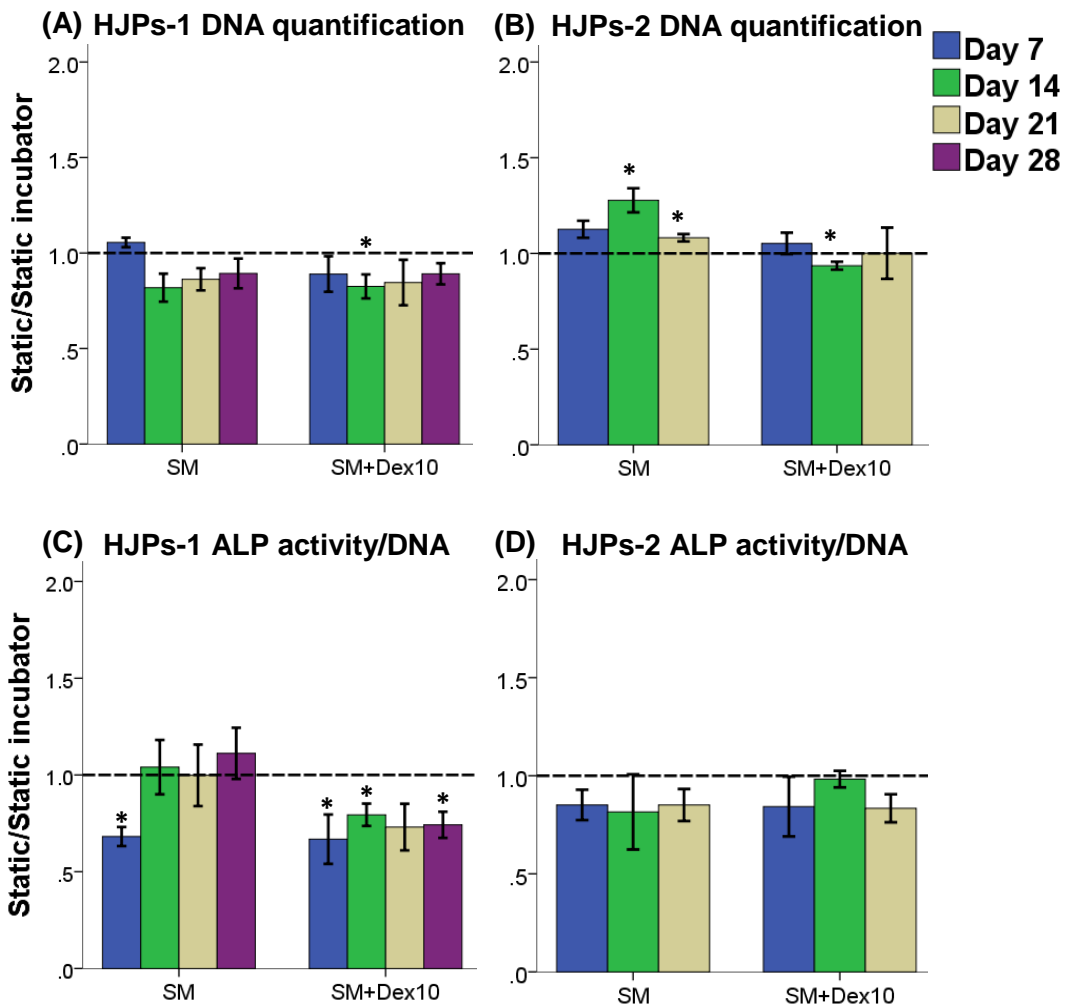


**Figure 4.7.1:** The effect of different temperatures for HJPs-1 and HJPs-2 cells cultured between the static and static incubator groups. The cells were cultured in the SM and SM+Dex10 media in monolayer and collected at 7, 14, 21, and 28 days, however, the HJPs-2 samples were collected until day 21. DNA quantification (A,B), ALP activity normalised to DNA (C,D) of static groups were normalised to static incubator groups of the HJPs-1 and HJPs-2, respectively, presented as mean  $\pm$  SE, (N=2, n=3), \*= $p < 0.05$  comparison between the static and the static incubator groups (dashed line), using One sample T test.

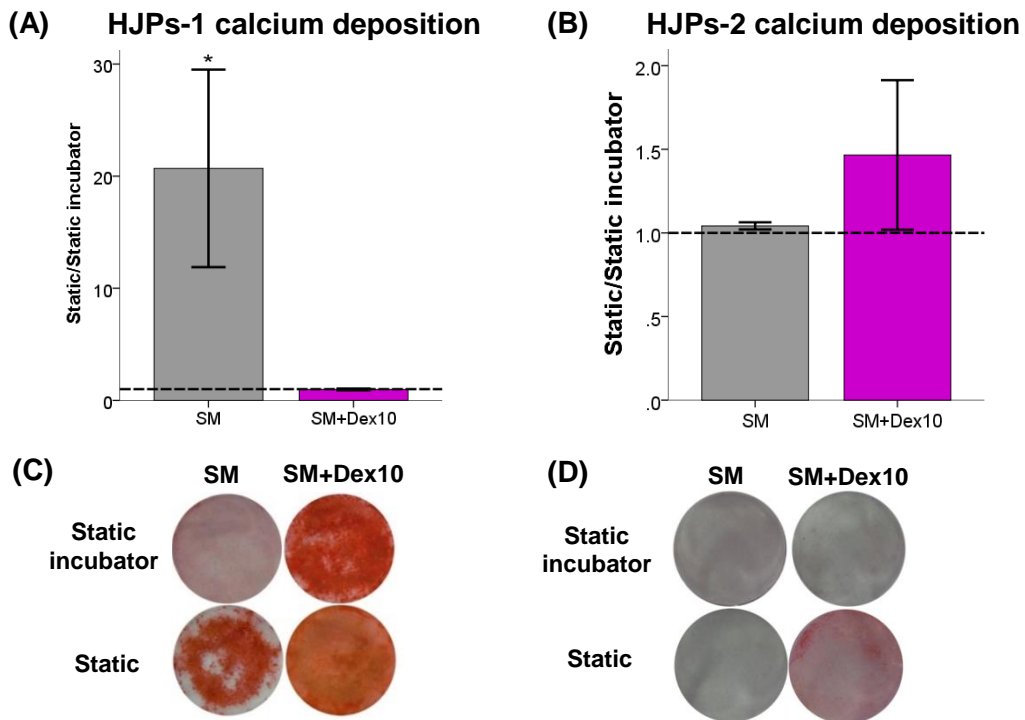


**Figure 4.7.2:** The effect of different temperature for HJPs-1 and HJPs-2 cells cultured between the static and static incubator groups. The cells were cultured in the SM and SM+Dex10 media on monolayer surface showed total calcium deposition after 21 days for HJPs-2 (B) and 28 days for HJPs-1 (A) using alizarin red staining. The photomicrographs show representative set of alizarin red staining of HJPs-2 (D) and HJPs-1 (C) on monolayer surface. Data is presented as mean  $\pm$  SE, (N=2, n=3),  $*=p<0.05$  comparison between the static and the static incubator groups (dashed line), using One sample T test.

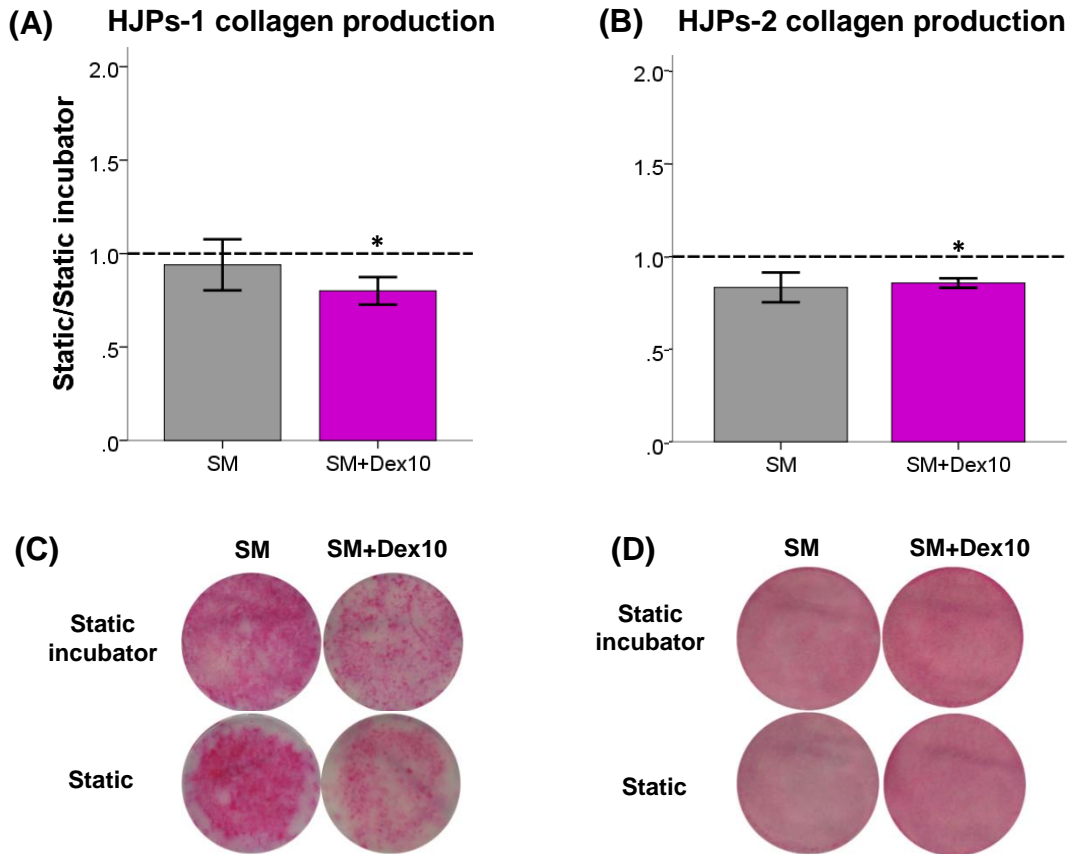


**Figure 4.7.3:** The effect of different temperatures for HJPs-1 and HJPs-2 cells cultured between the static and static incubator groups. The cells were cultured in the SM and SM+Dex10 media in monolayer. Total collagen production after 21 days for HJPs-2 (B) and 28 days for HJPs-1 (A) using picro-sirius red staining. The photoimages show representative set of picro-sirius red staining of HJPs-2 (D) and HJPs-1 (C) on monolayer surface. Data is presented as mean  $\pm$  SE, (N=2, n=3),  $*=p<0.05$  comparison between the static and the static incubator groups (dashed line), using One sample T test.

### 4.8. Discussion

It is known that hESMPs and HJPs can differentiate into osteogenic cells by adding Dex. These are promising cell sources for bone tissue engineering. OFF can enhance osteogenic differentiation and therefore may be of use as a pre-treatment in cleft palate bone tissue engineering. It was previously shown that OFF, using a standard see-saw rocker, performed at room temperature for 1 hour a day, 5 days per week up-regulates ALP, collagen and calcium in monolayer culture on hESMPs, the fluid flow stress between 0-0.051 Pa (Delaine-Smith et al., 2012). Others also applied OFF to monolayer cultures of hBMSCs or human fetal osteoblastic cells with the parallel plate flow chamber at a peak shear stress of up to 2 Pa (Jacobs et al., 1998, Li et al., 2004). hESMPs act as a model cells for evaluating a cell viability and effects on differentiation of a treatment on material. The HJPs from periosteum tissue and hBMSCs have been used clinically for bone reconstruction by using tissue engineering strategies. Therefore, the main objective of the work described in this chapter was to evaluate the effect of OFF on osteoprogenitor cells such as hESMPs, HJPs, and hBMSCs by using a standard see-saw rocker to mechanically stimulate cells. The three cell types have already been well demonstrated to have osteogenic differentiation potential (see chapter 3). This is the first study that I know of to subject HJPs to OFF using a standard see-saw rocker to enhance mineralized matrix production. Based on previous work on hESMPs we expected that this technique could enhance osteogenesis of HJPs whether they were cultured under osteogenic induction medium (Dex supplement) or supplemented medium (without Dex supplement). This may be a promising technique to enhance mineralization in bone tissue engineering and benefit patients who need bone graft for cleft palate reconstruction.

Applied OFF using a standard see-saw rocker was chosen in this study because this method has been showed to increase osteogenic differentiation in osteoprogenitor cells (Zhou et al., 2010, Lim et al., 2013, Delaine-Smith et al., 2012, Tucker et al., 2014). It is

a simple method, with high throughput, convenient to observe the cell morphology, and mineralized matrix production and it is cost effective. Several studies have used a parallel plate flow chamber to exert the fluid flow on the monolayer cell cultures in previous works (Nauman et al., 2001, Kreke et al., 2005, Jacobs et al., 1998), but this chamber has the weakness: 1] tubing at the inlet and outlet ports can leak and lead to cell culture infection, 2] stability of a fluid flow stress due to long distance from the pump, 3] high amount of cells, culture media, and reagents are required so studies of rare cell populations and using expensive chemical reagents are difficult (Brown and Larson, 2001), and 4] low throughput (Nauman et al., 2001). The parallel plate flow chamber is usually used to produce OFF stress ranging from 0-2 Pa, trough to peak. The critical fluid flow level which could remove half of attached cells on monolayer culture is typically is more than 1 Pa (McCoy and O'Brien, 2010). Therefore, the OFF induced by the standard see-saw rocker is less likely to detach cells from the culture surface. Delaine-Smith et al., (2012) used equations developed in Zhou et al., (2010) to calculate the shear stress in the circular 6 well-culture plate used in our lab and found that, for the rocking conditions used in these studies the peak shear stress at the center was at 0.041 Pa and at the periphery was 0.051 Pa. The oscillatory movement mimics the typical fluid flow in bone at the lacunar-canalicular system (Orr et al., 2006) and also in bone marrow on the endosteal surface which hBMSCs reside (Gurkan and Akkus, 2008, Yin and Li, 2006).

In studies to estimate shear stress on osteocytes within bone matrix it has been suggested that they are subjected to OFF at a peak shear stress of 2 Pa *in vivo* (Weinbaum et al., 1994), however, how that relates to the shear stress an osteoprogenitor would be subjected to *in vivo* is completely unknown. Birmingham et al., (2013) calculated the fluid flow on trabecular bone in the healthy bone marrow environment by using computational models and found that the fluid flow stress should range between 0.02-0.4 Pa depending on trabecular bone porosity. Studies on the *in*

*vitro* effect of OFF on osteocytes, osteoblasts, and MSCs have used the peak shear stresses of up to 3 Pa for cell stimulation (Weinbaum et al., 1994, Case et al., 2011, Birmingham et al., 2013). However if the Birmingham study is correct then the lower shear stress that we use may be more relevant for MSCs.

A limitation of this study is that in many cases only 2 experiments were performed in triplicate, however, some interesting differences were identified were found to be significant as follows. In this study DNA quantification indicated cell proliferation was not different between the rocking and static groups in all cell types (hESMPs, hBMSCs, and HJPs). This implies that OFF has not damaged the cells on monolayer culture but it also does not stimulate cell proliferation. These results are consistent with the study by Kreke et al., (2005) in which MSCs were subjected the steady fluid flow with the shear stress of 0.16 Pa had no effect on cell proliferation, but is in contrast to the studies of Nauman et al, (2001) in which on the rat tibial and femoral osteoprogenitor cells were subjected pulsatile fluid flow with the shear stress between 0.1 to 1.1 Pa and showed an increased cell proliferation on day 21. This study initiated the fluid flow stress on day 14 and further stimulated for 7 days whereas our study subjected the fluid flow stress to the cells on day 4 and further stimulated for 14 days (see chapter 2). These different time points of mechanical stimulation on the cells may affect cell proliferation. The response of immature osteoblastic cells to mechanical stimuli may depend on species of origin, fluid flow magnitude, and mode of flow such as steady, pulsatile, and oscillatory (Kreke et al., 2005). In our studies, a cell attachment time of 4 days was allowed before subjecting the cells to OFF to be consistent with 3D cultures for the next chapter (chapter 5). These time periods were previously observed to allow cell attachment to the culture surface before initiation of mechanical stimuli (McCoy and O'Brien, 2010).

The ALP activity in our study increased over time of culture, except that ALP activity of HJPs-1 on day 28 was significantly lower while at the same time-point they showed high calcium deposition. There were no effects of OFF on ALP activity between the

## CHAPTER FOUR

rocking and static groups under either the SM or SM with Dex supplements in all cell types (hESMPs, hBMSCs, and HJPs). This is consistent with the study of Nuaman et al., (2001) who found that the unidirectional pulsatile fluid flow on the rat osteoprogenitor cells had no effect on ALP activity whether they were cultured in the static condition or various magnitudes of flow with a parallel plate flow chamber on day 14. One potential reason is that ALP activity normally decreases before the beginning of mineralization (before day 21), therefore the ALP activity may lead to an apparent lack of response to OFF in conditions where mineralisation has been accelerated (Lian and Stein, 1995). Here we did measure ALP at three time points to try to capture any peak in activity and we did not appear to have reached the peak before 21 days. Due to problems with cell density (the cells became over confluent) we were only able to measure ALP at day 28 in HJPs-1, this data showed lower ALP at day 28 indicating that peak activity may have occurred around day 21. Therefore it is unlikely that we do not see higher ALP in rocked cultures just because the ALP peak occurred earlier in these cells. Yourek et al., (2010) found that the unidirectional fluid flow on hBMSCs under 100nM of Dex did not affect ALP in the cell lysate but did increase ALP levels in the media. He hypothesized that fluid flow may remove ALP from the cell membrane explaining why there is no apparent increase in ALP levels in the cell lysate even when other osteogenic markers are present. It would be interesting to measure media ALP in future studies.

Calcium deposition indicates the late state of osteogenic differentiation. Our study found that calcium deposition in the rocking groups under the 100nM of Dex medium in the hESMPs and the 10nM of Dex medium in both hBMSCs and HJPs was higher than the SM media. The combination of OFF and Dex supplementation can enhance osteoblastic differentiation especially in the late state by increasing calcium deposition. The 100nM of Dex medium allowed a higher calcium deposition than 10nM of Dex. It indicated that the concentration of Dex was directly related to the calcium deposition of

cells. Wozniak et al., (2000) and Sodek et al., (2000) stated that the osteogenic cells may respond to mechanical stimuli by secreting OPN in the extracellular matrix. OPN is a protein which is necessary for cellular proliferation and regulation of calcium deposition of cells on the ECM. Moreover, Wozniak et al., (2000) applied strain stress on hBMSCs using a 6-well Flexcell strain apparatus and reported that gap junctions increased, there are a cell-cell connection network. It has been suggested by several groups that even it only a few cells sense a mechanical stress it is passed to other cells in the culture via gap junctions leading to a co-ordinated response, this may be the reason for the more uniform calcium deposition observed in the OFF groups. Lastly, the OFF can stimulate the mineralization of cells either via mechanical or by secondary effects on nutrient distribution. In addition many study on bone cells OFF also increased intracellular calcium mobilization which is an important intracellular signals (Li et al., 2004). In this study we did not determine the pathway of OFF to induce osteogenic differentiation. Possible mechanisms of mechanotransduction have been studied and many researchers have noted mechanical stimulation of the mitogen activated protein kinase (MAPK) pathways which regulate the cell proliferation and osteogenic differentiation (see chapter 1) (Jaiswal et al., 2000, Pommerenke et al., 2002). Fluid flow has been shown to enhance osteogenic differentiation of osteoprogenitor cells and calcium deposition by several pathways such as the stretch-activated ion channels on the plasma membrane, the cell-cell interaction: gap junction, the cell-ECM interaction: focal adhesion complex, the biochemical signaling: PGE<sub>2</sub> (Einhorn, 2003) and OPN (Reilly et al., 2003, Bonnet and Ferrari, 2010), and the extracellular structure: primary cilia (Janmey and McCulloch, 2007, Orr et al., 2006).

Collagen production is also a marker of osteogenic differentiation on osteoprogenitor cells. Our studies showed that there were no differences between the rocking and static groups in total collagen production, indicating that the OFF had no effect in any cell type. This result is similar to the study by Li et al., (2004) who subject MSCs to OFF by

using a parallel plate flow chamber and found the gene expression of collagen type I was not affected by OFF. Nohutcu et al., (1997) reported that the gene expression of collagen type I was at the high level, following by reducing of this gene expression before the mineralization state. However, the opposite result was found with rat MSCs from bone marrow cultured on 3D scaffold using micro-vibration chamber, Zhou et al., (2011) found that the mechanical stimuli could enhance the collagen matrix production in osteoprogenitor cells although they were supplemented with Dex. Interestingly pulsatile fluid flow in a parallel plate flow chamber on rabbit tendon fibroblasts increased the expression of matrix metalloproteinase (MMP-1 and MMP-3) which act as collagen degradation in the enzymes remodelling of extracellular matrix (Kjaer et al., 2006, Archambault et al., 2002). This may be a reason why the collagen production in the rocking group was no different from the static group.

VEGF is an important cytokine to recruit endothelial cells for vasculogenesis. Our study showed no differences between the rocking and static groups, indicating that the OFF had no effect on VEGF secretion by hESMPs or hBMSCs. Lim et al's (2013) study on human MSCs derived from alveolar bone showed a similar result that the cells subjected to OFF by using rocking platform for 1 hour in the maximum magnitude at 0.00205 Pa slightly increased the VEGF secretion but by only 18.75% compared to the static group. In contrast, Thi et al's (2010) study on the osteoblastic mouse cell (MC3T3-E1), showed that the VEGF secretion was dramatically increased by pulsatile fluid flow (0.5 Pa) for 5 hours *in vitro*. They described that the increasing of PGE<sub>2</sub> production from OFF could stimulate the VEGF production. We did not measure PGE<sub>2</sub> secretion from the osteoprogenitor cells (hESMPs and hBMSCs), however, our group found that murine mature osteoblast cells (MLO-A5) respond to OFF by increasing PGE<sub>2</sub> secretion (Delaine-Smith et al., 2014b). Further studies consistently showed that osteoprogenitor cells can produce and accumulate PGE<sub>2</sub> in response to fluid flow (Nauman et al., 2001). However this increase PGE<sub>2</sub>, if it also occurred in these experiments does not seem to

enhance VEGF secretion. The shear stress in our system may be too low to stimulate VEGF secretion compared to other studies on hBMSCs in monolayer using the pulsatile parallel plate flow chamber. Using a high shear stress (2Pa) (Yuan et al., 2013) found that the VEGF secretion was higher than in the static conditions. In the HJPs study SM+Dex100 condition was not investigated due to the previous result that HJPs under various Dex supplementations on monolayer culture showed that the highest osteogenic differentiation was in the SM+Dex10 conditions (see chapter 3).

Cells were subjected to OFF at room temperature. Therefore there was some concern that the switch to room temperature and atmospheric CO<sub>2</sub> may in itself affect the cells. Temperature and CO<sub>2</sub> are a key environmental factor for cell culture and may have affected the cells. In order to check whether there was an effect of the switch to room temperature alone, regardless of rocking I tested the effect of temperature and CO<sub>2</sub> by comparing static cells cultured at room temperature, atmosphere (0.04%CO<sub>2</sub>) (static group) and continuous culture in the cell incubator at the 37 °C, 5%CO<sub>2</sub> (static incubator group). The results showed that that the DNA quantification which indicates cell number were not difference between the static and static incubator groups. Similarly, ALP activity, calcium deposition, and collagen production of both hESMPs and HJPs showed no differences. In all conditions of culture media without cells (SM, SM+Dex10, and SM+Dex100 media) in the static and static incubator groups showed no calcium precipitation. Therefore, all media required cells for mineralization. If cells are exposed to room temperature and atmosphere for a short enough period of time and moved back to the cell culture incubator, cell alteration can be prevented. Moreover, it would have taken some time for the cell culture medium to cool down, disturbing pH balance which involved a dissolved CO<sub>2</sub>, and affect the temperature of cell culture due to the medium volume were larger amount than the cell volume (Klein et al., 1996). Interestingly, the calcium deposition of HJPs-1 under the SM medium at the static conditions was much higher than the static incubator groups, these are the same cells

that did not show a significant response to rocking, however calcium levels were very high in all conditions, this effect of room temperature may explain the lack of effect of rocking, calcium deposition was already highly stimulated and therefore could not be further stimulated. HJPs-1 may be more sensitive to stress and produce higher amount of heat shock protein (HSP). Several studies on the culturing cells at low temperature (25-32°C) found that the cells increase the levels of heat shock protein (HSP-27, 70, and 90) which enhance osteogenic differentiation (Chen et al., 2013, Stolzing and Scutt, 2006, Neutelings et al., 2013, Fujita, 1999). The reason that this only occurred in HJPs-1 must be because of patient variation and site of tissue harvesting (Marolt et al., 2010, Akintoye et al., 2006). Therefore we would need more HJPs cell to evaluate the effect of OFF to osteogenic differentiation. A limitation of this study was that the effect of temperature and CO<sub>2</sub> on hBMSCs was not investigated. The hESMPs, hBMSCs, and HJPs showed similar results in osteogenic potential and the OFF effects. Therefore the results of room temperature and CO<sub>2</sub> effects on hBMSCs should be similar to the hESMPs and HJPs results on monolayer culture but would requires further investigation.

### 4.9. Conclusion

Isolated hBMSCs and HJPs can be autologous cell sources for bone tissue engineering. All cell types (hESMPs, hBMSCs, and HJPs) responded to OFF by using a standard see-saw rocker to stimulate osteogenic differentiation. The cells were more sensitive to OFF when subjected to biochemical stimulation, using Dex supplementation for enhancing calcium deposition. This may be a cost effective, high throughput, and simple pre-treatment for bone tissue engineering for small defects such as cleft palate. In general the cells were not affected by culturing in a short period of time at room temperature when considering cell morphology, cell proliferation, and osteogenic differentiation. It was important to test this as the specific rocker that we used was operated on the bench top at room temperature.

### 4.10. Summary

- Subjecting osteoprogenitor cells to short periods of OFF during culture results in increased calcium deposition.
- The hESMPs, hBMSCs, and HJPs cells all responded to OFF, confirming that hESMPs are a useful model and bone marrow derived MSCs and periosteum derived HJPs could be an autologous cell sources for future mechanical stimulation studies.
- Cell proliferation, ALP activity, VEGF secretion, and collagen production were not responsive to OFF.
- Calcium depositions in all cell types were enhanced by the combination of applying OFF and Dex supplementation.
- The cell morphology, cell proliferation, and osteogenic differentiation of both hESMPs and HJPs were not different between the static (room temperature, atmosphere CO<sub>2</sub>) and static incubator groups (37°C, 5% CO<sub>2</sub>).
- Therefore, the static group will be used as the control group (not subjected to OFF) to compare with the rocking group in OFF experiments.

### 4.11. Future work

The study showed a successful in enhancing osteogenic differentiation and calcium deposition on human osteogenic progenitor cells. This method could be used in the future studies, for example;

- Studying the response to OFF by cells in monolayer in order to better identify the optimal shear stresses for 3D bioreactor cultured and implanted tissues
- Studying the OFF responses on cells sourced from different aged donors, for example, children's periosteal cells may respond more robustly than adult periosteal cells.

## CHAPTER FOUR

- Studying the osteogenic differentiation of the cells is a wider range of OFF regimes such as loading period, loading day, and various biochemical supplementations (BMP-2, PGE<sub>2</sub>).

### CHAPTER FIVE: THE EFFECT OF OSCILLATORY FLUID FLOW AND NANOHYDROXYAPATITE ELECTROSPUN SCAFFOLD TO ENHANCE OSTEOGENIC DIFFERENTIATION OF OSTEOGENIC PROGENITOR CELLS

#### 5.1 Introduction

Tissue engineering could be an optional choice for bone reconstruction for cleft palate repair. The three basic principles of tissue engineering include firstly a promising cell source, secondly an appropriate engineered scaffold and lastly cultured under a suitably biochemical reagent. The promising cell sources and suitable biochemical reagent have been described in the previous chapters. Therefore this chapter will describe some prospective scaffold materials.

Electrospinning fabrication is a straightforward method to produce fibres in various diameters from 5nm to several micrometres (Zargarian and Haddadi-Asl, 2010). The effect of the physical properties of a scaffold has been of strong interest recently due to the development of novel scaffold materials with unique characteristics depended on the polymer chemistry. When bone tissue engineering is targeted, materials should have sufficient strength and flexibility and be able to support and promote the proliferation of osteoprogenitor cells. In recent studies, poly-D-lactide (PLA), poly( $\epsilon$ -caprolactone) (PCL), and polyhydroxybutyrate-co-polyhydroxyvalerate (PHBV) have been evaluated as biocompatible and biodegradable for tissue engineering materials. All materials: PLA, PCL, and PHBV are approved by the U.S. FDA for medical use (Hutmacher et al., 2001, Sikavitsas et al., 2005, Ji et al., 2008). These polymers were chosen for this studies due to their higher mechanical strength and lower rate of biodegradability than natural materials such as collagen type I (Jha et al., 2011) which could also be produced by electrospinning.

Recently, many biodegradable polymer electrospun scaffolds have been used for bone tissue engineering however they was no evidence for osteoconductivity or osteoinductivity (Polini et al., 2011). A bone graft substitute probably requires an active property to stimulate bone tissue regeneration which also does not have an adverse effect on the surrounding tissue. There have been many recent studies aimed at developing bioactive materials to enhance osteoconduction and osteoinduction using HA (Lao et al., 2011, Fang et al., 2009, Yin et al., 2010). HA is a calcium-phosphate which is non-toxic, osteoinductive, and osteoconductive. Nano particle hydroxyapatite (nHA) has been reported to enhance osteogenic differentiation of mouse MSCs compared with micro particle hydroxyapatite ( $\mu$ HA) (Li et al., 2009). They reported that the calcium atoms of nHA exposed on the mixture between chitosan and gelatine casting film scaffold surface could enhance osteogenic differentiation potential. Therefore the hypothesis of this study is that nHA included in electrospun scaffolds could enhance their ability to support osteogenesis of MSCs.

Bone is a natural composite material consisting of cells and the ECM which is composed of a collagen protein and HA based mineral plates. The microstructure of bone consists of the lacunocanalicular structure and ECM. As described in the introduction, bone is a dynamic tissue which responds to the mechanical stimuli that act on it. It has been reported in several studies that the osteogenic differentiation of human osteoprogenitor cells is enhanced by mechanical stimuli (Bancroft et al., 2002, Sikavitsas et al., 2003, Delaine-Smith et al., 2012). *In vitro* studies have estimated the effect of OFF on the osteogenic progenitor cells in monolayer culture. The cells cultured on electrospun scaffold are surrounded by fibres and connect to other cells in all direction therefore one could speculate that this environment better mimics their *in vivo* environment. Therefore, by subjecting cells to OFF in 3D culture the outcomes may be more similar to *in vivo* than monolayer culture and this may be a good model system for mechanotransduction studies.

In the chapter 4 have been demonstrated in chapter 4 that (OFF of human osteoprogenitor cells including; hESMPs, hBMSCs, and HJPs in monolayer culture enhances calcium deposition under supplementation with Dex, although there was no effect on ALP activity (an early marker of osteogenic differentiation) or VEGF secretion. Therefore these studies are a further investigate the potential of OFF to stimulate hESMPs and hBMSCs by subjecting cells to OFF in 3D culture to stimulate osteogenic differentiation. The calcium deposition of the cells was evaluated by using micro computed tomography (micro-CT).

The first objective of this chapter was to produce and characterise the selected polymer electrospun micro fibre scaffolds including PLA, PCL, and PHBV for bone tissue engineering. The second objective was to enhance osteogenic differentiation of mesenchymal progenitors by using an OFF and nHA incorporated into electrospun PCL scaffolds.

### **5.2. Fabrication and characterization of PLA, PCL, and PHBV electrospun scaffolds.**

#### **5.2.1. Methods**

##### **Preparation of polymer solution**

3.5g of polymer pellet (PLA, PCL, and PHBV) was added into 31.5 g or 23.7 mL of DCM (DCM density =  $1.33\text{g/cm}^3$ ). The mixture was stirred using a magnetic stirrer and dissolved at room temperature overnight to obtain the well mixed polymer solution with a concentration of 10wt%. The polymer solutions were spun using the electrospinning technique (see chapter 2). The scaffold morphology was measured from SEM images. The fibre diameter and their distribution were measured over 100 randomly selected fibres from 4 recorded SEM micrographs by using the image analysis software (ImageJ). Each picture was randomly overlaid with a square grid side  $2500\mu\text{m}^2$  using automatic ImageJ function and selected for 25 points (Figure 5.2.1). The fibre diameter

was measured for each fibre which was underneath the intersections of the lines. The volumetric porosity of the PCL, PDLA, and PHBV electrospun scaffolds were analysed from the ratio of the scaffold density and their bulk density.

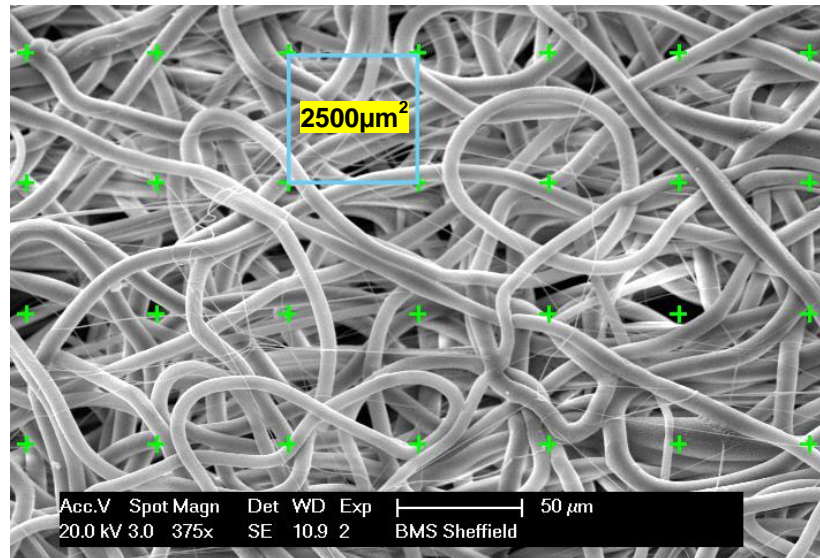


*Figure 5.2.1: Schematic of fibre diameter measuring from SEM image. The square grid lines size  $2500\mu\text{m}^2$  were overlaid on the image by using automatic image J function. The selected 25 points of underneath or nearest of the intersections of the lines had the fibre diameter measured.*

### 5.2.2 Results

PLA and PCL successfully produced fibres with a smooth fibre morphology without bead formation while the PHBV had a number of beads along with the fibres. Representative SEM images of the 10wt% PLA, PCL, and PHBV randomised electrospun scaffolds spun using DCM as a solvent are shown in Figure 5.2.2 A,B,C, respectively. The average fibre diameter of the three scaffolds (PLA, PCL, and PHBV) were significantly different ( $p < 0.05$ ) (Figure 5.2.2 G). PLA formed the thickest fibres with mean of 4.840  $\mu\text{m}$ , with a normal distribution between 1-7  $\mu\text{m}$  (Figure 5.2.2 D). The average fibre diameter of PCL was 2.682  $\mu\text{m}$ . The average of fibre diameter of PHBV was the lowest at about 0.773  $\mu\text{m}$ . The PHBV beads exhibited an average diameter of  $8.783 \pm 0.620 \mu\text{m}$  (average  $\pm$  SE), showing the narrowest size distribution (Figure 5.2.2 F). However, there were no significant differences between the volumetric porosity of the scaffolds (Figure 5.2.2 H).

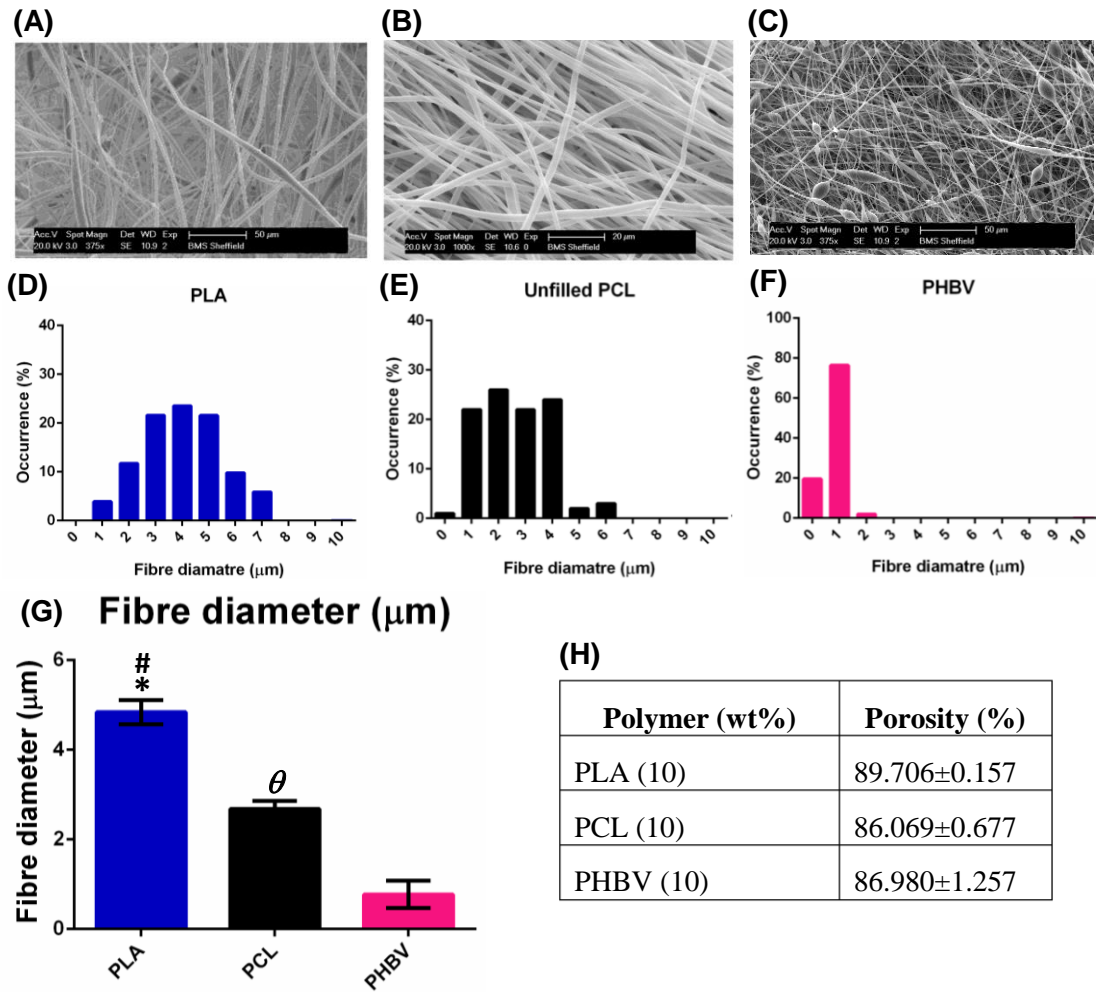


**Figure 5.2.2:** 10wt% PLA, PCL, and PHBV electrospun scaffold characterisations; SEM images of electrospun fibrous morphologies (A,B,C, respectively), fibre diameter distributions (D,E,F, respectively), average fibre diameter (G), and porosity of the scaffolds (H). The polymer pellets were dissolved in DCM and spun in the 40μL/min flow rate, 17kV, 17cm working distance, 300 rpm (rotating collector). The SEM images scale bar 50 μm for PLA and PHBV scaffolds and 20 μm for PCL scaffolds. The maximum value y-axis of the fibre diameter distributions bar graph D and E is 40 and graph F is 100. mean±SE (n=6 for porosity measurement and n=50 for fibre diameter measurement), \*=p<0.05 compared between PLA and PCL, #=p<0.05 compared between PLA and PHBV, θ=p<0.05 compared between PCL and PHBV, One way ANOVA, Tukey's multiple comparison test.

### 5.3 Optimizing cell seeding methods on scaffolds

#### 5.3.1 Methods

The cut PLA electrospun scaffolds and CellCrown™ inserts were sterilized, then the scaffolds were mounted into CellCrown™ and immersed in basal culture media ( $\alpha$ -MEM) overnight in the incubator at 37°C, 5% CO<sub>2</sub>, and a humidified atmosphere. 10<sup>5</sup> hESMPs were seeded on top of PLA scaffolds using 4 different methods; 1] small volume technique+1 hour: the small volume of cell suspension (no more than 100  $\mu$ L) is seeded on top of the scaffold, then left for 1 hour in an incubator then the appropriate media are added into the well plate (Figure 5.3.1 A), 2] small volume technique +2 hours (Figure 5.3.1 B), 3] low volume media technique: basal culture media was added up to the bottom surface of the scaffolds, then small volume technique used for cell seeding and cells left for attachment for 2 hours then the appropriate media are added into the well plate (Figure 5.3.1 C); and 4] large volume media technique: 1mL of basal culture media was added to cover the scaffolds, then the small volume technique was used for cell seeding and left for 24 hour for cell attachment (Figure 5.3.1 D) in the cell culture incubator.

The cell seeded scaffolds were removed to fresh well plates after 1 day, cell seeding efficiency was measured using the resazurin reduction assay. The number of viable cells which remained on the original tissue culture wells (fluorescence relative units: FRU) were compared with the FRU of the cells on tissue culture plates which were seeded with equivalent numbers as a control. Equation (1) adapted from (Seebach et al., 2010).

Percentage of cell attachment (%) =  $\frac{\text{FRU of control} - \text{FRU of remaining cells}}{\text{FRU of control}} \times 100$

$$\text{FRU of control} \quad (1)$$

The number of cells growing in the scaffolds was estimated by resazurin reduction assay on day 3, 5, and 7, which gives an indication of cell proliferation. Live/Dead staining was performed to visualize the cell distribution on scaffolds at day 7.

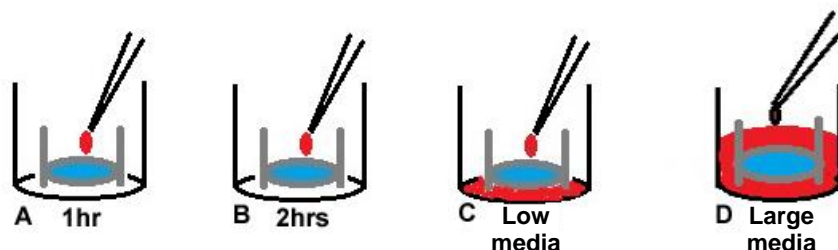


**Figure 5.3.1:** Schematic of cell seeding methods. A: small volume technique+1 hour, B: small volume technique+2 hours, C: low volume of media technique, and D: large volume of media technique. In the technique A, B, and C, after the samples were incubated, the appropriate media were added up to 1mL into the well plate. The cells were allowed to attach overnight in the cell culture incubator.

### 5.3.2 Results

Cell viability for all groups increased over-time points, however, the results were a quarter of the control result. No significant differences were found between the various conditions except for the TCP control group which was significantly higher than the others  $p < 0.05$  (Figure 5.3.2 A). The large volume of media group showed less variation compared to the other groups. Live/Dead staining images visualized by fluorescence microscopy showed viable (green) and died (red) cell distribution on the scaffolds. The 1 hour group showed isolated cells distributed on scaffolds (Figure 5.3.2 B-E). In the large volume of media cell seeding technique, there was less variability compared to the other methods (Figure 5.3.2 F). Therefore, the large volume media technique was selected for cell seeding in all future experiment.

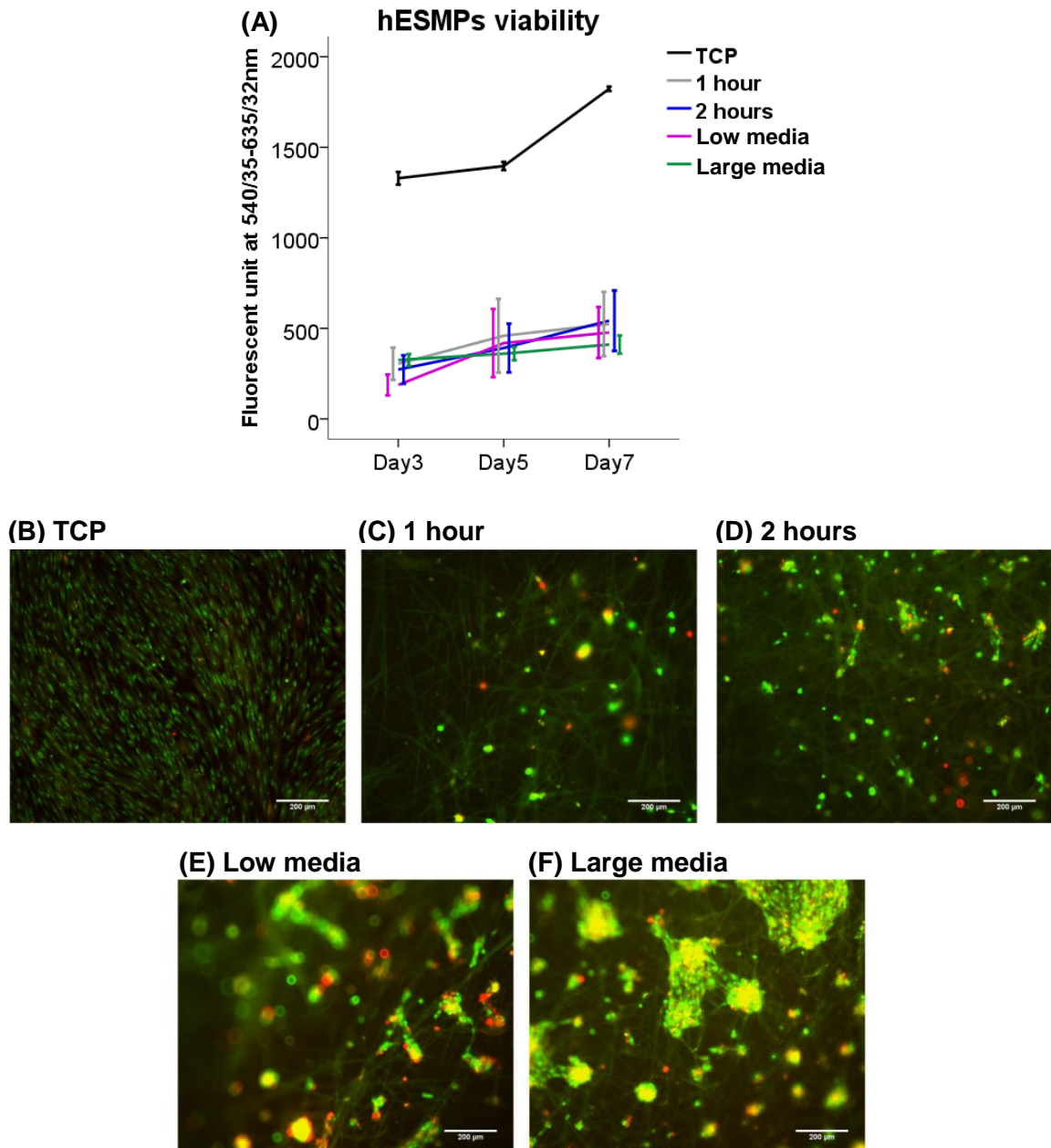


**Figure 5.3.2:** (A) The effect of 4 different cell seeding methods: 1] 1hour technique, 2] 2hours technique, 3] low media, and 4] large media groups of hES MP cells on PLA scaffold compared with the tissue culture plastic (TCP) group. The cell viabilities assayed using resazurin reduction test after 3, 5, and 7 days. mean $\pm$ SE, (N=1, n=3), Two-way ANOVA, Tukey's multiple comparison test,  $p < 0.05$ . The fluorescence images of hESMPs on PLA scaffolds in 4 different cell seeding methods using Live/Dead staining assay to examine cell viability after 7 days. B: tissue culture plate (TCP) group, C: 1hour, D: 2hours, E: low media, and F: large media groups. Scale bar = 200 $\mu$ m.

## 5.4 To evaluate cell viability on selected electrospun scaffolds (PLA, PCL, and PHBV) for hESMPs

### 5.4.1 Methods

- **Scaffold preparation**

Samples were divided into 3 groups depending on scaffold material; electrospun PLA, PCL, and PHBV scaffolds. The same amount of cells were cultured on TCP as a control. PCL, PLA, and PHBV were cut into disks using a cork borer with a diameter of 1.5 cm. The scaffolds were sterilized with 0.1% peracetic acid in PBS in steady rocking conditions for 3 hours then washed three times with PBS to remove the peracetic acid. The scaffolds were placed on top with sterilized stainless steel rings, then 1mL of basal culture media was added to each well and cell-scaffold constructs were cultured overnight to allow for serum protein attachment under sterile condition at 37°C, 5% CO<sub>2</sub>, and a humidified atmosphere incubator. Before cell seeding, the cell culture media was removed.

- **Cell seeding**

The 32.5µL mixture of 5x10<sup>4</sup> hESMP cells were seeded onto scaffolds with the large volume media technique as described previously. 5x10<sup>4</sup> cells were used in this experiment to complement an existing experiment for use as a figure in a publication (Bye et al., 2013). The samples were observed for their ability to support cells using a 25.1µg/mL (0.1mM) resazurin reduction test on days 1 and 7.

### 5.4.2. Results

Cell viability was used to evaluate cell attachment and cell proliferation of hESMPs on various types of scaffolds by using the resazurin reduction test at day 1 and 7 (Figure 5.4.1). The results showed that cell attachment between all groups was not significantly different on day 1 ( $p < 0.05$ ). By day 7, the cell viability was significantly higher for the control TCP group, however, the results of the PCL and PLA groups were less than half

of the TCP group. Moreover, they were not significantly different from day 1, indicating that cells had not proliferated. The cell viability on the PHBV group on day 7 was significantly lower than the other groups (PCL, PLA, and TCP groups), however, their cell viabilities on day 7 were also lower than at day1 with no significant difference, indicating cells didn't attach to the scaffold and there was cell arrest or even cell death.

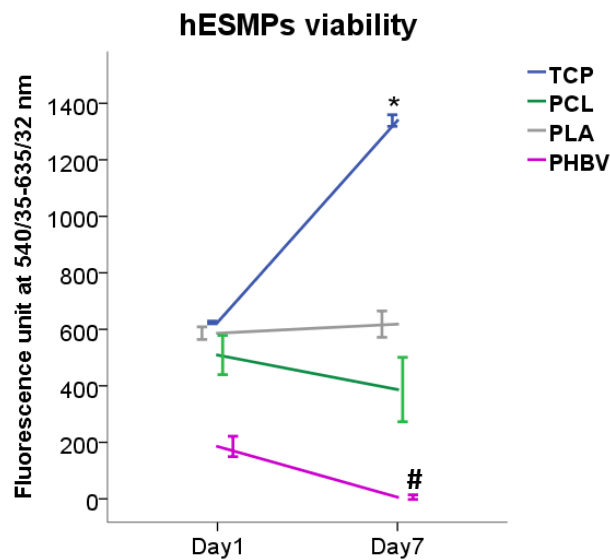


**Figure 5.4.2:** The ability of different electrospun scaffolds: PLA, PCL, PHBV, and TCP (tissue culture plastic control) to support cell viability over 7 days. The cell viability was assayed by resazurin reduction test after 1 and 7 days. mean±SE, (N=2, n=3 in all conditions except the TCP group N=1, n=3), \* =  $p < 0.05$  comparison between the TCP group with the other groups, # =  $p < 0.05$  comparison between the PHBV group with the other groups, Two-way ANOVA, Tukey's multiple comparisons.

## **5.5 To compare osteogenic differentiation of HJPs cultured on PCL and PLA scaffolds.**

### **5.5.1 Methods**

PCL and PLA were cut into circular disks (diameter 1.5cm). The sterilized scaffolds were seeded with  $10^5$  human jaw periosteal (HJP) cells from 2 donors (HJP-1 and HJP-2), passage numbers between 7 and 8 were used in this experiment.  $10^5$  cells were seeded using the large volume of media technique as described previously. The samples were cultured either in supplemented medium (SM group) which contained AA and  $\beta$ -GP, or in SM media with 10nM of Dex added, denoted 'SM+Dex10' group. The cell viability and osteogenic differentiation of the HJPs were measured using resazurin reduction test after day 7, 14, 21, and 28 and alizarin red staining after day 28. The scaffold sterilization and cell seeding as proceeded experiment 5.4.

### **5.5.2. Results**

A study was carried out to compare the osteogenic potential of HJPs-1 and HJPs-2 on PCL and PLA scaffolds. The resazurin reduction test was used to evaluate cell attachment on day 1 and cell viability on day 7, 14, 21, and 28 to compare PCL and PLA scaffolds. HJPs from both donors exhibited higher cell viability on PCL scaffolds than on PLA scaffolds (Figure 5.5.2). For both cell types the numbers increased over time in all conditions for 28 days indicating that cells proliferated (Figure 5.5.3). The cell viability of HJPs-1 under the SM+Dex10 medium was higher than the SM medium on both PCL and PLA scaffolds (Figure 5.5.3 A). This implies that the HJPs-1 on both PCL and PLA scaffolds under the SM+Dex10 medium underwent higher cell proliferation than in the SM medium. The cell viability of HJPs-2 on the PCL scaffold under the SM medium was higher than the Dex containing medium, in contrast, on the PLA scaffold cell viability was higher in SM+Dex10 medium than non Dex containing medium (Figure 5.5.3 B). Indicating that for HJPs-2 the PCL scaffold supported cell

proliferation better in SM but the PLA scaffold supported proliferation better under SM+Dex10 medium. The total calcium deposition of HJPs-1 was significantly higher in the PCL under SM+Dex10 medium (PCL-SM+Dex10) (Figure 5.5.4 A), however for HJPs-2, there was no significant difference between the 4 different groups (Figure 5.5.4 B). Alizarin red staining of HJPs-1 cell-deposited matrix showed darkest staining for the PCL-SM+Dex10 group (Figure 5.5.4 C), while the intensity of HJPs-2 staining was not different between the groups (Figure 5.5.4 D), indicating the HJPs were better support on PCL scaffolds.

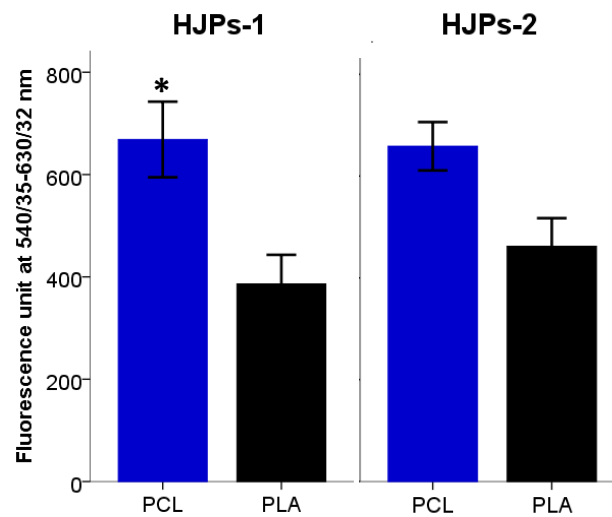


**Figure 5.5.2:** The ability of different electrospun scaffolds (PCL and PLA) to support HJPs attachment. The cell viability was measured using resazurin reduction results on day 1. mean±SE, (N=2, n=3), \* =  $p < 0.05$  comparison between PCL and PLA, One way ANOVA, Tukey's multiple comparison test.

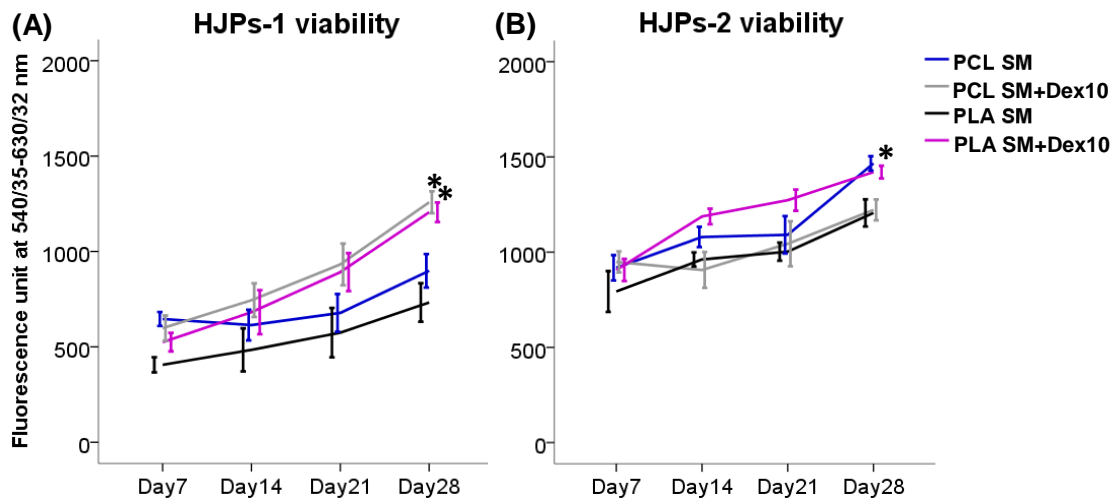


**Figure 5.5.3:** The ability of different electrospun scaffolds (PCL and PLA) to support HJPs growth under the supplemented media (SM) and the SM with 10nM of Dex (SM+Dex10). Cell viability was measured using resazurin reduction tests after 7, 14, 21, and 28 days. (A) First donor of HJPs: HJPs-1, and (B) second donor of HJPs: HJPs-2. mean  $\pm$  SE, (N=2, n=3), \*= $p < 0.05$  comparison between SM and SM+Dex10, # =  $p < 0.05$  comparison between PCL and PLA electrospun scaffolds, Two-way ANOVA, and Tukey's multiple comparison test.

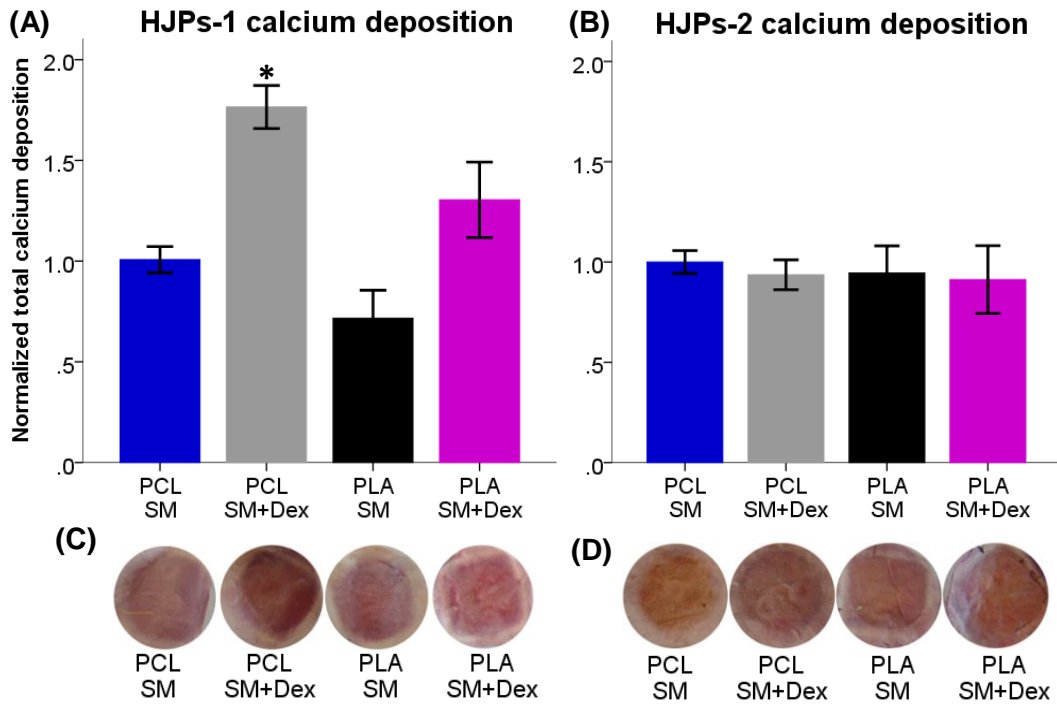


**Figure 5.5.4:** The ability of different electrospun scaffolds (PCL and PLA) to support osteogenic differentiation of HJPs under the supplemented media (SM) and the SM with 10nM of Dex (SM+Dex10). Deposited calcium was measured by alizarin red staining at day 28. Total calcium deposition normalized to cells cultured on the PCL under the SM medium (PCL-SM) groups (A) the first donor of HJP cells: HJPs-1, and (B) the second donor of HJP cells: HJPs-2. The photoimages show a representative set of alizarin red staining of HJPs-1(C) and HJPs-2 (D). mean  $\pm$  SE, (N=2, n=3), and  $*=p<0.05$  comparison between the SM and SM+Dex10 groups in the same scaffold, One-way ANOVA, Tukey's multiple comparison test.

## 5.6 Osteogenic differentiation of hESMPs on PCL scaffold

### 5.6.1 Methods

Circular PCL scaffolds with a diameter of 1.5cm were seeded with  $10^5$  hESMPs, passage numbers in the range 6 to 7. Samples were divided into 2 groups either the supplemented medium (SM) which contained basal  $\alpha$ -MEM supplemented with AA and  $\beta$ -GP, or the SM medium with 100nM of Dex added (SM+Dex100). The cell viability and osteogenic differentiation of the hESMPs were measured using resazurin reduction test after day 7, 14, 21, and 28 and alizarin red and picro-sirius red stainings after day 28, respectively. The scaffold sterilization and cell seeding as proceeded as experiment 5.4.

### 5.6.2 Results

The resazurin reduction test was used to evaluate cell viability on day 7, 14, 21, and 28. The cell viability of hESMPs increased overtime for 28 days at all conditions (Figure 5.6.2 A). Total calcium deposition by hESMPs was significantly higher in the SM+Dex100 than the SM group after 21 days and it was further significantly increased by 28 days ( $p<0.05$ ) (Figure 5.6.2 B). Total collagen production of the SM medium after 21 days was significantly lower than the other groups. However, there were no differences between the SM and SM+Dex100 groups after 28 days, ( $p<0.05$ ) (Figure 5.6.2 C). Alizarin red staining was darkest on the SM+Dex100 group after 28 days (Figure 5.6.2 D). The picro-sirius red stained images showed lightest staining on the SM group after 21 days (Figure 5.6.2 E). The intensities of picro-sirius red staining after 28 days were not different between the SM and SM+Dex100 groups, indicating that, although collagen deposition was slower in SM, Dex was not necessary to induce collagen production by 28 days of culture.

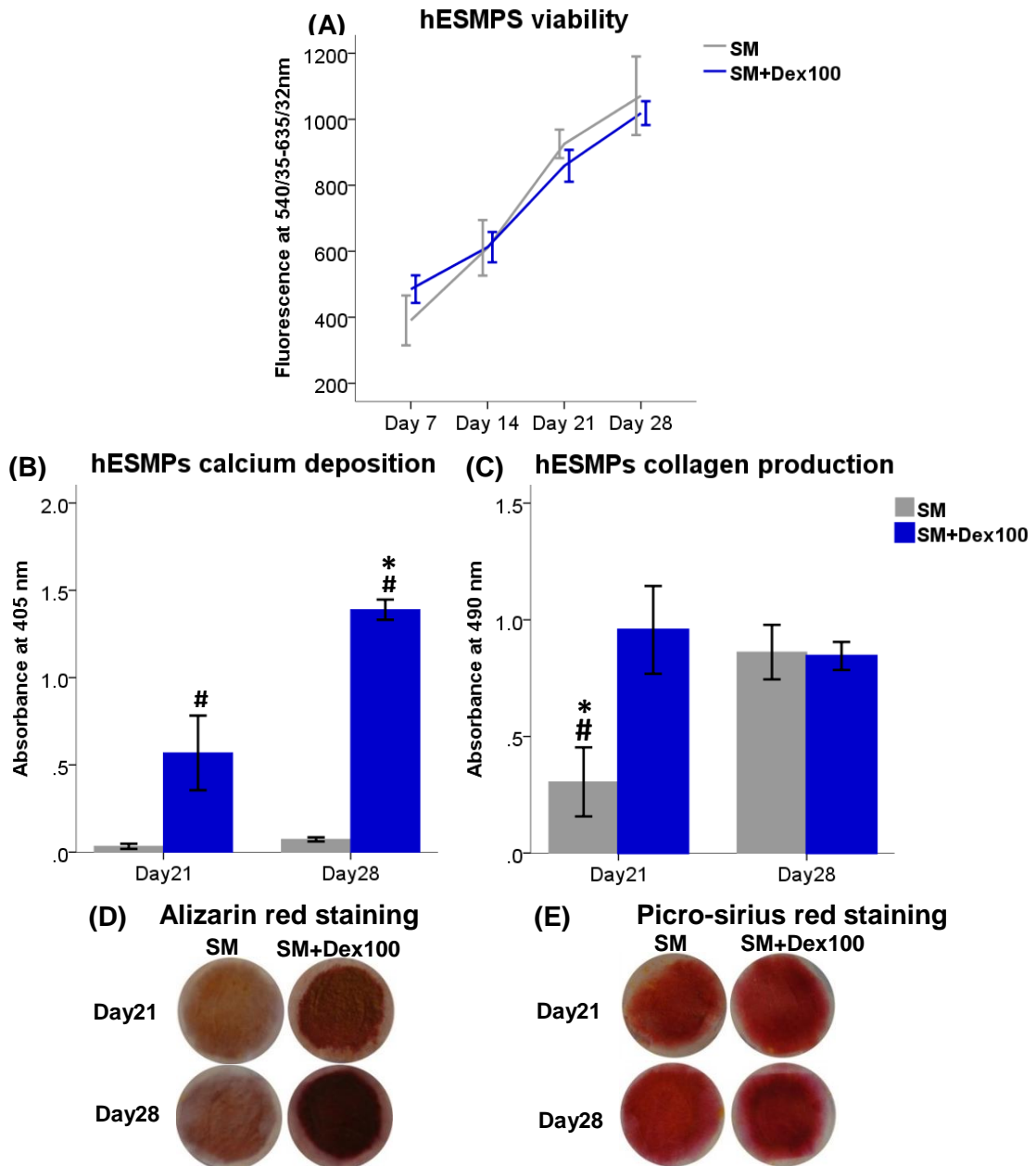


**Figure 5.6.2:** The ability of electrospun PCL scaffolds to support osteogenic differentiation of hESMPs under SM and SM+Dex100. (A) The cell viability of hESMPs was measured by using resazurin reduction test after day 7, 14, 21, and 28. Total calcium depositions (B) and total collagen production (C) were measured for hESMPs seeded on PCL scaffolds after day 21 and 28 using alizarin red and picro-sirius red staining assay, respectively. The photoimages show representative set of alizarin red staining (D) and picro-sirius red staining (E) on the hESMPs seeded on PCL scaffolds after 21 and 28 days. mean $\pm$ SE, (N=2, n=3), #= $p$ <0.05 comparison between the SM and SM+Dex100 groups in the same day, \*= $p$ <0.05 comparison between day 21 and 28 in the same medium, Two-way ANOVA, Tukey's multiple comparison test.

## **5.7: To evaluate the effect of OFF on hESMPs cultured on PCL electrospun scaffold.**

### **5.7.1. Methods**

$10^5$  cells of hESMPs in the passage number between 6 and 7 were seeded on PCL scaffolds. All cell seeded scaffolds were cultured with basal culture media along with the required supplements on day 1. The samples were divided into 2 groups; SM medium and SM medium with 100nM of Dex (SM+Dex100). The scaffold sterilization and cell seeding as proceeded as experiment 5.4. All samples were divided into two groups 1] Rocking and 2] Static groups at room temperature and atmospheric condition (0.04% CO<sub>2</sub>). The samples were subjected to OFF by using a standard see-saw rocker at room temperature for 1 hour a day, 5 days a week for 28 days (see chapter 2). The cell viability of the hESMPs were measured using resazurin reduction test after day 7, 14, 21, and 28. The osteogenic differentiation of the cells were measured using alizarin red and picro-sirius red staining for calcium deposition and collagen production after day 28.

### **5.7.2 Results**

The cell viability of hESMPs was assessed using resazurin reduction test after 7, 14, 21, and 28 days (Figure 5.7.2). Cell viability increased over time in all conditions (rocking SM, rocking SM+Dex100, static SM and static SM+Dex100 groups) except for in the rocking SM+Dex100 group where it was slightly decreased from day 21 to 28, and there were no significant differences between treatments ( $p < 0.05$ ). This implies that the cells in the rocking SM+Dex100 had lower cell proliferation than the other groups (Figure 5.7.2). Total calcium deposition by the rocking SM+Dex100 group was significantly higher compared to the other groups ( $P < 0.05$ ) (Figure 5.7.3 A). The SM groups deposited less calcium than the SM+Dex100 groups regardless of whether they were rocked. There were no differences in collagen production between any conditions (Figure 5.7.3 B). The alizarin red staining images confirmed these results with the

darkest staining in the rocking SM+Dex100 group (Figure 5.7.3 C) whereas the intensities of micro-sirius red staining images not different between conditions (Figure 5.7.3 D). VEGF secretion by the cells in SM media (during a 48 hours collecting period) was higher than in the SM+Dex100 media in both the rocking and static groups (Figure 5.7.4). At the day 28 time point, the static SM group had more secreted VEGF more than the others ( $p<0.05$ ).

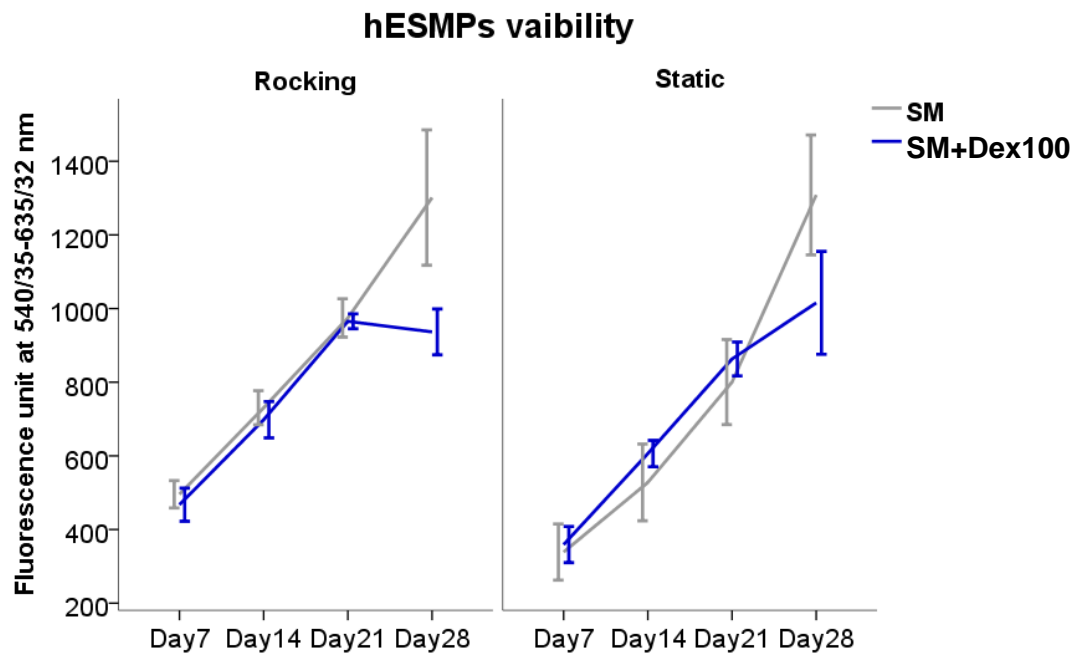


**Figure 5.7.2:** The effects of OFF to enhance osteogenic differentiation of hESMPs culture on PCL electrospun scaffolds under supplemented medium (SM) and SM added 100nM of Dex (SM+Dex100). The viability of hESMPs was measured using resazurin reduction test after 7, 14, 21, and 28 days. mean $\pm$ SE, (N=2, n=3), Two-way ANOVA, Tukey's multiple comparison test.

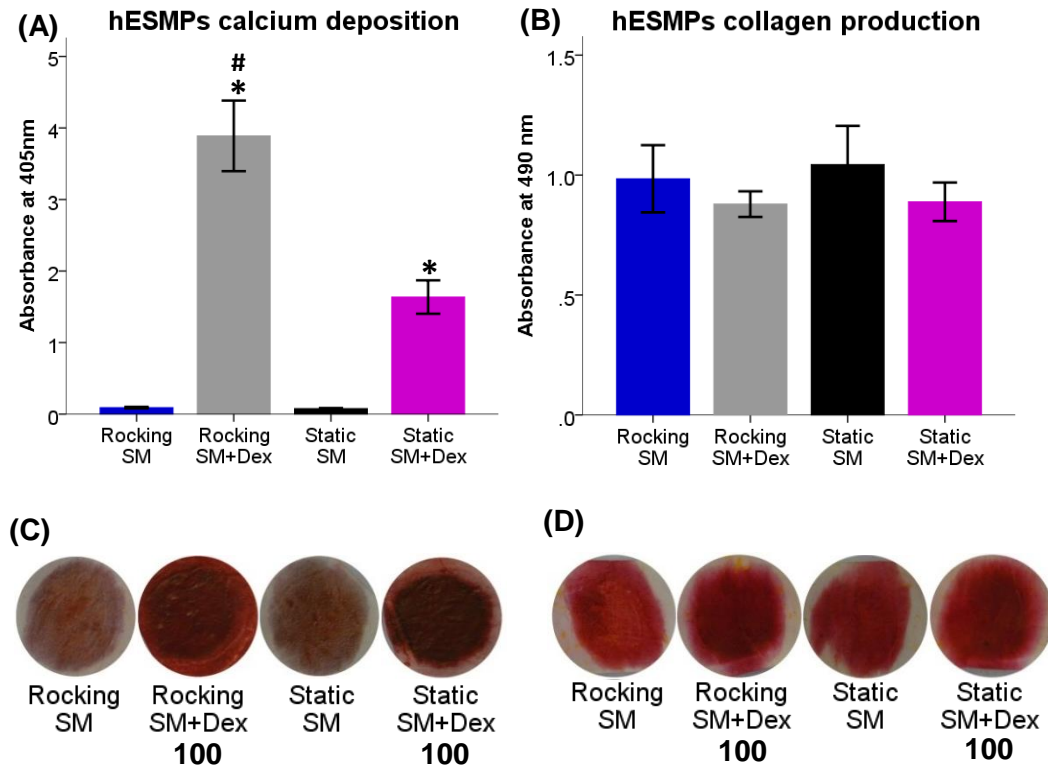


**Figure 5.7.3:** The effects of OFF to enhance osteogenic differentiation of hESMPs culture on PCL electrospun scaffolds under supplemented medium (SM) and SM with 100nM of Dex (SM+Dex100). Total calcium deposition in hESMPs was measured using alizarin red staining assay (A) and total collagen production using picro-sirius red staining assay (B) after 28 days. The photoimages show representative set of alizarin red (C) and picro-sirius red staining (D) of hESMPs.  $\text{mean} \pm \text{SE}$ , ( $N=2$ ,  $n=3$ ),  $*=p<0.05$  comparison between the SM and SM+Dex100 in the same condition,  $\# =p<0.05$  comparison between the rocking and static groups in the same medium, One-way ANOVA, Tukey's multiple comparison test.

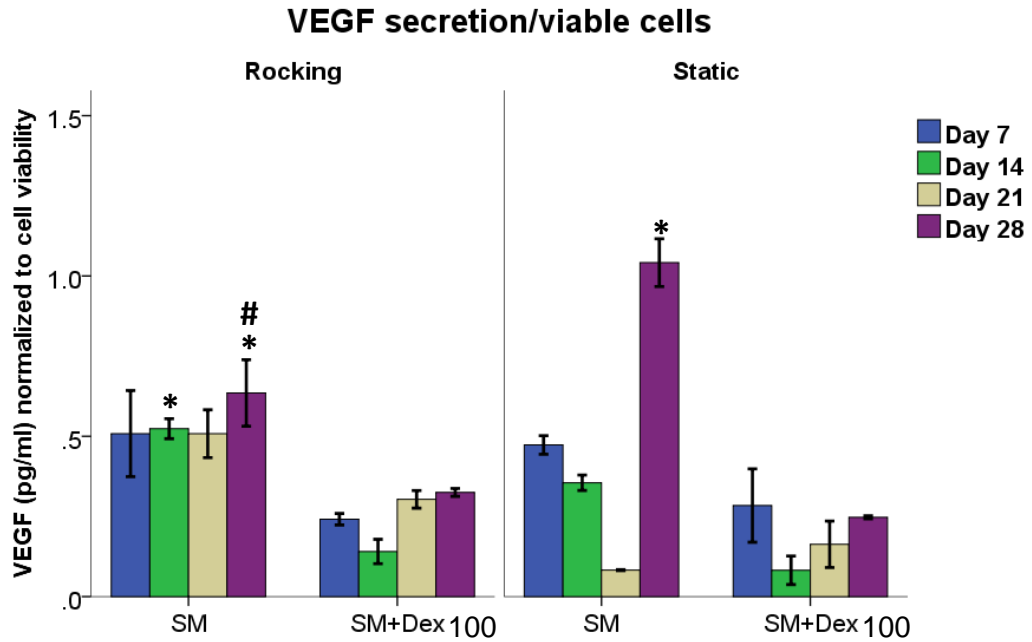


**Figure 5.7.4:** The effects of OFF on osteogenic differentiation of hESMPs cultured on PCL electrospun scaffolds under supplemented medium (SM) and SM added 100nM of Dex (SM+Dex100). VEGF secretion (during a 48 hour collection period) normalised to cell viability was measured using VEGF ELISA and resazurin reduction test, respectively after 7, 14, 21, and 28 days. mean $\pm$ SE, (N=1, n=3), \*= $p$ <0.05 comparison between SM and SM+Dex100 in the same condition, # =  $p$ <0.05 comparison between rocking and static groups in the same medium, Two-way ANOVA, Tukey's multiple comparison test.

## **5.8: To evaluate the effect of OFF on hBMSCs cultured on PCL electrospun scaffolds.**

### **5.8.1 Methods**

$10^5$  cells of hBMSCs (passage numbers between 2 and 3) were used in these experiments which were seeded on the PCL scaffold. All cell seeded scaffolds were cultured with basal culture media along with the required supplements on day1. The samples were divided into 2 groups; SM medium and SM medium with 10nM of Dex (SM+Dex10). The methods were as described for experiment 5.7.

### **5.8.2 Results**

The cell viability increased in all conditions (rocking SM, rocking SM+Dex10, static SM, and static SM+Dex10 groups) from day 7 to 28 (Figure 5.8.2). The rocking group in both the SM and SM+Dex10 media had lower cell proliferation than the static groups. There was no difference in cell viability between the SM and SM+Dex10 groups. Total calcium deposition by the rocking SM+Dex10 group was significantly higher compared to the other groups ( $P<0.05$ ) (Figure 5.8.3 A). The SM groups deposited less calcium than the SM+Dex10 groups regardless of whether they were rocked. There were no differences in collagen production between any conditions (Figure 5.8.3 B). The alizarin red staining images confirmed these results with the darkest staining in the rocking SM+Dex10 group (Figure 5.8.3 C) whereas the intensities of picro-sirius red staining images were no different between conditions (Figure 5.8.3 D). VEGF secretion (during a 48 hours collecting period) by the cells in SM+Dex10 media was lower than the SM media in both the rocking and static groups with no significant differences (Figure 5.8.4).

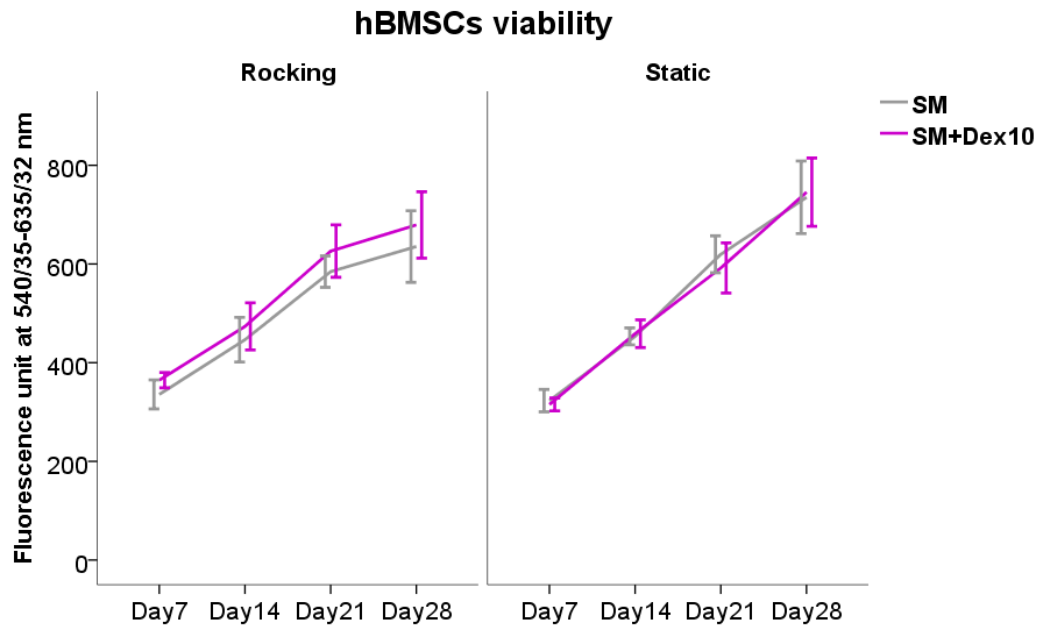


*Figure 5.8.2: The effects of OFF cultured under osteogenic media: supplemented media (SM) and SM with 10nM of Dex (SM+Dex10) of three donors of hBMSCs on PCL cultured after 7, 14, 21, and 28 days. The viability of hBMSCs was measured using resazurin reduction test. mean±SE, (N=3, n=3), Two-way ANOVA, Tukey's multiple comparison test.*

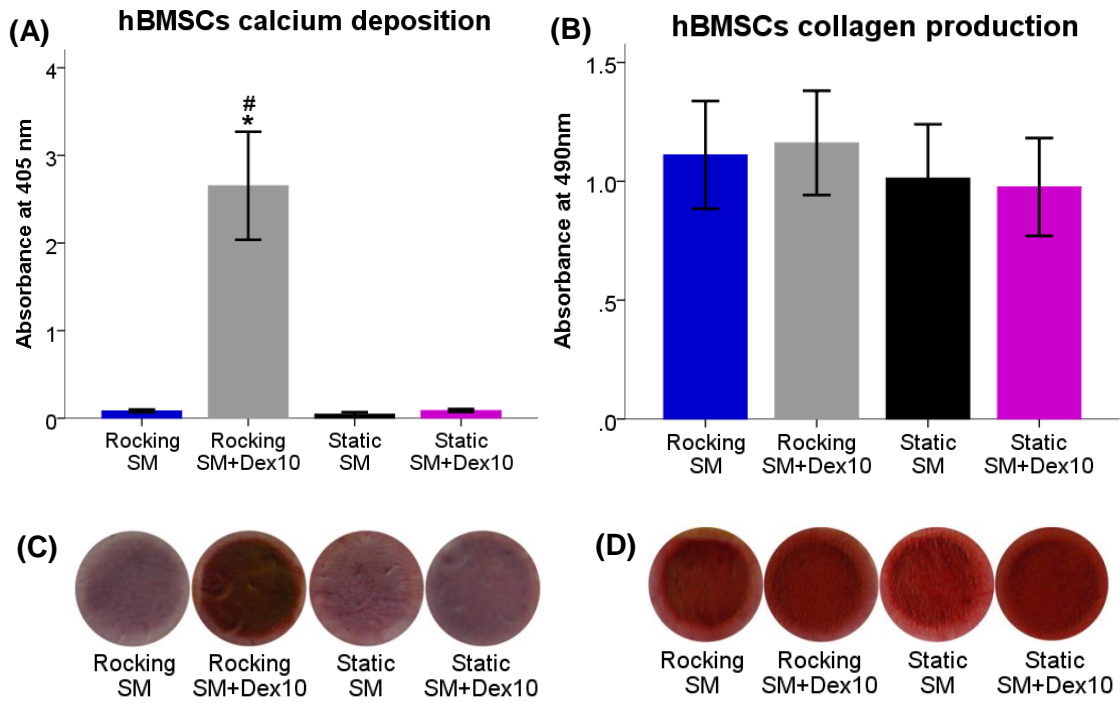


**Figure 5.8.3:** The effects of OFF and osteogenic media (SM and SM+Dex10 media) on the three donors of hBMSCs on PCL scaffolds cultured after 28 days. Total calcium deposition hBMSCs was measured using alizarin red staining assay (A) and total collagen production using picro-sirius red staining assay (B). The photomages showed representative sets of alizarin red (C) and picro-sirius red staining (D) of hBMSC cells. mean $\pm$ SE, (N=3, n=3), \*= $p$ <0.05 comparison between the SM and SM+Dex10 in the same group, # =  $p$ <0.05 comparison between the rocking and static groups in the same medium, One-way ANOVA, Tukey's multiple comparison test.

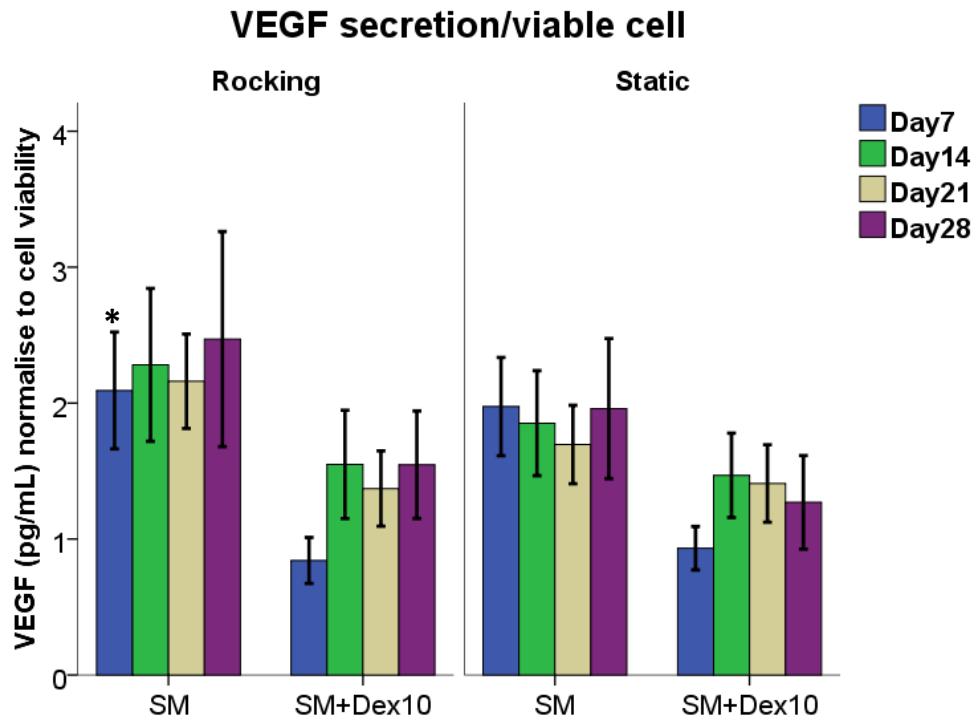


**Figure 5.8.4:** The effects of OFF and osteogenic media (SM and SM+Dex10 media) on the three donors of hBMSCs on PCL scaffolds cultured after 7, 14, 21, and 28 days. VEGF secretion (during a 48 hours collection period) normalised to cell viability. mean $\pm$ SE, (N=3, n=3), \*=p<0.05 comparison between SM and SM+Dex10 in the same condition, Two-way ANOVA, Tukey's multiple comparison test.

## **5.9. To incorporate nHA with PCL electrospun scaffolds for bone tissue engineering.**

### **5.9.1. Methods**

#### **• Scaffold preparation**

Various methods have been developed to fabricate calcium phosphate particles with poly( $\epsilon$ -caprolactone) electrospun scaffold (HA-PCL) for bone tissue engineering. This study will compare the three different fabrication methods of HA-PCL which have been used for bone tissue engineering; group 1: electrospinning (Lao et al., 2011, Fang et al., 2009), group 2: surface etching using a protocol modified from Choong et al., (2012) and Araujo et al., (2008), group 3: the alternate soaking process using a protocol modified from Jaiswal et al., (2012) and Taguchi et al., (2001).

#### **(Group 1) Electrospinning process**

0.35g of nHA with a particle size of no more than 200 nm was added into 31.5 g of DCM. The mixture was stirred using a magnetic stirrer for 15 minutes to disperse the nHA, followed by adding 3.5g of PCL pellet (80,000 Da) and dissolved at room temperature overnight to obtain a well mixed nHA-PCL suspension with a PCL concentration of 10wt%. 1wt% HA-PCL was the final concentration of the scaffold. The spinning parameter and process was the same as standard PCL (Figure 5.9.1 A).

#### **(Group 2) Surface etching process.**

The PCL scaffolds were submerged into a 0.1NaOH solution at 37°C for 1 hour. The scaffolds were then removed and washed with dH<sub>2</sub>O five times. The NaOH-treated PCL scaffolds were dipped in 1wt%HA in dH<sub>2</sub>O overnight. The scaffolds were then removed to a new container and left them dry. The HA-PCL was kept in the dry environment to be used in this experiment (Figure 5.9.1 B).

**(Group 3) Alternate soaking process.**

The PCL electrospun scaffold was functionalised on the surface by soaking in two different solutions as follows; The electrospun PCL scaffold was first submerged in 0.5M calcium chloride solution ( $\text{CaCl}_2$ ) in 0.05M Tris-HCL buffered solution at pH 7.4 for 30 minutes at  $37^\circ\text{C}$ , followed by washing with deionised water ( $\text{dH}_2\text{O}$ ) repeatedly. The PCL was then submerged in 0.3M disodium hydrogen phosphate ( $\text{Na}_2\text{HPO}_4$ ) in the 0.05M Tris-HCL buffered solution at pH 9 for 30 minutes at  $37^\circ\text{C}$ , followed by washing with  $\text{dH}_2\text{O}$  repeatedly. After this step the PCL was left in  $\text{dH}_2\text{O}$  for 1 hour at  $37^\circ\text{C}$  and dried for 24 hours. The HA-PCL was kept in the dry environment prior to use in this experiment (Figure 5.9.1 C).

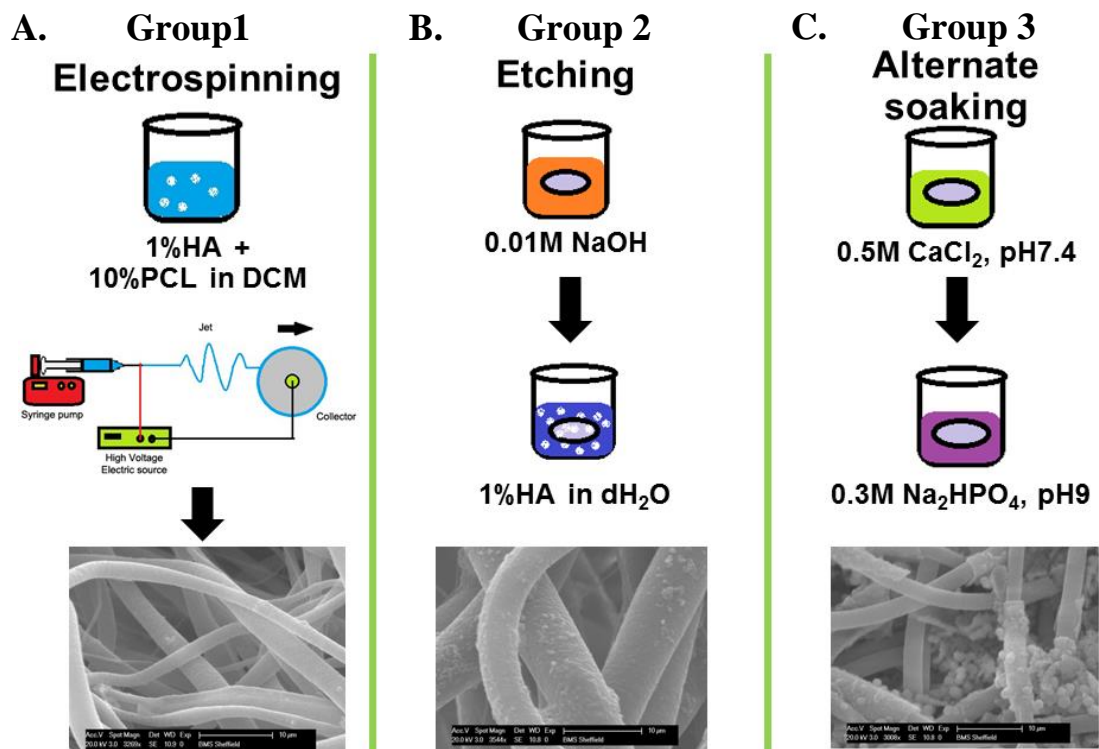


**Figure 5.9.1:** Schematic of the three different fabrication processes of hydroxyapatite incorporation with poly( $\epsilon$ -caprolactone) electrospun scaffold (HA-PCL) and the SEM images of the HA-PCL products in each process. (A) group1: electrospinning, (B) group2: surface etching, and (C) group3: alternated soaking process.

- **Cell preparation**

$10^5$  cells of hESMPs in the passage number in the range 6 to 7 were seeded on each type of nHA-PCL scaffold (standard PCL, electrospinning HA-PCL, surface etching process, and alternative soaking process). All cell seeded scaffolds were cultured with basal culture media along with the required supplements on day1. The samples were divided into 2 groups; SM medium and SM+Dex100 medium. The scaffold sterilization and cell seeding as proceeded as experiment 5.4. Cell viability of hESMPs was measured using resazurin reduction test on day 1, 4, and 7 and ALP activity was measured by using Alkaline Phosphatase Yellow (pNPP) Liquid Substrate System for ELISA on day 7 (see chapter 2).

### **5.9.2. Results**

The study characterised the samples from group 3 (alternate soaking process) using XPS survey spectra. Ca, P, and O peaks were present (Figure 5.9.2). The spectra analysed the chemistry and measured the amount of the chemical components in the samples by presenting in the percentage atomic concentration (At%) as shown in the table 5.9.2. Carbon (C), silicon (Si), boron (B), and sulphur (S) were impurities found in the sample surface in various At% from 0.24-26.79%. The mole fractions of the samples were received from percentage atomic concentration (At%) of the Ca and P as acronym “Ca/P” to distinguish the calcium phosphate phases. The measured Ca/P in this sample is 1.09 indicating that there is dibasic calcium phosphate dehydrate (DCPD or brushite) on the scaffold surface (Chusuei et al., 1999, Lu et al., 2000).

The XRD patterns for the various fabrication methods of HA-PCL scaffolds were detected in the  $2\theta = 20$  to 45 region (Figure 5.9.3). Standard PCL can be detected by specific XRD peaks at  $2\theta = 21.5^\circ$  and  $23.8^\circ$  indicated by the black arrows (Rezaei and Mohammadi, 2012). The HA and brushite patterns were matched with the database in the STOE STADI P diffractometer software (blue and red arrows, respectively). The

peaks for the alternative soaking process scaffolds corresponded to standard PCL, HA, and brushite, indicating that the brushite and HA components were on the scaffold. The XRD analysis of the electrospun HA-PCL scaffolds (group 1) indicated that the HA deposited in the scaffold and showed peaks corresponding to HA-PCL which had not change its chemical composition during the process.

The cell viability of hESMPs on HA-PCL scaffolds fabricated by the three methods and cultured in the SM or SM+Dex100 media was assayed using resazurin reduction tests to evaluate cell attachment on day 1 and cell viability on days 4 and 7 (Figure 5.9.4). The result showed that the cell viability for group 3 was lower than the other groups in both the SM and SM+Dex100 media on day 1. This implies that the cell attachment was the lowest on alternate soaked scaffolds. The cell viability for group 3 decreased after 4 and 7 days indicating that the cells must have died or detached from the scaffolds. Whereas the cell viabilities for the other groups (standard PCL, and group 1 and 2) increased overtime for 7 days. The cell viability for group 1 under the SM+Dex100 medium was higher than the other groups over time, indicating that group 1 supported the highest cell proliferation, compared to the other groups. The cells cultured under SM medium exhibited lower ALP activities at all conditions by day 7 (Figure 5.9.5). The group 3 cells under SM+Dex100 medium had a significantly lower ALP activity compared to the other groups ( $p < 0.05$ ).

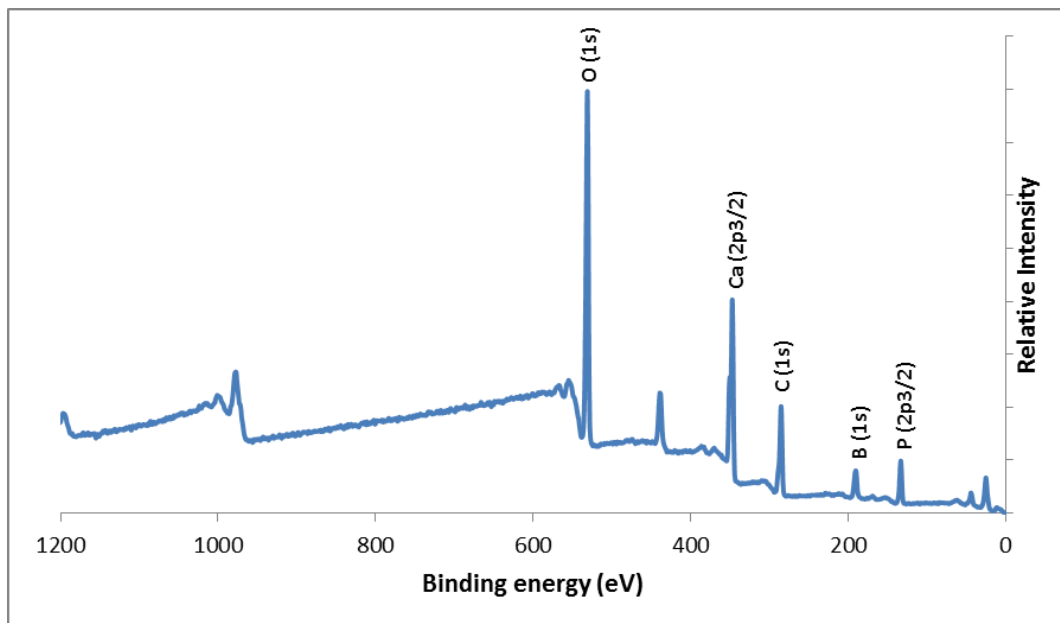


**Figure 5.9.2:** XPS survey spectrum of the HA-PCL samples from alternate soaking process (group 3). ( $N=1$ ,  $n=2$ )

Chemical components	Spectral line	Binding energy (eV)	At%
O	1s	531	31.06
Ca	2p <sub>3/2</sub>	347	11.18
C	1s	285	26.79
Si	2s	152	0.51
B	1s	190	20.01
S	2p <sub>3/2</sub>	169	0.24
P	2p <sub>3/2</sub>	133	10.2

**Table 5.9.2:** Chemical components, spectral line, binding energy and percentage atomic concentration (At%) of the sample in group 3 (alternate soaking process).

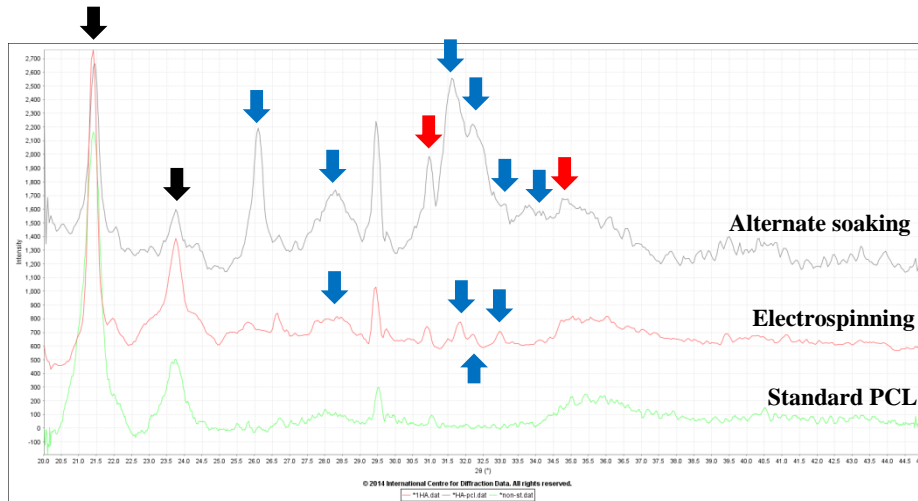


**Figure 5.9.3:** X-ray diffraction (XRD) patterns of the different HA fabrication techniques (alternate soaking: black line, electrospinning: red line, and standard PCL: green line). The red, blue, and black arrows present the identification of dibasic calcium phosphate dehydrate (DCPD, brushite), HA, and PCL, respectively. (N=1, n=3).

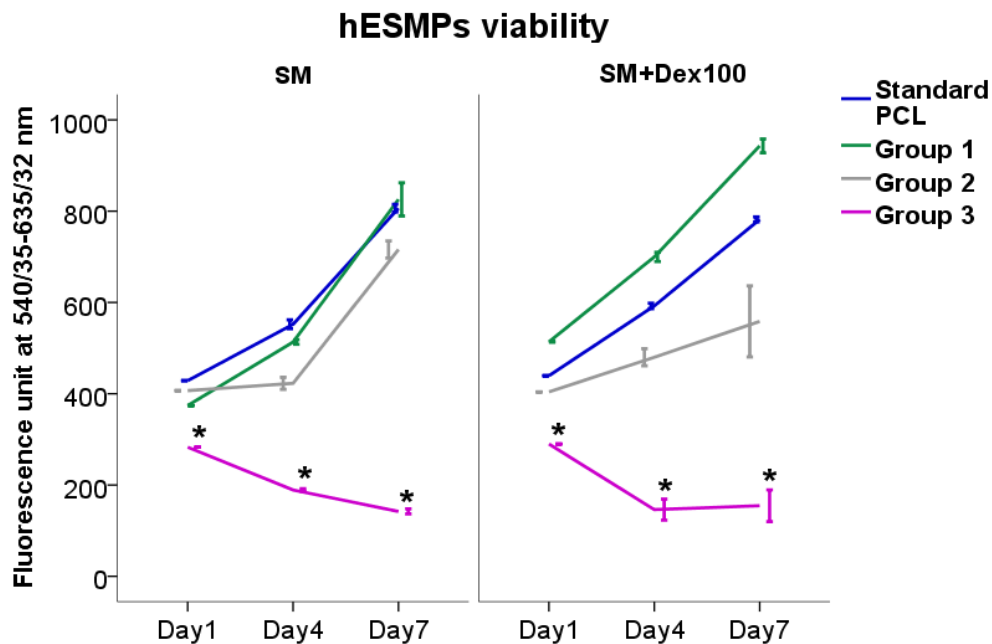


**Figure 5.9.4:** Comparison of the effect of three different fabrication techniques for hydroxyapatite poly( $\epsilon$ -caprolactone) electrospun scaffolds (HA-PCL) and standard PCL as a control. hESMPs seeded on HA-PCL scaffolds cultured under osteogenic media: supplemented medium (SM) and SM with 100nM of Dex (SM+Dex100) after 1, 4, and 7 days. The cell viabilities of hESMPs cultured on the scaffolds were measured using resazurin reduction test. mean $\pm$ SE, (N=1, n=3), \*=p<0.05 compare between the soaking with the other groups, Two-way ANOVA, Tukey's multiple comparison test.

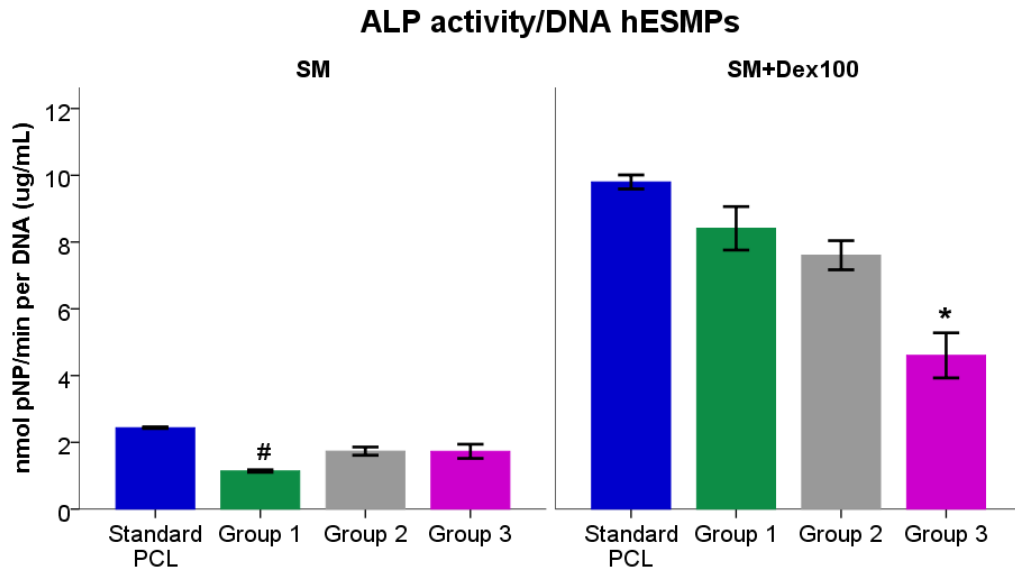


**Figure 5.9.5:** Comparison of the effect of four different HA-PCL fabrication processes (Standard PCL and group 1 to 3). hESMPs seeded on the HA-PCL scaffolds cultured under the SM and SM+Dex100 media. ALP activity normalised to DNA was measured after 7 days. mean $\pm$ SE, (N=1, n=3), \* =  $p < 0.05$  comparison between the group 3 and the other groups within the SM+Dex100 medium, # =  $p < 0.05$  comparison between the group 1 and the other groups within the SM medium, Two-way ANOVA, Tukey's multiple comparison test.

## 5.10: To select an appropriate concentration of nHA incorporated with PCL electropun scaffold for enhancing osteogenic differentiation of hESMPs

### 5.10.1. Methods

- **Preparation of HA-PCL scaffolds**

A pre-determined amount of the nHA powder for which the particle size was no more than 200 nm was added into 31.5 g of DCM. The mixture was stirred using a magnetic stirrer for 15 minutes to disperse the nHA, followed by adding 3.5g of PCL pellet (80,000 Da) and dissolving at room temperature overnight to obtain a well mixed nHA and 10wt% PCL suspension. The following is tabulated list of all the conditions for producing electrospun scaffolds in this study (table 5.10.1).

nHA		PCL (wt%)	Solvent system	Flow rate ( $\mu\text{L}/\text{minute}$ )	Voltage (kV)	Working distance (cm)	Collector speed (rpm)	Figure
wt%	g							
0	0	10	DCM	40	17	17	300	5.10.2A
1	0.35	10	DCM	40	17	17	300	5.10.2B
5	1.75	10	DCM	40	17	17	300	5.10.2C
10	3.50	10	DCM	40	17	17	300	5.10.2D

**Table 5.10.1:** Complete list of components and experiment parameters for electrospinning of PCL and HA-PCL scaffolds. PCL is Poly( $\epsilon$ -caprolactone), DCM is dichloromethane, nHA is nano particle hydroxyapatite. A rotating collector was used in all conditions.

- **Characterization of HA-PCL scaffolds**

The surface morphologies and fibre diameters of the HA-PCL scaffolds were observed from SEM images using ImageJ software. The compositions of scaffolds were determined by using FTIR and XRD analysis. The mechanical properties of the scaffolds were measured using the uni-directional tensile testing. The porosity of the scaffolds was determined by using micro-CT (Skyscan). The process, briefly, was that the scaffolds were scanned with

micro-CT and analysed using CTanalyzer software package. The scaffold porosity was estimated from the empty space of the scaffold. The ROI volume of the scaffold was subtracted to obtain the empty space. Dividing the empty space volume by the ROI volume gives the volumetric porosity of the scaffolds.

- **Cell culture**

$10^5$  cells of hESMPs were cultured on the four different concentrations of nano-hydroxyapatite polycaprolactone electrospun scaffolds (HA-PCL); 1] standard PCL, 2] 1%HA-PCL: 1wt%HA incorporating 10wt%PCL, 3] 5%HA-PCL: 5wt%HA incorporating 10wt%PCL, and 4] 10%HA-PCL: 10wt%HA incorporating 10wt%PCL. The scaffold sterilization and cell seeding as proceeded as experiment 5.4. The cell attachments and cell viabilities were assayed using resazurin reduction tests by day 1, 4, 7, 10, and 14. The osteogenic differentiation potential was evaluated using ALP activity after 7 and 14 days.

### 5.10.2 Results

The morphology and fibre diameter of the HA-PCL scaffolds was observed by SEM (Figure 5.10.2). The electrospun scaffolds were successfully fabricated without any bead formation in all ranges of compositions (Figure 5.10.2). The average fibre diameter of standard PCL was 2.682  $\mu\text{m}$  (Figure 5.10.2 A,E). PCL had a smaller average fibre diameter and more uniform fibre diameter distribution than the other groups (Table 5.10.2). The average fibre diameter of 10%HA-PCL was 3.012  $\mu\text{m}$  (Figure 5.10.2 D,H). It was bigger in fibre diameter than the other groups with a broader fibre diameter distribution. Both standard PCL and HA-PCL scaffolds contained a mix of micro- and nano-fibres. In standard PCL and 1%HA-PCL, fibre diameters of less than 1 $\mu\text{m}$  (nano-fibres) were less frequent or about 1% (Figure 5.10.2 E,F, respectively). In the 5% and 10%HA-PCL, the more frequent fibre diameter of nano-fibres were about 5% and 7% (Figure 5.10.2 G,H), respectively. The standard PCL had

the highest porosity and porosity decreased with increasing percentage of HA in the PCL (Figure 5.10.3 C, Table 5.10.2).

All HA-PCL scaffolds were stretched in unidirectional tension to generate stress/strain curves (Figure 5.10.4) to calculate their Young's modulus and Yield strength. The Young's modulus of the standard PCL was higher than the other groups. Whereas Young's modulus was lower in the HA groups and 5%HA-PCL had the lowest Young's modulus (Figure 5.10.3 A). The Yield strength was also lower in the HA groups in a similar pattern to Young's modulus results (Figure 5.10.3 B, Table 5.10.2).

The FTIR spectra of the various percentages of HA-PCL, standard PCL, and nHA powder (before electrospinning) provide details of the presence of the functional groups in the fibres to detect any possible chemical phase interaction or modification in the 480-3850  $\text{cm}^{-1}$  region (Figure 5.10.5). The typical FTIR bands of standard PCL are observed: the methylene group ( $\text{CH}_2$ ) stretching region was present as two bands, centre at 2945.2  $\text{cm}^{-1}$  which was assigned to the asymmetric  $\text{CH}_2$  stretching: green arrow and 2865.6  $\text{cm}^{-1}$  which was assigned to the symmetric  $\text{CH}_2$  stretching: green arrow. The peak at 1731.1  $\text{cm}^{-1}$  was assigned to the ester carbonyl stretching ( $\text{C}=\text{O}$ ): pink arrow. The FTIR spectra bands of nHA are observed: the phosphate group presented as two bands, centre at 574.2 and 1056  $\text{cm}^{-1}$  (black arrows). The peak at 3569  $\text{cm}^{-1}$  is assigned to the hydroxyl group (blue arrow). FTIR spectra of all various percentages of HA-PCL exhibited the strong absorbance band of PCL at 1731, 2945.2, and 2865.6  $\text{cm}^{-1}$  while the strong absorbance band of nHA at 574.2, 1056 and 3569  $\text{cm}^{-1}$ . The assignments of FTIR absorbance bands are tabulated in 5.10.3.

The XRD patterns of the various compositions of HA-PCL were detected in the  $2\theta = 20$  to 45 region (Figure 5.10.6). PCL can be detected by specific XRD peaks at  $2\theta = 21.5^\circ$  and  $23.8^\circ$  indicating by black arrows (Rezaei and Mohammadi, 2012). The HA patterns were matched with the database in the STOE STADI P diffractometer software (red

arrows). Peaks corresponding to both of HA and PCL were observed in the HA-PCL scaffolds indicating that the nHA was exposed in the electropun PCL scaffolds. The intensities of HA peaks increased with the increasing in the percentage of HA. Both FTIR spectra and XRD patterns in the 1wt%, 5wt%, and 10wt% HA-PCL scaffolds did not show a new band on both results indicating that there was not a new chemical component. Both FTIR spectra and XRD patterns of HA-PCL could be superimposed on the pure PCL and nHA traces. The relevant peak intensities may change depending on the concentration of HA in the compositions.

Cell viability using resazurin reduction test was used to evaluate cell attachment of hESMPs on scaffolds with various concentrations of HA on day 1 (Figure 5.10.7) and determine cell proliferation after day 4, 7, 10, and 14 (Figure 5.10.8). The results showed that the cell viabilities were not significantly different between all groups after 1 day, indicating that there were no differences in cell attachment. The cell viability of hESMPs on all HA-PCL scaffolds increased overtime from day 1 to 14, notably, the standard PCL groups had lower cell viability than the other groups in both the SM and SM+Dex100 media by day 14. This implies that the standard PCL groups supported cell proliferation less well than the other groups. Cells cultured under the SM medium had lower ALP activity than SM+Dex100 on day 14 (control) (Figure 5.10.9). The ALP activity of the 5%HA-PCL was highest whereas the 10%HA-PCL was significantly lower than the other groups ( $p < 0.05$ ). The results indicated that 5%HA-PCL can stimulate cells to osteogenic differentiation more than the other scaffolds.

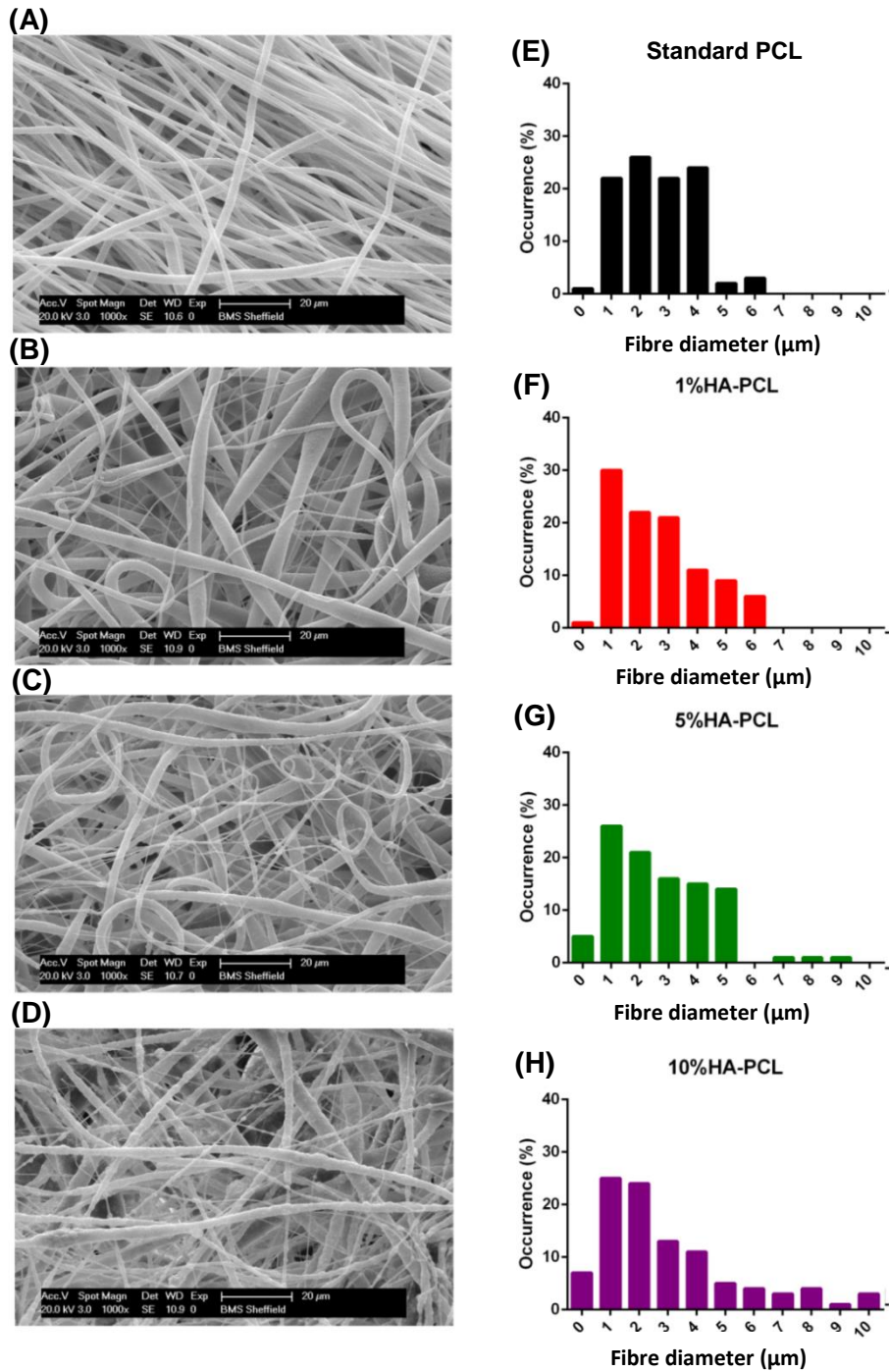


**Figure 5.10.2:** SEM images showed fibrous morphology of various percentages of nHA incorporated with 10wt% PCL dissolved in DCM (10wt% PCL) on the left column. The histogram shows fibre diameter distribution on the right column. (A,E):standard PCL, (B,F):1%HA-PCL, (C,G):5%HA-PCL, and (D,H):10%HA-PCL. Fibre diameter distributions are for 100 measured fibres (N=1, n=100).

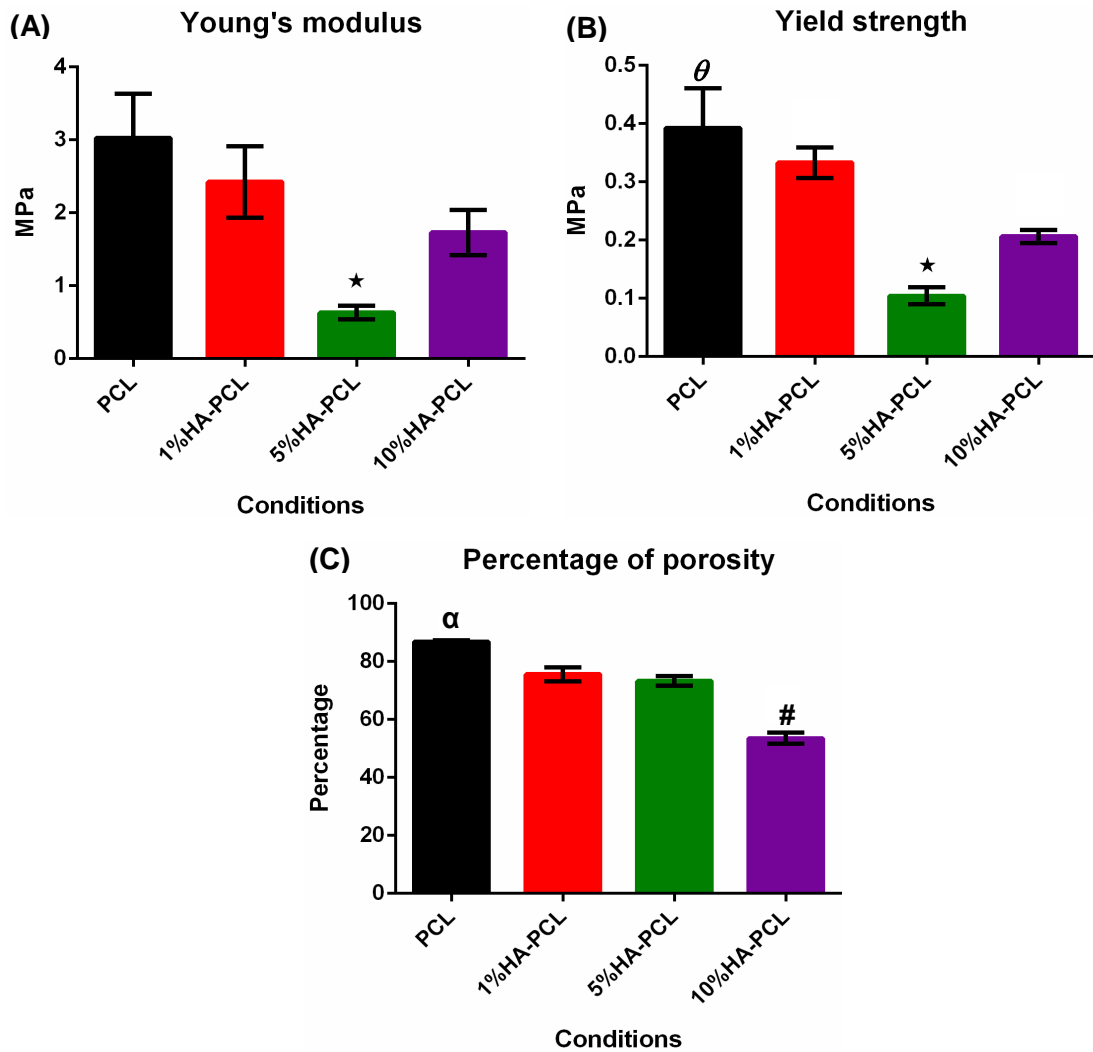


**Figure 5.10.3:** (A) Young's modulus, (B) Yield strength, and (C) percentage of porosity of various concentrations of nHA-PCL electrospun scaffolds (standard PCL as 'PCL'), 1%, 5%, and 10%HA-PCL). mean  $\pm$  SE, (N=1, n=3), \*=  $p < 0.05$  comparison between the 5%HA-PCL and the other groups,  $\theta = p < 0.05$  comparison between PCL and 10%HA-PCL,  $\alpha =$  PCL group was significantly higher than the others ( $p < 0.05$ ), # = 10%HA-PCL group was the significantly higher than the others ( $p < 0.05$ ), One-way ANOVA, Tukey's multiple comparison test.

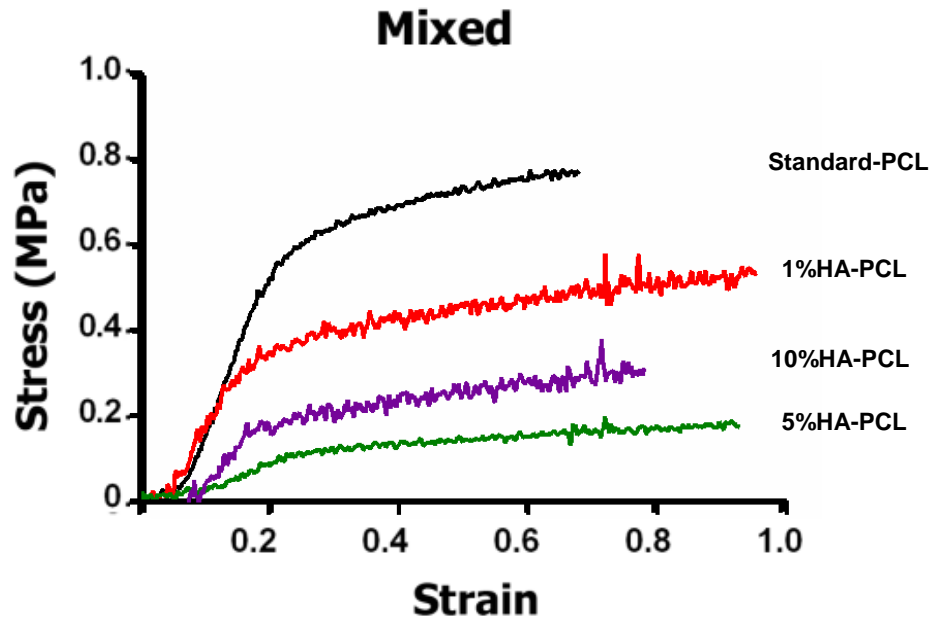


**Figure 5.10.4:** Stress-strain curves of various percentages of HA incorporated with PCL electrospun scaffolds: All percentages of HA incorporate with PCL: standard PCL (black line), 1%HA-PCL (red line), 5%HA-PCL (green line), and 10%HA-PCL (purple line). Scaffolds were cut into 20mm by 5mm and uni-tensile stretched at 0.1mm/sec to 100% strain. (N=1, n=3).

Conditions	Fibre diameter ( $\mu\text{m}$ )	Young's modulus MPa	Yield strength	%Porosity
Standard PCL	2.682 $\pm$ 0.129	3.027 $\pm$ 0.600	0.392 $\pm$ 0.068	86.79 $\pm$ 0.475
1%HA-PCL	2.609 $\pm$ 0.153	2.423 $\pm$ 0.490	0.332 $\pm$ 0.026	75.51 $\pm$ 2.392
5%HA-PCL	2.734 $\pm$ 0.173	0.630 $\pm$ 0.094	0.104 $\pm$ 0.015	73.21 $\pm$ 1.707
10%HA-PCL	3.012 $\pm$ 0.239	1.727 $\pm$ 0.313	0.206 $\pm$ 0.011	53.48 $\pm$ 1.935

**Table 5.10.2:** Physical and mechanical properties of the various HA-PCL electrospun scaffolds. mean $\pm$ SE, (N=1, n=3).

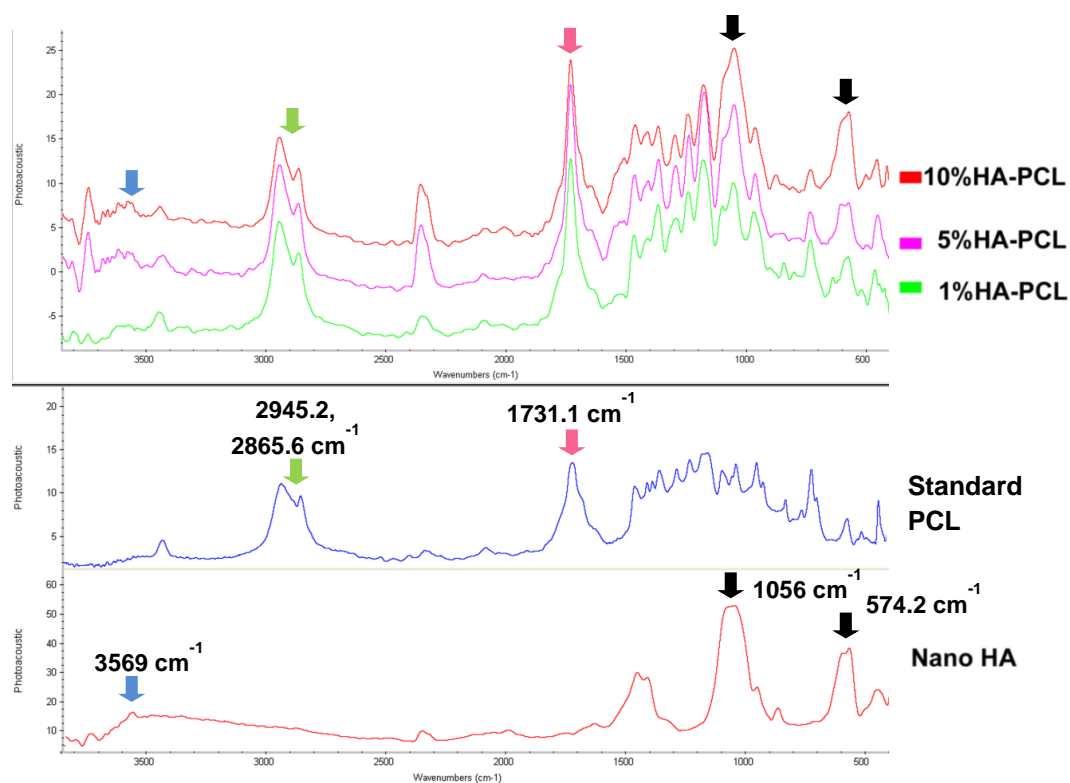


**Figure 5.10.5 :** Photoacoustic amplitude spectra in the length between  $480\text{-}3850\text{ cm}^{-1}$  of the various percentages of HA-PCL (standard PCL, 1%, 5%, and 10% HA-PCL groups) and nHA powder. At  $2945.2\text{ cm}^{-1}$  represent to  $\text{CH}_2$  stretching (green arrows), at  $2865.6\text{ cm}^{-1}$  represent to symmetric  $\text{CH}_2$  stretching (green arrow), at  $1731.1\text{ cm}^{-1}$  represent to carbonyl stretching (pink arrow), at  $574.2$  and  $1056\text{ cm}^{-1}$  represent to phosphate group (black arrow), and at  $3569\text{ cm}^{-1}$  represent to hydroxyl group (blue arrow). ( $N=1$ ,  $n=3$ ).

Stretching modes	FTIR spectral band ( $\text{cm}^{-1}$ )	References
PCL		(Doustgani et al., 2012)
$\text{CH}_2$ (asymmetric stretching)	2945.2	
$\text{CH}_2$ (symmetric stretching)	2865.6	
$\text{C}=\text{O}$ (carbonyl stretching)	1731.1	
HA		(Doustgani et al., 2012,
$\text{PO}_4^{-3}$ (Phosphate group)	574.2 and 1056	Rehman and Bonfield,
$-\text{OH}$ (hydroxyl group)	3569	1997)

**Table 5.10.3:** Observed infrared band positions from the nHA powder, and the various concentrations of HA-PCL electrospun scaffolds: standard PCL, 1%, 5%, and 10% by weight.

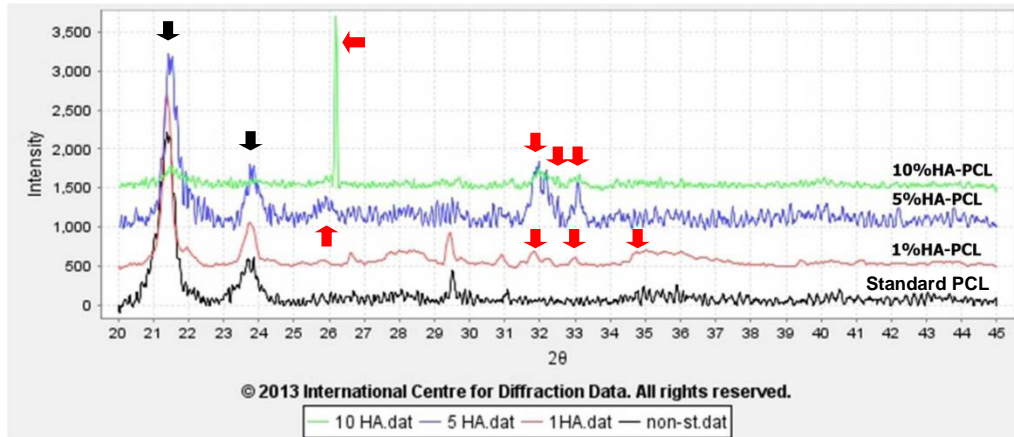


**Figure 5.10.6:** X-ray diffraction (XRD) pattern of the various concentrations of HA-PCL electrospun scaffolds. The red arrows referred to HA and the black arrows referred to PCL. The red arrows indicate that HA is clearly present in all scaffolds (1%, 5%, and 10% HA-PCL groups) except the standard PCL scaffolds. ( $N=1, n=3$ )

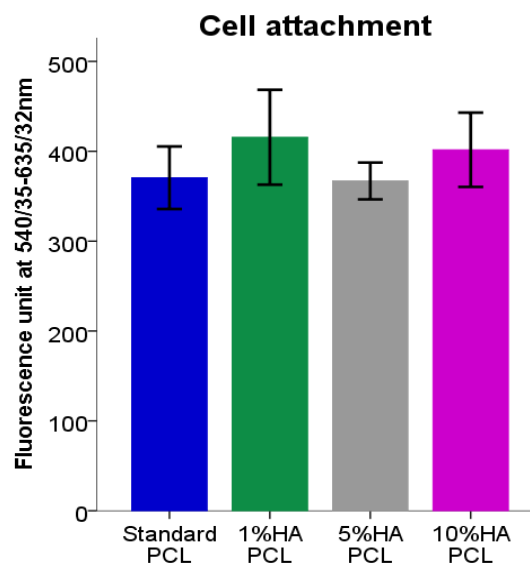


**Figure 5.10.7:** The effect of various concentrations of HA in PCL scaffolds on their ability to support hESMPs- (standard PCL, 1%, 5%, and 10% HA-PCL groups) cultured under basal culture medium  $\alpha$ -MEM after 24 hour cell seeding. The cell viabilities of hESMPs cultured on the scaffolds were measured using resazurin reduction test to indicate cell attachment.  $mean \pm SE$ , ( $N=2, n=3$ ), Two-way ANOVA, Tukey's multiple comparison test).

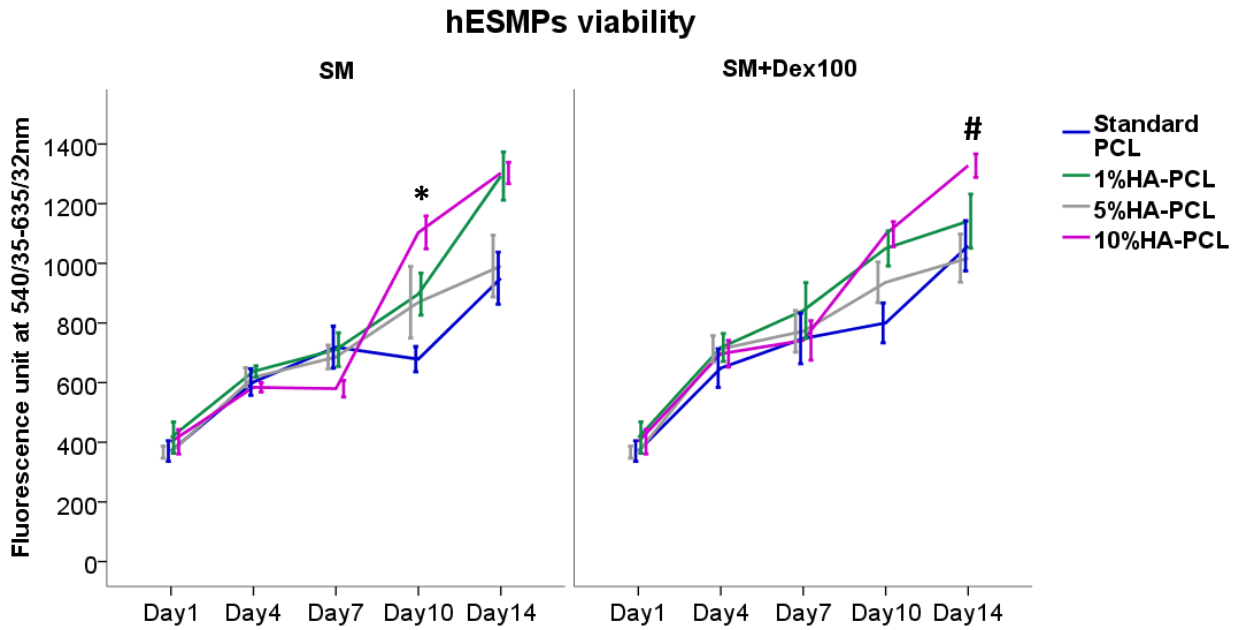


**Figure 5.10.8:** The effect of various concentration of HA-PCL (standard PCL, 1%, 5%, and 10% HA-PCL groups) cultured under osteogenic media: supplemented media (SM) and supplemented media with 100nMDex (SM+Dex100) of hESMPs after 1, 4, 7, 10, and 14 days. The cell viabilities of hESMPs cultured on the scaffolds were measured using resazurin reduction test. mean $\pm$ SE, (N=2, n=3), \* = $p < 0.05$  comparison between standard PCL and 10%HA-PCL groups within the SM medium, # = $p < 0.05$  comparison between standard PCL in the SM medium and 10%HA-PCL in the SM+Dex100 medium, Two-way ANOVA, Tukey's multiple comparison test.

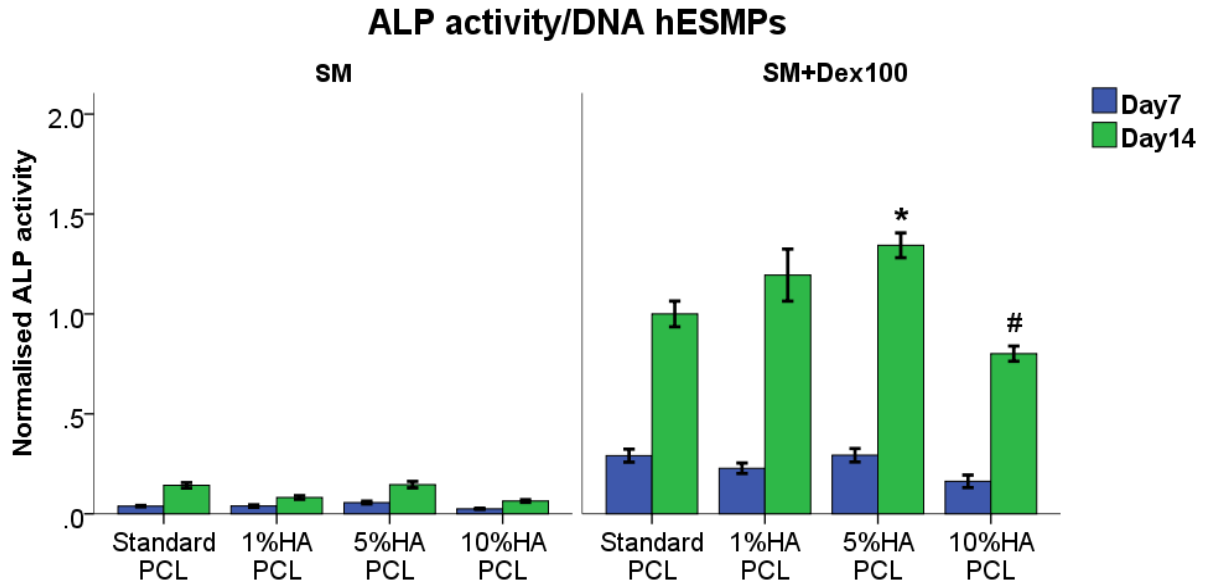


**Figure 5.10.9:** The effect of various concentrations of HA-PCL (standard PCL, 1%, 5%, and 10% HA-PCL groups) cultured under osteogenic media (the SM and SM+Dex100 groups) of hESMPs after 7 and 14 days. The bar graph showed ALP activity per DNA normalized to the results of the standard PCL under SM+Dex100 group on day 14. mean $\pm$ SE, (N=2, n=3), \* = $p$ <0.05 comparison between the standard PCL and the 5%HA-PCL groups, #= $p$ <0.05 comparison between the 10%HA-PCL and the other groups in the SM+Dex100 medium, Two-way ANOVA, Tukey's multiple comparison test.

### **5.11: To evaluate the effect of oscillatory fluid shear stress and nHA PCL electrospun scaffold for enhancing osteogenic differentiation of hESMPs**

#### **5.11.1 Methods**

- **Cell culture**

$10^5$  cells of hESMPs were seeded on either electrospun PCL or 5wt%HA-PCL scaffolds under the SM and SM+Dex100 media. Half of them were subjected to rocking using a standard see saw rocker and the others were cultured under static condition. The experimental method as proceeded as experiment 5.7. Samples were subjected to OFF as described for experiment 5.7. Cell viabilities and VEGF secretion were measured at the day 7, 14, 21, and 28 time-points using resazurin reduction test, and ELISA, respectively. The mineralized deposition was evaluated by using micro-computed tomography (micro-CT).

- **Application of micro-computed tomography (micro-CT) to analysis mineralized matrix deposition**

Micro-CT was used in this study because the HA-PCL scaffold itself stains with alizarin red with high background. It would be difficult to evaluate calcium deposition from cells on the HA-PCL scaffolds. The software package for analysing and reconstruction 3D realistic visualizations were used CTan and CTvol (both from Skyscan), respectively.

- **Region of interest (ROI)**

The region of interest (ROI) was cubic with dimensions of 18 mm in length and 35mm in width which covered the entire samples stack chosen for scanning. For measuring percentage bone volume (%BV), a cylindrical ROI with a diameter of 1.2 mm (inner diameter of metal ring) and height of 390 $\mu$ m (approximate scaffold thickness) was chosen. The ROI was sectioned into top, mid, and bottom portions with 130  $\mu$ m in each (Figure 5.11.1).

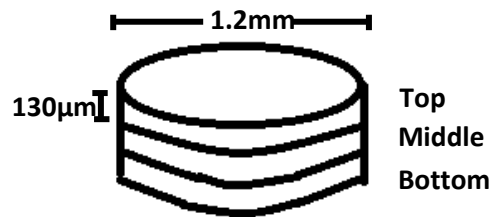


*Figure 5.11.1: The sectioning of the electrospun scaffold was used to analyse calcium deposition (%BV). The cylindrical ROI was diameter 1.2mm. The scaffold was divided into 3 layers with 130  $\mu$ m in each layer: top, middle, and bottom.*

- **Thresholding**

Three samples of standard PCL without cells, 5wt%HA-PCL without cells, and the rocking with SM+Dex100 group which showed mineralization from hESMPs on the standard PCL scaffolds were analysed with the aid of the CTanalyze software (Figure 5.11.2) to obtain the grey scale distributions (Figure 5.11.3 A). The mineralized deposition in a particular volume of ROI was expressed as %BV.

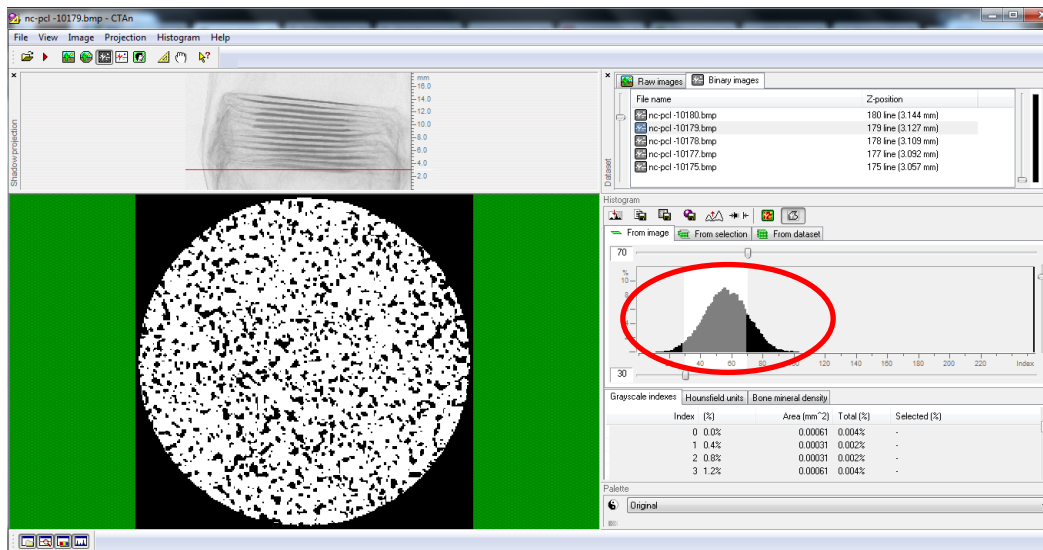


**Figure 5.11.2:** A window from CTanalyze software. The grey scale index (GSI) of the grey scale distribution (circle red) was used in the threshold ranges of standard PCL without cells, 5wt%HA-PCL without cells, and the rocking with SM+Dex100 group which showed mineralization from hESMPs on standard PCL scaffolds. (Circled red) The grey scale distribution histogram (a GSI: X-axis versus a percentage of brightness area: Y-axis) was used for evaluating threshold.

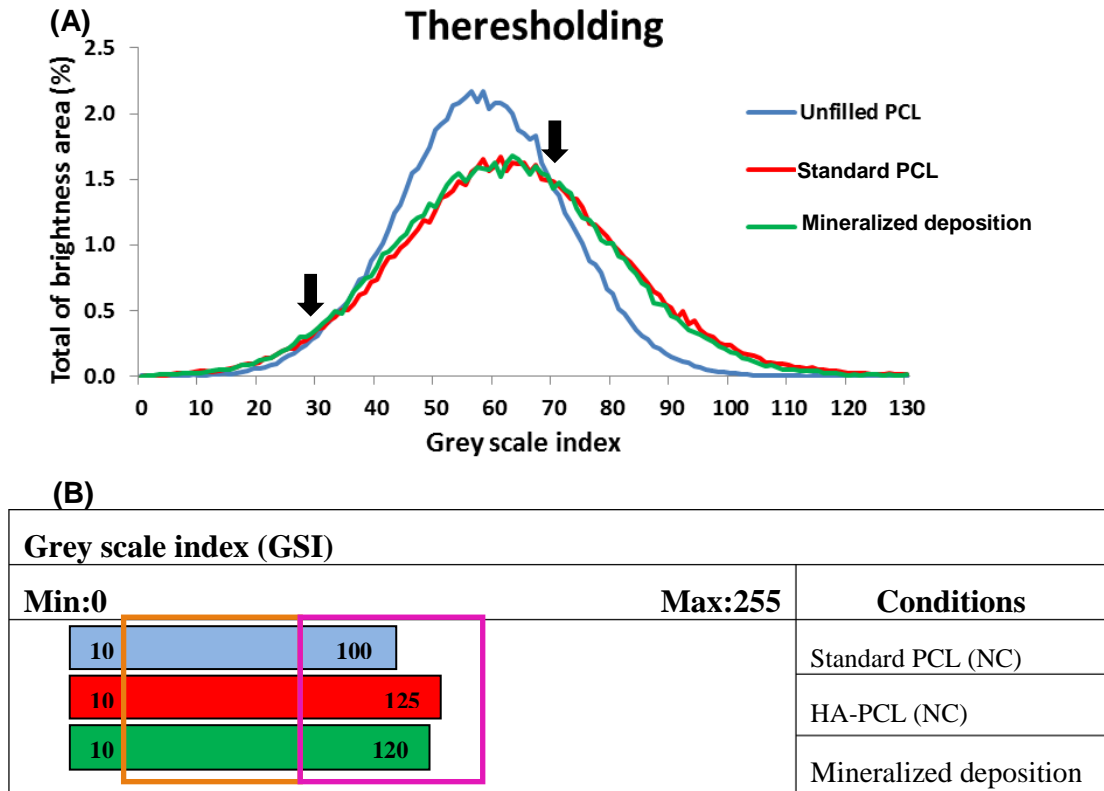
### 5.11.2 Results

The grey scale distribution of all samples : standard PCL, HA-PCL, and mineralized deposition of hESMPs cultured on PCL scaffolds in the rocking, SM+Dex100 group were plotted to evaluate the threshold (Figure 5.11.3 A). The hESMPs cultured on PCL scaffolds in the rocking, SM+Dex100 group was chosen because it definitely has calcium deposition based on alizarin red staining (experiment 5.7). The first and second interception points of three lines were at the GSI 30 and 70, respectively. The threshold was set in the range of 30-70 GSI to view the standard PCL, the threshold range above than 70 GSI was set to view a mineralized deposition and HA (Figure 5.11.3 B). It was possible to measure the scaffolds without any cells (background), subtraction of the background was used to determine a mineralized deposition on the samples.

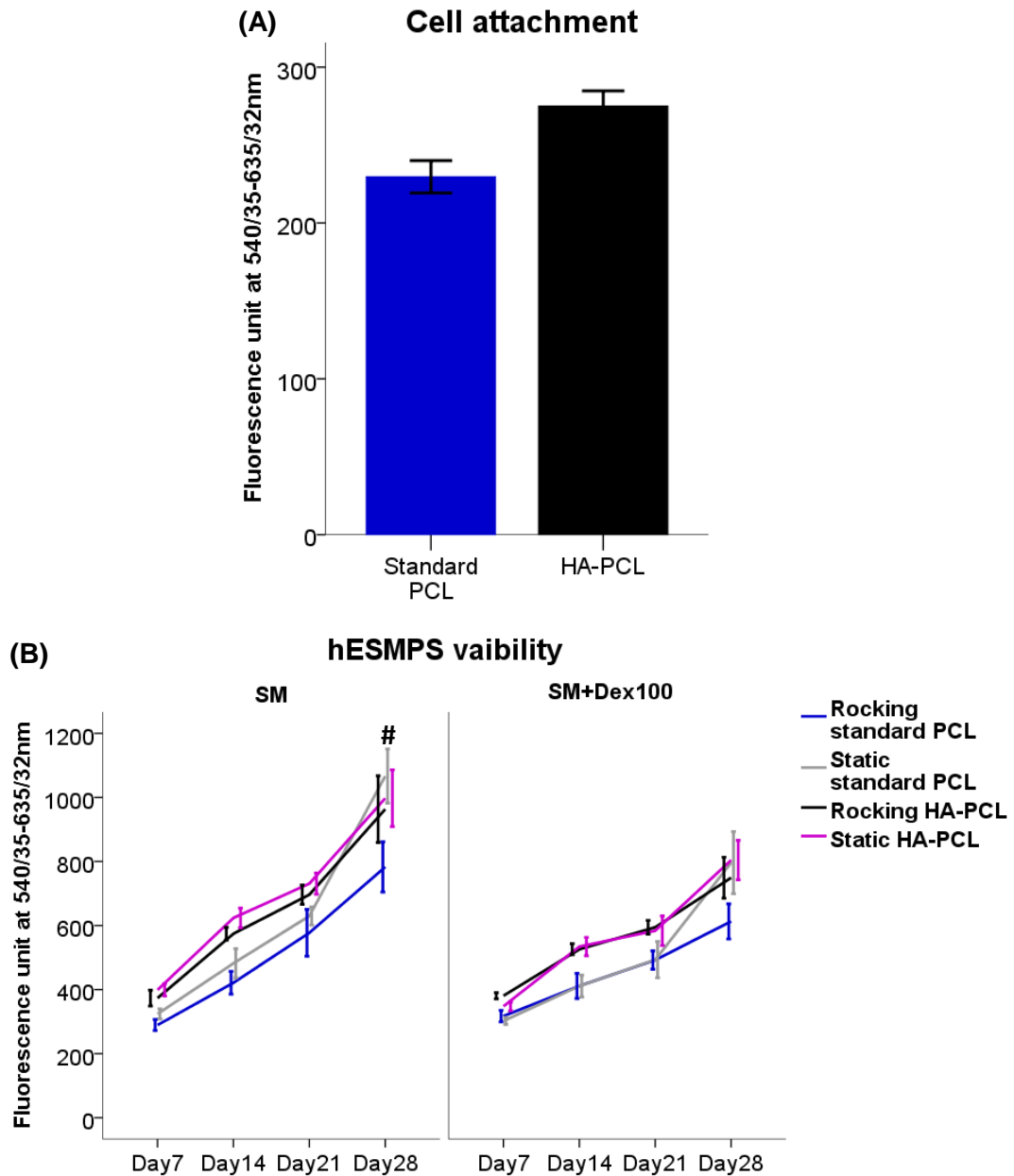
The cell viability of hESMPs on either standard PCL and HA-PCL scaffolds was assayed using resazurin reduction test after 1 day (Figure 5.11.4 A). The cell viability of the HA-PCL scaffold was higher than the standard PCL group indicating that the HA-PCL scaffolds supported higher cell attachment than the standard PCL. The cell viability increased in all conditions over-time points for 28 days with no significant differences, indicating an increased cell proliferation whether in the standard PCL or HA-PCL scaffolds. The static-SM group was significantly higher than the rocking-SM group on the standard PCL scaffold ( $p < 0.05$ ). VEGF secretion (during a 48 hour collection period) normalized to viable cells increased over-time points for 28 days (Figure 5.11.5). The SM groups secreted dramatically higher VEGF than the SM+Dex100 groups, as in our previous experiments 5.7 and 5.8. However, there was no effect either of HA in the scaffold or rocking, confirming our previous rocking data. The %BV indicated that there was mineralized deposition in the standard PCL after 28 days (Figure 5.11.6 A). The rocking SM+Dex100 group had significantly higher %BV in the top region than the middle and bottom regions within the same group and compared with the other groups ( $p < 0.05$ ). The middle region of the rocking SM+Dex100 group

had significantly higher %BV than the SM both rocking and static groups, indicating that this group has most mineralized deposition in the top and middle levels. This difference can be visualised in the three-dimensional (3D) reconstruction micro-CT images (Figure 5.11.6 B-K). The top surface of the rocking SM+Dex100 group has more yellow area (mineral) than the other groups (Figure 5.11.6 D). A side view image of a transverse cut through the scaffold from the rocking SM+Dex100 group shows that the top region is more yellow area than the other layers (red arrow head, Figure 5.11.6 I) and the top layer of the static-SM+Dex100 group (red arrow head, Figure 5.11.6 K). There were no significant differences in %BV of HA-PCL scaffolds between groups (rocking SM, rocking SM+Dex100, static SM, and static SM+Dex100) or in distribution through the layers (top, middle, and bottom) (Figure 5.11.7 A). Surprisingly, the %BV of the rocking SM+Dex100 on the standard PCL scaffold was higher than the rocking SM+Dex100 on the HA-PCL scaffold. The total %BV of the HA-PCL group was higher than the standard PCL group in all conditions except the standard PCL scaffolds were higher than the HA-PCL scaffold in the rocking SM+Dex100 group, indicating that the HA-PCL can enhance mineral deposition of hESMPs (Figure 5.11.8). In addition OFF also enhance mineralized deposition on standard PCL under Dex containing medium.

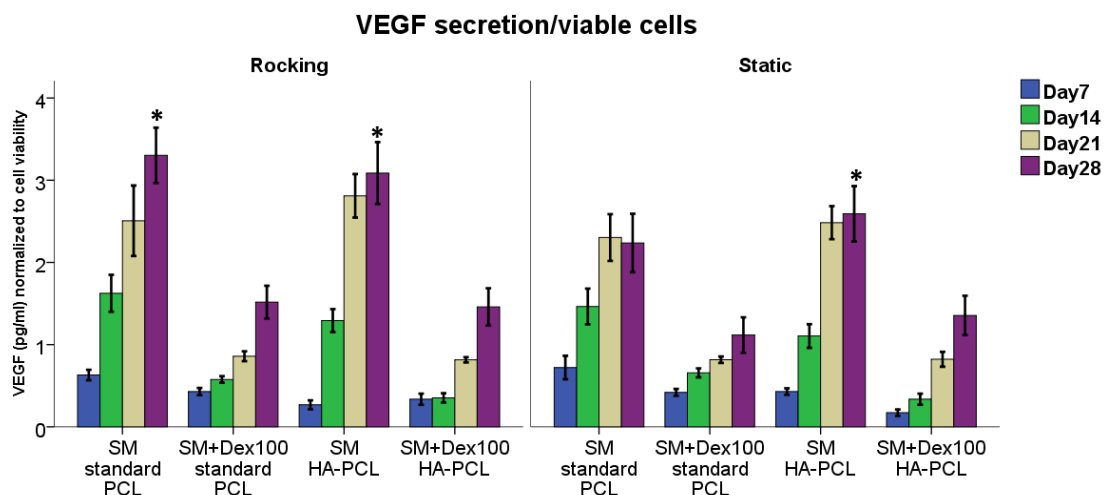
The SEM images of hESMPs seeded on the standard PCL scaffolds after 28 days showed that the cells were well adhered and spread on the surface and underneath of the scaffolds (Figure 5.11.9). The rocking SM+Dex100 group showed the more round particles on the ECM than the static SM+Dex100 group (Figure 5.11.9 C, E, respectively). These results indicate that the presence of OFF and Dex lead to enhance mineralized deposition confirming the previous results. The SEM images of HA-PCL also showed round particles on both ECM and fibres at all conditions, however, the rocking SM group showed fewer round particles than the others (Figure 5.11.10 B).



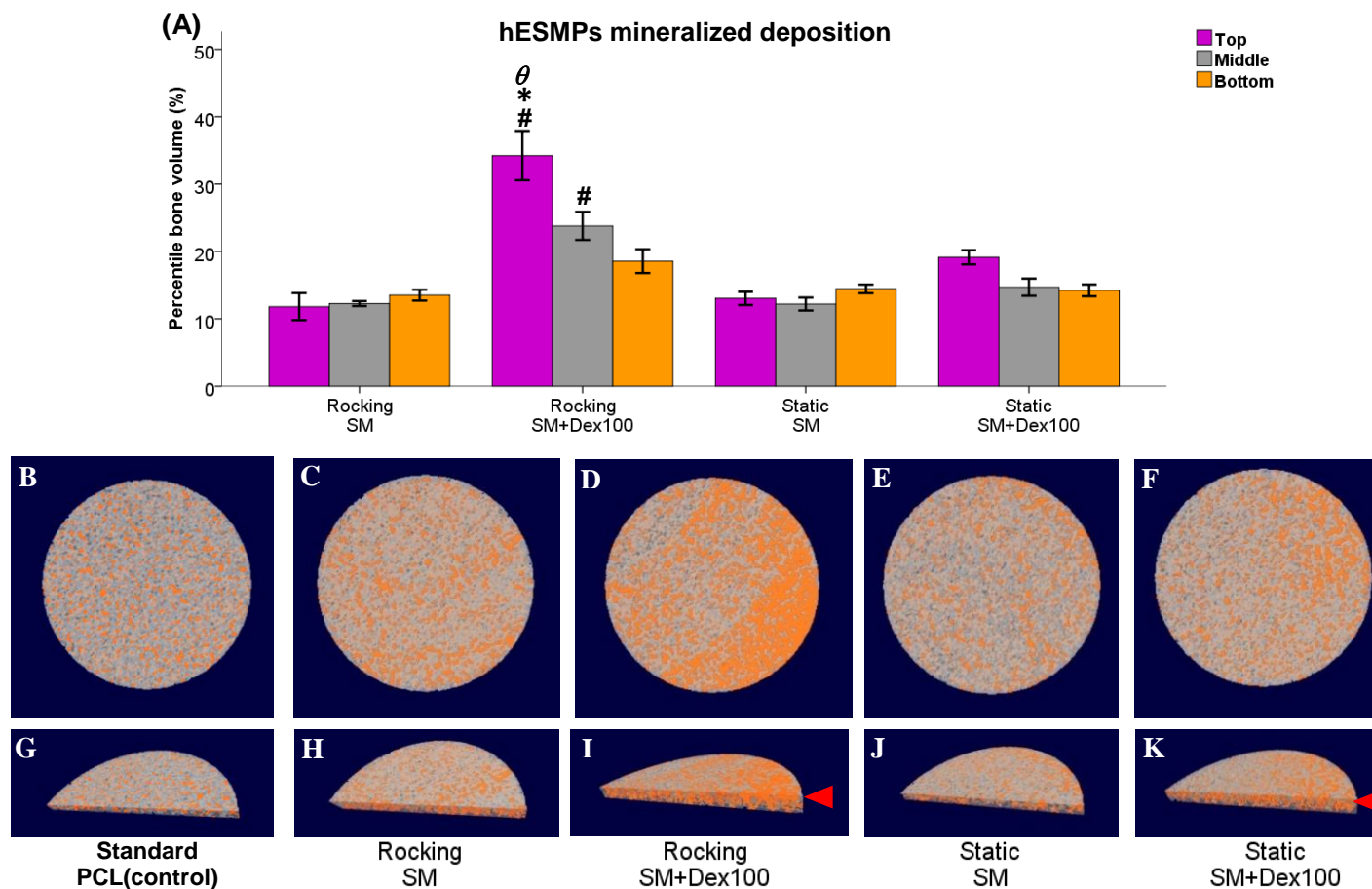
**Figure 5.11.3:** (A) The grey scale distribution showed the relationship between a grey scale index (GSI) and percentage of brightness area and (B) threshold range table of standard PCL, HA-PCL, and the rocking with SM+Dex100 group of hESMPs which showed calcium deposition on the scaffolds. The orange square from 30-70 GSI served to identify standard PCL scaffold. The purple square from 70-125 GSI served to identify calcium deposition and HA. (N=1, n=3)



**Figure 5.11.4:** (A) The effect of OFF with the hESMPS cultured on standard PCL and HA-PCL scaffolds assayed by using resazurin reduction test on day 1 to evaluate cell attachment. (B) To evaluate cell viability of the cells seeded on the scaffolds under the supplemented media (SM) and supplemented media with 100nM of Dex (SM+Dex100) were subjected to OFF after day 7, 14, 21, and 28. mean $\pm$ SE, (N=2, n=3), # =  $p < 0.05$  comparison between the rocking and static under the SM medium in the same scaffold, Two-way ANOVA, Tukey's multiple comparison tests).

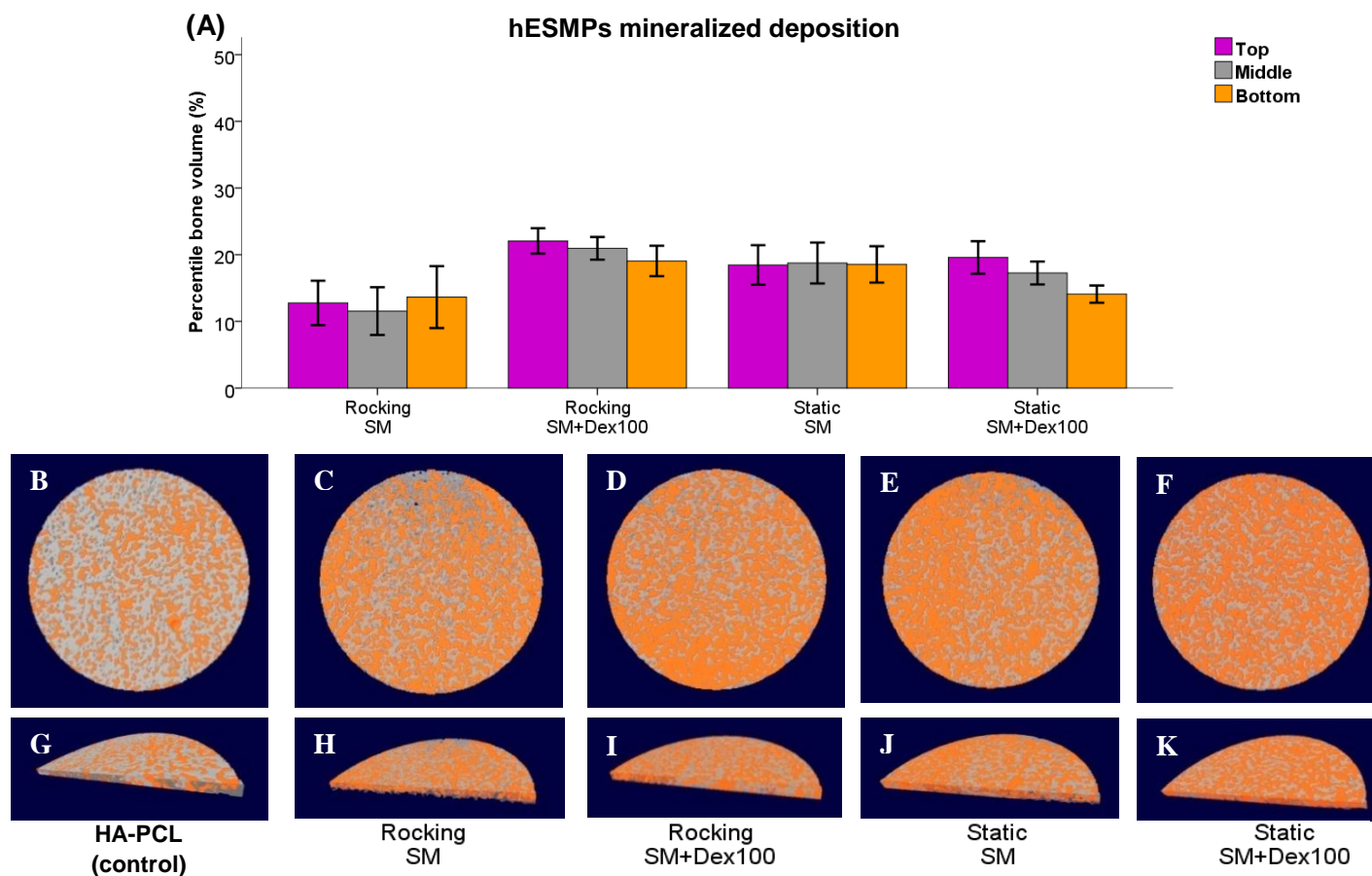


**Figure 5.11.5:** The effects of OFF with the hESMPs cultured on standard PCL and HA-PCL scaffolds under the SM and SM+Dex100 media by day 7, 14, 21, and 28. VEGF secretion (duration a 48 hour collection period) normalised to cell viability which measured using VEGF ELISA and resazurin reduction test, respectively. mean $\pm$ SE, (N=2, n=3), \* =  $p < 0.05$  comparison between SM and SM+Dex100 in the same condition and scaffold, Two-way ANOVA, Tukey's multiple comparison test.



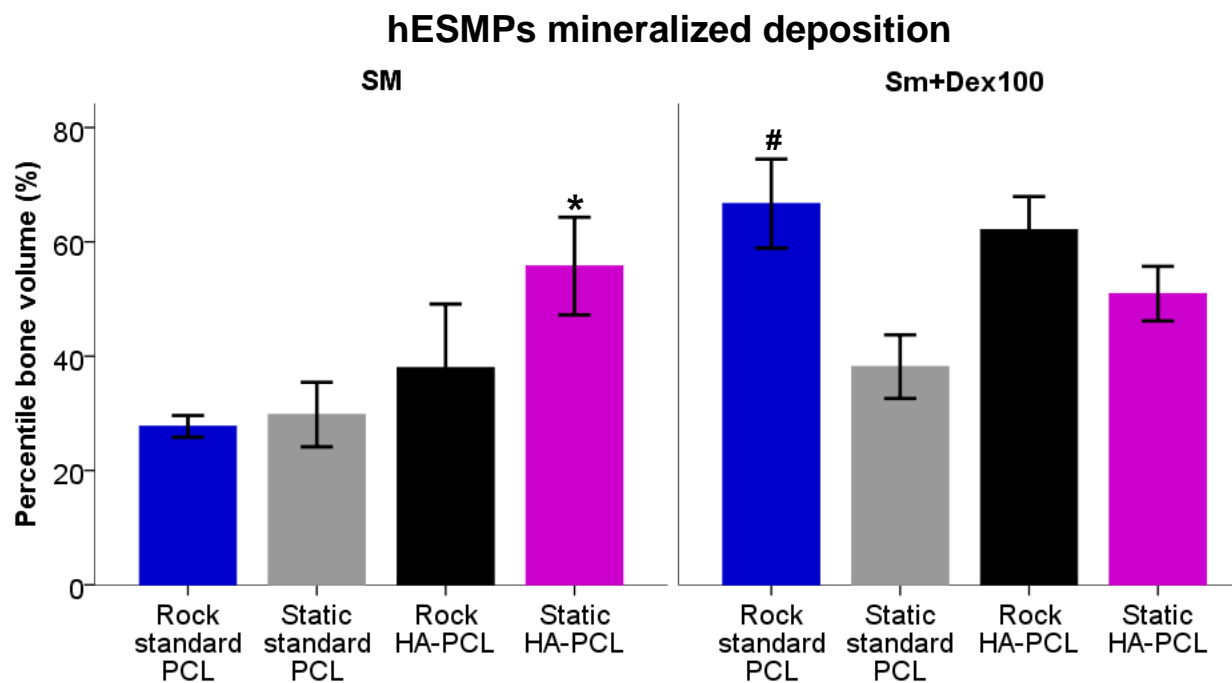
**Figure 5.11.6:** The effects of OFF on hESMPs cultured on standard PCL scaffolds under the osteogenic media (SM and SM+Dex100 media) after 28 days. (A) The %BV with subtraction of standard PCL scaffolds measured using micro-CT analyser. mean  $\pm$ SE, (N=2, n=3), # =  $p < 0.05$  comparison between SM and SM+Dex100 at the same level and condition, \* =  $p < 0.05$  the top level is higher than the other levels in the same group,  $\theta$  =  $p < 0.05$  comparison between the rocking and static conditions in the same level and medium, Two-way ANOVA, Tukey's multiple comparison test).

Microcomputed tomograph images of calcium deposition (orange area) in the scaffolds within the cylindrical region of interest. The upper row images show the top surface of the scaffolds (B-F) and lower row images showed the side view of half cut scaffolds (G-K). (I) The top level of the rocking-SM+Dex100 group contained more calcium than (K) the static-SMDex100 group (red arrow heads).

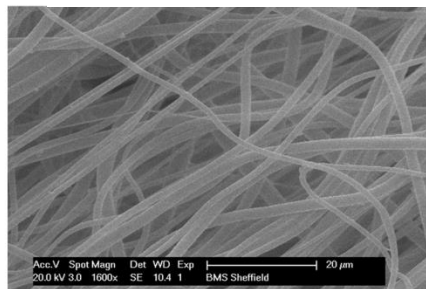
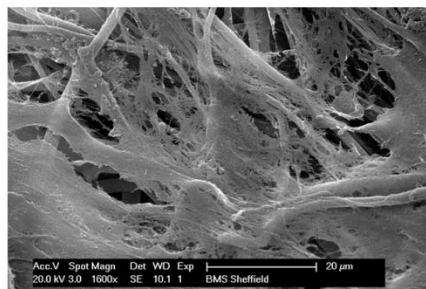
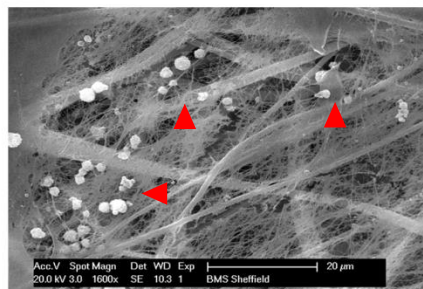
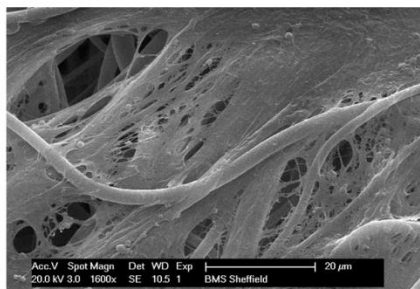
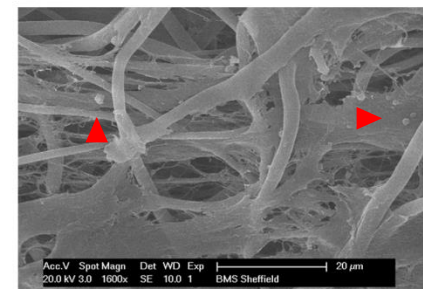


**Figure 5.11.7:** The effects of OFF on hESMPs cultured on HA-PCL scaffolds under osteogenic media (SM and SM+Dex100 media) after 28 days. (A) The %BV with subtraction of the nHA particles of the HA-PCL scaffolds measured using micro-CT analyser. mean  $\pm$ SE, (N=2, n=3),  $p < 0.05$ , Two-way ANOVA, Tukey's multiple comparison test.

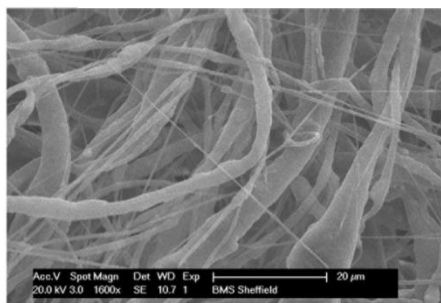
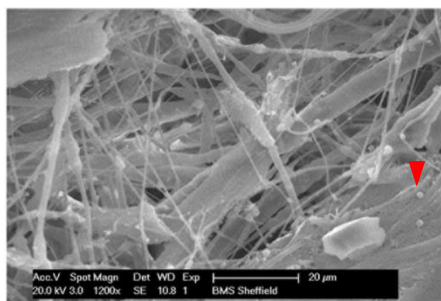
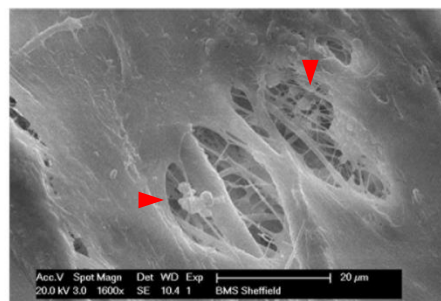
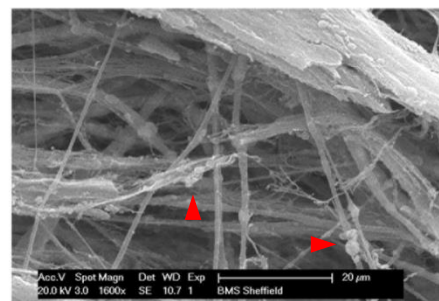
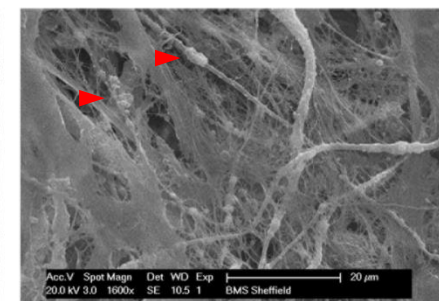
Microcomputed tomograph images of calcium deposition (orange area) in the scaffolds within the cylindrical region of interest. The upper row images show the top surface of the scaffolds (B-F) and lower row images showed the side view of half cut scaffolds (G-K).



**Figure 5.11.8:** The effects of OFF on hESMPs cultured on both standard PCL and HA-PCL scaffolds under the osteogenic media (SM and SM+Dex100 media) after 28 days. (A) The %BV of standard and HA-PCL scaffolds presented the mineralized deposition on the scaffolds using micro-CT analyser. mean  $\pm$  SE, (N=2, n=3), \* =  $p < 0.05$  comparison between the standard PCL and HA-PCL scaffolds in the same medium and conditions, # =  $p < 0.05$  comparison between rocking and static groups in the same medium and scaffold, Two-way ANOVA, Tukey's multiple comparison test.

**(A) Standard PCL (control)****(B) Rocking SM****(C) Rocking SM+Dex100****(D) Static SM****(E) Static SM+Dex100**

**Figure 5.11.9:** The SEM images of the hESMPs cultured on standard PCL scaffolds under the osteogenic media (SM and SM+Dex100 media) and subjected to OFF after 28 days. (C) The rocking group under the SM+Dex100 medium showed more white round particles (the red arrow heads) which indicated calcium nodules than the other groups. Scale bar = 20μm

**(A) HA-PCL (control)****(B) Rocking SM****(C) Rocking SM+Dex100****(D) Static SM****(E) Static SM+Dex100**

**Figure 5.11.10:** The SEM images of the hESMPs cultured on HA-PCL scaffolds under the osteogenic media (SM and SM+Dex100 media) and subjected to OFF after 28 days. The red arrow heads point to calcium depositions. Scale bar = 20 μm

**5.12 Discussion**

Bone tissue engineering aims to provide a biocompatible material capable of substituting autologous bone grafts for surgical reconstruction. The requirements of biodegradable polymer scaffolds are the mechanical strength and biological properties similar to native ECM for stimulating cell behaviour as a temporary ECM until regeneration occurs. The interaction from both the temporary ECM and the environment influence the cell behaviour by direct and indirect signalling.

The main aims of this study were to fabricate electrospun scaffolds for the bone part of a cleft palate reconstruction which would allow normal facial development. In order to do this first, I selected biodegradable polymer electrospun scaffolds were fabricated using FDA approved polymers such as PLA, PCL, and PHBV. Depending on the polymer type, the range of fibre diameter distribution was different. The results showed that both electrospun PLA and PCL micro fibre scaffolds were successfully fabricated with smooth fibre morphology without bead formation. PCL fibrous morphology was more uniform than for PLA scaffolds. In contrast, the PHBV electrospun scaffolds exhibited nano-fibres with a number of bead formations. These defects usually depend on the viscosity and surface tension of the polymer solution while spinning (Spasova et al., 2006). The bead formation is usually considered to be a defect in electrospun scaffolds. It decreases the ratio between surface area and volume of the scaffold, as a result, provides less surface for cell attachment and leads to reduce proliferation rate (Chen et al., 2007), indicating that a uniform fibre of electrospun scaffold is required for tissue engineering. We need a better understanding of this technique to improve fabrication in the PHBV scaffolds.

A limitation of this study is that in many cases only 2 experiments were performed in triplicate, however, some interesting differences were identified were found to be significant as follows. In these studies we used hESMPs as a cell model to detect cell

attachment and viability. Results of the cell seeded PCL and PLA groups showed good support for cell attachment, whereas, PHBV groups showed less cell attachment. This is in contrast to the good attachment of fibroblasts seen by my colleague (Bye et al., 2013). In the literature (Baek et al., 2012), PHBV was described as being supportive of the attachment of a mouse osteoblastic cell line but it has never been used for hESMPs. Discrepancy between this result and others may reflect the difficulty of handling PHBV. The cell viability in this experiment was detected while metal rings were placed on the samples, but these might limit the reaction between the resazurin salt solution and cells underneath the metal rings. The metal ring was removed for the cell viability method for subsequent experiments. The PHBV scaffold could be modified to increase cell attachment and proliferation to facilitate osteogenic differentiation. Firstly, the PHBV could overcome the bead formation which has a major effect on cell behaviour, for example adding methanol to increase permittivity of the polymer solution (Zuo et al., 2005). Moreover, various surface treatments could be used to modify the PHBV; 1] chemical modification: plasma polymerization or plasma spray, 2] coating materials: collagen, fibronectin and laminin (Cooke et al., 2008), 3] Incorporation of bioactive glass in to the scaffold (Levy et al., 2007) in order to enhance biocompatibility and osteogenic differentiation. However for my purposes, PCL and PLA were more likely candidate electrospun scaffolds so the PHBV was not continue working, and the ability of PCL and PLA scaffolds to support osteoprogenitor cells was investigated.

PLA and PCL scaffolds were selected to compare their ability to support osteogenesis of both groups of periosteal cells used in the previous chapter (see chapter 3 and 4) with the SM and SM+Dex10 media. PCL and PLA fibrous scaffolds were not significantly different in their ability to support HJPs and facilitate osteogenic differentiation. This is in contrast to a previous study in rat bone marrow cells, which found that the cell attachment and cell proliferation on PLA was higher than on PCL scaffolds (Conconi et al., 2009). PLA is an aliphatic polyester similar to PCL, however PLA has a different

chemical structure in the same molecular formula (isomer) (P-D-LA, P-L-LA, and P-DL-LA) and this lead to their different properties such as biodegradation and melting points. Although, PLA showed greater biocompatibility in other studies (Teresa et al., 2009), there are concerns about the effect of their degradation products in vivo, lactic acid, and they collapse and are difficult to handle when they are wet (Bye et al., 2013). This may affect cell growth when PLA scaffolds are used in long-term devices and cause difficulties for the surgeon when placing such a scaffold in the body. Whereas PCL has only one chemical structure, it may be less variable in material properties. From the fabrication point of view, PCL is a more straightforward polymer to blend with a wide range of bioactive materials due to its low melting temperature. The use of PCL scaffolds has been increases in tissue engineering research over last decade and they are clinically used in suture materials (Monocryl<sup>®</sup>, Ethicon, UK) and drug delivery devices under FDA approval (Cipitria et al., 2011). Therefore PCL was chosen to support human osteoprogenitor cells for cell proliferation and differentiation to osteoblast-like cells in the remaining experiments. HJPs are the good cell sources for future study, unfortunately, we lacked cell supply for further experiments. Schmelzeisen et al.,(2003), Schimming and Schmelzeisen, (2004) two clinical studies found HJPs could produce bone on the 3D scaffolds as a combination polymer of polyglactin and poly-p-dioxanone (Ethisorb, Ethicon, Germany) for maxillary augmentation and dental implant replacement afterward in majority of cases. Additionally, Ryu et al., (2011) *in vitro* study showed HJPs could mineralized on collagen scaffolds. Their studies showed results consistent with our study is that HJPs required 10nM of Dex for mineralization. It was confirmed that hESMPs, hBMSCs, and HJPs show similar results on both monolayer and 3D cultures is that they required Dex for osteogenic differentiation. Therefore, hESMPs and hBMSCs were used as model osteogenic cells.

PCL electrospun scaffolds were chosen for this study to evaluate cell supporting and osteogenic differentiation on hESMPs in long term culture for 28 days. Micro-fibrous PCL

scaffolds can mimic the architecture of ECM to enhanced cellular adhesion, proliferation and migration (Reed et al., 2009). This study presented that PCL scaffolds can support proliferation and osteogenic differentiation of hESMPs which is similar to the results of my colleague (Delaine-Smith, 2013). Calcium staining in the PCL scaffolds increased overtime at days 21 and 28. Calcium deposition of the SM+Dex100 group was higher than in the SM groups on the PCL scaffolds. Collagen staining in the SM+Dex100 groups was not difference compared to the SM groups. Therefore Dex was also required to stimulate osteoblastic differentiation in 3D culture.

To the best of our knowledge, no study has used a standard see-saw rocker as a method for mechanically stimulating cell culture on electrospun scaffolds. Having measured positive effects of the standard see-saw rocker induced OFF on cells in monolayer (Delaine-Smith et al., 2012). This technique was decided to investigate that could also be a way to further stimulate the osteogenic differentiation of the cells on a 3D scaffold. Our study showed that the effect of OFF from a standard see-saw rocker applied to both hESMPs and hBMSCs (3 donors) on porous PCL scaffolds (3D culture) under the presence of Dex supplemented media caused greater calcium deposition compared to the static cultures. The results presented here suggest that the combination of OFF and Dex during culture synergistically stimulates the osteogenic differentiation of both hESMPs and hBMSCs on PCL scaffolds. The OFF may benefit nutrients and oxygen transportation to cells in the scaffolds compared to the static culture (McCoy and O'Brien, 2010). For electrospun PCL scaffolds in our study are thin (about 300  $\mu\text{m}$  thickness) compared to typical porous scaffold (about 5 mm thickness) (Sittichokechaiwut et al., 2010) therefore a nutrient diffusion should be less of an issue. But cells should be 150  $\mu\text{m}$  from the nutrient source therefore cells in the centre would still have limited diffusion, especially as matrix forms and fills up the pores in longer term static cultures. In addition the OFF may enhance osteogenic marker expression such as OCN, OPN and mineral deposition by mechanotransduction (see chapter 1).

Regardless of the mechanism by which osteogenesis is stimulated it is clear that the use of osteoprogenitor cells seeded on the electrospun PCL scaffolds can produce a bone matrix structure. The 3D cultured results were parallel to the monolayer culture results (see chapter 4) which showed the rocking group under Dex supplemented medium had highest calcium deposition.

PCL was show to be a promising material for bone tissue engineering, however, the disadvantages of PCL are not only hydrophobic properties but also no osteoinductive potentials. It is well known that a bioactive properties of HA can enhance cell attachment, cell proliferation, and osteogenic differentiation (Li et al., 2007, Li et al., 2009). A hypothesis of this study is that incorporating HA into electrospun scaffold could enables accelerated osteogenesis compared to a polymer scaffold alone. Moreover, HA has been shown to improve compressive mechanical properties in other scaffolds (Chim et al., 2006). nHA incorporated with PCL scaffold (HA-PCL) was created to overcome the limitations of the standard electrospun PCL scaffolds for bone tissue engineering. The result of this study showed that the nHA incorporated with PCL using electrospinning technique was the best technique to create a composite HA-PCL scaffold with the best biocompatibility and to the ability to support osteogenic differentiation, compared to the etching or alternate soaking techniques. The electrospun HA-PCL showed reducing tensile mechanical properties with increasing percentage of HA. This result is consistent with some other studies, which have reported the reduction of tensile mechanical properties in the composite electrospun HA-PCL may reflect from the amount of HA loading, bad dispersion of nHA may cause insufficient interphasic mechanical interlock between the nHA and PCL (Zhang et al., 2010, Deb et al., 1996). Frohbergh et al., (2012) reported that the mechanical strength was not reduced if nHA is dispersed on or near the surface on the fibres. Therefore the alternate soaking technique was included in this study because it had previously been shown to improve the mechanical property of materials by coating on the surface of fibres (Jaiswal et al., 2012). In contrast, our

studies showed that this technique reduced their biocompatibility. The possible reasons for this could be an impurity of chemical components or a too high concentration of calcium phosphate particles on the processed scaffold.

XPS and XRD showed that other components excluding calcium and phosphate such as Boron, Silicon, and sulphur may form from the alternate soaking solution. In addition the XRD result showed that the alternate soaking process formed brushite (DCPD) on the fibre surfaces. Brushite was a more soluble than the nHA, therefore concentration of free calcium and phosphate ions in culture media may change and influence the cellular behaviour by reducing cell viability and osteogenic differentiation (Klammert et al., 2009). The etching technique used an aqueous hydroxide (0.1 M of NaOH) to improve the adhesive strength between the PCL and nHA by hydrolysing ester bond (R-COOR) of standard PCL to produce carboxylate group (R-COO<sup>-</sup>) on the surface, R referring to the rest of the molecule (Choong et al., 2012). The carboxylate group attracts calcium ions of the nHA and anchors them on the fibre surface (Oyane et al., 2005). Although this technique worked to a certain extent cell viability and osteogenic differentiation were not as good as with the electrospinning technique which showed a higher biocompatibility and allowed cells to undergo osteogenic differentiation under Dex supplementation media.

Having established that electrospinning was the best method of incorporating HA into the electrospun scaffold further work was undertaken to select the best concentration of HA for cell growth and differentiation. Different concentrations of HA-PCL solutions were spun using the same parameters as the PCL solution. HA-PCL electrospun scaffolds were successfully fabricated with no bead formation on the fibres. The average fibre diameter increased with increasing in the percentage of HA. The increasing percentage of HA can lead to higher concentration of solution and can restrict movement in the jet extruded from the metal needle and make it more difficult to eject the polymer solution. Although the nHA has no effect on the electrical

conductivity of the solution (Zargarian and Haddadi-Asl, 2010, Fridrikh et al., 2003). Fibre diameter distributions were more spread with increasing percentage of HA according to the unstable phase (whipping movement) of the polymer jet. The resulting mixture of nano and micro sized fibres is more similar to the natural ECM and may provide a more suitable environment for cell adhesion, proliferation, migration and differentiation (Borjigin et al., 2012, Vasita and Katti, 2006). However increasing the concentration of HA in HA-PCL scaffolds lead to lower Young's modulus (stiffness) and yield strength. It would be implied that the standard PCL electrospun scaffold has more stiffness and rigidity than the HA-PCL and the lowest mechanical property was the 5%HA-PCL. The high amount of HA can decrease a tensile property of the bio-composite material attribute to disrupt the stable of polymer formation and the intermediate adhesion between nHA and polymer was a very weak (Yang et al., 2008, Zhang et al., 2010). In addition, this may because of incomplete nHA dispersion along the fibres leading to tension distribution (Zargarian and Haddadi-Asl, 2010). Interestingly we have contrasting results in our group, where my colleague found that the composite electrospun PU either  $\mu$ HA or nHA scaffold improved tensile mechanical properties, Young's modulus and yield strength, compared to standard electrospun PU scaffold, this work is submission for publication (Tetteh et al., 2014). This indicates that the effect of HA can vary in different types of polymer, for instance PU is a much more elastic polymer than PCL. Moreover, their porosity and fibre size will also affect the scaffold mechanical properties and these were quite different for PU versus PCL. Ultimately for cleft palate repair we do not yet know what the ideal mechanical property would be. It would be the combination between flexibility, hand able and strength which extendable and does not break. Therefore, it may not necessary be the one with the highest Young's modulus and yield strength.

Estimating the porosity of the scaffolds by using micro-CT has many advantages. It is a non-destructive method requiring minimal sample preparation. The 3D morphology of

the scaffold can be visualized (Tuan and Hutmacher, 2005) enabling examination of the internal part of the scaffold. We compared the porosity measurements of standard PCL scaffold between gravitational porosity method (conventional method, see experiment 5.2) and using micro-CT. Both methods showed a similar porosity for the standard PCL scaffolds. The results showed that there were no differences in the porosity percentage from those methods, about 86%. Our results showed that the increase in HA concentration created less porous scaffolds. The nano-sized fibres accommodated in between the micro fibrous pore spaces lead to a decreased porosity of the scaffold. The high porosity is also crucial factor to enhance cells to migrate, attach, and access of cell culture media and removal of waste (Karageorgiou and Kaplan, 2005, Miao et al., 2008). The results of PAS-FTIR and XRD techniques confirmed the presence of nHA on the HA-PCL surface. The XRD technique detected HA on the fibre surface indicating that the nHA was exposed and had access to serum proteins and cells. None of the HA-PCL scaffolds had any new peaks compared to the standard PCL scaffold and nHA, indicating that there were no chemical interactions between the materials. The increase in intensities for the HA peak corresponded to the HA concentration in the scaffold. hESMPs were used for evaluating the suitable concentration of HA in the PCL scaffolds as model cell to evaluate cell attachment, cell viability, and osteogenic differentiation. There were no differences in cells attachment and cell viability which indicated similar cell proliferations between the various percentages of HA after day 1 and 14, respectively. Our results are similar to Kim et al, (2006b) who found that the MG63 (human osteosarcoma cell line) cultured on 12.5wt% HA in the PLA electrospun scaffolds improved cell attachment after day 1 however, the cell viabilities of the HA-PLA group was no different compared to the standard PLA fibre after day 28. ALP activity is an early marker to evaluate the bone forming potential of the cells. Our study showed that the cells with the highest ALP activity were 5wt % HA-PCL whereas the least ALP activity was 10wt%HA-PCL under osteogenic medium. Calcium and phosphate ions can be released from the HA-PCL which are important factors for

promoting osteogenic differentiation activity by stimulating osteogenic marker genes; such as ALP, collagen type 1, and OCN (Lin et al., 2009, Klammert et al., 2009). The possible pathway of HA's ability to stimulate osteogenic differentiation is to activate the c-jun and c-fos genes that lead to increased ALP gene expression at the early stage osteogenic differentiation (Lin et al., 2009). Maeno et al.,(2005) and Lin et al., (2009) reported that an excessive calcium and phosphate ions in the culture medium (more than 10mM of calcium) could be detrimental as they could lead to cell cytotoxicity. However, our study did not show any reduction of cell viability, although there was lower ALP in the high percentage of HA-PCL. The level of ALP activity can peak at matrix maturation, following by reducing of the activity in the mineralization period (Lian and Stein, 1995, Stein et al., 2004). Therefore the lower expression of ALP activity does not definitely lead to less differentiation of cells, it can because of the time-point of the collection of the sample. Considering the viability and osteogenic differentiation on the 5%wt HA-PCL may be useful to future experiments, regardless of its lower strength.

To our knowledge this is the first study to investigate whether there are any synergistic effects between the effects of incorporate nHA with PCL electrospun scaffold and those of mechanical stimulation on osteogenesis. This *in vitro* study evaluated the osteoinductive potential of the HA-PCL on the proliferation and differentiation of hESMPs seeded on HA-PCL scaffolds and subjected them to OFF using a standard see-saw rocker. The ultimate outcome of osteogenic differentiation is evaluated by the mineral deposition in the scaffolds which were scanned and analysed using micro-CT. The micro-CT has a benefit as a tool for real-time monitoring for tissue engineering as it is a non-destructive imaging technique to evaluate quantitative mineralization in the scaffolds is the %BV (Cartmell et al., 2004, Barbetta et al., 2012, Thimm et al., 2013). In addition it has been using widely in biomaterials for analysis of animal models because there is no need to biopsy the bone tissue for evaluation. The characterizations

of mineral deposition on electrospun scaffold using micro-CT have not been reported in many studies. The threshold for quantitative micro-CT analysis of bone usually used is the global threshold or automate global threshold such as Otsu's method (1979). However, this method has disadvantages as small amount of mineralized deposition would not be detected (Parkinson et al., 2008, Hahn et al., 1992). Individual threshold determinations were used in this study. The percentage porosity of the HA-PCL was less than the standard PCL (73.21 and 86.79%, respectively), indicating that the cells were more aggregated in the HA-PCL but this had no impact on cell proliferation. The presences of Dex have more effect on the mineral deposition on the standard PCL scaffold. The rocking SM+Dex100 group in the standard PCL scaffolds had the highest percentage of mineral deposition at the top level of the scaffolds than the middle and bottom levels. The reasons for this result were probably a greater cell density at the top of the scaffold, nutrient and oxygen transportation, waste removal, and an effective of OFF magnitude. The cells were seeded on the top of the scaffolds, as a result, more cells may adhere at the top of the scaffolds. Higher cell density can enhance osteogenic differentiation of human osteoprogenitor cells on the 3D culture by increasing ECM synthesis and cell-cell communication (Wang et al., 2010, Xue et al., 2013). Gap junction (cell-cell communication) plays a critical role in extracellular matrix in bone tissue engineering. Schiller et al., (2001) reported that the gap junctions stimulated OPN which promoted ECM mineralization.

In 3D culture, the shear stress may more strongly affect on the top level of the scaffold because the strength of flow will gradually decrease with scaffold depth assuming the scaffold is firmly attached to the well base. The calculations of shear stressed in a 6-well plate may not be very relevant when considering an electrospun scaffold because the fibres and pores will redirect the flow. One would need a computational model of fluid flow through a porous medium to calculate what the shear stress is on the walls of the electrospun fibres, such as those used for other types of porous scaffolds (Sandino and

Lacroix, 2011, Birmingham et al., 2013). Fluid flow has been shown to increase osteogenic differentiation and mineralization in osteoprogenitor cells cultured in the 3D scaffolds (Sikavitsas et al., 2003, Yeatts et al., 2012). Yeatts et al., (2012) studied the effect of fluid flow shear stress on hBMSCs cultured on alginate bead 3D constructs and reported that fluid flow up-regulated OPN expression compared to static culture.

In this study they appears to be a synergistic relationship between OFF and cell density which causes improved mineral deposition, especially at the top level of scaffold. It is interesting to note that in the middle level of the standard PCL the rocking with Dex group deposited higher mineral than both the rocking without Dex and the static with Dex groups, this implies that the rocking improved distribution of Dex to the middle level of the scaffold compared to static culture, where there was a surprisingly small effect of Dex.

Our results show that the HA-PCL scaffolds show a greater cell attachment than the standard PCL scaffolds. nHA particle on fibre surfaces have been show to absorb more serum proteins such as fibronectin and vitronectin than standard scaffolds leading to increase cell attachment and differentiation of hESMPs (Li et al., 2009, Sawyer et al., 2005). The mineralization of hESMPs on HA-PCL in our study showed no differences in the each level (top, middle, and bottom), indicating that the cells distributed throughout the HA-PCL scaffold. Incorporation nHA into PCL can enable it to be more hydrophilic, resulting in cells with a better distribution even they though less porous than the standard PCL (Choong et al., 2012, Oyane et al., 2005). In addition, the HA-PCL scaffold also showed relatively stronger ALP activity than the standard PCL scaffold (experiment 5.10). Total mineral deposition in all levels within the HA-PCL scaffolds were higher than the standard PCL scaffolds, regardless culture media conditions (supplemented and supplemented media contained with Dex). This result agrees with many studies that reported that the HA releases calcium and phosphate ions into culture medium which there were the essential sources for mineralization (Chang et

al., 2000b, Ma et al., 2005). The rocking group cultured in the SM+Dex100 on both the standard PCL and HA-PCL scaffolds were not different. They may have reached their limitation for mineral deposition according to their pore space, accessibility of nutrient and waste. The lower porosity of the HA-PCL than the standard PCL scaffold may manipulate cells to aggregate, resulting in enhancement of osteogenic differentiation (Karageorgiou and Kaplan, 2005). There were no differences in mineralization between rocking and static groups. The rocking group under SM medium was lower mineralization than the static group, it may be because the nHA came out from the HA-PCL scaffold after rocking. To address this comparison of the HA-PCL scaffold before and after rocking could be measured. The effect of nHA on the tensile mechanical properties of fibres decreased in their stiffness and rigidity, however, the HA-PCL could enhance mineralization compared to the standard PCL scaffolds. A limitation of this study is that only two experimental repeats were performed. It is not quite clear that nHA have relevant effect or not. More repeats would have answered the question whether mineralization was influenced by OFF.

Vasculogenesis is an important factor for bone repair by providing nutrients and excreting waste. VEGF secretion has been measured to evaluate the effect of incorporating HA into electrospun PCL scaffold (HA-PCL) and mechanical stimuli on undergoing. Our results showed that VEGF secretion decreased in the all Dex contained media, and there were no effects of OFF or HA-PCL. This is the same results as the experiments 5.7 and 5.8 of hESMPs and hBMSCs, respectively which showed that the OFF had no effect on VEGF secretion. Moreover, this result was as similar as the applied OFF on monolayer cultures (see chapter 4). However in the VEGF secretion of hESMPs under SM+Dex10 group increased to the same amount as the SM group on the late state of cell culture. Dex may be a crucial factor to reduce the VEGF secretion (see chapter 4). The further work could establish a concentration of Dex suitable for both mineral deposition and VEGF secretion.

### 5.13 Conclusion

The main objective of this chapter is to evaluate suitable scaffold materials to repair the bone part of cleft palate and allow normal facial development. This objective was completed in that it was demonstrated that PCL could be a suitable material as it showed good biocompatibility and allowed osteogenic differentiation of osteogenic progenitor cells. The large volume of media of cell seeding method was shown to be suitable for future work. The next objective was to find a method of increasing osteogenic differentiation of osteoprogenitor cells on scaffold. This objective was a success in that OFF induced by a standard see-saw rocker could increase the mineralization of the cells on scaffolds and that fabricating the nHA incorporated with scaffold. 5%wt nHA-PCL electrospun scaffold was a suitable technique to investigate whether it is worthwhile to incorporate HA into a bone tissue engineering PCL scaffold. However, our study showed that there was no synergistic effect of OFF and HA incorporating into PCL scaffolds on mineralized matrix deposition. In addition, we have evaluated the cellular mineralization of scaffolds by using micro-CT to localize the effect of OFF either on standard PCL and HA-PCL. The top level of the standard PCL scaffolds showed the greatest response to OFF. HA-PCL increased matrix mineralization on the static group under both SM and SM+Dex100 media.

Total mineral deposition of hESMPs within the HA-PCL was improved compared to the standard PCL regardless at mechanical stimulation.

### 5.14 Summary

- Electrospun PCL scaffolds are suitable for bone tissue engineering.
- HJPs and hBMSCs are a good cell source for bone matrix production in electrospun scaffolds, hESMPs behave similarly to hBMSCs in electrospun scaffolds and are therefore a useful model cell with which to study the system.

- Both hESMPs and hBMSCs on PCL scaffolds are responsive to OFF by significantly increasing mineralization.
- 5wt% nHA incorporated with PCL scaffolds by using electrospun technique enhanced ALP activity of hESMPs under osteogenic medium although it did not affect mineralised matrix deposition.
- Micro-CT is a minimally invasive technique to detect and locate cellular mineralization without any sample preparation.
- The top level of the standard PCL scaffolds showed the greatest respond to OFF for enhancing the cellular mineralization of hESMPs.
- Cells in HA-PCL scaffolds deposited more mineralised matrix over 28 days compared to standard PCL scaffolds however they did not exhibit any detectable increase in mineralisation in response to fluid flow.
- The VEGF secretion of both hESMPs and hBMSCs were inhibited by Dex. Neither OFF or HA incorporation into PCL scaffolds had an effect on VEGF secretion.
- The use of osteoprogenitor cells seeded on the electrospun PCL scaffolds can produce a bone matrix structure which can be implanted to the cleft palate bone defect.

### 5.15. Future work

- Future work could further evaluate osteogenic differentiation of the cells on HA-PCL scaffolds by detecting osteogenic gene expression.
- Different concentrations of HA-PCL could be produced to evaluate the suitable HA-PCL electrospun scaffold for improving osteogenic differentiation such as 2.5 or 7.5 wt% HA-PCL.
- To determine the increasing mineralization related from OFF or the number of cells on the top level of scaffolds. The cell distribution should be determined throughout scaffolds in the both standard PCL and HA-PCL.

## CHAPTER FIVE

- To compare the effect of OFF on mineralization of cells present on the external and internal surfaces of the scaffold.
- To develop a bioreactor to provide mechanical stimulation at 37°C, 5%CO<sub>2</sub> rather than room temperature, 0.04% CO<sub>2</sub>.
- To evaluate the suitable Dex concentration for enhance osteogenic stimulation and VEGF secretion on osteoprogenitor cells.
- To use computer models of fluid flow to estimate the shear stress applied on different regimes of the scaffold under flow conditions.

**CHAPTER SIX: A TRI-LAYER POLYCAPROLACTONE MEMBRANE FOR CO-CULTURE OF FIBROBLASTS AND OSTEOGENIC PRECURSORS FOR CLEFT PALATE REPAIR.****6.1. Introduction**

The most common complication following palatal closure is a severe inhibition of mid-face growth due to scar tissue formation at the palatal and alveolar regions (Smahel et al., 2009, Payne et al., 2014, Ross, 1987a). Many in the maxillofacial reconstruction field have stated that an alternative cell source for bone augmentation should be investigated further to improve cleft palate repair (Lohberger et al., 2013, Bueno et al., 2009). Tissue engineering (cells combined with a supportive biomaterial scaffold) may be a suitable treatment for cleft palate repair. MSCs have been used for bone regenerative medicine due to their ability to differentiate into either osteoblasts, osteocytes, or adipocytes under specific culture media, and have shown satisfactory clinical outcomes (George et al., 2006, Hibi et al., 2006, Behnia et al., 2009). Recently, tissue engineering strategies using the patient's own MSCs as the cell source showed much promise for repairing a cleft defect on the alveolar ridge region; resulting in a successful repair and support of tooth eruption in the 2 following years (Hibi et al., 2006). A suitable graft for cleft palate repair should separate the oral and nasal cavities, and allow normal facial development by supporting the bone growth and preventing the soft tissue intrusion into the bone formation site.

PCL electrospun scaffolds are biocompatible, porous, biodegradable and have suitable mechanical properties to support both soft tissue and bone growth (Hutmacher et al., 2001, Reed et al., 2009, Delaine-Smith et al., 2014a) as demonstrated in chapter 5. My colleague recently developed a method of spinning tri-layer scaffolds in which two micro-fibre layers were separated by a nano-fibre layer (Bye et al., 2013) The tri-layer

electrospun scaffold could support two different cell types and maintain their separation over 11 days of culture.

The objective of this study was to test a facile one-step process to create a single-polymer tri-layer electrospun scaffold and to investigate whether it can support cell attachment, proliferation and differentiation. The aim is to maintain separation between the bone and soft-tissue layers of a multi-tissue scaffold for cleft palate repair. Therefore, we addressed the question of whether the scaffold can support bone matrix formation and separate two different cell types; human osteoprogenitor cells and HDFs.

### **6.2. Methods**

#### **6.2.1. Micro/nano-fibre PCL tri-layer scaffold fabrication**

A PCL micro-fibre solution with a concentration of 10% w/w was prepared by dissolving PCL Mn=80,000 in DCM. A PCL nano-fibre solution with a concentration of 5% w/w was prepared by dissolving PCL in a mixture of methanol and DCM in the weight ratio of 10/90 (methanol/DCM). Both solutions were stirred for a minimum of 24 hours at room temperature.

Scaffolds were fabricated using an electrospinning rig as previously described in chapter 2 (Bye et al., 2013, Delaine-Smith et al., 2014a). The fabrication was performed by my colleague Frazer Bye as part of his PhD project, briefly; a tri-layer of PCL micro-fibres was fabricated at 17kV, with a flow rate of 40 $\mu$ L/min, a working distance of 17cm, and a drum rotation speed of 300 rpm at room temperature. The syringe pumps were located on the left and right and left sides, of the collector. Voltage was applied independently to each syringe pumps. The electrospinning parameters were as for the micro-fibre scaffolds (above) except that for the nano-fibre fabrication the working distance was 10 cm. 2mls of micro-fibre solution per needle was used to create the first layer. Then 1ml of nano-fibre solution per needle was dispensed while the 1ml of

micro-fibre solution was continuously spun to create the second layer. This was followed by 2ml per needle of micro-fibre solution only to create the third layer.

On receiving the tri-layer scaffolds were characterised it by using SEM to determine the size distribution and fibre diameter by measuring over 100 randomly selected fibres from 4 recorded SEM micrographs in each layer (width 200µm each layer) using image analysis software (ImageJ) (see chapter 5). To investigate the cell deposited matrix and mineralization, scaffolds were collected on day 7 and 28 of HDFs and hESMPs culture, respectively and were dehydrated in a series of alcohols (see chapter 2).

### **6.2.2. Cell seeding on micro-fibre PCL scaffolds.**

Scaffolds were cut and sterilised with 0.1% peracetic acid in PBS for 3 hours then washed three times with PBS. The scaffolds were submerged overnight in the basal culture medium for serum protein coating. Before cell seeding, the cell culture media was removed. The cells were detached using Trypsin-EDTA.  $10^5$  cells of HDFs in a 100µl of media were seeded onto the scaffolds and left to attach for 24 hours in an incubator. The next day, the scaffolds were moved to fresh well plates. HDF cells were cultured either in DMEM basal culture medium or basal culture medium supplemented with 50µg/mL AA. The cell viability and collagen production tests used were MTS assay and picro-sirius red staining after 14 and 21 days of cultures.

### **6.2.3. Cell seeding, proliferation on tri-layer electrospun PCL scaffold.**

Three different cell types were used in the present study: 1] hESMPs, 2] hBMSCs, and 3] HDFs. The scaffolds were cut into 15mm diameter circles using a cork borer. The scaffolds and CellCrown™ culture inserts were sterilised with 0.1% peracetic acid in PBS under steady rocking. Scaffolds were placed within the CellCrown™ assembly and submerged overnight in the basal culture media. Before cell seeding, the cell culture media were removed.  $10^5$  cells in a small volume suspension (no more than 100µl) were seeded on top of the scaffold within the inner diameter of CellCrown™ and left for 24

hours for cell attachment in a cell culture incubator. The next day, the scaffolds attached to CellCrown™ inserts were removed to fresh well plates. hESMPs or hBMSCs were seeded on one side of the tri-layer scaffolds and grown in either SM+Dex100 or SM+Dex10 media, respectively from day 1 to 21. The HDFs were stained with CellTracker™ by adding 10µM CellTracker™Green (in media without serum) to HDFs cultured in T-75 flasks for 45 minutes, followed by removal of the CellTracker™Green solution, then washed twice with PBS. The cells were incubated for 30 minutes further under fresh basal medium. Trypsin-EDTA was added to the flasks, which were centrifuged at 1000 rpm to collect the cell pellet.  $10^5$  of labelled cells were seeded on the opposite side of the CellCrown™ to the hESMPs or hBMSCs and the entire construct was cultured in SM medium for a further 7 days.

#### **6.2.4. XO fluorescent staining for assessment of osteogenesis**

XO ( $C_{31}H_{28}N_2O_{13}SNa_4$ ) was added into culture medium in a 1:1000 dilution at a final concentration of 20µM, and incubated for at least 12 hours before imaging (Kuhn et al., 2010). The XO solution was removed and washed with PBS twice and replaced with fresh medium without β-GP to reduce fluorescence background from unbound XO. The location of mineralised tissue (containing osteogenic progenitor cells) and HDFs co-cultured on the tri-layer scaffolds was analysed using confocal laser scanning microscopy (CLSM). (see chapter 2)

#### **6.2.5. Sample preparation for CLSM**

The scaffolds were gently rinsed with PBS solution to remove non-attached dyes and cells until no more colour eluted into the PBS solution. After the rinsing step, the scaffolds were detached from the CellCrown™ insert and cut to a thickness of 0.5 mm by using a sharp sterilised surgical scalpel. The scaffolds were viewed with CLSM and not covered with a coverslip to avoid possible damage of the cells on the side view of the scaffolds. Consequently, the CLSM consisted of a EC plan-Neofluar objective with magnification 20x. An Argon/2 laser with wavelength 488 nm and HeNe laser with

wavelength 543 nm were used to visualize XO and CellTracker™Green staining respectively. The obtained digital images were merged into 515 KB RGB (red-green-blue) images using Zeiss LSM Image Browser software package and the images were overlaid using the ImageJ.

### 6.3. Results

The cell viability of HDFs increased between days 14 to 21 in media supplemented with AA (basal+AA) (Figure 6.3.1 A). Total collagen production in the basal+AA group was similar to that in media without AA after 14 and 21 days (Figure 6.3.1 B).

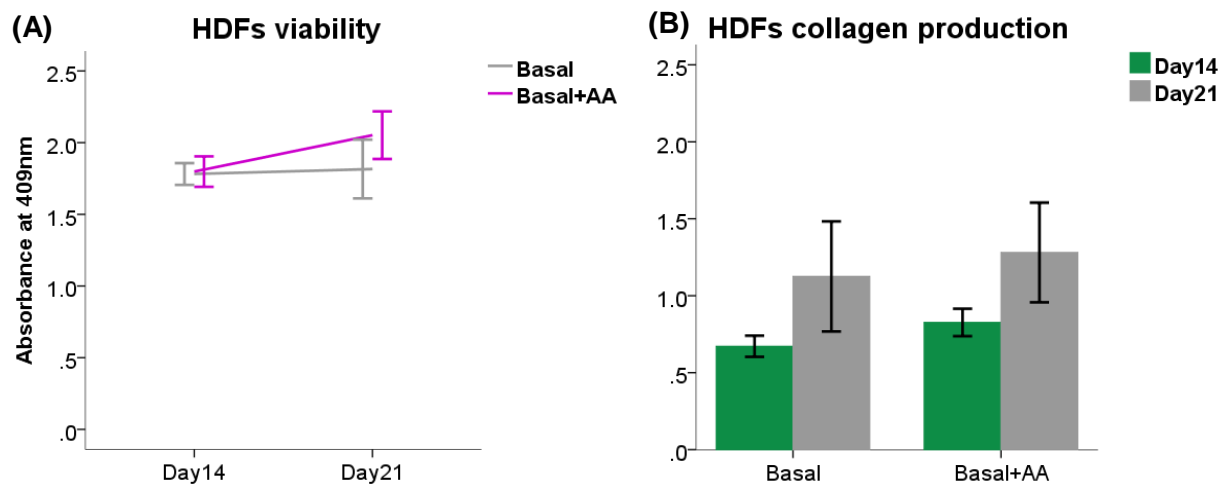


**Figure 6.3.1:** The effect of ascorbic acid-2-phosphate (AA) on human dermal fibroblasts (HDFs) on PCL scaffolds. (A) The cell viability of HDFs were measured using MTS after day 14, 21. (B) Total collagen production was measured using picro-sirius red staining assay after day 14 and 21, mean $\pm$ SE, (N=2, n=3), One-way ANOVA, Tukey's multiple comparison test.

SEM images of the tri-layer scaffold showed there was a mixture of micro- and nano-scale fibres present. However, as predicted there were differences in the frequency of size distribution depending on the parameters used for a specific layer (200µm per layer) (Figure 6.3.2). In the top layer, the most prevalent fibre diameter is between 7-9 µm and more than 95% of fibres are micro-fibres (Figure 6.3.2 C). In the middle layer, the most frequent occurrence of fibre diameter range is less than 1 µm and more than 40% are nano-fibres (Figure 6.3.2 B). In the bottom layer, the most prevalent fibre diameter is between 5-7 µm and more than 90% are micro-fibres (Figure 6.3.2 A). When either hESMPs or hBMSCs were co-cultured with HDFs they deposited calcium nodules by 28 days (Figure 6.3.3 upper and bottom rows, respectively). HDFs were clearly present on the opposite side in a dense layer after 7 days of culture (Figure 6.3.3 B and E, respectively), indicating that soft tissue can be cultured in the adjacent layer to the mineralised tissue. SEM images of the side views of the scaffolds, hESMPs/HDFs and hBMSCs/HDFs (Figure 6.3.3 C,F) showed no cells present in the central nano-fibre layer. CLSM fluorescence images of the co-culture of hESMPs/HDFs and hBMSCs/HDFs (Figure 6.3.4 C,F, respectively) confirmed mineral deposition was only present on one side of the scaffold (Figure 6.3.4 B,E, respectively) and HDFs were only present on the other side (Figure 6.3.4 A,D, respectively). There is a black space in between the red fluorescent (mineralisation) and green fluorescent (fibroblast) surfaces indicating that there were no cells crossing over the nano-fibre central layer, confirming the evidence from the SEM images.

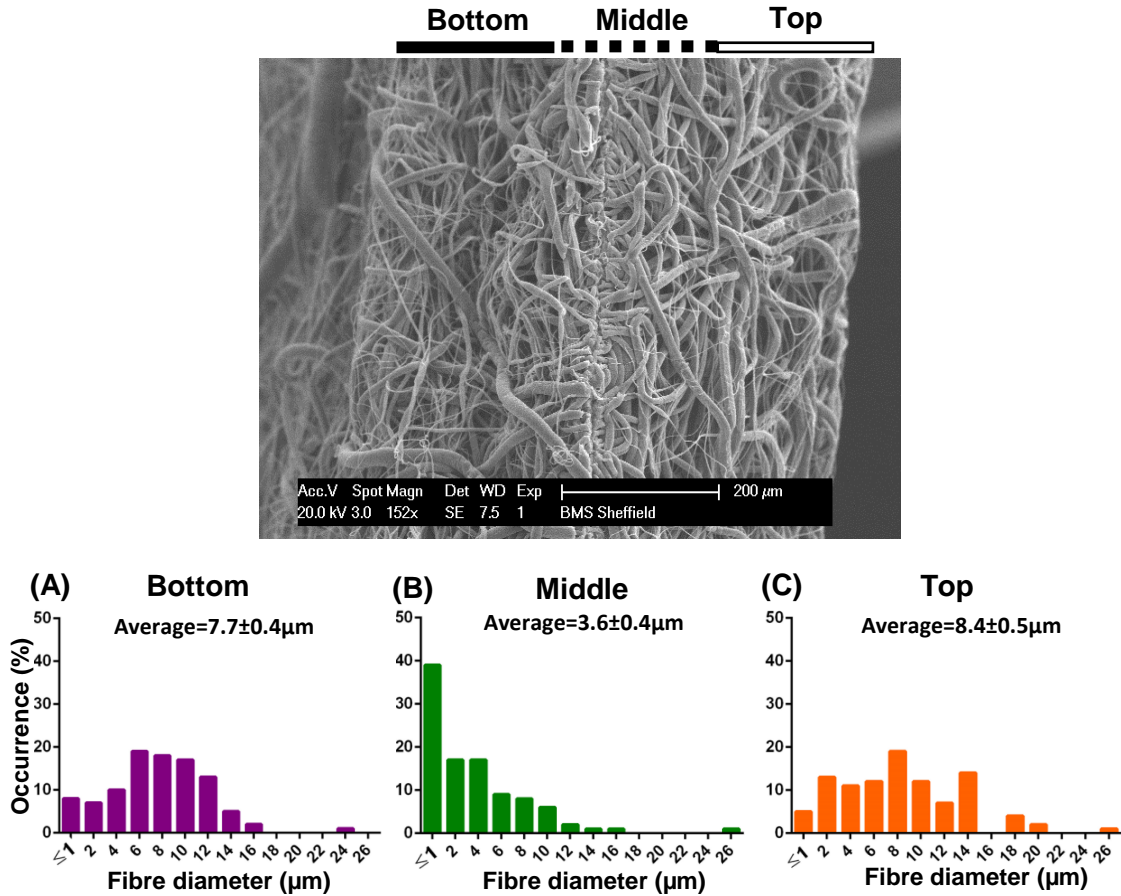


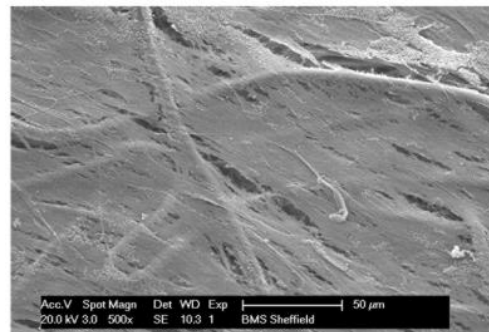
**Figure 6.3.2:** SEM image of the tri-layer electrospun PCL scaffold in side view (top). Frequency of distribution against fibre diameter in the bottom layer (A), the middle layer (B), and the top layer (C). The scale  $\leq 1$  on the X-axis indicates a fibre diameter of less than  $1 \mu\text{m}$  (nano-fibre). average=mean $\pm$ SE, (N=1, n=100), measurements from 4 SEM images in each layer). Scale bar:  $200 \mu\text{m}$ .

## hESMPs /HDFs

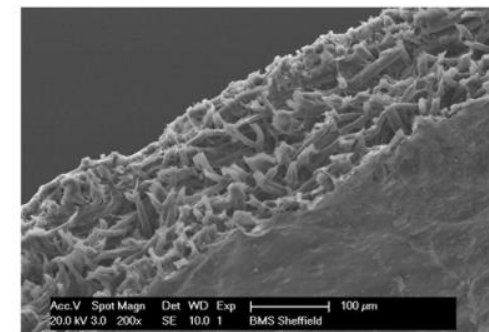
(A)



(B)

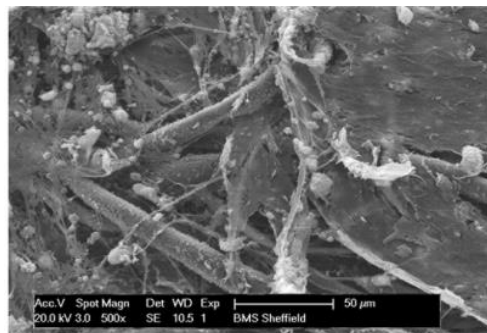


(C)

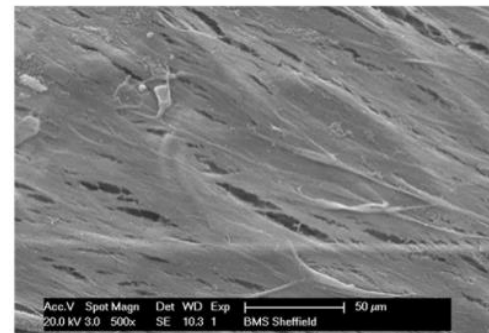


## hBMSCs/HDFs

(D)



(E)



(F)

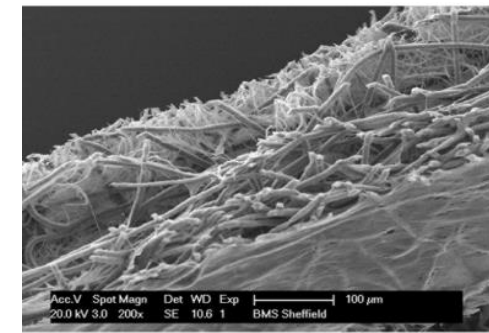
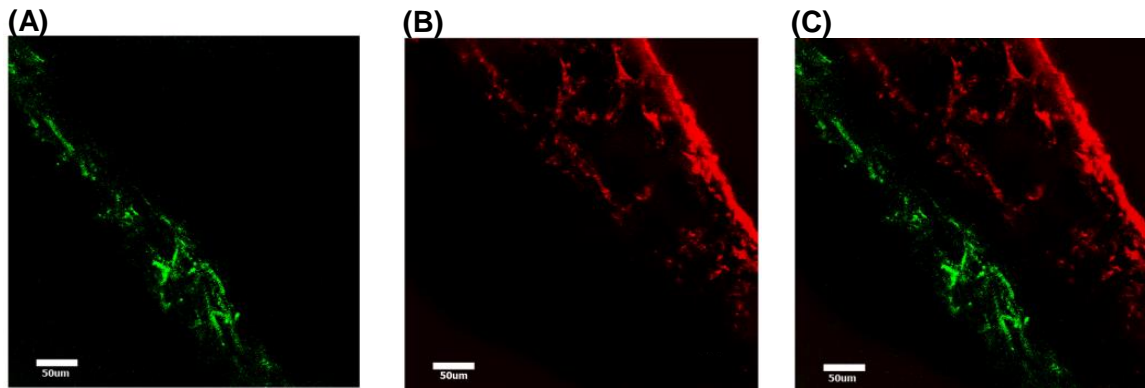


**Figure 6.3.3:** SEM images of the co-culture of hESMPs/HDFs (upper row) and hBMSCs/HDFs (bottom row) on tri-layer scaffolds. Matrix mineralization surfaces of hESMPs (A) and hBMSCs (D) on one side of the scaffolds on 28 days. (B,E) The opposite side of the scaffolds on 7 days culture with HDFs. Side views of the scaffolds co-cultured with hESMPs/HDFs (C) and hBMSCs/HDFs (F) showed the scaffolds could support two different cell types and maintain their separation over 7 days of culture. (N=2, n=2)

## hESMPs/HDFs



## hBMSCs/HDFs

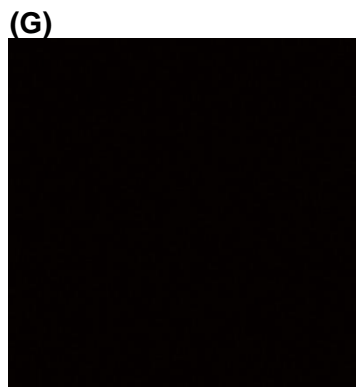
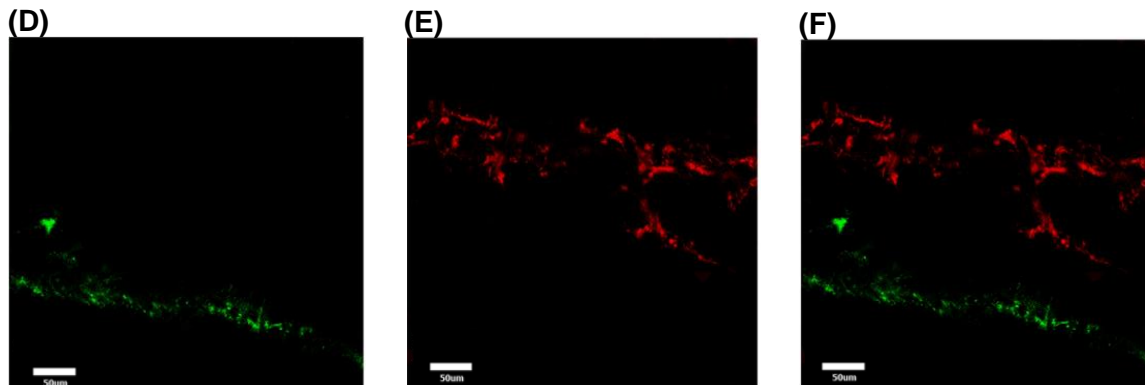


**Figure 6.3.4:** CLSM fluorescence images of the side views of the co-cultured hESMPs/HDF (upper row) and hBMSCs/HDFs (bottom row) on the tri-layer scaffolds. The matrix mineralization of both hESMPs and hBMSCs were assessed by labelling using xylenol orange XO (red colour) staining after 28 days of culture (B and E, respectively). The HDFs were labelled with CellTracker™Green (green colour) prior to 7 days of culture on the opposite side of the scaffolds of the co-cultured hESMPs/HDF (A) and hBMSCs/HDFs (D). Both images indicate there is a space (no cells or mineral deposition) in the central region of the scaffold corresponding to the nanofibrous layer over 7 days of culture (C and F). The PCL scaffold with no staining was visualized to show that it was no auto-fluorescence (G). (Scale bar =50  $\mu\text{m}$ ), (N=2, n=2).

**6.4. Discussion**

As discussed in the previous chapters there are many limitations to current cleft palate repair. In this study we demonstrated the use of a tissue engineering approach for the treatment of cleft palate. Therefore the single-polymer tri-layer electrospun scaffold was created to support osteoblasts and fibroblasts with potential for filling the cleft defect while it maintained two different types of tissues.

The electrospinning technique was chosen in this study for fabricating tissue engineering scaffolds because it is a versatile technique for producing the polymer fibres in diameters from a nano-scale to micro-scale and can be used with various types of polymers as described and shown in chapter 2 and 5. However, the disadvantage of the technique is the low production rate (Rim et al., 2013). My research group was previously successful in producing a tri-layer scaffold which contained a mixture of nano- and micro-scale fibre diameters using PHBV for the nano-fibrous layer and PLA for the micro-fibrous layers (Bye et al., 2013). However the polymers used in that preliminary work were probably not optimal for bone-forming tissue due to the high degradation rate of PLA. Here that procedure was modified to produce a tri-layer scaffold from PCL alone.

Analysis of the tri-layer scaffold indicated that the top and bottom-layers showed a higher percentage of the micro-fibres than nano-fibres and were occupied by osteoprogenitor cells (hESMPs and hBMSCs) on the bone part. Whereas, the middle layer showed the highest percentage of nano-fibres which acted as separation membrane and did not allow the cells to cross-over to the opposite side of the scaffold.

A limitation of this study is that in many cases only two experimental repeats were performed in duplicated or triplicate, however, some interesting appearances were identified as followed. HDFs cells were chosen to represent the soft tissue layer. The results showed that the PCL electrospun scaffold can support HDF proliferation and

allow ECM production in agreement with the study of Hutmacher et al., (2001). In the clinic, a potential approach may be to harvest oral fibroblasts from oral mucosa, similar to my colleague's previous work (Selim et al., 2011). The oral mucosa could be received through routine cleft lip and palate treatment. The first surgery for cleft treatment is a lip closure (cheiloplasty) and during this procedure a small amount of oral mucosa is usually discarded.

CellTracker™Green was capable of enabling the tracking of HDF cells on the scaffold during 7 days of culture. XO, which becomes fluorescent when it chelates calcium, was used to indicate mineralization of the osteogenic cells. It has not commonly used for tissue engineering but may be a great technique to visualised mineralised tissue in 3D scaffolds. Animal model, *in vivo* the XO stain is used for continuous monitoring a new bone formation by injecting this stain into the blood stream in the curtained time-point where it likely newly mineralized formation (Kuhn et al., 2010, Wang et al., 2006).

CLSM overlaid images showed that cells co-cultured on tri-layer scaffolds can maintain separation on their specific regions; the black space in the middle region visible in side view indicates that there were neither fibroblasts nor mineralising cells in this region. The SEM images of the scaffold cross sections confirmed that there were no cells present in this region. This supports our hypothesis that cells would not be able to penetrate the nano-fibrous layer due to their low porosity and is in agreement with my group previous results on tri-layer membranes made from other polymers.

Although the XO staining data alone does not confirm that the osteoprogenitor cells did not cross the nano-fibrous membrane, an undergraduate student under my supervision undertook a separate experiment to verify this issue. Her results show that all hESMPs were only resident on the same side of the scaffold on which they were seeded and there was no evidence of the cells crossing over the central region of the tri-layer membrane.

Development of new blood vessels in this construct should be addressed as it is critical for the successful of this implant. Nutrient and O<sub>2</sub> supply, and waste removal diffuse into the cell construct from surrounding environment (around 150-200µm) until the construct become vascularised (Kanczler and Oreffo, 2008). Hypoxia conditions may occur because the scaffold thickness (600µm) and could up-regulate VEGF secretion (see chapter 3). It would be beneficial to a new blood vessel formation in the construct. The suitable pore size of scaffold for blood vessel formation is 400µm (see chapter 1). Although the tri-layer scaffold was not measured the pore size in each layer, the top and bottom layers of the scaffold were micro-fibres, they may be a suitable pore size for a new blood vessel formation. Whereas, the middle layer of the scaffold was a majority of nano-fibre, lead to reduce the pore size. As the aim of this study is that the cells could not reside at the middle of the scaffold, therefore, the thickness and pore size of the scaffold may be an advantage for vascularisation of the construct.

### **6.5. Conclusion**

Our study indicates that the tri-layer scaffold can support the co-culture of cells (between osteoprogenitor cells and HDFs) and allow osteogenic progenitor cell (hESMPs and hBMSCs) differentiation. The scaffold did not allow the cells to crossover for 28 days due to the low porosity in the middle layer of the scaffold. The benefit of this tri-layer scaffold design is that it could support and separate both soft and hard tissue repair until the new tissues are mature enough to maintain separation. We propose that as a result the soft tissue which is a fast healing would not intrude into the hard tissue region which is slower healing. This would reduce scar formation at the surgical site following a cleft palate surgery and the inhibition of palate growth that occurs when bone graft is performed too early. This scaffold may be useful for any oral maxillofacial reconstruction which involves more than one type of tissue such as guided tissue regeneration for periodontal surgical treatment and alveolar ridge augmentation for tooth implantation.

### 6.6. Summary

- The single-polymer tri-layer electrospun scaffold was demonstrated to support cell attachment and allow cell proliferation and differentiation over 28 days while it maintained a separation of two tissue types between soft and bone forming tissues.
- The tri-layer PCL electrospun scaffold is a promising material for cleft palate repair.

### 6.7. Future work

- Evaluate and localize the collagen production on both sides of the scaffold over long term culture.
- Move on to *in vivo* study to test how both cells behave on the tri-layer membrane in short and long term, for example; detect their retention and maintain their separation between two cell types.
- Incorporate VEGF into the membrane with VEGF for inducing vasculogenesis in the graft.

### **CHAPTER SEVEN: CONCLUSION AND FUTURE DIRECTIONS.**

Current treatments of cleft palate repair have many drawbacks such as multiple surgical steps, donor site morbidity from bone harvesting, and the long time over which complete treatment takes place. A bone tissue engineering strategy may overcome those drawbacks; such a strategy, consisting of cells, biomaterial scaffolds, and other chemical reagents has emerged as a new approach for maxillofacial reconstruction and cleft palate repair.

#### **7.1 Human mesenchymal progenitor/stem cells (human MSCs)**

Human MSCs have been used widely in bone tissue engineering and their differentiation stimulated by chemical reagents, the mechanical environment, scaffolds topography and chemical surface coatings. Our studies confirmed that hESMPs, hBMSCs, and HJPs have osteogenic potential and can be differentiated to osteoblastic-like cells and deposit calcium on their ECM under Dex supplementation. Interestingly, all these cell types dramatically increased calcium deposition when they were subjected to OFF compared to static culture. The use of HJPs which can be easily harvested from the oral cavity would be a less invasive intervention at the donor site compared to the harvesting the hBMSCs from bone marrow.

VEGF is an important protein produced by osteoblast-like cells which stimulates vasculogenesis. It aids to improve the success of bone tissue engineering at the implanted side by facilitating surrounding endothelial cells to produce new blood vessels. Our studies on both hESMPs and hBMSCs seeded on scaffolds showed that VEGF secretion was significantly suppressed in the Dex supplemented group. Therefore, we examined the effect of Dex concentration on monolayer culture and found that by 21 days of culture, cells with Dex were able to secrete as much VEGF as those without, indicating vasculogenesis may be delayed by Dex treatment but not completely inhibited.

The ideal cell source for bone tissue engineering has not yet to be identified and may well depend on the location of the defect (e.g. maxillofacial or long bone), the age of the patient and the disease state. In the case of cleft palate there is still more work needed to determine the most suitable cell source. Future work in this area could include:

- Investigating other markers of osteogenic differentiation of the cells such as surface antigens, cytokines, and the expression of genes involved in the initial stages of differentiation e.g. Runx2, osterix (OSX), activating transcription factor 4 (ATF4), collagen type I, ALP, BMP-2 (Malgorzata, 2012).
- Investigate multiple donors of osteoprogenitor cells to better understand the variability between cells from different individuals.
- Comparing the osteogenic differentiation of the osteoprogenitor cells from different anatomical harvesting sites
- Mineral deposition analysis by FT-IR, XRD, or EDX to evaluate the quality of mineralization relative to a real bone and whether it's nano-structure and mechanical properties are sufficient to maintain the palate intact.
- Mechanical properties analysis on the cells-seeded scaffold samples to evaluate whether the cell seeded scaffold construct could support cells and withstand mechanical force when they were implanted into the defected regions.

### **7.2. 3D model for bone tissue engineering**

Many technologies have been used for fabricating a porous scaffold. Electrospinning has been proven to be a simple and adjustable method of producing fibres in a wide size range from nano- to micro- sized fibre diameters. Electrospun PCL scaffolds were used in our study due to their mechanical properties which are suitable for bone and their biocompatibility with surrounding tissue. PCL scaffolds can support hESMPs, hBMSCs, and HJPs for proliferation, and osteogenic differentiation with the addition of Dex. However their limitations are that they do not have osteoinductive nor

osteoconductive properties. Therefore, nHA was incorporated with PCL (HA-PCL) to overcome the limitations. Our study found that the 5wt%HA-PCL electrospun scaffold was a suitable material for cell support, proliferation, and enhancing osteogenic differentiation however it reduced scaffold mechanical properties. The cellular calcium deposition on both standard and HA-PCL scaffolds was evaluated by using micro-CT. HA-PCL scaffolds showed an increase of calcium deposition compared to standard PCL scaffold in the static culture in medium which did not contain Dex, however, there were no differences in the calcium deposition in the media supplemented with Dex, or the same media without Dex in the rocking groups. Moreover, there were no differences between standard-PCL and HA-PCL scaffolds in the cellular calcium deposition in the rocking under SM+Dex100 group. Further investigation will be needed to:

- Analyse osteogenic gene expression on both standard PCL and HA-PCL scaffolds to indicate osteogenic differentiation, for instance, the early state: ALP, collagen type I, BMP-2 or late stage: OPN and OCN.
- Quantify the amount of calcium and phosphate ions in the culture media to indicate the effect of nHA on matrix mineralization of cells on the HA-PCL scaffold.
- Improve mechanical properties of HA-PCL scaffolds to be suitable for integration with the adjacent region and function until the mature development of tissue.
- Compare the mechanical properties of the scaffold with ECM construct produced on standard and HA-PCL scaffolds.
- Quantify nHA distribution in the HA-PCL scaffolds and degradation rate.
- To evaluate a suitable amount of nHA particles for improving their mechanical properties. .

### 7.3 External mechanical force

OFF is a form of external mechanical stimulation has been reported to enhance cell proliferation, ECM, and calcium deposition in many cell types. Our study showed that

OFF applied by using a standard see-saw rocker with a requirement of Dex can enhance calcium deposition on both monolayer and 3D cultures in three cells types; 1] hESMPs, 2] hBMSCs, and 3] HJPs. However, we did not test the effect of OFF on the HJPs in the 3D culture, because of an insufficient cell supply. The hESMPs and hBMSCs on the standard PCL scaffolds responded to OFF resulting in increased calcium deposition at the top surface of the scaffolds, moreover, they showed a significantly higher %BV over the top layer of HA-PCL scaffolds under the osteogenic induction medium (Dex supplementation).

Our study found that OFF had no effect on VEGF secretion for the osteoprogenitor cells seeded on either standard PCL or HA-PCL scaffolds. Therefore, this study did not solve a crucial limitation of a large scale tissue engineer graft, which is a lack of vasculature. The low cell survival rate which has been shown at the centre of the graft due to nutrient supply and excretion of waste may still exist.

The future of OFF stimuli to enhance osteogenic differentiation of osteoprogenitor cells should clearly be investigated to fulfil the current void in knowledge around bone tissue engineering. Many factors will influence the cellular response such as the frequency, magnitude, and type of flow, the insertion of rest period, and chemical supplements to stimulate osteogenesis. These factors could be scaled-up to clinical application for bone graft substitutes for cleft palate repair and other bone tissue engineering constructs. To improve a method to enhance vasculogenesis by the cells, it would be beneficial to integrate between the bone graft and the surrounding implanted region. Characterisation of the fluid flow on the 3D scaffold from this loading system needs to be evaluated using mathematical and computer modelling of the loading system. This would hopefully enable a better characterisation of the local stresses and strains which are applied throughout the scaffold. In addition, the mechanism of OFF induced osteogenic differentiation in osteoprogenitor cells is very complex with many signalling pathways involved (Liu et al., 2010). To elucidate this mechanism it would be useful to provide a

better understanding of what mechanical signal the cells respond to or are sensing from this type of loading system. This could help to create the graft construction without the need for biochemical reagents such as Dex or by substituting with another chemical e.g. vitamin D or BMP-2 (Jorgensen et al., 2004). Substitution of Dex could overcome the Dex-dependant inhibition of VEGF secretion and reduce the concern about long term use of Dex which risks causing osteoporosis or osteonecrosis if it is included in the construct implanted into bone (Li et al., 2005).

### **Future work**

- Characterise the stress and strain from OFF on the cell seeded PCL scaffolds using mathematics and computer modelling.
- To evaluate the suitable percentage of HA in HA-PCL scaffolds to provide a more homogenous distribution of HA in the electrospun scaffold, to improve mechanical properties of HA-PCL scaffolds.
- Another material e.g. PU which is a more flexible may also be a suitable scaffold for OFF stimulation. Such polymers should be compared with PCL to determine the best candidate for cleft palate repair.

### **7.4 Tri-layer membrane scaffold**

Many studies have attempted to devise a tissue engineering approach for craniofacial reconstruction and determine what scaffold materials and architectures would work best. The design and fabrication of scaffolds can be controlled to mimic the natural craniofacial structure. Our proposed design is tri-layer scaffold of electrospun PCL attempts to mimic the structure of craniofacial organs by having soft tissue and bone separated by a membrane (*in vivo* this is the periosteum). HDFs were seeded on one side within a micro-fibre layer and human osteoprogenitor cells on the other side also within a micro-fibre layer and these were separated by the nano-fibrous layer at the middle of the scaffold. We found that this scaffold was can support cells and allowed the

osteoprogenitor cells to undergo osteogenic differentiation while the scaffold maintained separation of the two cells types in long term culture (28 days). Further work is required to:

- Move to an animal model by using the co-culture graft at the non-bone environment (ectopic bone formation) to detect cell localisation, and cell-graft survival on the scaffold of both cell types.
- Test the mechanical properties of the graft to address whether it is strong enough for loading within an oral cavity.
- Optimise the degradation rate of the scaffold to match the new tissue formation of both soft and hard tissues in the body.
- Incorporate drugs e.g. antibiotic (doxycycline, colistin) into the tri-layer membrane scaffold to prevent infection post-operation.

### **7.5 Clinical applications of maxillofacial reconstruction**

The current cleft palate repair procedure recommends treatment when the child is 6-12 months old, this may disrupt the development of craniofacial structure in many directions such as vertical, antero-posterior, and transverse directions, because of tissue fibrosis at the defect region. Then cleft repair at the alveolar (teeth bearing region on the palate) occurs later about 8-9 years using autologous bone graft which is recommended to take place before the permanent canine teeth erupt on the defect region, this can also can severely inhibit maxillary growth (Wolford and Stevao, 2002). The suitable timing for cleft palate repair is still controversial. Rochrich et al., (2004) studied the long-term follow up of the cleft palate patients who underwent palatal closer surgeries designed to complete the cleft palate repair before 2 years of age. As the reasons, are to establish normal speech development and reduce risk of hearing loss in the patients. The drawbacks of current autologous bone graph are insufficient quantity and quality of grafts, and of allografts is their immunogenic potential and the risk of pathogen

transmission to the recipient. To reconstruct the function of cleft palate in the field of bone tissue engineering may overcome the drawbacks of the current treatment. An important advantage of bone tissue engineering is that a small healthy tissue biopsy can be taken from the body, the cells expanded under a cell culture conditions, incorporated with biocompatible materials, and re-implanted them back into patients.

The ideal timing for cleft palate treatments using a tissue engineering strategy are not yet known. It would ideally be before 2 years of age to allow speech development and decrease risk of hearing loss, and also reduce the number of surgical treatments. Hopefully the patient would then avoid further surgery, for instance, autologous bone graft procedure. Alternatively, it would be at 8-9 years of age to prepare the bone support for tooth eruption. This procedure would reduce donor site morbidity and length of surgical time compared to autologous bone graft surgery from iliac bone (current treatment). In my opinion, the tissue engineering strategy can benefit cleft palate treatment whichever time point is selected compared to the current treatment.

Meijer et al, (2008) reported a successful clinical study for bone augmentation (increase in alveolar ridge side) by using bone tissue engineering and placed the dental implants in the reconstructed bone afterwards. They reported no any adverse effects from the pathogen contamination from animal or corticosteroid while they cultured the cells under the 10%FBS and Dex to induce osteogenic differentiation. In contrast, using serum free medium for culturing the cells, resulting in a low cell adhesion and proliferation and also lead to cell apoptosis (Heng et al., 2004, Wong and Tuan, 1993). However, the development of the suitable hBMSCs culture conditions for clinical use is still required.

Our study demonstrated that both HJPs and hBMSCs had multi-potent ability to differentiate to osteogenic cells and formed ECM and calcium deposition on the biocompatible and biodegradable 3D constructs. Moreover mechanical stimulation

using OFF with the requirement of Dex enhanced calcium deposition. OFF was most effective at stimulating mineralisation at the top surface of the scaffolds as detected by micro computed tomography (micro-CT). This method could be applied to evaluation bone formation on 3D constructs after implanting into patients by using clinical CT. There are still many obstacles to be overcome before bone tissue engineering can be used for routine clinical protocol. Both short and long-term studies of the bone tissue engineering after implantation are required to evaluate the effective outcome compared to the current approach with an important consideration being whether the new treatment improves patient outcome.

### 7.6 Final conclusion

- The human cell line (hESMPs) and primary osteoprogenitor cells (HJPs and hBMSCs) showed the osteogenic potential by producing calcium deposition on both monolayer (chapter 3) and 3D constructs (chapter 5) under culture condition with presence of Dex.
- PCL is a suitable temporary ECM for bone tissue engineering (chapter 5).
- VEGF secretion was reduced by Dex supplementation conditions in 3D culture (chapter 5) and was delayed in monolayer culture (chapter 4).
- OFF enhanced the calcium deposition of all cell types on both monolayer (chapter 4) and 3D constructs (chapter 5) in Dex supplemented conditions. The strongest effect of OFF was at the top surface of the scaffolds.
- The cellular calcium depositions on HA-PCL was increased compared to standard PCL under the supplemented medium. But there were no effects of OFF (chapter 5).
- A tri-layer PCL scaffold could support and separate two different cell types HDFs and human osteoprogenitor cells: both hESMPs and hBMSCs) and allow osteogenic differentiation for 28 days (chapter 6).

**APPENDIX****Oral presentations**

1. Thai/UK stem cell meeting: ‘Optimising cell sources and materials for cleft palate repair’, 29<sup>th</sup> March 2011, the University of Sheffield, Sheffield.
2. Biomaterials and Tissue Engineering Group: ‘Oscillatory fluid shear stress enhances matrix production of Human embryonic mesenchymal progenitor stem cells (hES-MP) on biodegradable electrospun polycaprolactone scaffold’, 17<sup>th</sup> December 2012, the University of York.

**Poster presentations**

1. The 6<sup>th</sup> UK Mesenchymal Stem cell meeting: ‘Optimizing cell sources and materials for cleft palate repair’, 15<sup>th</sup> June 2012, University of Southampton, Southampton.
2. Tissue and Cell Engineering 2012: ‘Optimizing cell sources and materials for cleft palate repair’, 4<sup>th</sup>-6<sup>th</sup> July 2012, the University of Liverpool, Liverpool.
3. 3<sup>rd</sup> World Congress Tissue Engineering International & Regenerative Medicine: ‘Optimizing cell sources and materials for cleft palate repair’, 5<sup>th</sup>-8<sup>th</sup> September 2012, Vienna, Austria.
4. The 7<sup>th</sup> UK Mesenchymal Stem cell meeting: ‘Fluid shear stress enhances matrix production by Mesenchymal stem cells’, 12<sup>th</sup>-13<sup>th</sup> September 2013, Aston University, Birmingham
5. 5<sup>th</sup> International Conference on Mechanics of Biomaterials and Tissues: ‘Fluid shear stress enhances matrix production by mesenchymal progenitor cells on biodegradable electrospun scaffolds’, 8<sup>th</sup>-12<sup>th</sup> December 2013, Sitges, Spain.

**Awards**

Three travel grants awarded from Learned Society the University of Sheffield (2012, 2013, and 2014).

**Publications**

1. **[Abstract]** ‘Optimizing cell sources and materials for cleft palate repair’ in Journal European Cells and Materials, Vol.23, Suppl. 4, 2012 (page88).

## REFERENCES

- ADVANI, S., LAFRANCIS, D., BOGDANOVIC, E., TAXEL, P., RAISZ, L. G. & KREAM, B. E. 1997. Dexamethasone suppresses in vivo levels of bone collagen synthesis in neonatal mice. *Bone*, 20, 41-46.
- AKINTOYE, S. O., LAM, T., SHI, S. T., BRAHIM, J., COLLINS, M. T. & ROBEY, P. G. 2006. Skeletal site-specific characterization of orofacial and iliac crest human bone marrow stromal cells in same individuals. *Bone*, 38, 758-768.
- ARAUJO, J. V., MARTINS, A., LEONOR, I. B., PINHO, E. D., REIS, R. L. & NEVES, N. M. 2008. Surface controlled biomimetic coating of polycaprolactone nanofiber meshes to be used as bone extracellular matrix analogues. *Journal of Biomaterials Science-Polymer Edition*, 19, 1261-1278.
- ARCHAMBAULT, J. M., ELFERVIG-WALL, M. K., TSUZAKI, M., HERZOG, W. & BANES, A. J. 2002. Rabbit tendon cells produce MMP-3 in response to fluid flow without significant calcium transients. *Journal of Biomechanics*, 35, 303-309.
- AVISS, K. J., GOUGH, J. E. & DOWNES, S. 2010. Aligned electrospun polymer fibres for skeletal muscle regeneration. *European Cells & Materials*, 19, 193-204.
- BACABAC, R. G., SMIT, T. H., MULLENDER, M. G., DIJCKS, S. J., VAN LOON, J. & KLEIN-NULEND, J. 2004. Nitric oxide production by bone cells is fluid shear stress rate dependent. *Biochemical and Biophysical Research Communications*, 315, 823-829.
- BAEK, J.-Y., XING, Z.-C., KWAK, G., YOON, K.-B., PARK, S.-Y., PARK, L. S. & KANG, I.-K. 2012. Fabrication and Characterization of Collagen-Immobilized Porous PHBV/HA Nanocomposite Scaffolds for Bone Tissue Engineering. *Journal of Nanomaterials*.
- BALL, M. D., BONZANI, I. C., BOVIS, M. J., WILLIAMS, A. & STEVENS, M. M. 2011. Human Periosteum Is a Source of Cells for Orthopaedic Tissue Engineering: A Pilot Study. *Clinical Orthopaedics and Related Research*, 469, 3085-3093.
- BANCROFT, G. N., SIKAVITSAST, V. I., VAN DEN DOLDER, J., SHEFFIELD, T. L., AMBROSE, C. G., JANSEN, J. A. & MIKOS, A. G. 2002. Fluid flow increases mineralized matrix deposition in 3D perfusion culture of marrow stromal osteoblasts in a dose-dependent manner. *Proceedings of the National Academy of Sciences of the United States of America*, 99, 12600-12605.
- BANFI, A., MURAGLIA, A., DOZIN, B., MASTROGIACOMO, M., CANCEDDA, R. & QUARTO, R. 2000. Proliferation kinetics and differentiation potential of ex vivo expanded human bone marrow stromal cells: Implications for their use in cell therapy. *Experimental Hematology*, 28, 707-715.
- BARBETTA, A., BEDINI, R., PECCI, R. & DENTINI, M. 2012. Role of X-ray microtomography in tissue engineering. *Annali Dell Istituto Superiore Di Sanita*, 48, 10-18.
- BEHNIA, H., KHOJASTEH, A., SOLEIMANI, M., TEHRANCHI, A., KHOSHZABAN, A., KESHEL, S. H. & ATASHI, R. 2009. Secondary repair of alveolar clefts using human mesenchymal stem cells. *Oral Surgery Oral Medicine Oral Pathology Oral Radiology and Endodontology*, 108, E1-E6.
- BERGLAND, O., SEMB, G. & ABYHOLM, F. E. 1986. ELIMINATION OF THE RESIDUAL ALVEOLAR CLEFT BY SECONDARY BONE-GRAFTING AND SUBSEQUENT ORTHODONTIC TREATMENT. *Cleft Palate Journal*, 23, 175-205.
- BERKOWITZ, S., DUNCAN, R., EVANS, C., FRIEDE, H., KUIJPERS-JAGTMAN, A. M., PRAHL-ANDERSON, B. & ROSENSTEIN, S. 2005. Timing of cleft palate closure should be based on the ratio of the area of the cleft to that of the palatal segments and not on age alone. *Plastic and Reconstructive Surgery*, 115, 1483-1499.
- BIRMINGHAM, E., GROGAN, J. A., NIEBUR, G. L., MCNAMARA, L. M. & MCHUGH, P. E. 2013. Computational modelling of the mechanics of trabecular bone and marrow using fluid structure interaction techniques. *Annals of Biomedical Engineering*, 41, 814-826.
- BLACKWOOD, K. A., MCKEAN, R., CANTON, I., FREEMAN, C. O., FRANKLIN, K. L., COLE, D., BROOK, I., FARTHING, P., RIMMER, S., HAYCOCK, J. W., RYAN, A. J. & MACNEIL, S. 2008.

## REFERENCES

- Development of biodegradable electrospun scaffolds for dermal replacement. *Biomaterials*, 29, 3091-3104.
- BONNET, N. & FERRARI, S. L. 2010. Exercise and the skeleton: How it works and what it really does. 7. [Accessed 22 December 2013].
- BORJIGIN, M., STROUSE, B., NIAMAT, R. A., BIALK, P., ESKRIDGE, C., XIE, J. & KMIEC, E. B. 2012. Proliferation of Genetically Modified Human Cells on Electrospun Nanofiber Scaffolds. *Molecular Therapy-Nucleic Acids*, 1.
- BOXALL, S. A. & JONES, E. 2012. Markers for characterization of bone marrow multipotential stromal cells. *Stem cells international*, 2012, 975871-975871.
- BROWN, D. C. & LARSON, R. S. 2001. Improvements to parallel plate flow chambers to reduce reagent and cellular requirements. *BMC immunology*, 2, 9-9.
- BUENO, D. F., KERKIS, I., COSTA, A. M., MARTINS, M. T., KOBAYASHI, G. S., ZUCCONI, E., FANGANIELLO, R. D., SALLES, F. T., ALMEIDA, A. B., RAPOSO DO AMARAL, C. E., ALONSO, N. & PASSOS-BUENO, M. R. 2009. New source of muscle-derived stem cells with potential for alveolar bone reconstruction in cleft lip and/or palate patients. *Tissue Engineering Part A*, 15, 427-435.
- BURGER, C., HSIAO, B. S. & CHU, B. 2006. Nanofibrous materials and their applications. *Annual Review of Materials Research*, 36, 333-368.
- BYE, F. J., BISSOLI, J., BLACK, L., BULLOCK, A. J., PUWANUN, S., MOHARAMZADEH, K., REILLY, G. C., RYAN, A. J. & MACNEIL, S. 2013. Development of bilayer and trilayer nanofibrous/microfibrous scaffolds for regenerative medicine. *Biomaterials Science*, 1, 942-951.
- CAPLAN, A. I. 2005. Mesenchymal stem cells: Cell-based reconstructive therapy in orthopedics. *Tissue Engineering*, 11, 1198-1211.
- CARRIER, R. L., RUPNICK, M., LANGER, R., SCHOEN, F. J., FREED, L. E. & VUNJAK-NOVAKOVIC, G. 2002. Perfusion improves tissue architecture of engineered cardiac muscle. *Tissue Engineering*, 8, 175-188.
- CARTMELL, S., HUYNH, K., LIN, A., NAGARAJA, S. & GULDBERG, R. 2004. Quantitative microcomputed tomography analysis of mineralization within three-dimensional scaffolds in vitro. *Journal of Biomedical Materials Research Part A*, 69A, 97-104.
- CASE, N., SEN, B., THOMAS, J. A., STYNER, M., XIE, Z., JACOBS, C. R. & RUBIN, J. 2011. Steady and Oscillatory Fluid Flows Produce a Similar Osteogenic Phenotype. *Calcified Tissue International*, 88, 189-197.
- CASPER, C. L., STEPHENS, J. S., TASSI, N. G., CHASE, D. B. & RABOLT, J. F. 2004. Controlling surface morphology of electrospun polystyrene fibers: Effect of humidity and molecular weight in the electrospinning process. *Macromolecules*, 37, 573-578.
- CHANG, B. S., LEE, C. K., HONG, K. S., YOUN, H. J., RYU, H. S., CHUNG, S. S. & PARK, K. W. 2000a. Osteoconduction at porous hydroxyapatite with various pore configurations. *Biomaterials*, 21, 1291-1298.
- CHANG, Y. L., STANFORD, C. M. & KELLER, J. C. 2000b. Calcium and phosphate supplementation promotes bone cell mineralization: Implications for hydroxyapatite (HA)-enhanced bone formation. *Journal of Biomedical Materials Research*, 52, 270-278.
- CHAO, Y.-H., WU, H.-P., CHAN, C.-K., TSAI, C., PENG, C.-T. & WU, K.-H. 2012. Umbilical cord-derived mesenchymal stem cells for hematopoietic stem cell transplantation. *Journal of biomedicine & biotechnology*, 2012, 759503-759503.
- CHEN, D., SHEN, H., SHAO, J., JIANG, Y., LU, J., HE, Y. & HUANG, C. 2011. Superior mineralization and neovascularization capacity of adult human metaphyseal periosteum-derived cells for skeletal tissue engineering applications. *International Journal of Molecular Medicine*, 27, 707-713.

## REFERENCES

- CHEN, H. H., DECOT, V., OUYANG, J. P., STOLTZ, J. F., BENSOUSSAN, D. & DE ISLA, N. G. 2009. In vitro initial expansion of mesenchymal stem cells is influenced by the culture parameters used in the isolation process. *Bio-Medical Materials and Engineering*, 19, 301-309.
- CHEN, J., SHI, Z.-D., JI, X., MORALES, J., ZHANG, J., KAUR, N. & WANG, S. 2013. Enhanced Osteogenesis of Human Mesenchymal Stem Cells by Periodic Heat Shock in Self-Assembling Peptide Hydrogel. *Tissue Engineering Part A*, 19, 716-728.
- CHEN, J.-H., LIU, C., YOU, L. & SIMMONS, C. A. 2010. Boning up on Wolff's Law: Mechanical regulation of the cells that make and maintain bone. *Journal of Biomechanics*, 43, 108-118.
- CHEN, J. C. & JACOBS, C. R. 2013. Mechanically induced osteogenic lineage commitment of stem cells. *Stem Cell Research & Therapy*, 4.
- CHEN, L. J. & WANG, M. 2002. Production and evaluation of biodegradable composites based on PHB-PHV copolymer. *Biomaterials*, 23, 2631-2639.
- CHEN, M., PATRA, P. K., WARNER, S. B. & BHOWMICK, S. 2007. Role of fiber diameter in adhesion and proliferation of NIH 3T3 fibroblast on electrospun polycaprolactone scaffolds. *Tissue Engineering*, 13, 579-587.
- CHEN, T. L. 2006. Inhibition of growth and differentiation of osteoprogenitors in mouse bone marrow stromal cell cultures by increased donor age and glucocorticoid treatment (vol 35, pg 83, 2004). *Bone*, 38, 604-604.
- CHENG, S. L., YANG, J. W., RIFAS, L., ZHANG, S. F. & AVIOLI, L. V. 1994. Differentiation of human bone-marrow osteogenic stromal cells *in vitro*-induction of the osteoblast phenotype by dexamethasone. *Endocrinology*, 134, 277-286.
- CHEUNG, H. Y., LAU, K. T., LU, T. P. & HUI, D. 2007. A critical review on polymer-based bio-engineered materials for scaffold development. *Composites Part B-Engineering*, 38, 291-300.
- CHIM, H., HUTMACHER, D. W., CHOU, A. M., OLIVEIRA, A. L., REIS, R. L., LIM, T. C. & SCHANTZ, J. T. 2006. A comparative analysis of scaffold material modifications for load-bearing applications in bone tissue engineering. *International Journal of Oral and Maxillofacial Surgery*, 35, 928-934.
- CHOI, I. H., CHUNG, C. Y., CHO, T. J. & YOO, W. J. 2002. Angiogenesis and mineralization during distraction osteogenesis. *Journal of Korean Medical Science*, 17, 435-447.
- CHOI, K.-M., SEO, Y.-K., YOON, H.-H., SONG, K.-Y., KWON, S.-Y., LEE, H.-S. & PARK, J.-K. 2008. Effect of ascorbic acid on bone marrow-derived mesenchymal stem cell proliferation and differentiation. *Journal of Bioscience and Bioengineering*, 105, 586-594.
- CHOONG, C., YUAN, S., THIAN, E. S., OYANE, A. & TRIFFITT, J. 2012. Optimization of poly( $\epsilon$ -caprolactone) surface properties for apatite formation and improved osteogenic stimulation. *Journal of Biomedical Materials Research Part A*, 100A, 353-361.
- CHUSUEI, C. C., GOODMAN, D. W., VAN STIPDONK, M. J., JUSTES, D. R. & SCHWEIKERT, E. A. 1999. Calcium phosphate phase identification using XPS and time-of-flight cluster SIMS. *Analytical Chemistry*, 71, 149-153.
- CICCONETTI, A., SACCHETTI, B., BARTOLI, A., MICHENZI, S., CORSI, A., FUNARI, A., ROBEY, P. G., BIANCO, P. & RIMINUCCI, M. 2007. Human maxillary tuberosity and jaw periosteum as sources of osteoprogenitor cells for tissue engineering. *Oral Surgery Oral Medicine Oral Pathology Oral Radiology and Endodontology*, 104.
- CIPITRIA, A., SKELTON, A., DARGAVILLE, T. R., DALTON, P. D. & HUTMACHER, D. W. 2011. Design, fabrication and characterization of PCL electrospun scaffolds-a review. *Journal of Materials Chemistry*, 21, 9419-9453.
- CLARKE, B. 2008. Normal bone anatomy and physiology. *Clinical Journal of the American Society of Nephrology*, 3, S131-S139.

## REFERENCES

- COELHO, M. J. & FERNANDES, M. H. 2000. Human bone cell cultures in biocompatibility testing. Part II: effect of ascorbic acid, beta-glycerophosphate and dexamethasone on osteoblastic differentiation. *Biomaterials*, 21, 1095-1102.
- CONCONI, M. T., CARAMPIN, P., LORA, S., GRANDI, C. & PARNIGOTTO, P. P. 2009. *Polyphosphazenes for Biomedical Applications*, Hoboken, New Jersey, John Wiley & Sons, Inc.
- COOKE, M. J., PHILLIPS, S. R., SHAH, D. S. H., ATHEY, D., LAKEY, J. H. & PRZYBORSKI, S. A. 2008. Enhanced cell attachment using a novel cell culture surface presenting functional domains from extracellular matrix proteins. *Cytotechnology*, 56, 71-79.
- D'ADDONA, A. & NOWZARI, H. 2001. Intramembranous autogenous osseous transplants in aesthetic treatment of alveolar atrophy. *Periodontology 2000*, 27, 148-161.
- DATTA, N., PHAM, Q. P., SHARMA, U., SIKAVITSAS, V. I., JANSEN, J. A. & MIKOS, A. G. 2006. In vitro generated extracellular matrix and fluid shear stress synergistically enhance 3D osteoblastic differentiation. *Proceedings of the National Academy of Sciences of the United States of America*, 103, 2488-2493.
- DAUD, M. F. B., PAWAR, K. C., CLAEYSSENS, F., RYAN, A. J. & HAYCOCK, J. W. 2012. An aligned 3D neuronal-glia co-culture model for peripheral nerve studies. *Biomaterials*, 33, 5901-5913.
- DE BARI, C., DELL'ACCIO, F., KARYSTINO, A., GUILLOT, P. V., FISK, N. M., JONES, E. A., MCGONAGLE, D., KHAN, I. M., ARCHER, C. W., MITSIADIS, T. A., DONALDSON, A. N., LUYTEN, F. P. & PITZALIS, C. 2008. A biomarker-based mathematical model to predict bone-forming potency of human synovial and periosteal mesenchymal stem cells. *Arthritis and Rheumatism*, 58, 240-250.
- DE BARI, C., DELL'ACCIO, F., VANLAUWE, J., EYCKMANS, J., KHAN, Y. M., ARCHER, C. W., JONES, E. A., MCGONAGLE, D., MITSIADIS, T. A., PITZALIS, C. & LUYTEN, F. P. 2006. Mesenchymal multipotency of adult human periosteal cells demonstrated by single-cell lineage analysis. *Arthritis and Rheumatism*, 54, 1209-1221.
- DE PEPPO, G. M., SVENSSON, S., LENNERAS, M., SYNNERGREN, J., STENBERG, J., STREHL, R., HYLLNER, J., THOMSEN, P. & KARLSSON, C. 2010. Human embryonic mesodermal progenitors highly resemble human mesenchymal stem cells and display high potential for tissue engineering applications. *Tissue Engineering Part A*, 16, 2161-2182.
- DEB, S., WANG, M., TANNER, K. E. & BONFIELD, W. 1996. Hydroxyapatite polyethylene composites: Effect of grafting and surface treatment of hydroxyapatite. *Journal of Materials Science-Materials in Medicine*, 7, 191-193.
- DELAINE-SMITH, R. 2013. *Mechanical and physical guidance of osteogenic differentiation and matrix production*. Doctor of Philosophy, The University of Sheffield.
- DELAINE-SMITH, R. M., GREEN, N. H., MATCHER, S. J., MACNEIL, S. & REILLY, G. C. 2014a. Monitoring Fibrous Scaffold Guidance of Three-Dimensional Collagen Organisation Using Minimally-Invasive Second Harmonic Generation. *PLoS ONE*, 9, e89761.
- DELAINE-SMITH, R. M., MACNEIL, S. & REILLY, G. C. 2012. Matrix production and collagen structure are enhanced in two types of osteogenic progenitor cells by a simple fluid shear stress stimulus. *European Cells & Materials*, 24, 162-174.
- DELAINE-SMITH, R. M. & REILLY, G. C. 2011. The effects of mechanical loading on mesenchymal stem cell differentiation and matrix production. *Vitamins and Hormones: Stem Cell Regulators*, 87, 417-480.
- DELAINE-SMITH, R. M., SITTICHOKECHAIWUT, A. & REILLY, G. C. 2014b. Primary cilia respond to fluid shear stress and mediate flow-induced calcium deposition in osteoblasts. *FASEB Journal*, 28, 430-439.
- DEMPSTER, D. W., ARLOT, M. A. & MEUNIER, P. J. 1983. Mean wall thickness and formation periods of trabecular bone packets in corticosteroid-induced osteoporosis. *Calcified Tissue International*, 35, 410-417.
- DOLL, B. A. 2005. *Bone Tissue Engineering*, Florida 33431, CRC Press, 2000 N.W. Corporate Blvd.

## REFERENCES

- DOMINICI, M., LE BLANC, K., MUELLER, I., SLAPER-CORTENBACH, I., MARINI, F. C., KRAUSE, D. S., DEANS, R. J., KEATING, A., PROCKOP, D. J. & HORWITZ, E. M. 2006. Minimal criteria for defining multipotent mesenchymal stromal cells. The International Society for Cellular Therapy position statement. *Cytotherapy*, 8, 315-317.
- DOUGLAS, T. E. L., MESSERSMITH, P. B., CHASAN, S., MIKOS, A. G., DE MULDER, E. L. W., DICKSON, G., SCHAUBROECK, D., BALCAEN, L., VANHAECKE, F., DUBRUEL, P., JANSEN, J. A. & LEEUWENBURGH, S. C. G. 2012. Enzymatic Mineralization of Hydrogels for Bone Tissue Engineering by Incorporation of Alkaline Phosphatase. *Macromolecular Bioscience*, 12, 1077-1089.
- DOUSTGANI, A., VASHEGHANI- FARAHANI, E., SOLEIMANI, M. & HASHEMI-NAJAFABADI, S. 2012. Physical and Chemical Investigation of Polycaprolactone, Nanohydroxyapatite and Poly (Vinyl Alcohol) Nanocomposite Scaffolds. 6.
- EINHORN, T. A. 2003. COX-2: where are we in 2003? The role of cyclooxygenase-2 in bone repair. *Arthritis Research & Therapy*, 5, 5-7.
- ENGLER, A. J., SEN, S., SWEENEY, H. L. & DISCHER, D. E. 2006. Matrix elasticity directs stem cell lineage specification. *Cell*, 126, 677-689.
- FANG, B., WAN, Y.-Z., TANG, T.-T., GAO, C. & DAI, K.-R. 2009. Proliferation and Osteoblastic Differentiation of Human Bone Marrow Stromal Cells on Hydroxyapatite/Bacterial Cellulose Nanocomposite Scaffolds. *Tissue Engineering Part A*, 15, 1091-1098.
- FERGUSON, M. W. J. 1988. PALATE DEVELOPMENT. *Development*, 103, 41-60.
- FREY, S. P., JANSEN, H., DOHT, S., FILGUEIRA, L. & ZELLWEGER, R. 2013. Immunohistochemical and molecular characterization of the human periosteum. *TheScientificWorldJournal*, 2013, 341078-341078.
- FRIDRIKH, S. V., YU, J. H., BRENNER, M. P. & RUTLEDGE, G. C. 2003. Controlling the fiber diameter during electrospinning. *Physical Review Letters*, 90.
- FROHBERGH, M. E., KATSMAN, A., BOTTA, G. R., LAZAROVICI, P., SCHAUER, C. L., WEGST, U. G. K. & LELKES, P. I. 2012. Electrospun hydroxyapatite-containing chitosan nanofibers crosslinked with genipin for bone tissue engineering. *Biomaterials*, 33, 9167-9178.
- FROST, H. M. 1994. Wolff law and bones structural adaptations to mechanical usage-an overview for clinician. *Angle Orthodontist*, 64, 175-188.
- FUJII, T., UENO, T., KAGAWA, T., SAKATA, Y. & SUGAHARA, T. 2006. Comparison of bone formation ingrafted periosteum harvested from tibia and calvaria. *Microscopy Research and Technique*, 69, 580-584.
- FUJITA, J. 1999. Cold shock response in mammalian cells. *Journal of Molecular Microbiology and Biotechnology*, 1, 243-255.
- FURUMATSU, T., SHEN, Z. N., KAWAI, A., NISHIDA, K., MANABE, H., OOHASHI, T., INOUE, H. & NINOMIYA, Y. 2003. Vascular endothelial growth factor principally acts as the main angiogenic factor in the early stage of human osteoblastogenesis. *Journal of Biochemistry*, 133, 633-639.
- GEESIN, J. C., DARR, D., KAUFMAN, R., MURAD, S. & PINNELL, S. R. 1988. ASCORBIC-ACID SPECIFICALLY INCREASES TYPE-I AND TYPE-III PROCOLLAGEN MESSENGER-RNA LEVELS IN HUMAN-SKIN FIBROBLASTS. *Journal of Investigative Dermatology*, 90, 420-424.
- GEORGE, J., KUBOKI, Y. & MIYATA, T. 2006. Differentiation of mesenchymal stem cells into osteoblasts on honeycomb collagen scaffolds. *Biotechnology and Bioengineering*, 95, 404-411.
- GLUCKSMANN, A. 1942. The role of mechanical stresses in bone formation in vitro. *Journal of Anatomy*, 76, 231-239.
- GOGOLEWSKI, S., JOVANOVIĆ, M., PERREN, S. M., DILLON, J. G. & HUGHES, M. K. 1993. Tissue-response and *in-vivo* degradation of selected polyhydroxyacids-poly(lactides) (PLA), poly(3-hydroxybutyrate) (PHB), and poly(3-hydroxybutyrate-co-3-hydroxyvalerate) (PHB/VA). *Journal of Biomedical Materials Research*, 27, 1135-1148.

## REFERENCES

- GRAYSON, W. L., BHUMIRATANA, S., CANNIZZARO, C., CHAO, P. H. G., LENNON, D. P., CAPLAN, A. I. & VUNJAK-NOVAKOVIC, G. 2008. Effects of initial seeding density and fluid perfusion rate on formation of tissue-engineered bone. *Tissue Engineering Part A*, 14, 1809-1820.
- GUAN, J. J., FUJIMOTO, K. L., SACKS, M. S. & WAGNER, W. R. 2005. Preparation and characterization of highly porous, biodegradable polyurethane scaffolds for soft tissue applications. *Biomaterials*, 26, 3961-3971.
- GUELCHER, S. A. 2008. Biodegradable polyurethanes: Synthesis and applications in regenerative medicine. *Tissue Engineering Part B-Reviews*, 14, 3-17.
- GUNATILLAKE, P. A. & ADHIKARI, R. 2003. Biodegradable synthetic polymers for tissue engineering. *European Cells & Materials*, 5, 1-16.
- GURKAN, U. A. & AKKUS, O. 2008. The mechanical environment of bone marrow: a review. *Annals of Biomedical Engineering*, 36, 1978-1991.
- HAHN, M., VOGEL, M., POMPESIUSKEMPA, M. & DELLING, G. 1992. TRABECULAR BONE PATTERN FACTOR - A NEW PARAMETER FOR SIMPLE QUANTIFICATION OF BONE MICROARCHITECTURE. *Bone*, 13, 327-330.
- HE, J., GENETOS, D. C. & LEACH, J. K. 2010. Osteogenesis and Trophic Factor Secretion are Influenced by the Composition of Hydroxyapatite/Poly(Lactide-Co-Glycolide) Composite Scaffolds. *Tissue Engineering Part A*, 16, 127-137.
- HE, P., SAHOO, S., NG, K. S., CHEN, K., TOH, S. L. & GOH, J. C. H. 2013. Enhanced osteoinductivity and osteoconductivity through hydroxyapatite coating of silk-based tissue-engineered ligament scaffold. *Journal of Biomedical Materials Research Part A*, 101A, 555-566.
- HEISS, J. D., PAPAVALASSIOU, E., MERRILL, M. J., NIEMAN, L., KNIGHTLY, J. J., WALBRIDGE, S., EDWARDS, N. A. & OLDFIELD, E. H. 1996. Mechanism of dexamethasone suppression of brain tumor-associated vascular permeability in rats - Involvement of the glucocorticoid receptor and vascular permeability factor. *Journal of Clinical Investigation*, 98, 1400-1408.
- HENG, B. C., CAO, T., STANTON, L. W., ROBSON, P. & OLSEN, B. 2004. Strategies for directing the differentiation of stem cells into the osteogenic lineage in vitro. *Journal of Bone and Mineral Research*, 19, 1379-1394.
- HERMANN, C., ZEIHNER, A. M. & DIMMELER, S. 1997. Shear stress inhibits H<sub>2</sub>O<sub>2</sub>-induced apoptosis of human endothelial cells by modulation of the glutathione redox cycle and nitric oxide synthase. *Arteriosclerosis Thrombosis and Vascular Biology*, 17, 3588-3592.
- HIBI, H., YAMADA, Y., UEDA, M. & ENDO, Y. 2006. Alveolar cleft osteoplasty using tissue-engineered osteogenic material. *International Journal of Oral and Maxillofacial Surgery*, 35, 551-555.
- HILD, N., SCHNEIDER, O. D., MOHN, D., LUECHINGER, N. A., KOEHLER, F. M., HOFMANN, S., VETSCH, J. R., THIMM, B. W., MUELLER, R. & STARK, W. J. 2011. Two-layer membranes of calcium phosphate/collagen/PLGA nanofibres: in vitro biomineralisation and osteogenic differentiation of human mesenchymal stem cells. *Nanoscale*, 3, 401-409.
- HITOMI, K., TORII, Y. & TSUKAGOSHI, N. 1992. INCREASE IN THE ACTIVITY OF ALKALINE-PHOSPHATASE BY L-ASCORBIC-ACID 2-PHOSPHATE IN A HUMAN OSTEOBLAST CELL-LINE, HUO-3N1. *Journal of Nutritional Science and Vitaminology*, 38, 535-544.
- HOEY, D. A., TORMEY, S., RAMCHARAN, S., O'BRIEN, F. J. & JACOBS, C. R. 2012. Primary cilia-mediated mechanotransduction in human mesenchymal stem cells. *Stem Cells*, 30, 2561-2570.
- HOLLAND, S. J., JOLLY, A. M., YASIN, M. & TIGHE, B. J. 1987. Polymers for biodegradable medical devices .2. hydroxybutyrate-hydroxyvalerate copolymers-hydrolytic degradation studies *Biomaterials*, 8, 289-295.
- HUTMACHER, D. W., SCHANTZ, T., ZEIN, I., NG, K. W., TEOH, S. H. & TAN, K. C. 2001. Mechanical properties and cell cultural response of polycaprolactone scaffolds designed and fabricated via fused deposition modeling. *Journal of Biomedical Materials Research*, 55, 203-216.

## REFERENCES

- INGBER, D. E. 2006. Cellular mechanotransduction: putting all the pieces together again. *Faseb Journal*, 20, 811-827.
- ISHIKAWA, K., DUCHEYNE, P. & RADIN, S. 1993. Determination of the Ca/P ratio in calcium-deficient hydroxyapatite using x-ray diffraction analysis. *Journal of Materials Science-Materials in Medicine*, 4, 165-168.
- JACOBS, C. R., YELLOWLEY, C. E., DAVIS, B. R., ZHOU, Z., CIMBALA, J. M. & DONAHUE, H. J. 1998. Differential effect of steady versus oscillating flow on bone cells. *Journal of Biomechanics*, 31, 969-976.
- JAISWAL, A. K., CHANDRA, V., BHONDE, R. R., SONI, V. P. & BELLARE, J. R. 2012. Mineralization of nanohydroxyapatite on electrospun poly(L-lactic acid)/gelatin by an alternate soaking process: A biomimetic scaffold for bone regeneration. *Journal of Bioactive and Compatible Polymers*, 27, 356-374.
- JAISWAL, R. K., JAISWAL, N., BRUDER, S. P., MBALAVIELE, G., MARSHAK, D. R. & PITTENGER, M. F. 2000. Adult human mesenchymal stem cell differentiation to the osteogenic or adipogenic lineage is regulated by mitogen-activated protein kinase. *Journal of Biological Chemistry*, 275, 9645-9652.
- JANMEY, P. A. & MCCULLOCH, C. A. 2007. Cell mechanics: Integrating cell responses to mechanical stimuli. *Annual Review of Biomedical Engineering*, 9, 1-34.
- JAQUIERY, C., SCHAEREN, S., FARHADI, J., MAINIL-VARLET, P., KUNZ, C., ZEILHOFER, H. F., HEBERER, M. & MARTIN, I. 2005. In vitro osteogenic differentiation and in vivo bone-forming capacity of human isogenic jaw periosteal cells and bone marrow stromal cells. *Annals of Surgery*, 242, 859-868.
- JEON, O. H., JEONG, S. H., YOO, Y.-M., KIM, K. H., YOON, D. S. & KIM, C. H. 2012. Quantification of temporal changes in 3D osteoclastic resorption pit using confocal laser scanning microscopy. *Tissue Engineering and Regenerative Medicine*, 9, 29-35.
- JHA, B. S., AYRES, C. E., BOWMAN, J. R., TELEMECO, T. A., SELL, S. A., BOWLIN, G. L. & SIMPSON, D. G. 2011. Electrospun Collagen: A Tissue Engineering Scaffold with Unique Functional Properties in a Wide Variety of Applications. *Journal of Nanomaterials*.
- Jl, Y., LI, X.-T. & CHEN, G.-Q. 2008. Interactions between a poly(3-hydroxybutyrate-co-3-hydroxyvalerate-co-3-hydroxyhexanoate) terpolyester and human keratinocytes. *Biomaterials*, 29, 3807-3814.
- JILKA, R. L., WEINSTEIN, R. S., BELLIDO, T., PARFITT, A. M. & MANOLAGAS, S. C. 1998. Osteoblast programmed cell death (apoptosis): Modulation by growth factors and cytokines. *Journal of Bone and Mineral Research*, 13, 793-802.
- JONAT, C., RAHMSDORF, H. J., PARK, K. K., CATO, A. C. B., GEBEL, S., PONTA, H. & HERRLICH, P. 1990. Antitumor promotion and antiinflammation-down-modulation of AP-1 (fos jun) activity by glucocorticoid hormone. *Cell*, 62, 1189-1204.
- JORGENSEN, N. R., HENRIKSEN, Z., SORENSEN, O. H. & CIVITELLI, R. 2004. Dexamethasone, BMP-2, and 1,25-dihydroxyvitamin D enhance a more differentiated osteoblast phenotype: validation of an in vitro model for human bone marrow-derived primary osteoblasts. *Steroids*, 69, 219-226.
- KANCZLER, J. M. & OREFFO, R. O. C. 2008. Osteogenesis and angiogenesis: The potential for engineering bone. *European Cells & Materials*, 15, 100-114.
- KARAGEORGIU, V. & KAPLAN, D. 2005. Porosity of 3D biomaterial scaffolds and osteogenesis. *Biomaterials*, 26, 5474-5491.
- KARLSSON, C., EMANUELSSON, K., WESSBERG, F., KAJIC, K., AXELL, M. Z., ERIKSSON, P. S., LINDAHL, A., HYLLNER, J. & STREHL, R. 2009. Human embryonic stem cell-derived mesenchymal progenitors-Potential in regenerative medicine. *Stem Cell Research*, 3, 39-50.

## REFERENCES

- KARNER, E., UNGER, C., SLOAN, A. J., AHRLUND-RICHTER, L., SUGARS, R. V. & WENDEL, M. 2007. Bone matrix formation in osteogenic cultures derived from human embryonic stem cells in vitro. *Stem Cells and Development*, 16, 39-52.
- KATTA, P., ALESSANDRO, M., RAMSIER, R. D. & CHASE, G. G. 2004. Continuous electrospinning of aligned polymer nanofibers onto a wire drum collector. *Nano Letters*, 4, 2215-2218.
- KAVEH, K., IBRAHIM, R., ABU BAKAR, M. Z. & IBRAHIM, T. A. 2011. Mesenchymal Stem Cells, Osteogenic Lineage and Bone Tissue Engineering: A Review. *Journal of Animal and Veterinary Advances*, 10, 2317-2330.
- KHOO, M. L. M., SHEN, B., TAO, H. & MA, D. D. F. 2008. Long-Term Serial Passage and Neuronal Differentiation Capability of Human Bone Marrow Mesenchymal Stem Cells. *Stem Cells and Development*, 17, 883-896.
- KIM, B. I., JEONG, S. H., JANG, S. O., KIM, K. N., KWON, H. K. & PARK, Y. D. 2006a. Tooth whitening effect of toothpastes containing nano-hydroxyapatite.
- KIM, H.-W., LEE, H.-H. & KNOWLES, J. C. 2006b. Electrospinning biomedical nanocomposite fibers of hydroxyapatite/poly(lactic acid) for bone regeneration. *Journal of Biomedical Materials Research Part A*, 79A, 643-649.
- KINI, U. & NANDEESH, B. N. 2012. Physiology of bone formation, remodelling, and metabolism. In: FOGELMAN, I., GNANASEGEGARAN, G. & VAN DER WALL, H. (eds.) *Radionuclide and hybrid bone imaging*. Berlin, German: Springer.
- KJAER, M., MAGNUSSON, P., KROGSGAARD, M., MOLLER, J. B., OLESEN, J., HEINEMEIER, K., HANSEN, M., HARALDSSON, B., KOSKINEN, S., ESMARCK, B. & LANGBERG, H. 2006. Extracellular matrix adaptation of tendon and skeletal muscle to exercise. *Journal of Anatomy*, 208, 445-450.
- KLAMMERT, U., REUTHER, T., JAHN, C., KRASKI, B., KUEBLER, A. C. & GBURECK, U. 2009. Cytocompatibility of brushite and monetite cell culture scaffolds made by three-dimensional powder printing. *Acta Biomaterialia*, 5, 727-734.
- KLEIN, B. Y., GAL, I. & BENBASSAT, H. 1996. Cell-mediated mineralization in culture at low temperature associated with subtle thermogenic response. *Journal of Cellular Biochemistry*, 63, 229-238.
- KLEINMAN, H. K., KLEBE, R. J. & MARTIN, G. R. 1981. Role of collagenous matrices in the adhesion and growth of cells. *Journal of Cell Biology*, 88, 473-485.
- KOTNIS, M. A., OBRIEN, G. S. & WILLETT, J. L. 1995. Processing and mechanical-properties of biodegradable poly(hydroxybutyrate-co-valerate)-starch compositions. *Journal of Environmental Polymer Degradation*, 3, 97-105.
- KREKE, M. R., HUCKLE, W. R. & GOLDSTEIN, A. S. 2005. Fluid flow stimulates expression of osteopontin and bone sialoprotein by bone marrow stromal cells in a temporally dependent manner. *Bone*, 36, 1047-1055.
- KUHN, L. T., LIU, Y., ADVINCULA, M., WANG, Y.-H., MAYE, P. & GOLDBERG, A. J. 2010. A Nondestructive Method for Evaluating In Vitro Osteoblast Differentiation on Biomaterials Using Osteoblast-Specific Fluorescence. *Tissue Engineering Part C-Methods*, 16, 1357-1366.
- KWON, R. Y., MEAYS, D. R., TANG, W. J. & FRANGOS, J. A. 2010. Microfluidic enhancement of intramedullary pressure increases interstitial fluid flow and inhibits bone loss in hindlimb suspended mice. *Journal of Bone and Mineral Research*, 25, 1798-1807.
- LABAR, B., SUCIU, S., WILLEMZE, R., MUUS, P., MARIE, J.-P., FILLET, G., BERNEMAN, Z., JAKSIC, B., FEREMANS, W., BRON, D., SINNIGE, H., MISTRIK, M., VREUGDENHIL, G., DE BOCK, R., NEMET, D., GILOTAY, C., AMADORI, S., DE WITTE, T. & GRP, E. L. 2010. Dexamethasone compared to prednisolone for adults with acute lymphoblastic leukemia or lymphoblastic lymphoma: final results of the ALL-4 randomized, phase III trial of the EORTC Leukemia Group. *Haematologica-the Hematology Journal*, 95, 1489-1495.

## REFERENCES

- LAMOUREUX, F., BAUD'HUIN, M., DUPLOMB, L., HEYMANN, D. & REDINI, F. 2007. Proteoglycans: key partners in bone cell biology. *Bioessays*, 29, 758-771.
- LANGER, R. & TIRRELL, D. A. 2004. Designing materials for biology and medicine. *Nature*, 428, 487-492.
- LAO, L., WANG, Y., ZHU, Y., ZHANG, Y. & GAO, C. 2011. Poly(lactide-co-glycolide)/hydroxyapatite nanofibrous scaffolds fabricated by electrospinning for bone tissue engineering. *Journal of Materials Science-Materials in Medicine*, 22, 1873-1884.
- LEE, H., PARK, J. B., LEE, S., BAEK, S., KIM, H. & KIM, S. J. 2013. Intra-osseous injection of donor mesenchymal stem cell (MSC) into the bone marrow in living donor kidney transplantation; a pilot study. *Journal of Translational Medicine*, 11.
- LEUKERS, B., GULKAN, H., IRSEN, S. H., MILZ, S., TILLE, C., SCHIEKER, M. & SEITZ, H. 2005. Hydroxyapatite scaffolds for bone tissue engineering made by 3D printing. *Journal of Materials Science-Materials in Medicine*, 16, 1121-1124.
- LEVY, S., VAN DALEN, M., AGONAFER, S. & SOBOYEJO, W. O. 2007. Cell/surface interactions and adhesion on bioactive glass 45S5. *Journal of Materials Science-Materials in Medicine*, 18, 89-102.
- LI, C. Y., YANG, X. J., ZHANG, L. Y., CHEN, M. F. & CUI, Z. D. 2007. In vivo histological evaluation of bioactive NiTi alloy after two years implantation. *Materials Science & Engineering C-Biomimetic and Supramolecular Systems*, 27, 122-126.
- LI, J., DOU, Y., YANG, J., YIN, Y., ZHANG, H., YAO, F., WANG, H. & YAO, K. 2009. Surface characterization and biocompatibility of micro- and nano-hydroxyapatite / chitosan-gelatin network films. *Materials Science & Engineering C-Biomimetic and Supramolecular Systems*, 29, 1207-1215.
- LI, S., PIOTROWICZ, R. S., LEVIN, E. G., SHYY, Y. J. & CHIEN, S. 1996. Fluid shear stress induces the phosphorylation of small heat shock proteins in vascular endothelial cells. *American Journal of Physiology-Cell Physiology*, 271, C994-C1000.
- LI, X. D., JIN, L., CUI, Q. J., WANG, G. J. & BALIAN, G. 2005. Steroid effects on osteogenesis through mesenchymal cell gene expression. *Osteoporosis International*, 16, 101-108.
- LI, Y. J., BATRA, N. N., YOU, L. D., MEIER, S. C., COE, I. A., YELLOWLEY, C. E. & JACOBS, C. R. 2004. Oscillatory fluid flow affects human marrow stromal cell proliferation and differentiation. *Journal of Orthopaedic Research*, 22, 1283-1289.
- LIAN, J. B. & STEIN, G. S. 1995. Development of the osteoblast phenotype: molecular mechanisms mediating osteoblast growth and differentiation. *The Iowa orthopaedic journal*, 15, 118-40.
- LIDRAL, A. C. & MURRAY, J. C. 2004. Genetic approaches to identify disease genes for birth defects with cleft lip/palate as a model. *Birth Defects Research Part a-Clinical and Molecular Teratology*, 70, 893-901.
- LIM, K. T., KIM, J., SEONWOO, H., CHANG, J. U., CHOI, H., HEXIU, J., CHO, W. J., CHOUNG, P. H. & CHUNG, J. H. 2013. Enhanced Osteogenesis of Human Alveolar Bone-Derived Mesenchymal Stem Cells for Tooth Tissue Engineering Using Fluid Shear Stress in a Rocking Culture Method. *Tissue Engineering Part C-Methods*, 19, 128-145.
- LIN, L., CHOW, L. & LENG, Y. 2009. Study of hydroxyapatite osteoinductivity with an osteogenic differentiation of mesenchymal stem cells. *Journal of Biomedical Materials Research Part A*, 89A, 326-335.
- LIU, L., YUAN, W. & WANG, J. 2010. Mechanisms for osteogenic differentiation of human mesenchymal stem cells induced by fluid shear stress. *Biomechanics and Modeling in Mechanobiology*, 9, 659-670.
- LIU, W., THOMOPOULOS, S. & XIA, Y. 2012. Electrospun nanofibers for regenerative medicine. *Advanced Healthcare Materials*, 1, 10-25.
- LOHBERGER, B., PAYER, M., RINNER, B., KALTENEGGER, H., WOLF, E., SCHALLMOSER, K., STRUNK, D., ROHDE, E., BERGHOLD, A., PEKOVITS, K., WILDBURGER, A., LEITHNER, A., WINDHAGER,

## REFERENCES

- R. & JAKSE, N. 2013. Tr-lineage potential of intraoral tissue-derived mesenchymal stromal cells. *Journal of Cranio-Maxillofacial Surgery*, 41, 110-118.
- LU, H. B., CAMPBELL, C. T., GRAHAM, D. J. & RATNER, B. D. 2000. Surface characterization of hydroxyapatite and related calcium phosphates by XPS and TOF-SIMS. *Analytical Chemistry*, 72, 2886-2894.
- LU, T., LI, Y. & CHEN, T. 2013. Techniques for fabrication and construction of three-dimensional scaffolds for tissue engineering. *International Journal of Nanomedicine*, 8, 337-350.
- LUU, Y. K., KIM, K., HSIAO, B. S., CHU, B. & HADJIARGYROU, M. 2003. Development of a nanostructured DNA delivery scaffold via electrospinning of PLGA and PLA-PEG block copolymers. *Journal of Controlled Release*, 89, 341-353.
- MA, J., HE, X. & JABBARI, E. 2011. Osteogenic differentiation of marrow stromal cells on random and aligned electrospun poly(L-lactide) nanofibers. *Annals of Biomedical Engineering*, 39, 14-25.
- MA, P. X. & ZHANG, R. 1999. Synthetic nano-scale fibrous extracellular matrix. *Journal of Biomedical Materials Research*, 46, 60-72.
- MA, S., YANG, Y., CARNES, D. L., KIM, K., PARK, S., OH, S. H. & ONG, J. L. 2005. Effects of dissolved calcium and phosphorous on osteoblast responses. *The Journal of oral implantology*, 31, 61-7.
- MACHEIN, M. R., KULLMER, J., RONICKE, V., MACHEIN, U., KRIEG, M., DAMERT, A., BREIER, G., RISAU, W. & PLATE, K. H. 1999. Differential downregulation of vascular endothelial growth factor by dexamethasone in normoxic and hypoxic rat glioma cells. *Neuropathology and Applied Neurobiology*, 25, 104-112.
- MAENO, S., NIKI, Y., MATSUMOTO, H., MORIOKA, H., YATABE, T., FUNAYAMA, A., TOYAMA, Y., TAGUCHI, T. & TANAKA, J. 2005. The effect of calcium ion concentration on osteoblast viability, proliferation and differentiation in monolayer and 3D culture. *Biomaterials*, 26, 4847-4855.
- MAES, C. & CARMELIET, G. 2008. Vascular and nonvascular roles of VEGF in bone development. *Molecular Biology Intelligence Unit*, 79-90.
- MALGORZATA, W.-Z. 2012. Biochemistry, Genetics and Molecular biology. In: YUNFENG, L. (ed.) *Transcriptional control of osteogenesis*. Intech open science: Intech open science.
- MALLADI, P., XU, Y., CHIOU, M., GIACCIA, A. J. & LONGAKER, M. T. 2006. Effect of reduced oxygen tension on chondrogenesis and osteogenesis in adipose-derived mesenchymal cells. *American Journal of Physiology-Cell Physiology*, 290, C1139-C1145.
- MAROLT, D., KNEZEVIC, M. & NOVAKOVIC, G. V. 2010. Bone tissue engineering with human stem cells. *Stem Cell Research & Therapy*, 1.
- MARTINEZ-ALVAREZ, C., BONELLI, R., TUDELA, C., GATO, A., MENA, J., O'KANE, S. & FERGUSON, M. W. J. 2000. Bulging medial edge epithelial cells and palatal fusion. *International Journal of Developmental Biology*, 44, 331-335.
- MAUNEY, J. R., SJOSTORM, S., BLUMBERG, J., HORAN, R., O'LEARY, J. P., VUNJAK-NOVAKOVIC, G., VOLLOCH, V. & KAPLAN, D. L. 2004. Mechanical stimulation promotes osteogenic differentiation of human bone marrow stromal cells on 3-D partially demineralized bone scaffolds in vitro. *Calcified Tissue International*, 74, 458-468.
- MCCOY, R. J. & O'BRIEN, F. J. 2010. Influence of shear stress in perfusion bioreactor cultures for the development of three-dimensional bone tissue constructs: a review. *Tissue Engineering Part B-Reviews*, 16, 587-601.
- MEHRABANIAN, M. & NASR-ESFAHANI, M. 2011. HA/nylon 6,6 porous scaffolds fabricated by salt-leaching/solvent casting technique: effect of nano-sized filler content on scaffold properties. *International Journal of Nanomedicine*, 6, 1651-1659.
- MEIJER, G. J., DE BRUIJN, J. D., KOOLE, R. & VAN BLITTERSWIJK, C. A. 2008. Cell based bone tissue engineering in jaw defects. *Biomaterials*, 29, 3053-3061.

## REFERENCES

- MENG, Z. X., LI, H. F., SUN, Z. Z., ZHENG, W. & ZHENG, Y. F. 2013. Fabrication of mineralized electrospun PLGA and PLGA/gelatin nanofibers and their potential in bone tissue engineering. *Materials Science & Engineering C-Materials for Biological Applications*, 33, 699-706.
- MI, L. Y., BASU, M., FRITTON, S. P. & COWIN, S. C. 2005. Analysis of avian bone response to mechanical loading, Part Two: Development of a computational connected cellular network to study bone intercellular communication. *Biomechanics and Modeling in Mechanobiology*, 4, 132-146.
- MIAO, X., TAN, D. M., LI, J., XIAO, Y. & CRAWFORD, R. 2008. Mechanical and biological properties of hydroxyapatite/tricalcium phosphate scaffolds coated with poly(lactic-co-glycolic acid). *Acta Biomaterialia*, 4, 638-645.
- MIN, J.-H., KO, S.-Y., CHO, Y.-B., RYU, C.-J. & JANG, Y.-J. 2011. Dentinogenic potential of human adult dental pulp cells during the extended primary culture. *Human Cell*, 24, 43-50.
- MISHRA, N., GOYAL, A. K., KHATRI, K., VAIDYA, B., PALIWAL, R., RAI, S., MEHTA, A., TIWARI, S., VYAS, S. & VYAS, S. P. 2008. Biodegradable polymer based particulate carrier(s) for the delivery of proteins and peptides. *Anti-Inflammatory & Anti-Allergy Agents in Medicinal Chemistry*, 7, 240-251.
- MOSSEY, P. A., LITTLE, J., MUNGER, R. G., DIXON, M. J. & SHAW, W. C. 2009. Cleft lip and palate. *Lancet*, 374, 1773-1785.
- MOY, P. K., LUNDGREN, S. & HOLMES, R. E. 1993. Maxillary sinus augmentation-histomorphometric analysis of graft materials for maxillary sinus floor augmentation. *Journal of Oral and Maxillofacial Surgery*, 51, 857-862.
- MURRAY, J. C. 2002. Gene/environment causes of cleft lip and/or palate. *Clinical Genetics*, 61, 248-256.
- NAKAMURA, S., YAMADA, Y., BABA, S., KATO, H., KOGAMI, H., TAKAO, M., MATSUMOTO, N. & UEDA, M. 2008. Culture medium study of human mesenchymal stem cells for practical use of tissue engineering and regenerative medicine. *Bio-Medical Materials and Engineering*, 18, 129-136.
- NANDAKUMAR, A., FERNANDES, H., DE BOER, J., MORONI, L., HABIBOVIC, P. & VAN BLITTERSWIJK, C. A. 2010. Fabrication of bioactive composite scaffolds by electrospinning for bone regeneration. *Macromolecular Bioscience*, 10, 1365-1373.
- NAUMAN, E. A., SATCHER, R. L., KEAVENY, T. M., HALLORAN, B. P. & BIKLE, D. D. 2001. Osteoblasts respond to pulsatile fluid flow with shortterm increases in PGE(2) but no change in mineralization. *Journal of Applied Physiology*, 90, 1849-1854.
- NEUTELINGS, T., LAMBERT, C. A., NUSGENS, B. V. & COLIGE, A. C. 2013. Effects of Mild Cold Shock (25 degrees C) Followed by Warming Up at 37 degrees C on the Cellular Stress Response. *Plos One*, 8.
- NOHUTCU, R. M., MCCAULEY, L. K., KOH, A. J. & SOMERMAN, M. J. 1997. Expression of extracellular matrix proteins in human periodontal ligament cells during mineralization in vitro. *Journal of Periodontology*, 68, 320-327.
- O'BRIEN, J., WILSON, I., ORTON, T. & POGNAN, F. 2000. Investigation of the Alamar Blue (resazurin) fluorescent dye for the assessment of mammalian cell cytotoxicity. *European Journal of Biochemistry*, 267, 5421-5426.
- OGATA, K., SATOH, C., TACHIBANA, M., HYODO, H., TAMURA, H., DAN, K., KIMURA, T., SONODA, Y. & TSUJI, T. 2005. Identification and hematopoietic potential of CD45(-) clonal cells with very immature phenotype (CD45(-)CD34(-)CD38(-)Lin(-)) in patients with myelodysplastic syndromes. *Stem Cells*, 23, 619-630.
- OGURA, N., KAWADA, M., CHANG, W.-J., ZHANG, Q., LEE, S.-Y., KONDOH, T. & ABIKO, Y. 2004. Differentiation of the human mesenchymal stem cells derived from bone marrow and enhancement of cell attachment by fibronectin. *Journal of oral science*, 46, 207-13.

## REFERENCES

- OLBRICH, M., RIEGER, M., REINERT, S. & ALEXANDER, D. 2012. Isolation of osteoprogenitors from human jaw periosteal cells: a comparison of two magnetic separation methods. *Plos One*, 7.
- OLIVEIRA, J. M., RODRIGUES, M. T., SILVA, S. S., MALAFAYA, P. B., GOMES, M. E., VIEGAS, C. A., DIAS, I. R., AZEVEDO, J. T., MANO, J. F. & REIS, R. L. 2006. Novel hydroxyapatite/chitosan bilayered scaffold for osteochondral tissue-engineering applications: Scaffold design and its performance when seeded with goat bone marrow stromal cells. *Biomaterials*, 27, 6123-6137.
- ORIMO, H. 2010. The Mechanism of Mineralization and the Role of Alkaline Phosphatase in Health and Disease. *Journal of Nippon Medical School*, 77, 4-12.
- ORR, A. W., HELMKE, B. P., BLACKMAN, B. R. & SCHWARTZ, M. A. 2006. Mechanisms of mechanotransduction. *Developmental Cell*, 10, 11-20.
- ORTIZMON.F, SERRANO, A., BARRERA, G., RODRIGUE.H & VINAGERA.E 1966. A study of untreated adult cleft palate patients. *Plastic and Reconstructive Surgery*, 38, 36-&.
- OSIPOVA, E. Y., SHAMANSKAYA, T. V., KURAKINA, O. A., NIKITINA, V. A., PURBUEVA, B. B., USTUGOV, A. Y., KACHANOV, D. Y., SKOROBOGATOVA, E. V., DISHLEVAYA, Z. M. & ROUMIANTSEV, S. A. 2011. Biological characteristics of mesenchymal stem cells during Ex Vivo expansion. 1.
- OSYCZKA, A. M., DAMEK-POPRAWA, M., WOJTOWICZ, A. & AKINTOYE, S. O. 2009. Age and skeletal sites affect BMP-2 responsiveness of human bone marrow stromal cells. *Connective Tissue Research*, 50, 270-277.
- OTROCK, Z. K., MAKAREM, J. A. & SHAMSEDDINE, A. I. 2007. Vascular endothelial growth factor family of ligands and receptors: Review. *Blood Cells Molecules and Diseases*, 38, 258-268.
- OTSU, N. 1979. A threshold selection method from Grey-Level Histograms. 9.
- OYANE, A., UCHIDA, M., CHOONG, C., TRIFFITT, J., JONES, J. & ITO, A. 2005. Simple surface modification of poly(epsilon-caprolactone) for apatite deposition from simulated body fluid. *Biomaterials*, 26, 2407-2413.
- PARK, J.-B., BAE, S.-S., LEE, P.-W., LEE, W., PARK, Y.-H., KIM, H., LEE, K. & KIM, I. 2012. Comparison of Stem Cells Derived from Periosteum and Bone Marrow of Jaw Bone and Long Bone in Rabbit Models. *Tissue Engineering and Regenerative Medicine*, 9, 224-230.
- PARKINSON, I. H., BADIEI, A. & FAZZALARI, N. L. 2008. Variation in segmentation of bone from micro-CT imaging: implications for quantitative morphometric analysis. *Australasian Physical & Engineering Sciences in Medicine*, 31, 160-164.
- PAYNE, K. F. B., BALASUNDARAM, I., DEB, S., DI SILVIO, L. & FAN, K. F. M. 2014. Tissue engineering technology and its possible applications in oral and maxillofacial surgery. *British Journal of Oral & Maxillofacial Surgery*, 52, 7-15.
- PEDERSEN, J. A. & SWARTZ, M. A. 2005. Mechanobiology in the third dimension. *Annals of Biomedical Engineering*, 33, 1469-1490.
- PETER, B. & PETER, B. 2009. Quantifying Cytotoxicity of Thiostrepton on Mesothelioma Cells using MTT Assay and the Epoch™ Microplate Spectrophotometer. 10-Dec-09 ed.: Application note, BioTek Instruments, INS., Winooski, Vermont, 05404.
- PETERS, H., NEUBUSER, A., KRATOCHWIL, K. & BALLING, R. 1998. Pax9-deficient mice lack pharyngeal pouch derivatives and teeth and exhibit craniofacial and limb abnormalities. *Genes & Development*, 12, 2735-2747.
- PETERSON-FALZONE, S. J., HARDIN-JONES, M. A. & KARNELL, M. P. 2001. *Cleft palate speech*, St. Louis, Missouri, Mosby.
- PHAM, I., UCHIDA, T., PLANES, C., WARE, L. B., KANER, R., MATTHAY, M. A. & CLERICI, C. 2002. Hypoxia upregulates VEGF expression in alveolar epithelial cells in vitro and in vivo. *American Journal of Physiology-Lung Cellular and Molecular Physiology*, 283, L1133-L1142.

## REFERENCES

- PHILLIPS, C. L., COMBS, S. B. & PINNELL, S. R. 1994. Effects of ascorbic acid on proliferation and collagen-synthesis in relation to the donor age of human dermal fibroblasts. *Journal of Investigative Dermatology*, 103, 228-232.
- PINNELL, S. R. 1985. REGULATION OF COLLAGEN BIOSYNTHESIS BY ASCORBIC-ACID - A REVIEW. *Yale Journal of Biology and Medicine*, 58, 553-559.
- POLINI, A., PISIGNANO, D., PARODI, M., QUARTO, R. & SCAGLIONE, S. 2011. Osteoinduction of Human Mesenchymal Stem Cells by Bioactive Composite Scaffolds without Supplemental Osteogenic Growth Factors. *Plos One*, 6.
- POMMERENKE, H., SCHMIDT, C., DURR, F., NEBE, B., LUTHEN, F., MULLER, P. & RYCHLY, J. 2002. The mode of mechanical integrin stressing controls intracellular signaling in osteoblasts. *Journal of Bone and Mineral Research*, 17, 603-611.
- PRYDSO, U., HOLM, P. C. A., DAHL, E. & FOGHANDERSEN, P. 1974. Bone-formation in palatal cleft subsequent to palato-vomer plasty-influence on transverse maxillary growth *Scandinavian Journal of Plastic and Reconstructive Surgery and Hand Surgery*, 8, 73-78.
- PUELACHER, W. C., VACANTI, J. P., FERRARO, N. F., SCHLOO, B. & VACANTI, C. A. 1996. Femoral shaft reconstruction using tissue-engineered growth of bone. *International Journal of Oral and Maxillofacial Surgery*, 25, 223-228.
- RAMASAMY, R., TONG, C. K., YIP, W. K., VELLASAMY, S., TAN, B. C. & SEOW, H. F. 2012. Basic fibroblast growth factor modulates cell cycle of human umbilical cord-derived mesenchymal stem cells. *Cell Proliferation*, 45, 132-139.
- REED, C. R., HAN, L., ANDRADY, A., CABALLERO, M., JACK, M. C., COLLINS, J. B., SABA, S. C., LOBOA, E. G., CAIRNS, B. A. & VAN AALST, J. A. 2009. Composite tissue engineering on polycaprolactone nanofiber scaffolds. *Annals of Plastic Surgery*, 62, 505-512.
- REHMAN, I. & BONFIELD, W. 1997. Characterization of hydroxyapatite and carbonated apatite by photo acoustic FTIR spectroscopy. *Journal of Materials Science-Materials in Medicine*, 8, 1-4.
- REILLY, G. C., HAUT, T. R., YELLOWLEY, C. E., DONAHUE, H. J. & JACOBS, C. R. 2003. Fluid flow induced PGE(2) release by bone cells is reduced by glycocalyx degradation whereas calcium signals are not. *Biorheology*, 40, 591-603.
- RENEKER, D. H., YARIN, A. L., FONG, H. & KOOMBHONGSE, S. 2000. Bending instability of electrically charged liquid jets of polymer solutions in electrospinning. *Journal of Applied Physics*, 87, 4531-4547.
- REUTELINGSPERGER, C. P. M., VANGOOL, R. G. J., HEIJNEN, V., FREDERIK, P. & LINDHOUT, T. 1994. The rotating-disc as a device to study the adhesive properties of endothelial cells under differential shear stresses. *Journal of Materials Science-Materials in Medicine*, 5, 361-367.
- REZAEI, A. & MOHAMMADI, M. R. 2012. Development of Hydroxyapatite Nanorods-Polycaprolactone Composites and Scaffolds Derived from a Novel In-Situ Sol-Gel Process. *Tissue Engineering and Regenerative Medicine*, 9, 295-303.
- RIDDLE, R. C., TAYLOR, A. F., GENETOS, D. C. & DONAHUE, H. J. 2006. MAP kinase and calcium signaling mediate fluid flow-induced human mesenchymal stem cell proliferation. *American Journal of Physiology-Cell Physiology*, 290, C776-C784.
- RIM, N. G., SHIN, C. S. & SHIN, H. 2013. Current approaches to electrospun nanofibers for tissue engineering. *Biomedical Materials*, 8.
- ROGER, K. 2011. *Bone and muscle: structure, force, and motion*, 29 East 21st street, New York, NY 10010, Britannica Educational Publishing.
- ROHRICH, R. J. & GOSMAN, A. A. 2004. An update on the timing of hard palate closure: A critical long-term analysis. *Plastic and Reconstructive Surgery*, 113, 350-352.
- ROHRICH, R. J., ROWSELL, A. R., JOHNS, D. F., DRURY, M. A., GRIEG, G., WATSON, D. J., GODFREY, A. M. & POOLE, M. D. 1996. Timing of hard palatal closure: A critical long-term analysis. *Plastic and Reconstructive Surgery*, 98, 236-246.

## REFERENCES

- ROSS, R. B. 1987a. Treatment variables affecting facial growth in complete unilateral cleft lip and palate. *The Cleft palate journal*, 24, 5-77.
- ROSS, R. B. 1987b. Treatment variables affecting facial growth in complete unilateral cleft-lip and palate-treatment affecting growth-presurgical orthopedic treatment-alveolar repair and bone grafting-repair of the cleft lip-timing of palate repair-techniques of palate repair-an overview of treatment and facial growth. *Cleft Palate Journal*, 24, 1-77.
- RYU, Y.-M., HAH, Y.-S., PARK, B.-W., KIM, D. R., ROH, G. S., KIM, J.-R., KIM, U.-K., RHO, G.-J., MAENG, G.-H. & BYUN, J.-H. 2011. Osteogenic differentiation of human periosteal-derived cells in a three-dimensional collagen scaffold. *Molecular Biology Reports*, 38, 2887-2894.
- SAIJO, H., MORI, Y., FUJIHARA, H., KANNO, Y., CHIKAZU, D., OHKUBO, K., HIKIJI, H., IINO, M., YONEHARA, Y. & TAKATO, T. 2010. Evaluation and analysis of formation of bone at the palate in patients with cleft lip and palate after palatoplasty based on computed tomograms and three-dimensional data. *Journal of Plastic Surgery and Hand Surgery*, 44, 21-25.
- SAITOH, S., TAKAHASHI, I., MIZOGUCHI, I., SASANO, Y., KAGAYAMA, M. & MITANI, H. 2000. Compressive force promotes chondrogenic differentiation and hypertrophy in midpalatal suture cartilage in growing rats. *Anatomical Record*, 260, 392-401.
- SALBACH, J., RACHNER, T. D., RAUNER, M., HEMPEL, U., ANDEREGG, U., FRANZ, S., SIMON, J.-C. & HOFBAUER, L. C. 2012. Regenerative potential of glycosaminoglycans for skin and bone. *Journal of Molecular Medicine-Jmm*, 90, 625-635.
- SALGADO, A. J., COUTINHO, O. P. & REIS, R. L. 2004. Bone tissue engineering: State of the art and future trends. *Macromolecular Bioscience*, 4, 743-765.
- SAMEE, M., KASUGAI, S., KONDO, H., OHYA, K., SHIMOKAWA, H. & KURODA, S. 2008. Bone morphogenetic protein-2 (BMP-2) and vascular endothelial growth factor (VEGF) transfection to human periosteal cells enhances osteoblast differentiation and bone formation. *Journal of Pharmacological Sciences*, 108, 18-31.
- SANDINO, C. & LACROIX, D. 2011. A dynamical study of the mechanical stimuli and tissue differentiation within a CaP scaffold based on micro-CT finite element models. *Biomechanics and Modeling in Mechanobiology*, 10, 565-576.
- SAUNDERS, M. M., YOU, J., TROSKO, J. E., YAMASAKI, H., LI, Z., DONAHUE, H. J. & JACOBS, C. R. 2001. Gap junctions and fluid flow response in MC3T3-E1 cells. *American Journal of Physiology-Cell Physiology*, 281, C1917-C1925.
- SAWYER, A. A., HENNESSY, K. M. & BELLIS, S. L. 2005. Regulation of mesenchymal stem cell attachment and spreading on hydroxyapatite by RGD peptides and adsorbed serum proteins. *Biomaterials*, 26, 1467-1475.
- SCHILLER, P. C., D'IPPOLITO, G., BALKAN, W., ROOS, B. A. & HOWARD, G. A. 2001. Gap-junctional communication mediates parathyroid hormone stimulation of mineralization in osteoblastic cultures. *Bone*, 28, 38-44.
- SCHIMMING, R. & SCHMELZEISEN, R. 2004. Tissue-engineered bone for maxillary sinus augmentation. *Journal of Oral and Maxillofacial Surgery*, 62, 724-729.
- SCHMELZEISEN, R., SCHIMMING, R. & SITTINGER, M. 2003. Making bone: implant insertion into tissue-engineered bone for maxillary sinus floor augmentation - a preliminary report. *Journal of Cranio-Maxillofacial Surgery*, 31, 34-39.
- SCHWECKENDIEK, W. 1978. Primary veloplasty-long-term results without maxillary deformity-25 years report. *Cleft Palate Journal*, 15, 268-274.
- SEEBACH, C., SCHULTHEISS, J., WILHELM, K., FRANK, J. & HENRICH, D. 2010. Comparison of six bone-graft substitutes regarding to cell seeding efficiency, metabolism and growth behaviour of human mesenchymal stem cells (MSC) in vitro. *Injury-International Journal of the Care of the Injured*, 41, 731-738.

## REFERENCES

- SEELEY, R. R., STEPHEN, T. D. & TATE, P. 2008. *Anatomy and Physiology*, The McGraw-Hill companies, Inc. 1221 Avenue of the Americas, New York, NY 10020, McGraw-Hill Higher Education.
- SELIM, M., BULLOCK, A. J., BLACKWOOD, K. A., CHAPPLE, C. R. & MACNEIL, S. 2011. Developing biodegradable scaffolds for tissue engineering of the urethra. *Bju International*, 107, 296-302.
- SEMENZA, G. L. 1999. Regulation of mammalian O<sub>2</sub> homeostasis by hypoxia-inducible factor 1. *Annual Review of Cell and Developmental Biology*, 15, 551-578.
- SENGER, D. R., GALLI, S. J., DVORAK, A. M., PERRUZZI, C. A., HARVEY, V. S. & DVORAK, H. F. 1983. Tumor-cells secrete a vascular-permeability factor that promotes accumulation of ascites-fluid. *Science*, 219, 983-985.
- SHISHATSKAYA, E. I., VOLOVA, T. G., PUZYR, A. P., MOGILNAYA, O. A. & EFREMOV, S. N. 2004. Tissue response to the implantation of biodegradable polyhydroxyalkanoate sutures. *Journal of Materials Science-Materials in Medicine*, 15, 719-728.
- SIKAVITSAS, V. I., BANCROFT, G. N., HOLTORF, H. L., JANSEN, J. A. & MIKOS, A. G. 2003. Mineralized matrix deposition by marrow stromal osteoblasts in 3D perfusion culture increases with increasing fluid shear forces. *Proceedings of the National Academy of Sciences of the United States of America*, 100, 14683-14688.
- SIKAVITSAS, V. I., BANCROFT, G. N., LEMOINE, J. J., LIEBSCHNER, M. A. K., DAUNER, M. & MIKOS, A. G. 2005. Flow perfusion enhances the calcified matrix deposition of marrow stromal cells in biodegradable nonwoven fiber mesh scaffolds. *Annals of Biomedical Engineering*, 33, 63-70.
- SITTICHOKECHAIWUT, A., EDWARDS, J. H., SCUTT, A. M. & REILLY, G. C. 2010. Short bouts of mechanical loading are effective as dexamethasone at inducing matrix production by human bone marrow mesenchymal stem cells. *European Cells & Materials*, 20, 45-57.
- SLOAN, A. J. & WADDINGTON, R. J. 2009. Dental pulp stem cells: what, where, how? *International Journal of Paediatric Dentistry*, 19, 61-70.
- SMAHEL, Z., VELEMINSKA, J., TREFNY, P. & MUELLEROVA, Z. 2009. Three-Dimensional Morphology of the Palate in Patients With Bilateral Complete Cleft Lip and Palate at the Stage of Permanent Dentition. *Cleft Palate-Craniofacial Journal*, 46, 399-408.
- SODEK, J., GANSS, B. & MCKEE, M. D. 2000. Osteopontin. *Critical Reviews in Oral Biology & Medicine*, 11, 279-303.
- SOLIMAN, S., SANT, S., NICHOL, J. W., KHABIRY, M., TRAVERSA, E. & KHADEMHOSEINI, A. 2011. Controlling the porosity of fibrous scaffolds by modulating the fiber diameter and packing density. *Journal of Biomedical Materials Research Part A*, 96A, 566-574.
- SOLTAN, M., SMILER, D. & SOLTAN, C. 2009. The Inverted Periosteal Flap: A Source of Stem Cells Enhancing Bone Regeneration. *Implant Dentistry*, 18, 373-379.
- SOMBATMANKHONG, K., SANCHAVANAKIT, N., PAVASANT, P. & SUPAPHOL, P. 2007. Bone scaffolds from electrospun fiber mats of poly (3-hydroxybutyrate), poly(3-hydroxybutyrate-co-3-hydroxyvalerate) and their blend. *Polymer*, 48, 1419-1427.
- SOMMERFELDT, D. W. & RUBIN, C. T. 2001. Biology of bone and how it orchestrates the form and function of the skeleton. *European Spine Journal*, 10, S86-S95.
- SPASOVA, M., MINCHEVA, R., PANEVA, D., MANOLOVA, N. & RASHKOV, I. 2006. Perspectives on: Criteria for complex evaluation of the morphology and alignment of electrospun polymer nanofibers. *Journal of Bioactive and Compatible Polymers*, 21, 465-479.
- SROUJI, S., KIZHNER, T., SUSS-TOBI, E., LIVNE, E. & ZUSSMAN, E. 2008. 3-D Nanofibrous electrospun multilayered construct is an alternative ECM mimicking scaffold. *Journal of Materials Science-Materials in Medicine*, 19, 1249-1255.
- STANIER, P. & MOORE, G. E. 2004. Genetics of cleft lip and palate: syndromic genes contribute to the incidence of non-syndromic clefts. *Human Molecular Genetics*, 13, R73-R81.

## REFERENCES

- STEIN, G. S., LIAN, J. B., VAN WIJNEN, A. J., STEIN, J. L., MONTECINO, M., JAVED, A., ZAIDI, S. K., YOUNG, D. W., CHOI, J. Y. & POCKWINSE, S. M. 2004. Runx2 control of organization, assembly and activity of the regulatory machinery for skeletal gene expression. *Oncogene*, 23, 4315-4329.
- STOLZING, A., JONES, E., MCGONAGLE, D. & SCUTT, A. 2008. Age-related changes in human bone marrow-derived mesenchymal stem cells: Consequences for cell therapies. *Mechanisms of Ageing and Development*, 129, 163-173.
- STOLZING, A. & SCUTT, A. 2006. Effect of reduced culture temperature on antioxidant defences of mesenchymal stem cells. *Free Radical Biology and Medicine*, 41, 326-338.
- SUBIA, B., KUNDU, J. & KUNDU, S. C. 2010. *Biomaterial scaffold fabrication techniques for potential tissue engineering applications*, InTech.
- SULTANA, N. & KHAN, T. H. 2012. In Vitro Degradation of PHBV Scaffolds and nHA/PHBV Composite Scaffolds Containing Hydroxyapatite Nanoparticles for Bone Tissue Engineering. *Journal of Nanomaterials*.
- SWETHA, M., SAHITHI, K., MOORTHY, A., SRINIVASAN, N., RAMASAMY, K. & SELVAMURUGAN, N. 2010. Biocomposites containing natural polymers and hydroxyapatite for bone tissue engineering. *International Journal of Biological Macromolecules*, 47, 1-4.
- TAGUCHI, T., MURAOKA, Y., MATSUYAMA, H., KISHIDA, A. & AKASHI, M. 2001. Apatite coating on hydrophilic polymer-grafted poly(ethylene) films using an alternate soaking process. *Biomaterials*, 22, 53-58.
- TAKAHARA, A., HERGENROTHER, R. W., COURY, A. J. & COOPER, S. L. 1992. Effect of soft segment chemistry on the biostability of segmented polyurethanes .2. in vitro hydrolytic degradation and lipid sorption *Journal of Biomedical Materials Research*, 26, 801-818.
- TAKAHASHI, I., ONODERA, K., SASANO, Y., MIZOGUCHI, I., BAE, J. W., MITANI, H. & KAGAYAMA, M. 2003. Effect of stretching on gene expression of beta 1 integrin and focal adhesion kinase and on chondrogenesis through cell-extracellular matrix interactions. *European Journal of Cell Biology*, 82, 182-192.
- TANAKA, S. M., SUN, H. B., ROEDER, R. K., BURR, D. B., TURNER, C. H. & YOKOTA, H. 2005. Osteoblast responses one hour after load-induced fluid flow in a three-dimensional porous matrix. *Calcified Tissue International*, 76, 261-271.
- TAYLOR, G. 1964. Disintegration of Water Drops in an Electric Field. *Proceedings of the Royal Society of London. Series A. Mathematical and Physical Sciences*, 280, 383-397.
- TERESA, C. M., PAOLO, C., SILVANO, L., CLAUDIO, G. & PAOLO, P. P. 2009. *Polyphosphazenes for Biomedical Application*, Hoboken, New Jersey., John Wiley & Sons, Inc.
- TETTEH, G., KHAN, A. S., DELAINE-SMITH, R., GWENDOLEN, R. & U, R. I. 2014. Electrospun Polyurethane/Hydroxyapatite Bioactive Scaffolds for Bone Tissue Engineering: Therole of Solvent and Hydroxyapatite Particles. Elsevier.
- THI, M. M., SUADICANI, S. O. & SPRAY, D. C. 2010. Fluid Flow-induced Soluble Vascular Endothelial Growth Factor Isoforms Regulate Actin Adaptation in Osteoblasts. *Journal of Biological Chemistry*, 285, 30931-30941.
- THIMM, B. W., WECHSLER, O., BOHNER, M., MULLER, R. & HOFMANN, S. 2013. In Vitro Ceramic Scaffold Mineralization: Comparison Between Histological and Micro-Computed Tomographical Analysis. *Annals of Biomedical Engineering*, 41, 2666-2675.
- THOMAS, J. M. D., CHAKRABORTY, A., SHARP, M. K. & BERSON, R. E. 2011. Spatial and Temporal Resolution of Shear in an Orbiting Petri Dish. *Biotechnology Progress*, 27, 460-465.
- THOMSON, R. C., WAKE, M. C., YASZEMSKI, M. J. & MIKOS, A. G. 1995. Biodegradable polymer scaffolds to regenerate organs. *Biopolymers li*, 122, 245-274.
- TISCHER, E., MITCHELL, R., HARTMAN, T., SILVA, M., GOSPODAROWICZ, D., FIDDES, J. C. & ABRAHAM, J. A. 1991. The human gene for vascular endothelial growth-factor-multiple protein forms are encoded through alternative exon splicing. *Journal of Biological Chemistry*, 266, 11947-11954.

## REFERENCES

- TORMIN, A., LI, O., BRUNE, J. C., WALSH, S., SCHUTZ, B., EHINGER, M., DITZEL, N., KASSEM, M. & SCHEDING, S. 2011. CD146 expression on primary nonhematopoietic bone marrow stem cells is correlated with in situ localization. *Blood*, 117, 5067-5077.
- TRAUTVETTER, W., KAPS, C., SCHMELZEISEN, R., SAUERBIER, S. & SITTINGER, M. 2011. Tissue-Engineered Polymer-Based Periosteal Bone Grafts for Maxillary Sinus Augmentation: Five-Year Clinical Results. *Journal of Oral and Maxillofacial Surgery*, 69, 2753-2762.
- TU, C. F., CAI, Q., YANG, J., WAN, Y. Q., BEI, J. Z. & WANG, S. 2003. The fabrication and characterization of poly(lactic acid) scaffolds for tissue engineering by improved solid-liquid phase separation. *Polymers for Advanced Technologies*, 14, 565-573.
- TUAN, H. S. & HUTMACHER, D. W. 2005. Application of micro CT and computation modeling in bone tissue engineering. *Computer-Aided Design*, 37, 1151-1161.
- TUCKER, R. P., P., H., FRANKLIN, S. L., CHEN, D., VENTIKOS, Y., BOMPHREY, R. J. & THOMPSON, M. S. 2014. See-saw rocking: an *in vitro* model for mechanotransduction research. *Journal of the royal society interface*, 11, 1-9.
- TULLBERG-REINERT, H. & JUNDT, G. 1999. In situ measurement of collagen synthesis by human bone cells with a Sirius Red-based colorimetric microassay: effects of transforming growth factor beta 2 and ascorbic acid 2-phosphate. *Histochemistry and Cell Biology*, 112, 271-276.
- VAN GAALEN, S. M., KRUYT, M. C., GEUZE, R. E., DE BRUIJN, J. D., ALBLAS, J. & DHERT, W. J. A. 2010. Use of Fluorochrome Labels in In Vivo Bone Tissue Engineering Research. *Tissue Engineering Part B-Reviews*, 16, 209-217.
- VASITA, R. & KATTI, D. S. 2006. Nanofibers and their applications in tissue engineering. *International Journal of Nanomedicine*, 1, 15-30.
- VERBORGT, O., GIBSON, G. J. & SCHAFFLER, M. B. 2000. Loss of osteocyte integrity in association with microdamage and bone remodeling after fatigue in vivo. *Journal of Bone and Mineral Research*, 15, 60-67.
- VERBRUGGEN, S. W., VAUGHAN, T. J. & MCNAMARA, L. M. 2014. Fluid flow in the osteocyte mechanical environment: a fluid-structure interaction approach. *Biomechanics and Modeling in Mechanobiology*, 13, 85-97.
- VOLKMER, E., DROSSE, I., OTTO, S., STANGELMAYER, A., STENGELE, M., KALLUKALAM, B. C., MUTSCHLER, W. & SCHIEKER, M. 2008. Hypoxia in static and dynamic 3D culture systems for tissue engineering of bone. *Tissue Engineering Part A*, 14, 1331-1340.
- WAGNER, W., HORN, P., CASTOLDI, M., DIEHLMANN, A., BORK, S., SAFFRICH, R., BENES, V., BLAKE, J., PFISTER, S., ECKSTEIN, V. & HO, A. D. 2008. Replicative Senescence of Mesenchymal Stem Cells: A Continuous and Organized Process. *Plos One*, 3.
- WALSH, D. & AVASHIA, J. 1992. Glucocorticoids in clinical oncology. *Cleveland Clinic Journal of Medicine*, 59, 505-515.
- WALSH, S., JORDAN, G. R., JEFFERISS, C., STEWART, K. & BERESFORD, J. N. 2001. High concentrations of dexamethasone suppress the proliferation but not the differentiation or further maturation of human osteoblast precursors in vitro: relevance to glucocorticoid-induced osteoporosis. *Rheumatology*, 40, 74-83.
- WANG, H., PANG, B., LI, Y., ZHU, D., PANG, T. & LIU, Y. 2012. Dexamethasone has variable effects on mesenchymal stromal cells. *Cytotherapy*, 14, 423-430.
- WANG, L., DORMER, N. H., BONEWALD, L. F. & DETAMORE, M. S. 2010. Osteogenic Differentiation of Human Umbilical Cord Mesenchymal Stromal Cells in Polyglycolic Acid Scaffolds. *Tissue Engineering Part A*, 16, 1937-1948.
- WANG, Y., WAN, C., DENG, L., LIU, X., CAO, X., GILBERT, S. R., BOUXSEIN, M. L., FAUGERE, M.-C., GULDBERG, R. E., GERSTENFELD, L. C., HAASE, V. H., JOHNSON, R. S., SCHIPANI, E. & CLEMENS, T. L. 2007. The hypoxia-inducible factor a pathway couples angiogenesis to osteogenesis during skeletal development. *Journal of Clinical Investigation*, 117, 1616-1626.

## REFERENCES

- WANG, Y.-H., LIU, Y., MAYE, P. & ROWE, D. W. 2006. Examination of mineralized nodule formation in living osteoblastic cultures using fluorescent dyes. *Biotechnology Progress*, 22, 1697-1701.
- WATT, S. M., GULLO, F., VAN DER GARDE, M., MARKESON, D., CAMICIA, R., KHOO, C. P. & ZWAGINGA, J. J. 2013. The angiogenic properties of mesenchymal stem/stromal cells and their therapeutic potential. *British Medical Bulletin*, 108, 25-53.
- WEI, F., QU, C., SONG, T., DING, G., FAN, Z., LIU, D., LIU, Y., ZHANG, C., SHI, S. & WANG, S. 2012. Vitamin C treatment promotes mesenchymal stem cell sheet formation and tissue regeneration by elevating telomerase activity. *Journal of Cellular Physiology*, 227, 3216-3224.
- WEINBAUM, S., COWIN, S. C. & ZENG, Y. 1994. A model for the excitation of osteocytes by mechanical loading-induced bone fluid shear stresses. *Journal of Biomechanics*, 27, 339-360.
- WILLIAMS, J. M., ADEWUNMI, A., SCHEK, R. M., FLANAGAN, C. L., KREBSBACH, P. H., FEINBERG, S. E., HOLLISTER, S. J. & DAS, S. 2005. Bone tissue engineering using polycaprolactone scaffolds fabricated via selective laser sintering. *Biomaterials*, 26, 4817-4827.
- WOLFORD, L. M. & STEVAO, E. L. L. 2002. Correction of jaw deformities in patients with cleft lip and palate. *Proceedings (Baylor University. Medical Center)*, 15, 250-4.
- WONG, M. Y. & TUAN, R. S. 1993. nuserum, a synthetic serum replacement, supports chondrogenesis of embryonic chick limb bud mesenchymal cells in micromass culture. *In Vitro Cellular & Developmental Biology-Animal*, 29A, 917-922.
- WOODRUFF, M. A., LANGE, C., REICHERT, J., BERNER, A., CHEN, F., FRATZL, P., SCHANTZ, J.-T. & HUTMACHER, D. W. 2012. Bone tissue engineering: from bench to bedside. *Materials Today*, 15, 430-435.
- WOZNIAK, M., FAUSTO, A., CARRON, C. P., MEYER, D. M. & HRUSKA, K. A. 2000. Mechanically strained cells of the osteoblast lineage organize their extracellular matrix through unique sites of  $\alpha(v)\beta(3)$ -integrin expression. *Journal of Bone and Mineral Research*, 15, 1731-1745.
- XUE, R., LI, J. Y.-S., YEH, Y., YANG, L. & CHIEN, S. 2013. Effects of matrix elasticity and cell density on human mesenchymal stem cells differentiation. *Journal of Orthopaedic Research*, 31, 1360-1365.
- YANG, D., JIN, Y., MA, G., CHEN, X., LU, F. & NIE, J. 2008. Fabrication and Characterization of Chitosan/PVA with Hydroxyapatite Biocomposite Nanoscaffolds. *Journal of Applied Polymer Science*, 110, 3328-3335.
- YANG, X. B., ROACH, H. I., CLARKE, N. M. P., HOWDLE, S. M., QUIRK, R., SHAKESHEFF, K. M. & OREFFO, R. O. C. 2001. Human osteoprogenitor growth and differentiation on synthetic biodegradable structures after surface modification. *Bone*, 29, 523-531.
- YASZEMSKI, M. J., PAYNE, R. G., HAYES, W. C., LANGER, R. & MIKOS, A. G. 1996. Evolution of bone transplantation: Molecular, cellular and tissue strategies to engineer human bone. *Biomaterials*, 17, 175-185.
- YEATTS, A. B., GEIBEL, E. M., FEARS, F. F. & FISHER, J. P. 2012. Human mesenchymal stem cell position within scaffolds influences cell fate during dynamic culture. *Biotechnology and Bioengineering*, 109, 2381-2391.
- YIN, T. & LI, L. H. 2006. The stem cell niches in bone. *Journal of Clinical Investigation*, 116, 1195-1201.
- YIN, Z., CHEN, X., CHEN, J. L., SHEN, W. L., NGUYEN, T. M. H., GAO, L. & OUYANG, H. W. 2010. The regulation of tendon stem cell differentiation by the alignment of nanofibers. *Biomaterials*, 31, 2163-2175.
- YOSHIDA, K., OIDA, H., KOBAYASHI, T., MARUYAMA, T., TANAKA, M., KATAYAMA, T., YAMAGUCHI, K., SEGI, E., TSUBOYAMA, T., MATSUSHITA, M., ITO, K., ITO, Y., SUGIMOTO, Y., USHIKUBI, F., OHUCHIDA, S., KONDO, K., NAKAMURA, T. & NARUMIYA, S. 2002. Stimulation of bone

## REFERENCES

- formation and prevention of bone loss by prostaglandin E EP4 receptor activation. *Proceedings of the National Academy of Sciences of the United States of America*, 99, 4580-4585.
- YOSHIMOTO, H., SHIN, Y. M., TERAJ, H. & VACANTI, J. P. 2003. A biodegradable nanofiber scaffold by electrospinning and its potential for bone tissue engineering. *Biomaterials*, 24, 2077-2082.
- YOU, J., REILLY, G. C., ZHEN, X. C., YELLOWLEY, C. E., CHEN, Q., DONAHUE, H. J. & JACOBS, C. R. 2001. Osteopontin gene regulation by oscillatory fluid flow via intracellular calcium mobilization and activation of mitogen-activated protein kinase in MC3T3-E1 osteoblasts. *Journal of Biological Chemistry*, 276, 13365-13371.
- YOUREK, G., MCCORMICK, S. M., MAO, J. J. & REILLY, G. C. 2010. Shear stress induces osteogenic differentiation of human mesenchymal stem cells. *Regenerative Medicine*, 5, 713-724.
- YSUNZA, A., PAMPLONA, M. C., QUIROZ, J., YUDOVICH, M., MOLINA, F., GONZALEZ, S. & CHAVELAS, K. 2010. Maxillary growth in patients with complete cleft lip and palate, operated on around 4-6 months of age. *International Journal of Pediatric Otorhinolaryngology*, 74, 482-485.
- YUAN, L., SAKAMOTO, N., SONG, G. & SATO, M. 2013. High-level Shear Stress Stimulates Endothelial Differentiation and VEGF Secretion by Human Mesenchymal Stem Cells. *Cellular and Molecular Bioengineering*, 6, 220-229.
- ZARGARIAN, S. S. & HADDADI-ASL, V. 2010. A Nanofibrous Composite Scaffold of PCL/Hydroxyapatite-chitosan/PVA Prepared by Electrospinning. *Iranian Polymer Journal*, 19, 457-468.
- ZHANG, R. Y. & MA, P. X. 1999. Poly(alpha-hydroxyl acids) hydroxyapatite porous composites for bone-tissue engineering. I. Preparation and morphology. *Journal of Biomedical Materials Research*, 44, 446-455.
- ZHANG, Y., REDDY, V. J., WONG, S. Y., LI, X., SU, B., RAMAKRISHNA, S. & LIM, C. T. 2010. Enhanced Biomineralization in Osteoblasts on a Novel Electrospun Biocomposite Nanofibrous Substrate of Hydroxyapatite/Collagen/Chitosan. *Tissue Engineering Part A*, 16, 1949-1960.
- ZHOU, X., LIU, D., YOU, L. & WANG, L. 2010. Quantifying fluid shear stress in a rocking culture dish. *Journal of Biomechanics*, 43, 1598-1602.
- ZHOU, Y., GUAN, X., ZHU, Z., GAO, S., ZHANG, C., LI, C., ZHOU, K., HOU, W. & YU, H. 2011. Osteogenic differentiation of bone marrow-derived mesenchymal stromal cells on bone-derived scaffolds: effect of microvibration and role ERK1/2 activation. *European Cells & Materials*, 22, 12-25.
- ZIEGLERHEITBROCK, H. W. L. & ULEVITCH, R. J. 1993. CD14-cell surface receptor and differentiation marker. *Immunology Today*, 14, 121-125.
- ZINK, D., SADONI, N. & STELZER, E. 2003. Visualizing chromatin and chromosomes in living cells. *Methods*, 29, 42-50.
- ZONG, X. H., BIEN, H., CHUNG, C. Y., YIN, L. H., FANG, D. F., HSIAO, B. S., CHU, B. & ENTCHEVA, E. 2005. Electrospun fine-textured scaffolds for heart tissue constructs. *Biomaterials*, 26, 5330-5338.
- ZUO, W. W., ZHU, M. F., YANG, W., YU, H., CHEN, Y. M. & ZHANG, Y. 2005. Experimental study on relationship between jet instability and formation of beaded fibers during electrospinning. *Polymer Engineering and Science*, 45, 704-709.